UNIVERSITÉ DE STRASBOURG

ÉCOLE DOCTORALE SCIENCE DE LA TERRE, DE L'UNIVERS ET DE L'ENVIRONNEMENT

Laboratoire Image Ville Environnement

UMR 7362

THÈSE

présentée par :

Manon KOHLER

Date de soutenance: 8 juin 2015

pour obtenir le grade de : **Docteur de l'université de Strasbourg**

Discipline/ Spécialité: Géographie / Climat urbain

Apport de la modélisation météorologique à l'évaluation des besoins énergétiques des bâtiments

THÈSE dirigée par :

M. Clappier Alain	PR, LIVE-UMR 7362, Université de Strasbourg

RAPPORTEURS :

M. Richard Yves	PR, CRC-UMR 6282, Université de Bourgogne
M. Frankhauser Pierre	PR, ThéMa-UMR 6049, Université de Franche-Comté

EXAMINATEURS :

Mme Weber Christiane	DR, LIVE-UMR 7362, Université de Strasbourg
Mme Myriam Lopes	Assistant professor, CESAM, Université d'Aveiro

UNIVERSITÉ DE STRASBOURG

ÉCOLE DOCTORALE SCIENCE DE LA TERRE, DE L'UNIVERS ET DE L'ENVIRONNEMENT

Laboratoire Image Ville Environnement

UMR 7362

THESIS

presented by :

Manon KOHLER

PhD defense: 8th june 2015

for the award of the grade of: **Doctor of sciences from the université de Strasbourg**

Discipline/ Speciality: **Geography / Urban climate**

Assessement of the building energy requirements : added value of the use of the urban climate modeling

Research director:

M. Clappier Alain	PR, LIVE-UMR 7362, Université de Strasbourg

REPORTERS :

M. Richard Yves	PR, CRC-UMR 6282, Université de Bourgogne
M. Frankhauser Pierre	PR, ThéMa-UMR 6049, Université de Franche-Comté

REVIEWERS :

Mme Weber Christiane	DR, LIVE-UMR 7362, Université de Strasbourg
Mme Myriam Lopes	Assistant professor, CESAM, Université d'Aveiro

---

INVITED members:

Mme Blond Nadège	Chargée de recherche CNRS, LIVE-UMR 7362, Strasbourg (co-director)
M. Rivière Emmanuel	Directeur adjoint de l'Association pour la Surveillance et la Prévision de la qualité de l'Air, Strasbourg

Abstract

The climate change and the depletion of most of the affordable tanks of conventional fossil fuels in the next century challenge the contemporaneous societies in designing post-carbon society. In France, buildings are a key point of the energy policies. They represent about 40% of the French final energy consumption and are characterized by a high potential of energy savings due to the building long life cycle. In the past decades, sophisticated climate modeling systems that implement three dimensional urban effect canopy parameterizations and simplified building energy models in mesoscale atmospheric models, have been developed to consider the cross-scaled processes involve in the urban climate and its linkage with the building energy use. With the reinforcement of the role of the local authorities in the climate change mitigation strategies, those climate modeling systems seem a promising tool in helping transferring the climatic and energetic knowledge in the urban planning instruments.

This study aims to assess the capability of such climate modeling systems in helping urban planners to implement energy saving strategies in the context of climate change and aims to provide new insight on the interactions between the urban form, the urban climate and the building energy use for designing sustainable cities.

For this, we used the WRF/ARW-BEP+BEM climate modeling system provided by the American atmospheric research center and performed various sensitivity tests considering firstly, the territory of the city council of Strasbourg (France) in 2010, and secondly, the residential development of the Strasbourg-Kehl urban region by 2030. At last, we developed a canopy interface model (CIM) to improve the surface representations in the climate modeling systems. The philosophy is that microscale climate models and sophisticate building energy use models can better consider the heterogeneity of the surface and can compute more accurately the surface fluxes accounting for the topology of the obstacles than traditional urban canopy parameterizations. The results of the sensitivity analyses revealed that the climate modeling system achieves estimating the building energy requirement of a given area and period, but is highly sensitive to the intrinsic building properties and internal heat gains. In addition, we found that the urban form has few incidences on the building energy requirements and that building forms are prevailing factors in the building energy requirements. We therefore plaided in favor of down scaling the scale of investigation at the level of the neighborhood. To such extent, the CIM interface model seems appropriated to bridge the gap between the microscale and the mesoscale climate models.

Keywords: *Urban climate, planning policies, urban form, building energy, climate modeling system, mesoscale atmospheric model, 3D urban canopy parameterization*

REMERCIEMENTS

C'est un moment émouvant lorsque l'on en vient à écrire les dit-remerciements. Emouvant, parce qu'usuellement c'est à ce moment précis que l'on réalise que l'aventure thèse touche à sa fin. Ce qui est en soi assurément une bonne nouvelle ! Là, je pense en premier lieu à mes encadrants Nadège et Alain ainsi qu'à Cécile (Tannier) que je remercie tous trois chaleureusement de m'avoir épaulée et encadrée avec amitié durant ces années. Ensuite, je pense aux rapporteurs de mon jury que je remercie d'avance de l'attention qu'ils porteront à mes travaux et de leur présence. Enfin mes pensées se dirigent vers le personnel du LIVE, de la MSHE Nicolas Ledoux, et de ThéMa qui m'ont accueilli et qui ont contribué tout à chacun à la réalisation de cette thèse notamment Rahim Aguejdad, Estelle Baehrel, Grégoire Skupinski, Jean-Christophe Foltête, Armelle Kaufmant-Couillet et Damien Roy. Je remercie également Alberto Martilli du CIEMAT pour ses précieux conseils et sa disponibilité. Emouvant aussi, parce que l'on se remémore toutes les personnes que l'on a rencontrées et qui ont permis de ramifier nos connaissances et pensées. Ces personnes sont nombreuses: de l'UFR de géographie notamment Jean-Luc Mercier et George Najjar au Jardin des Sciences de l'université de Strasbourg et de Bogota à Besançon! Ces rencontres ont été diverses: furtives et fortuites, planifiées et prolongées et ont toujours été enrichissantes et belles.
Emouvant enfin, parce que l'on pense à toutes les personnes qui ont supporté tout un arc en ciel d'humeurs au cours de ces dernière années. Les pauvres ! Je remercie mes collègues de bureau, Dasaraden et Sajjad qui ont su égayer mes journées. Je remercie mes proches qui ont su se montrer patients et qui ont cru en moi (souvent même, un peu plus que moi!). Et je pense enfin à l'équipe de grimpeurs du SUAPS. De l'air frais, des parois, des montagnes, des personnes chaleureuses et du fromages, ça fait toujours du bien aux neurones et au moral! Merci à vous!

Bref ! Plutôt que de continuer sur une litanie et quelques psaumes et de dresser une liste non exhaustive des personnes qui ont compté, pensons bien, mais vite ! Je vous remercie tous. Tous ? oui, tous ! J'ai pris plaisir à échanger avec chacun de vous durant ces années. Moi qui voulait voyager, j'ai été servi! *Un voyage se passe de motifs. Il ne tarde à prouver qu'il se suffit lui-même. On croit qu'on va faire un voyage, mais bientôt c'est le voyage qui vous fait, ou vous défait.* - Nicolas Bouvier.
Et la thèse est, en effet ,un sacrée voyage !

Je vous souhaite à tous une bonne route, des circonvolutions, des bifurcations, des errances, des questionnements, des trouvailles et des rencontres! De manière plus concrète puisque vous entamez ces pages, je vous souhaite une bonne lecture.

ACKNOWLEDGMENTS

Ce travail a été financé par le CNRS dans le cadre de l'ANR TVU et le programme CCTV, par le projet FEDER ODIT, la ZAEU et le réseau REALISE. Les données utilisées dans cette étude ont été fournies par le service régional de Météo France, l'association pour la surveillance et la protection de la qualité de l'air de Strasbourg (Source d'information ASPA - 12121203 - TD), la Communauté Urbaine de Strasbourg, la coopération CIGAL, l'IGN et l'INSEE. Le méso-centre de calcul HPC et les unités mixte de recherche Image Ville Environnement (Strasbourg, UMR 7362) et ThéMa (Besançon, UMR 6049) ont fourni les ressources informatiques et logistiques nécessaires à ce projet.

Contents

List of Figures

List of Tables

Chapter 1

Introduction

Since the 1970's-1980's, the rapid growth of the world energy use raises increasingly concerns for energy supply and energy-related environmental impacts. In particular, climate change becomes one of the major scientific and political preoccupations [Pérez-Lombard et al., 2008, UN, 2012]. To date, climate change is unequivocal and is observed both in the mean and variability of the climate properties. The global surface temperature has increased by +0.74°C over the past 100 years (1906-2005), and twelve of the latest years are ranked among the warmest years. The driver of the present warming is with a "very high confidence" attributed to the unprecedented increase of atmospheric greenhouse gases (GHG) concentrations such as methane, ozone, and carbon dioxide. The combustion of fossil fuels by human activities and by-products represents 70% to 75% of the carbon dioxide emissions in the atmosphere [Hoel and Kverndokk, 1996]. To date, the carbon dioxide atmospheric concentration exceeds from far the natural maximum ranges recorded over at least the last 800,000 years. Due to the long time scales associated with climate processes and feedbacks as well as the long GHG life cycle, the resilience of many ecosystems will be exceeded in the next century [IPCC, 2007]. The urban ecosystem, in the absence of mitigation and adaptation strategies, is one such.

IEA [2008] estimated that around 84% of the world energy supplies up to 2030 will come from fossil fuels. Considering the finite affordable reserves of fossil fuels and maximum world productions (the peak oil) the reserves of oil are estimated to be equal to 40 years, 60 years for natural gas and 350 to 150 years for coal [Shafiee and Topal, 2009]. As a consequence, this urges the energy transition of our contemporaneous society. Nevertheless, the peak oil may be delayed depending on the population growth and fuel price, the international energy policies of the OPEP countries, the discovering of additional tanks, the use of unconventional hydrocarbons as well as the improvement of oil salvage technologies (by now only one third of the tank is exploited according to IAURIF [2008]) [IEA, 2012].

1.1 The energy challenge in urban areas

In the one hand, although urban areas represent approximatively 2% of the emerged Earth surface, they concentrated around the half of the world population in cities of 100,000 to 500,000 inhabitants or megacities of more than 10 millions of people. By 2050, the World Health Organization estimates that 7 out 10 people will be urban

dwellers [UN, 2012]. In France, urban areas represent 21.8% of the metropolitan territory in 2010 and gather in 2007 more than 77.5% of the metropolitan population [INSEE, 2011].

Due to this high population density, more than two third of the total world energy consumption occur in cities. More, it is expected to be 73% by 2030 with the worldwide demographic and economic growths[IEA, 2008]. The building sector is one of the largest world energy end-use sectors accounting approximatively for the entire daily oil production of the OPEP countries and almost 40% of the final energy use [Santamouris, 2001, OECD and IEA, 2008]. In France it represents 44% of the final energy use, far ahead from the transportation sector in which residential houses count for the two third [ADEME, 2012]. Thermal comfort remains the main energy use. In particular, space heating accounts for 54% of building energy use in the IEA countries and 68.3% in France [OECD and IEA, 2008, ADEME, 2012]. The energy mix in buildings is dominated by the electricity and natural gases [IEA, 2013]. In France, they count respectively for 38% and 32%. Oil (16%), renewable energies (14%), and coal and peat (0.4%) supply the remaining energy requirements [Global-Chance, 2010]. In the world, fossil fuels mainly supply the electricity generation. Coal represents 41.3% and natural gas 21.9%, respectively. By 2030, a rise in the building energy requirements is projected due to the improvement of life standards and demographic growth [Santamouris et al., 2001]. On the new power generation capacity that is built for 2035, one third is already needed to replace the production of aging power plants. A half will be supplied by renewables energies while the remaining by coal [IEA, 2012].

A focus on the French situation points out that the building sector is less dependent than the others to the fossil fuel reserves. Indeed, 50% of the building energy use is supplied by electrical power. In contrast to other countries, a large share of the power generation in France is supplied by nuclear energy (74.8% of the power generation in France and 11.7% in other countries according to the world energy outlook in 2012). In France, hydropower represents the second source of electricity accounting for 11.8% of the total generated power. It is mainly used to offset the variations of the energy demand. As nuclear and hydro-power generations depend both on the water supplies, climate change may alter the efficiency of the electricity generation along with the reduction of water discharge and availability of cooling liquid in nuclear power plants [US Climate change science program, 2008]. A fortiori, nuclear power plants and electricity grids come in age. In 2011 only 80.7% of the potential of power production by nuclear power has been used due to maintenance operations [RTE, 2012]. Meantime according

to the electricity supply company the electricity demand has raised by +2.4% per year since 2002 [RTE, 2012]. The rise is partly explained by the development of electric heating system in new constructions (60% of them are supplied by electricity) and by the increasing use of specific electricity for telecommunication and informatics. Other socio-economic factors due to an ageing population structure are also mentioned: such as smaller household size and hence, an increasing demand in energy per dwelling unit [ADEME, 2012, Castéarn and Ricroch, 2008].

In the other hand, since the 60's the rapid urbanization has been accompanied by urban sprawl, the spatial extension of urban areas out of their fringe within the rural countryside [INSEE, 2011]. In France it is the equivalent of one district (610,000 km^2) each 7 years that is built up to the detriment of crops and meadows. More than building areas, impervious built-up areas dedicated to transport and commercial activities and urban green areas (defined as the whole vegetative areas located within or at vicinity of an urban area [Selmi et al., 2013]) count for the highest rise [Agreste, 2011]. Hence, the radiative, thermal and aerodynamics surface properties are modified. Over cities, the substitution of the humid and vegetative areas by impervious built-up areas leads to the formation of a warm atmospheric dome (*i.e.* the urban boundary layer) above and downwind to the urban areas. This urban boundary layer is often several degrees warmer than the rural boundary layer and is characterized by convective uplifted wind motions [Oke, 1987]. This phenomenon is called the Urban Heat Island (UHI) and results from the expression at regional scale (mesoscale) of physical processes occurring at street and building scales that are listed below:

i) Surface shadowing effect and multiple interceptions of short waves and longwaves radiations due to numerous obstacle vertical facets modify the amount of radiative energy absorbed at the surface;

ii) The higher thermal admittance of construction materials allow the absorption and storage of large amount of energy in the urban fabric materials;

iii) Since vegetation-covered soils are fewer in urban areas compared to rural areas (*e.g.*vegetation areas represent 57% to 0.01% of the total urban surface in Arcadia and in Mexico, respectively according to Grimmond and Oke [1999b]), the incoming solar radiative energy is mainly partitioned into heat (*i.e.* sensible heat) and ground heat fluxes that contributes to warm the air at local scale (street);

iv) Additional ejections in the street of heat and humidity as well as particles and greenhouse gases emissions due to human activities reinforce the air warming;

v) At last, friction and drag forces acting on the obstacles facets reduce the natural ventilation in the streets. Deflections occur at building edges leading to wind speed reduction and formation of recirculation regions at the top of the obstacles, and at its upwind and downwind sides. The recirculation regions are characterized by the presence of turbulent eddies and vortices that may interfere according to the obstacle density [Baik and Kim, 2003].

With the global warming the heat wave are expected to be more frequent, and the UHI is expected to harsher the urban dwellers heat stress in summer as the European 2003 heat wave witnessed. Although, UHI may have negative feedbacks on energy requirements in winter, it has positive feedbacks in summer enhancing the use of electricity and the production of anthropogenic heat due to the use of air conditioning in buildings [Hunt and Watkiss, 2011, Yang et al., 2014]. More, several studies showed that the energy demand is more sensitive to weather conditions when using electricity heating or cooling system than when using oil or natural gas-fired boiler plants. Akbari et al. [2001] reported a +2 to +4% rise of the urban peak electricity demand each 1°C rise in the daily maximum temperature ranging above 15-20°C for six American cities; Global-Chance [2010] reported a doubling of the peak electricity demand for space heating between 2009 and 1996 concomitant with an increasing number of heating electrical systems in houses. As a conclusion the UHI effect may enhance the thermal stress of the urban dwellers in summer, while a shift in the seasonal energy demand is expected with an increasing share of the electrical power energy in the building energy mix.

1.2 Mitigation and adaptation strategies to cope with the climate change impacts

Mitigation strategies, which refer to lessen GHG emissions to reduce the magnitude of changes cannot cope alone with the climate change impacts. Even more if the magnitude of the climate change impacts is projected to increase with time [IPCC, 2007]. Adaptation strategies are then required in addition. In this context cities, as driver of political and socio-economical changes and land-use planning, are relevant places for driving such strategies.

1.2.1 Mitigation strategies

By 2050, a limitation of the temperature rise to +2°C is agreed as the related impacts are still judged acceptable. To fit with this limitation, anthropogenic CO2 atmospheric emissions are targeted [IPCC, 2007]. Thus, the French government targets a reduction by a factor 4 of the GHG emissions with respect to the 1990's GHG emissions. To this extent, buildings, which contribute to 25% of the total French CO2 emissions, offer a high potential of reduction of the GHG emissions.

The substitution of low carbon or renewables energies (EnR) for power generation and direct heating could achieve those objectives. In France the use of nuclear generated electricity plays a key role in mitigation policies. However, is the use of electricity efficient in reducing GHG emission? To such extent, Global-Chance [2010] demonstrated that the reduction in GHG emissions between 1997 and 2007 by using nuclear produced electricity in new houses despite fossil fuels (natural gas) is few. It represents less than 1% of the building total emissions. A fortiori, higher variations of the electricity demand and decrease of the nuclear power generation capacity due to the aging of the power system will reinforce the use of thermal power plants that used hydrocarbon fuels to supply the electricity demand [RTE, 2012]. Moreover, the use of nuclear energy raises ethical issues: radioactive cores are finite and thousand years estimated [National academy of technology of France, 2004], while the safety of the installations, the retirement of the long timescale radioactive wastes, and the potential military usages of this civil technology are far to achieve any opinion consensus in the population on the sustainability of the nuclear energy supplied-power generation.
In parallel, the share of the EnR in the space heating energy mix is projected to increase by 33% since 2050. The biomass, which counts for the two third of the EnR energy mix, represents 85% of the 2015 objectives [IAURIF, 2008]. The biomass presents the advantage that it could be used for power generation as well as for direct heating. Although considered as "clean energies", the analysis of its lifecycle shows non null contributions to GHG emissions. It contributes to the ozone formation and emits methane and nitrous protoxide, which have a 4 fold and 100 fold higher global warming potential than carbon dioxide. A fortiori large conversions of arable toward non-alimentary productions and deforestation of ecologically rich forested lands are ethical issues associated with the biomass exploitation. Pressure on the water resources, eutrophication of the aquatic biotope and impoverishment of soil organic matter are other related environ-

mental concerns [Pehnt, 2006]. In conclusion even with the EnR, the production of energy remains economically and environmentally costly: the adaptation of the power transmission system requirs almost 1,224 million Euros in 2012, while the support of the EnR penetration on the energy mix markets is mainly provided through short-term subsides and taxes incentives that ensure artificial competitiveness [RTE, 2012].

For these reasons, other ways such as energy conservation measures should be investigated. Energy conservation relies on the enhancement of the building energy efficiency, and acts both on the energy production and demand patterns. To this extent, new constructions have the largest potential as a significant proportion of the consumed energy might be wasted during the buildings lifespan due to defaults in their construction and design [Wang et al., 2012]. The French thermal regulation sets the maximum energy requirements at 50 kWh since 2012. More, by 2020, the whole new constructions should produce from renewables more energy than used. However building stock in France is dominated by energy intensive buildings built before 1974, the first thermal regulation, in which oil and gas-fired boiler plants were widely used. With an existing building replacement rate equal to about 1% per year, ADEME [2005] estimated a 1974's building park turnover of about 100 years. For this reason,the French law Grenelle 1 adopted in 2009 sets a renovation rate of 400,000 lodgments per year so as to reduce the building energy consumption by 38% by 2020 for existing buildings. Although a reduction of -44% of the heating consumption between 2001 and 1973 is attributable to renovations [ADEME, 2005], the energy savings due to building renovations are limited. The renovations are often done once after the building purchase and focused mainly on the building shell (*e.g.* thermal insulation and reflective coatings) as the improvements of the thermal envelope can reduce the space heating requirements by factor two to four at a few percent of the total cost of residential buildings [IPCC, 2007, Desjardin et al., 2011].

Additionally, occupant behavior, culture and consumer choice are major determinant of energy conservation measures [IPCC, 2007]. Several studies on rebound effect [Greening et al., 2000, Herring and Roy, 2007, Brännlund and Ghalwash, 2007], indeed, pointed out that the price elasticity resulting from the enhancement of the building efficiency may result in the increase of the building energy consumption. Abrahamse [2005] demonstrated that frequent feedbacks on energy use through monitoring and monetary reward are efficient strategies to reduce energy use. And Yang et al. [2014] reported a cooling energy savings of about 30% when increasing the set point temperature. As a consequence, it seems that the energy consumption has a socio-economical

dimension relative to the thermal comfort perception that is socio-culturally determined and that is often neglected in mitigation studies [IEA, 2008].
Indeed, technical proven solutions are rather considered to alleviate the forthcoming disaster as they are more *"transferable and readily applicable to other technically similar solutions"* than behavioral ones [Guy, 2004]. A fortiori thinking on the social dimension of the energy consumption can raise issues on the human own nature and its linkage with its environments as humans are often described as rational actors taking rational decisions: so how believe that the result of myriad rational choices (behaviors) can lead to such unprecedented threat?

1.2.2 Adaptation strategies

According to Smit and Wandel [2006] adaptation strategies refer to the long-term adjustment of the system behavior and characteristics that enhance its ability to cope with or take advantage of a stimuli, here, the forthcoming global warming. Improving of the urban climate is one of them [Bitan, 1992, Landsberg, 1973]. Bitan [1992] pointed out that most of the adaptation strategies refer to the building scale and the adoption of vernacular architecture principles such as: the optimization of the building orientation and glazing systems to take advantage of natural ventilation and solar passive gain, the reduction of the envelope surface exchange with the atmosphere by adopting compact and semi-detached houses, the optimization of the building density for improving the natural ventilation of the streets and taking advantage of the shadowing of the building facets [Oke, 1988], the use of high-reflective surfaces [Akbari et al., 2001] and so on. Other adaptation strategies rather refer to behavioral measures such as the renunciation of certain activities that produce anthropogenic wasted heat according to the weather conditions.

Among adaptation strategies, the enlargement of urban green areas in urban areas have more and more recognition in alleviating climate change impacts through the optimized usages of their ecological functions at building, city-block and city scales [Gill et al., 2008]. Indeed urban green areas, more than ensuring the ecological diversity, provide many other ecosystem services. Among them, ventilation of appropriate space, the provision of cooler air at building and neighborhood scales through direct shading of the surface, and at lesser extent through evapotranspiration is of interest [Dimoudi and Nikolopoulou, 2003, Kuttler, 2012]. To date, the research and public

institution communities have mainly focused their investigations on three types of vegetation: trees, green roofs that could be intensive (tall vegetation) or extensive (low vegetation), and green parks.

- **Trees**

  Trees, in particular veteran trees with densely foliated crowns, have focused the attention of the researcher communities in the past decades and forester the development of urban forestry services in urban areas [Nowak, 2004, 2006]. Akbari et al. [1997] observed a potential cooling energy savings ranging from -30% up to -50% by planting trees when surveying two experimental houses in Sacramento. Heisler et al. [1986] and Akbari and Taha [1992] reported energy savings in winter of 23% to 25% and 10% to 15% due to the trees wind-shielding effects. In contrast Shashua-Bar et al. [2009] and Huang et al. [1987] emphasized that trees could harsher thermal comfort and increase the cooling energy demand: trees intercept longwave radiations from the ground and neighboring building surfaces and inhibit as well the natural ventilation. To such extent, Kuttler [2012] showed that placing a tree in the middle of the road bordering by trees should be avoid because the tunnel effect created could lead to street-level exhaust-gas accumulation, and hence reduce the street natural ventilation. In parallel, Simpson and McPherson [1998] also outlined a +2.8% rise of the space heating demands due to shading of the building surface by branches and trunks. The effects of trees on building energy saving is therefore controversial.

- **Green roof**

  Recently, green roof biotechnologies are regularly cited as the solution of the future temperature rise mitigation. Green roofs consist in a layered system comprising a waterproofing membrane, growing medium and the vegetation itself. Roofs, indeed, are waste surfaces that are located within the human habitat and that absorb the largest amount of solar radiation [Alexandri and Jones, 2008, Castleton et al., 2010]. An investigation on the future of Manchester in 2080 reported a temperature reduction by -7.6°C by greening all the roofs by 2080 [Gill et al., 2008]. For building energy performance, Liu and Minor [2005] reported from a field campaign a reduction of the heat gains of building shell in summer by -70 to -90% and a reduction of winter heat losses by -10 to -30% resulting in

a decrease in the building energy load.

- **Green park**

  At last, green parks are often cited as cool oasis in urban areas. Several studies like IAU [2010] reported that green parks lessen the air temperatures up to 1-2°C around 100 m downwind the parks. Green parks could, however, stress the human comfort when dry as they then act as bare and impervious soils. Their wide use may also originate extensive use of lands that are energy intensive urban form [Chang et al., 2007, Mehdi et al., 2012, Haines, 1986] and may reduce the convective mixing of the air above urban areas by lowering the boundary layer height and thus, increase the concentration of the pollutant in the streets.

Thus, the benefits of the vegetation in lessen the air temperature and save building energy is mitigated. More, some urban green forms, such as green parks that provide other ecological services for urban dwellers (*e.g.* recreative, physchological, aesthetic, educational) seem to have unwanted effects on the urban development with generalized usage. Therefore, how to conciliate the urban dweller's desire for nature and the preservation of the ecological services provided by green areas?

Since the 1987's the urban planning receive increasing recognition in helping optimizing the use of the natural resources, and in framing the different elements of the urban ecosystem [Holden and Norland, 2005].
By controlling the location of the urban activities (*e.g.* residential, work, leisure and so on) the local development plans act simultaneously on the energy production and consumption chains. The home to work distance influences the automobile traffic and the correlated use of fossil fuels. Again the home-to-work distance, and the land use policies and prices influence the homebuyers residential choices as well as the residential housing types (*e.g.*individual, collective) that are often associated with particular building energy performance properties (*i.e.*insulation, surface on volume ratio). As a consequence, several planning instruments include energy efficiency and climate quality dimensions [Chanard et al., 2011]. As an example, the French *Plan Climat Energie Territorial* (PCET) that is set mandatory since 2012 for agglomerations of 50,000 residents and more aims to inventory the energy use and GHG emissions over the administrative limits of the urban agglomerations; it determines objectives and action plans in matter of GHG emissions reduction and building energy performance.

In the past, two contrasted urban forms were assigned to produce sustainable urban ecosystems: the compact city and the short-cycle city. The sustainability of the compact city relies on the statement that urban sprawl by originating numerous individual cars home-to-work commuting, low dense human settlements and segregations of activities are urban form that enhance the energy use. The idea, mainly promoted by the works of Newman and Kenworthy on the home-to-work trips of several megacities in the world, is that high-density development of built-up areas close to or within an existing built-up areas with a mixture of activities may result in promoting public transportation services, pedestrian trips, multi-family dwellings that are characterized by high energy use per capita. Although the compact city concept has entrenched many policies, high density has been demonstrated to have prohibitive effects. Bailly and Bourdeau-Lepage [2011] stressed that compact cities are unrealistic and undesirable as they do not answer to the individual's desire of privacy and nature that urban dwellers have to find elsewhere such as in compensatory long-distance travels [Holden and Norland, 2005, Desjardin et al., 2011] The Commissariat général au développement durable [2010] also highlighted that the scale economy due to high-density disappears after a given marginal cost threshold at which rural towns modify their planning policies leading to push farthest away the population settlements. At last ,although high density can improve the winter climate quality by enhancing the UHI intensity in particular in high-latitudes, it may cause other problems associated with the melting of the permafrost and may harsher thermal comfort in summer in middle-latitudes [Hinkel et al., 2003, Taha, 1997, Smith and Levermore, 2008]. Other studies questioned a fortiori the assumption that has originated the compact city theory [Haines, 1986, Dujardin et al., 2014]. Dujardin et al. [2014] demonstrated that the age of construction rather determined the energy efficiency than the urban form and that energy efficient urban from could be found also in rural and semi-rural less dense built-up settlements.

At the opposite, short-cycle cities seem to be energy efficient alternatives to compact cities and dispersed cities [Haines, 1986]. It relies on a local conception of the environmental sustainability as Ebenezer Howard theorized in the Garden Cities. It consists in decentralized concentration of population and activities, and short-circuit production-consumption patterns for energy and agriculture. The provision of periurban agricultural lands can indeed offer a larger access for urban dwellers for natural services and amenities that can attenuate the urban sprawl. Short-circuit in particular for energy can forester the use of renewable energies and the recycling of wastes. At last short-circuit also promote the mix of usage, economical functions and dwelling

social obedience at local scale.
In contrast to the compact city, the short-cycle city rather consists in an urban hierarchical network in which intermediate cities play a key role in attracting population and activities by proposing public transport offers, mix usages and proximity services. To such extent, Tannier [2009] demonstrated that fractal cities can promote short-cycle as fractal elements are invariant or quasi-invariant in scales and therefore provide a greater access to natural amenities and services than other urban form. As a drawback, it seems that this urban form is more convenient for new towns in which the efficiency of the whole urban system could be anticipated at the planning stage. To date, concretized short-cycles realizations are rather found at city-block scale in the form of Eco-neighborhoods that favor energy efficient building (compact semi-detached zero energy housings), social and local economical activities mixes, local and periurban agriculture that could figure as familial gardens or AMAP associations (a direct association between a producer and consumers), local energy production and cogeneration principles, and at last, waste and water recycling circuits. The public spaces such as the pathways are then thinking as multifunctional lanes that can be used for soft transportation ways (bicycles, pedestrian), and for ensuring the connectivity of the ecological network. Individual cars are often excluded like in the German eco-neighborhood Vauban in Freiburg-im-Breisgau or their use mutualized. However, in real, it seems that the ownership in such neighborhood rather concerns a social elite class. More, although the projects have flourished during the last decades, short-cycle patterns figure more as an exception than a norm. As a conclusion, the question of sustainable urban form is still open.

In designing sustainable cities, Landsberg [1973] considered the *"climatologist as a Johnny-come-lately"*. Oke [1984] estimated that *little of the large body of knowledge concerning urban climate has permeated through to working planners"*. Inversely, the non-accurate appreciation of the urban planning scales in meteorological models that are used to foretell the climatic conditions over urban areas, explains partly the lack of communications between urban planners and urban climatologists.
In the one hand, operational mitigation and adaptation strategies issued from urban planning rather work at city-block or building scales: *i)* the urban morphology can not be dramatically changed as it is often inherited from long term planning policies on transportation and accommodation [Anderson et al., 1996]; and *ii)* the operational planning regulatory instruments are rather set for building or building lots. For instance, the local French development plan (PLU) gives the main 5-10 years planning

orientations in matter of social diversity, optimization of the land-usage between natural resources, agricultural lands, and built-up areas, but even more provides the building codes and operational legal informations for each building lots. Indeed the PLU defines the thermal regulation in vigor for the lots, the maximum built-up areas per lots, the maximum construction height that all have direct impacts on building energy performance and local climate. A fortiori, urban planning operations are often delegated to property developers that limit the architectural coherence and the scope of the mitigation and adaptation strategies at the city scale.

1.3 A brief review of the building energy performance methodologies: their actual limits and opportunities

With the forced energy transition, diagnostics of building energy performance and estimations of building energy consumption become necessary to design sustainable cities. Several building scale- or regional scale-focused methods exist that assess the building energy performance. Most of them rely on a bottom-up approach in which the knowledge of the building energy use intensity (EUI) (*i.e.* the energy consumptions per floor square meter, the energy losses per floor square meter, the energy requirements per square meter) of a benchmarked building owning to a particular segment of the building stock provides the overall building energy performance knowing the share of this segments in the whole building stock.
The EUIs are often provided by building energy use sub-metering campaigns, desegregations of energy bills per end-uses or analysis of the radiant energy emitted by the buildings in thermal infrared images. Although those methods permit to consider quickly the changes induced by the urban development on the building energy performance of a given area through the compilation of up-dated dwelling datasets, the EUIs neglect the interactions between the building and the local climate.
In the EUIs that consider the variation of the climate, numerical building energy use models enables to dynamically assess the building energy requirements of a prototype building by resolving the heat and humidity diffusion in the building materials that constitute the building envelope. Nevertheless, the outdoor climate conditions are often inherited from fix meteorological synoptic stations that are located out of the built-up areas leading to over-estimate the building energy requirements.

With the climate change, the enhancement of the local extreme phenomenon such as the UHI those methods seems no more appropriated as they do not reproduce the local climate interactions with the building energy requirements. More, the release of anthropogenic heat in atmosphere due to the human activities are recognized to increase the air temperature by +2°C, and the urban heat island intensity in particular in winter and at night when the solar forcing is low. Kikegawa et al. [2003] besides, found an increase in the cooling energy demand due to the activation of the heat ventilation air conditioning system in summer.

To include the energetic and dynamic alterations of the regional airflow due to the presence of urban areas and anthropogenic activities, some studies used numerical regional atmospheric models like ASPA [2012] to produce more accurate air temperature and the climate correction by using the degree-day as climate correction factor. The degree-day represents the cumulative temperature differences over a period of the daily outdoor temperatures taken from the closest meteorological stations and a pre-defined base temperature. The latter corresponds to the temperature at which there are no more building energy needs. It is often taken at 17°C or 18°C and appears to be particularly sensible to the building types (residential, commercial) and fuels [Valor et al., 2001]. The daily outdoor temperatures are usually provided by the fix observational meteorological networks, which are often located out of the urban areas. The estimates of the building energy requirements thus, neglect the effect of the urban heat island on the building energy requirements. To such extent, Taha [1997], Spitz [2012] demonstrated that the non consideration of the local warming induced by the built-up areas results in the over-estimations of the building energy requirements by +30% .

The regional atmospheric models in contrast resolve a set of mathematical equations that depict the physics of the atmosphere to compute the meteorological fields over a coarse domain of thousand kilometers such as the air temperature, the humidity, the wind speed and orientation. The effect of the urban areas are then considered in average in each grid cells of the domain by adapting the surface properties of the natural lands, and in particular by increasing the thermal admittance and the roughness of the built-up areas compared to natural lands. Nevertheless, in the past 20 decades, the increasing computing capacities have spurred the development of sophisticated urban parameterizations that reproduce the three dimensional energetic and dynamic effects of the buildings on the atmosphere (*e.g.* shadowing effect, multi reflection, and so on). They are able, therefore, to reproduce the urban heat island effect. In addition, some of the sophisticated urban parameterizations include simplified building energy models [Kusaka et al., 2001, Kusaka and Kimura, 2004, Salamanca et al., 2010, Krpo, 2009], and shape as a whole a climate modeling system able to dynamically assess the building

energy use considering jointly the complexity of the urban climate, the influence of the urban heat island on the building energy requirements, and the particular features of the urban surface.They therefore held a renewal potential for studying various urban environmental issues [Chen et al., 2011].

As a conclusion, accurate estimations of the building energy requirements are required for guiding the necessary energy transition in urban areas. A particular attention has to be paid for accounting for the urban climate interactions with the building energy requirements. To such extent the newly developed climate modeling systems seem promising tools. More details on the building energy performance methodologies are found in chapter 2.

1.4 Research objectives

The present study aims to develop a methodology able to quantitatively and dynamically assess the building energy performance in terms of building energy requirements over any area and period by considering the complexity of the urban climate that is at the origin of the urban heat island phenomenon, as well as the consequences of the residential development on the local climate and building energy needs.
Relying on the recent advance in the urban atmospheric modeling capacities, the study aims also to investigate the ability of the regional atmospheric models and their sophisticated urban surface parameterizations to provide accurate building energy and climate informations to urban planners and any urban stakeholders. In particular, the question of the sustainable urban form is raises.

1.5 Structure of the thesis

Firstly, a review of the building energy performance assessment methods is presented. We particularly developed the numerical approach that enables considering various possible futures. The basis in atmospheric physical modeling is given meanwhile a

presentation of the atmospheric modeling system is carried on.
Second, we investigate the ability of climate modeling systems to provide urban planning guidelines. For this, we simulate the meteorological fields and building energy requirements of the Eurodistrict region. The climate modeling system that is used includes the WRF/ARW research mesoscale atmospheric model [Skamarock et al., 2008], the BEP three dimensional building effects parameterization [Martilli et al., 2002] and the BEM building energy model [Salamanca et al., 2010]. Particular attentions were given to depict as much as possible realistic study case. We analyze a broad set of fine resolution geospatial databases of the region to assign the physical properties of the surface (*e.g.* land cover type, albedo, heat capacity, and so on) in each atmospheric grid that describe the study area .
Doing so a significant correlation between the simulated building energy requirements for space heating and the daily outdoor temperatures is found. Like in the degree-day method, we proposed to linearly fit the building energy requirements-outdoor temperature function to define two parameters: the base temperature and the cold sensitivity. The first is the interception of the linear fit with the outdoor temperature axis. The second is the slope of the linear fit. Their determination allows us to quickly estimate the building energy requirements for any period knowing the air temperature distributions over the period or at least the annual average air temperature. The linear fit is referred to the statistical model. The study case, the settings of the climate modeling system, and the statistical model are presented in chapter 3.

Then, we propose to use the statistical model to assess the impacts of urban sprawl countermeasures on the building energy requirements (chapters 4 and 5).
Chapter 4 is dedicated to the simulation of contrasted and archetypal urban development scenarios over the Eurodistrict region. Chapter 5 focuses on the impacts of those urban development scenarios on the building energy requirements. The modified version of the american urban growth cellular automata model SLEUTH* [Doukari et al., 2013] is used to simulate the urban development for each scenario meanwhile the MorphoLim and Graphab computing programs [Tannier et al., 2011, Foltête et al., 2012] help to: *i)* constrain the urban development either within the morphological areas or at their vicinity; and *ii)* consider in addition ecological network preservation policies. We demonstrate that the climate modeling system achieves reproducing the changes in the building energy requirements with respect to the simulated built-up patterns. Nevertheless, the changes seem to be mainly due to changes in the building volume to be heated between the urban development scenarios whereas the location of the urban development seems to have no influence on the building energy requirements.

No changes in the urban heat island intensity according to the urban development scenarios are found. It seems that local changes induced by the urban development are too small to be "seen" by the climate modeling system.

At last, we propose a canopy interface model (CIM) to improve the computation of the vertical structure of the wind speed and air temperature in the urban canopy layer. Several studies pointed out that local thermal conditions and air ventilation produce non-negligible effects on the building energy requirements. They stressed in addition that urban parameterizations, although being more and more complex, still do not simulate correctly the near surface temperature and wind speed [Müller, 2007, Salamanca et al., 2011, Kusaka and Kimura, 2004, Britter and Hanna, 2003].
The CIM model computes the vertical wind speed profiles for a high resolution column that is immersed in the canopy layer. It considers explicitly the presence of the obstacles in the largest atmospheric grid through volume and surface porosities. This porosities enable us to reduce the momentum exchange in the canopy layer and consider any obstacle shape. In this first version, obstacles are modeled like parallelograms which dimensions vary with the height in x-and y- directions. Moreover, the CIM model is developed so as to interface any surface fluxes model that could come either from urban parameterizations or from more sophisticate micro-scale models to take benefit from the finest resolution of the latter type of model (meter). The development of the CIM model is presented in chapter 6 of the thesis. We discuss the possible influence of the model on the building energy requirement estimations when implementing in climate modeling system like the WRF/ARW-BEP+BEM.

Chapter 2

Methodologies allowing for the assessment of the building energy requirements

Abstract

This chapter addresses a review of most of the usual methods used for assessing the building energy performance. Several quantitative bottom-up methods have been developed in the past to address energy issues. In the quantitative methods, numerical physically based methods present in particular a certain advantage: they dynamical consider the meteorological conditions over a given spatial elements (a building, a region) and can be used for investigating probable futures (changes in the surface properties, changes in the global climate, and so on). At regional or city scale, *"mesoscale atmospheric model-based"* climate modeling systems seem promising tools to address building energy issues. They include regional atmospheric models that compute the meteorological field over domains of thousand kilometers and sophisticated urban surface representations (or parameterizations) that account for the three dimensional effects of the buildings on the energetics and dynamics of the atmosphere and the building energy requirements. Hence, a particular focus is given in this chapter to the mesoscale atmospheric model-based climate modeling systems. Their basics in physics and their urban parameterizations are described. Nevertheless, due to their coarse resolutions (few kilometers) the mesoscale atmospheric model-based climate modeling systems are, however, limited for operational climate applications. The resolution of the atmospheric grids are too coarse to represent in details realist urban surface conditions that are required at the level of the local developers, and it seems that the definition of the urban entity also suffer from a lack of consensus between the climatologist and the urban planners. It can be problematic even more when several studies showed the sensitivity of the operational guidelines with the urban area delimitations. Recently, new attempts are inventoried in the climatologists, geographers and urban planners communities to transfer climate and energy knowledge in the urban planning instruments. They have been listed in this chapter.

Keywords: *Urban canopy parameterization-mesoscale climate models- building energy performance -urban areas*

2.1 Introduction

This chapter aims to present the actual set of quantitative building energy requirements methods. In particular the numerical physically based mesoscale atmospheric modeling approach is developed. Indeed, new surface parameterizations designed for representing with more accuracy the three-dimensional radiative, aerodynamic and thermal effects of buildings on the thermodynamic of the atmosphere and simplified building energy models that estimate the building energy requirements for space heating or cooling have recently been developed and implemented in regional atmospheric models. Thus, the whole atmospheric scales involves in the urban climate is by now represented in such climate modeling systems. It is then expected to provide new opportunities to assess the building energy efficiency, and to provide climate and building energy guidelines for urban planners in the climate change and energy transition background.
Nevertheless, the transfer of the climate knowledge in the urban planners' community is still harshening by the physical approximations adopted in the mesoscale climate modeling systems. The atmospheric grids are usually ranging from 1 km to 5 km width to consider homogeneous surfaces and average meteorological quantities that enable to simplify the classical mathematical equations used to depict the airflow dynamics and energetics. Basically, it leads to neglect the sub-grid advective effects due to the surface heterogeneity. The sub-grid heterogeneity is, however, represented by computing separately the heat, moisture and momentum that are exchanged between the surface and the atmosphere (the surface fluxes) for each types of land cover included in the atmospheric grids, and by considering latter an average of all of them accounting for the coverage of each type of land cover. Although this approach (tile approach) is recognized to produce accurate meteorological field, it is far to represent realistic surface conditions, especially the urban heterogeneity observed at the neighborhood scale and at the level of the urban planners. More the surface conditions are recognized to be crucial for representing accurate local climate and hence, building energy requirements. Therefore, more and more studies try to improve the representation of the surface in the climate modeling systems by using high resolution surface datasets. The latter are then expected to bridge the gap between the level of accuracy required by the urban planners and the coarse resolution of the climate modeling systems. In this chapter, we firstly present the atmospheric scales and inherent physical mechanisms that influence the urban climate, and hence, the building energy requirements. Then, the different methods used for assessing the building energy performance in the urban planners and climatologist communities are addressed. In particular, numerical physically-based climate models and their underlying physics are developed. A focus is

given on the mesoscale climate models, and their surface parameterizations. At last, a review of the existing attempts for providing operational climate guidance at the level of the urban planners is proposed.

2.2 The climate scales and the existing building energy performance assessment methodologies

2.2.1 Modeling the building energy requirements: a multi-scale problem

2.2.1.1 The horizontal scales

The building energy demand is closely linked with the surrounding building microclimate. The latter results from physical processes of length and time scales ranging from global to local scales and from years to less than one hour. Figure 2.1 shows the time and length scale related to the building energy requirement. Governing factors are outlined for each scale.

The climate at a given site is first influenced by the atmospheric circulations occurring **at global scale (A)** and the succession of weather conditions. The global atmospheric circulation is first driven by the difference all around the Globe in the solar irradiance, *i.e. the part of the solar radiations that reaches the ground.* The solar irradiance may vary with time according to long quasi-periodic astronomic cycles, the Milankovitch cycles (*e.g.* 100,000 years, 40,000years and 20,000 years), that influence the elliptic courses of the Earth around the sun as well as the distance between the Earth and the sun, and according to shorter periods of 11 years during when the intensity of the solar activity may change. Other climate system forcings are the atmospheric concentration in greenhouse gases (like the carbon dioxide CO_2 and the water vapor H_2O) and the changes in the surface properties due to changes of the global land cover. Indeed surfaces may absorb, emit and transmit radiative energy according to various patterns. Ice cover may absorb only a little fraction (10%) of the incident solar radiative energy, while the forested areas and water bodies may absorb quasi the total-

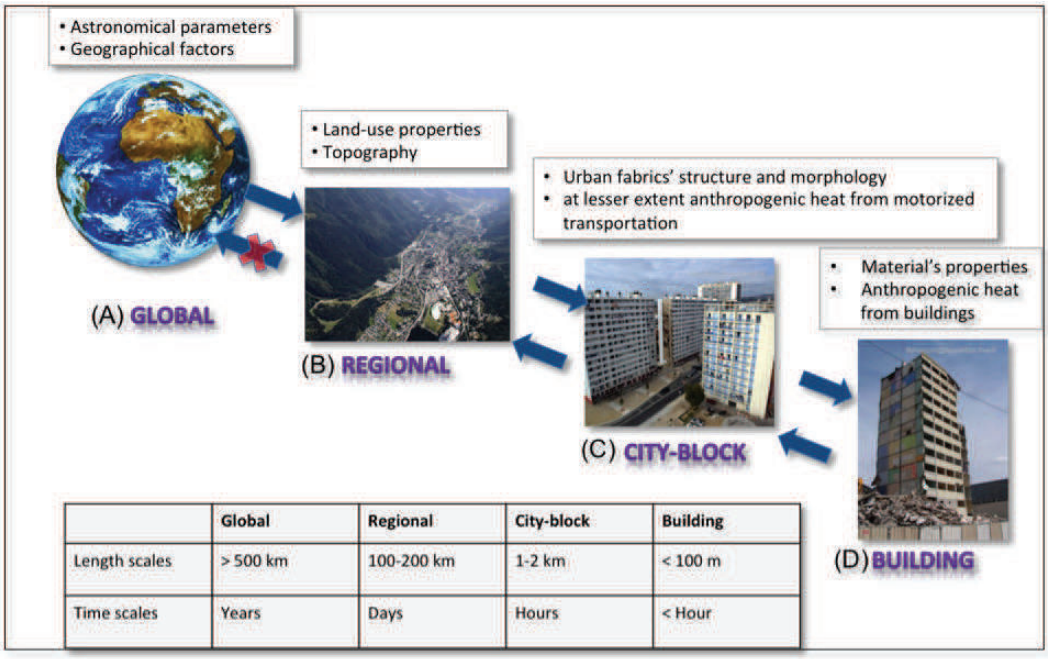

	Global	Regional	City-block	Building
Length scales	> 500 km	100-200 km	1-2 km	< 100 m
Time scales	Years	Days	Hours	< Hour

Figure 2.1: Representation of the horizontal spatial scales involved in determining the building energy requirement (adapted from Mauree [2014]).

ity of the incident solar energy. Changes in the land covers may, hence, alter the global temperature and the atmospheric circulation. Mahmood et al. [2013] indeed reported that land cover changes influence as much the extreme temperatures as a doubling in the CO_2 atmospheric concentration. At last, episodical volcanic eruptions by emitting particles and water vapor in the upper atmosphere may cause annual global cooling by directly scattering the sunlight and serving as condensation nuclei for clouds [Zhang et al., 2013].

At **regional scale** (or mesoscale, **(B)**) the heterogeneous mosaic of land-covers offers contrasting thermal responses to the radiative forcing because of their different properties and energy balances. At this scale, urban areas represent warmer (cooler) and rougher spots in humid (arid) areas compare to its surroundings [Rothach, 1999, Mahmood et al., 2013]. The presence of such surfaces directly modifies the vertical structure of the planetary boundary layer, *i.e. the part of the troposphere that is influenced by the surface in timescale of about one hour or less.* Fully-developed daily turbulent convective and warm boundary layers over urban areas are often reported during clear sky and calm wind weather conditions. This effect is known as the Urban Heat Island (UHI). Advection effects such as evaporating cooling and fetch effects that depict modifications of climate phenomena with changes in the land covers along the

transition area are of particular interest. Hence, the differential in warming between urban and rural areas may produce countryside breezes from rural to urban areas while the differential in air moisture may trigger under calm wind, precipitations downwind to the urban areas. To such extent, Unger [1999] described an excess of humidity at night and in winter over urban areas due to the release of water vapor and combustion particles by the anthropogenic activities that can serve as condensation nuclei. At night, stable atmospheric conditions may retain this humid air mass in the nocturnal urban boundary layer while the dewfall reduce the air moisture availability in rural areas. With the sunrise the faster air mass convection in urban areas may push the humid urban air mass downwind to the urban area producing a saturation in water vapor of the rural air mass (increase air moisture due to sunrise evaporative dewfall and evapotranspiration, advection of urban moisture, lower temperature and dew-point temperature compared to urban areas) and originate frequent precipitation episodes. In the same way, Bornstein and Lin [2000]observed in summer a maximum cumulus convective clouds activities and more frequent precipitation episode downwind to the Atlanta urban areas due to the enormous production of hygroscopic condensation nuclei, water vapor and heat by human activities.
At last, the topography induces local radiative variations and specific winds patterns across the slopes of the rough elements. Wind sheltering effects, anabatic and katabatic winds across the slope of a valley, gravity waves damping and secondary turbulent circulations as well, are some often inventoried topographical effects.

By downscaling at **city block scale (C)**, the myriad of surfaces have unique combination of intrinsic properties and spatial configuration that originate complex turbulent structures and thermal zones [Roth, 2000]. City-blocks form uniform morphological units composed by regular pattern of buildings and infrastructure networks [Long, 2003]. Its surfaces due to their specific properties could be wet or dry, shaded or sunlit inducing local differentials in cooling and heating that nourish in addition local advections of heat, mass and moisture plumes.

At last, processes occurring at **building scales (D)** directly affect the human living conditions. Usually the morphological unit is the street-canyon. It is composed by a street and its adjacent building. The presence of one or more obstacle induces secondary turbulent recirculation flows across the individual rough elements and wind deflections at the windward side of the obstacles. The turbulent recirculation structures reduce the momentum and energy exchanges between the street and the above lying atmosphere. In particular Baik and Kim [2003] found interfering turbulent struc-

tures and disconnections of the street flow with the above lying flow with dense urban fabrics. In addition with dense urban fabrics the absorption of the solar radiation in the street-canyon is attenuated meanwhile the longwave radiations emitted by the facets of the street-canyon are trapped in the canyon. Then, the orientation of the building facets and the radiative and thermal properties of the construction materials influence the interactions between the building envelop and the atmosphere. In particular, construction materials are characterized by higher thermal admittance and hence have a stronger thermal inertia than vegetative areas. It is then common to observe over urban area a slower nocturnal cooling compared to the rural countryside cooling leading to a difference in the air temperatures between the urban and rural areas. Note that the differences in the air temperatures are the highest few hours after sunset. Because buildings home also economical and residential activities, additional wasted anthropogenic heat and moisture may be ejected in the atmosphere. It could raise the air temperature up to +2°C [Sailor, 2011] in particular in high latitudes and winter when the contribution of the solar radiation in the surface energy budget is low. The anthropogenic heat alters in turn the space heating and cooling energy requirements.

2.2.1.2 The vertical scales

Commonly the atmosphere is divided into several layers characterized by contrasting vertical thermal gradient. The troposphere is the lower ones and reaches up to 7 km at poles and 17 km at equator [Seinfeld and Pandis, 2012]. The lower part of the troposphere that is directly influenced by the surface is the Planetary Boundary Layer (PBL). It is divided in:
i) the mixing layer (ML) that is highly turbulent during day. The ML grows during the day because surfaces continuously warm up and generate convective motions, and also by the entrainment of the upper air parcels from the transition zone or capping inversion zone;
*ii)*the surface layer (SL) only represents 10% of the PBL but is of particular concerns as the phenomena that occur there directly impact the human living conditions. Its elevation is referred below as z_i. Figure 2.2 sketches the vertical structure of the SL.

The surface layer (SL) is by convention divided into the urban canopy layer (UCL), which extents from the ground up to the average height H of the obstacles, the roughness sublayer (RSL), which extents from the ground up to z^*, with $z^* \approx$ 1.5H- 3H, and the inertial sublayer (ISL), which extends from z^* to the ISL top. Oke [1988]

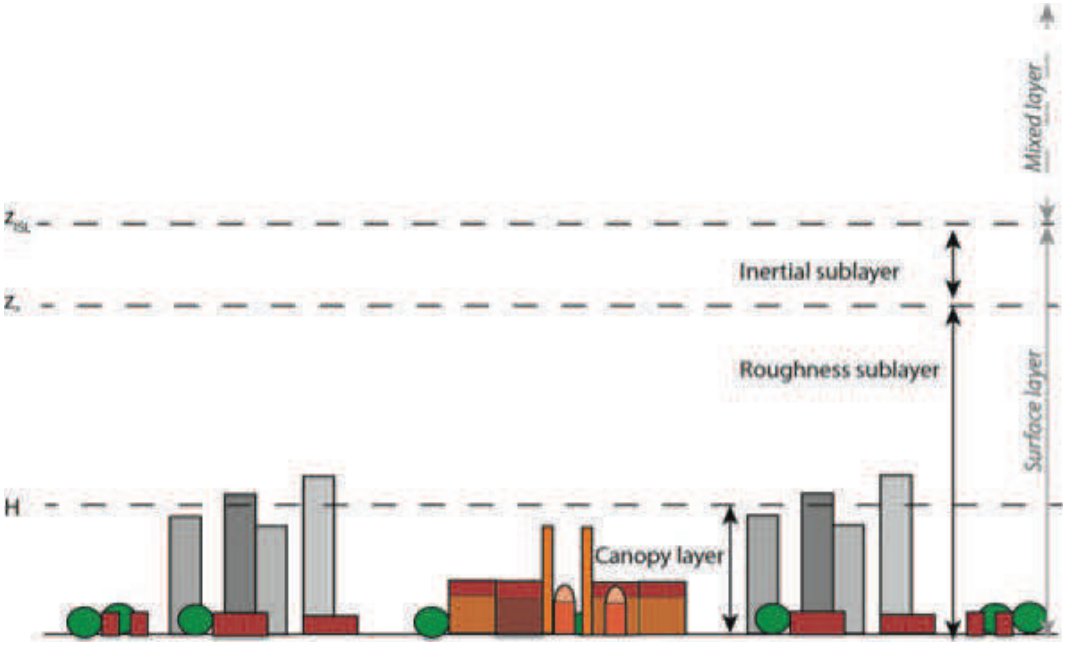

Figure 2.2: Vertical structure of the surface layer (after Rotach [1993])

assumed that the ISL top is equal to be $z_{ISL} = 0.1z_i$. The typical features of each of this atmospheric layers included in the SL are given in table 2.1.

Layers	Features
the UCL	-Surface forcings: drag forces, up-take of radiative energy, surface exchanges of heat and moisture with the atmosphere, attenuation of the solar radiation absorption (shading effects), longwave radiations multi-reflections (trapping effects), emission of anthropogenic heat and so on. -Morphological site's characteristics dependence of the flow dynamic and thermodynamics that induce complex dynamical processes (airflow ducting and trapping) [Collier, 2006a].
the RSL	- Non-permanent and horizontal inhomogeneous turbulent flows that are influenced by length scales associated with the individual roughness elements and heat and moisture local-scales advections [Roth, 2000].
the ISL	- Homogeneous horizontal turbulent flows those are quasi-constant with height [Rothach, 1999, Collier, 2006a]. - Semi-logarithmic vertical profiles of meteorological variables

Table 2.1: Description of the vertical structure of the surface layer. UCL=Urban canopy layer; RSL=roughness sub-layer, ISL=inertial sub-layer

2.2.1.3 Scales interactions

Even though, the interactions of the whole scales is at the origin of the well known mesoscale urban heat island effect, *i.e. a differential in the surface heating and cooling between the urban and the nearby humid areas*, it is commonly accepted that the local climate does not have direct and significant influences on the global climate. The urban areas represents only about 2% of the global land area and the urbanization does not produce intense land cover changes that are able to affect the climate of remote regions [Parker, 2006]. Therefore at global scale, the impact of the land cover changes in the climate are limited to the changes in the vegetative covers due to reforestations, afforestations and expansions of irrigated agriculture [Mahmood et al., 2013]. The influence of the urban areas on the global climate has been then limited to their contribution in increasing the anthropogenic greenhouse gas emissions. Recent studies like Zhang et al. [2013], however, suggested that the energy consumption of the urban areas can disturb on a relative short time the global atmospheric circulation. Note that the energy consumption intensities (*i.e.* energy consumption per atmospheric grid areas) are directly incorporating in the physical equations of the lowest layer (Δz=130 m)

of the National Center for Atmospheric Research (NCAR) Community Atmosphere model (CAM3) as a time invariant heat source. It could therefore over-estimate the impact of the heat release due to the human activities on the global climate.

2.2.2 The building energy requirement quantitative methods

Recently energy quantitative approaches that rely on the construction of quantifiable building Energy Performance indicators (EPIs) such as building energy use intensity (EUI in kWh/m^2), have received more recognition in helping local authorities to implement more sustainable energy policies [Jones et al., 2007]. The EPIs can be determined by measurements-based, calculation-based or any hybrid approaches [Wang et al., 2012]. Although in the following sub-sections the whole methods will be introduce, degree day and numerical physically-based modeling methods will be more specifically developed. The first one is a fast and simple method used to estimate building energy consumption over any region of interest while the second has the advantage to consider the complexity of the urban climate system, and in particular the feedback of the urban heat island intensity on the building energy consumption.

2.2.2.1 Measurement based techniques

In-situ energy use monitoring, disaggregation of building energy consumption from energy bills, and analysis of building thermal images are measurement-based techniques that could only be applied to existing building.

- **In situ monitoring**

  End-use sub-metering is an intrusive method for investigating the building energy performance. Usually real instantaneous energy consumptions are measured periodically over period of 15 or 20 years so as to depict various patterns of energy loads. The energy consumptions can be given in litter for gas and oil, in Watt hour (Wh) for electricity for each end-use as in Asdrubali et al. [2013]. One of the advantage of the method is that energy data when reading are instantaneously accessible compared to utility bill that are given few days or weeks after

the reading of the energy meters. Because the Heat Ventilation and Air Conditioning system, the light and other appliances are often installed in the same electrical circuit, sub-metering can be difficult to install and a disaggregation of the electricity consumption could be necessary for analyzing specific end-uses. Limitations of the method arise as real consumptions are only periodically monitored and therefore involved the implications of occupants and building managers to complete the energy consumption time series over the entire year. In the other hand, the method is often applied on few sample of buildings that are assumed to be representative of a given segment of the building stock. Asdrubali et al. [2013] for instance chose 9 buildings and sample flats in each of them that share similar floor area and number of occupants to carry on the in-situ monitoring. However, the energy consumption may not only change with the number of occupants but also with the structure of the household (*e.g.* age, median income). More than assessing the building energy performance or consumption alone, the method seems to measure also the social dimension of the energy consumption and the penetration of energy conservation policies like in Abrahamse [2005]. The interpolation of the results of the monitoring campaign for the whole urban areas should be then be done cautiously.

- **Remote and non-intrusive measurement methods**

  - *Disaggregation of energy bills*

    The utility bills are delivered by every companies of energy suppliers. The utility bills provide a large set of informations. They usually indicate the interval between readings, the corresponding number of days, the total energy consumption, the cost, the maximum electrical demand measured during that interval. By using such informations it is possible to derive the energy use intensity in kWh/yr/m^2, in energy cost \$/yr/m^2 or, the load factor (*i.e.* the ratio of the total energy consumption on the maximum peak energy demand) that indicates how steady an electrical load is over time. Thus, by analyzing such a document it is possible to depict the patterns of energy use in buildings. It can show how the heating load is spread over the year, how the consumption has changed relative to a same period of previous years due to the arrival of a new occupants, the installation of new boilers, appliances or new insulation systems.

The energy disaggregation on its own refers to the method that breaks down the whole building energy consumption into appliance level itemized bills (or into end-uses) and time-of-use. The disaggregation relies on autoregressive analysis. The use of the energy bills is, however, limited as monthly utility bills are too coarse to provide time-use energy and a disaggregation into hourly energy consumption data is pre-requested for studying the daily profile of energy loads. More, the survey is usually carried over few buildings (7-10 buildings) and cannot be easily extended at city scale.

– *Thermal images*

Thermal images represent the spatial mapping of the thermal infra-red radiations emitted by the buildings and streets facets. The radiant energy emitted by the surface is indeed captured by a camera placed on an aircraft (300 m elevation) during expensive campaign or taken from the ground. The principle relies on the association of a color scale with a correspondent thermal energy level. Thermal images are often used to provide a rapid overview of the building energy performance in terms of building energy losses of a given areas and help identifying defaults in the construction of the buildings FLIR services [2011]. To such extent APUR [2011] performed 505 thermographs of sampled buildings that are classified according to their date of construction to provide an overview of the energy performance of the building stock of Paris in 2009.
It should be however stressed that the monitored radiant energies that are emitted by the surfaces are integrated energy signals that combines different sources of energy. The energy stored in the construction of the materials during a diurnal cycle, the radiant solar energy reflected by the surface during the day, the internal heat gains due to the human activities are as much sources of energy that are then monitored. It is then difficult to address one specific energy end-uses.
More, the method suffers from the weather conditions and the resulting energy signal is corrected from the climate conditions. The presence of water droplets, greenhouse gases and particles may absorb a part of the emitted infrared thermal radiations while the energy losses through humid surfaces may be under-estimated due to their lower skin temperatures. In addition, contrasts in thermal inertia of the buildings cause interpretation errors of the signal because the thermal balance is not achieve at the same time for

all the buildings. At last, it should be stressed that thermal images taken from the ground for characterizing an entire building stock may suffer from the sampling techniques, while the thermal images taken from an aircraft over-estimate the contributions of the roofs compared to walls and integrate in addition the radiative response of the streets.

2.2.2.2 Statistical techniques

- **Statistical multivariate analysis**

Statistical multivariate analysis is often employed when evaluating and mapping the building energy consumption over extended areas. The *energy cadastre* proceeds of such a method. It relies on a bottom-up approach in which the EUIs of prototype buildings owning to a particular segment of the building stock are statistically interpolated over a given area knowing the share of this particular segment in the total building stock [ANAH, 2008, CUS, 2008, ASPA, 2012].
The segmentation of the building stock is determined according to building physical descriptors that permit assumptions on the building energy performance. For instance, the building age seems to be well correlated with the building insulation performance and types of fuel as demonstrated by CUS [2008]. The air quality association of Strasbourg (France), called ASPA, also used such technique to map the 2010 estimated building energy consumption [ASPA, 2012]. The ASPA took advantage of the well-described INSEE dwelling database in which figure the age of the construction, the nature of the building (*e.g.* single or multifamily) the type of fuel, the number of occupants, the number of rooms, the surface of the floors and so on and that is available for several urban planning scales (*e.g.* municipalities, county). In parallel, they used the energy consumptions of prototype buildings (unitary coefficients for a given end-use) provided by the CEREN (Centre d'Etude et de Recherche Economique sur l'éNergie) that details the end-uses and fuel types. For the space heating, the unitary coefficient results from the survey of a panel of 3,500 households characterized according to the type of the lodgment, the type of heating system and the type of the fuel. Note that the energy consumption is corrected from the climate variations.
Thus a broad set of data is required when using such method. It present the advantage to relies on datasets that are directly at the disposal of the urban planners' services. It allows to account dynamically for the influence of the ur-

ban growth on the building energy consumptions as showed by Viejo-Garcia and Keim [2008] in their "Stuttgart 2030" case study, but it neglects the influence of the climate on the energy consumption: the dynamic of the weather conditions is then often reconstructed by using a climate severity index to weight the building energy consumptions. The latter relies most of the time on the well-known degree day method.

- **The Degree day methods**

The degree-day method is a simple and fairly reliable procedure for assessing dynamically the building energy demand for cooling (CDD) or heating (HDD) when internal temperature, thermal gains (*e.g.* occupant and equipment wasted heat, solar energy) and building properties are relatively constant over time. The method relies on the strong empirical linkage found by previous empirical studies between the air temperatures and the heating or cooling energy consumptions that are provided by energy companies or energy institutions and documented since the 1950's [Thom, 1954]. Such a relationship exhibits a non-linear form over a year. In winter the building energy consumptions decrease with the air temperature rise. In summer the building energy consumptions increase with the air temperature rise. A temperature threshold that rather shapes a plateau is found In between the winter and summer trends. It represents the building energy uses that are non-sensitive with climate variations and mainly due to the use of light, hot sanitary water, or cooking devices.

Although the function is non-linear, several studies proposed to consider separately the winter and the summer branches and to model each of the branche by a linear fitting as sketched in figure 2.4 [Quayle and Diaz, 1980, Valor et al., 2001]. The resulting slope P represents the sensitivity of the building with cold or warm temperatures (in Wh/°C) while the interception of the linear fits with the air temperature axis defines the base temperature (or balance point) temperature T_0. It is the temperature at which there is no more needs of energy, or thetemperature at which the internal and solar energy gains offset the building energy losses through its envelop.

From such relationship one can define the degree-day which mathematical formulation is given in equation2.1. The degree-day is a proxy-measure of the heating or cooling energy requirement considering the relationship between the building

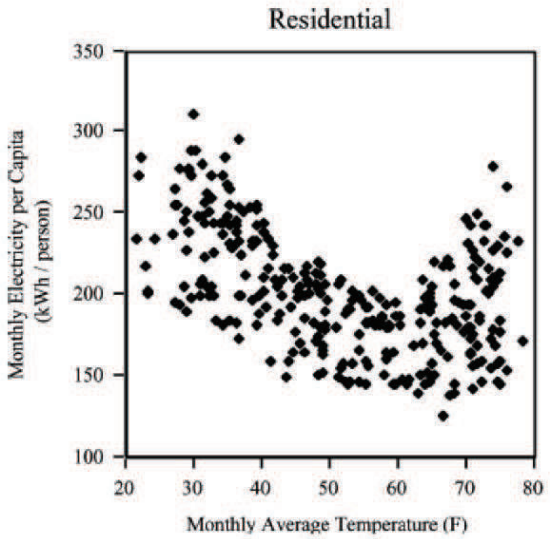

Figure 2.3: The non-linear relationship between the residential monthly electricity consumption and the monthly average temperature found by Amato et al. [2005] across Massachusetts between 1977 and 2001

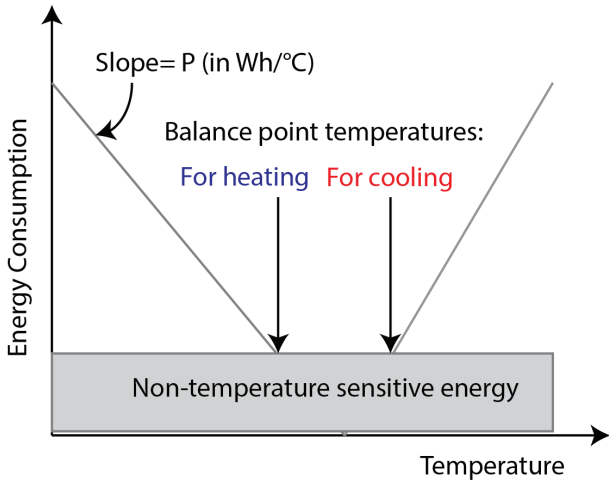

Figure 2.4: Theoretical relationship between energy consumption and air temperatures (adapted from Amato et al. [2005])

energy requirements and the thermal loads between the building and its surrounding. Thermal loads are the temperature differences between the base temperature (or balance point temperature) T_0, and the outdoor temperature T_i that could be computed like in equations 2.2 or 2.3.

The energy requirements Q_J over a period Δt are then calculated by using the time integration over the time period Δt of the distributions of the thermal loads when the outdoor temperature are below (for space heating) or above (for space

cooling) the base temperatures, and by considering the sensitivity of the building energy requirement with the temperature rise P like in equation 2.4. Usually, the integrating time step δt is taken to be 1 hour. Actually, several definitions of degree-days co-exist in the literature. Christenson et al. [2006] computed the thermal load as the difference between the base temperature taken at 20°C and the outdoor temperatures and integrated the latter difference when the outdoor temperature is below the chosen base temperature T_0. Cartalis et al. [2001] considered in addition the efficiency of the heating system by using the coefficient of performance of the heat pump system (COP).

$$D = \sum_{i=1}^{\Delta t} min(T_i - T_0; 0) \tag{2.1}$$

$$T_i = \frac{1}{24} \sum_{j=1}^{24} T_j \tag{2.2}$$

$$T_i = \frac{(T_{j,max} - T_{j,min})}{2} \tag{2.3}$$

$$Q_J = \sum_{i=1}^{\Delta t} Q_i = P \sum_{i=1}^{\Delta t} min(T_i - T_0; 0)\delta t \tag{2.4}$$

Where the base temperature could be defined as:

$$T_0 = T_{room} - \frac{\Delta g}{P} \tag{2.5}$$

With D the degree-day, ΔT the period of investigation, δt the period of integration in hours, T_i the daily averaged outdoor temperatures, T_j the hourly temperature, $T_{j,max}$ the maximum hourly temperature of the day i, $T_{j,min}$ the minimum hourly temperature of the day i.T_0 is the base temperature, T_{room} the room set point temperature and Δg the passive energy gains from solar radiations and internal heat gains (equipment and human metabolism). P is the sensitivity of the building energy conditions to the outdoor temperatures, and at last Q_i is the building energy requirements in Watt hours (Wh).

The base temperature is often set predefined. The American Society of Heating, Refrigerating and Air Conditioning Engineers (ASHRAE) standard recommends

the use of base temperatures set equal to 10°C and 18.3°C (65°F) for heating and cooling respectively. Christenson et al. [2006] chose base temperatures set equal to 8°C, 10°C and 12°C that correspond better to the Switzerland building standards. Indeed the base temperature T_0 depends on the room thermostat set point temperature T_{room} and the passive energy gains Δg that can come from the penetration of longwave and shortwave radiations from outdoor, equipment and occupant wasted heat, and walls heat storage.

The outdoor temperatures are often taken from fix observational meteorological networks that provide long temperature time series. For this, the airport meteorological stations is often used. Several studies have however showed that the use of synoptic stations instead of local weather stations cause discrepancies in the estimations of the building energy use. Hence, the heating degree days reported by Taha [1997] over the 1993-2006 periods by using successively observational stations located in the urban core and at the airport for several US cities show an average relative difference of about +12% that could be up to +46% for Los Angeles meaning that the energy use will be over-estimated when considering the airport temperatures. The use of airport data series is often justified as the urban meteorological field campaigns are often intensive and concentrated on one year (*e.g.* BUBBLE in Basel (Switzerland) and CAPITOUL in Toulouse (France)) or less over summer periods (*e.g.* ESCOMTE in Fos-Marseille (France), DESIREX in Madrid (Spain)).

So as to bend this drawback, recent studies have investigated the benefits of using outputs from numerical meteorological models to reproduce the distribution of the degree-day over an entire year. For instance, the ASPA [ASPA, 2012] used daily air temperatures issued from the 3 km-urban grids of the AtmoRhena regional model and a base temperature set equal to 17°C to build according to equation 2.1 a climate severity index.

2.2.2.3 Methodology using numerical physically-based models

As cheaper and faster technique, numerical physically-based building energy models are of regain interest with climate change as it allows predicting future meteorological conditions and forthcoming stresses on human thermal comfort and building energy use. On the contrary to the heating or cooling degree day method, the whole meteo-

rological field is explicitly addressed.

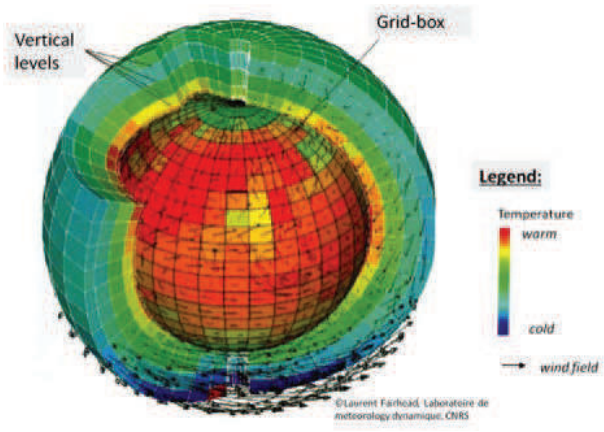

Figure 2.5: Sketch of the grid of a global numerical climate model (La météorologie 2000).

Indeed meteorological numerical models forecast the wind velocity, the temperature, the mass and the moistures field over a domain of interest Ω that is discretized into elementary volume, the grid-boxes (Figure 2.5). The evolution of the meteorological variables are obtained by solving mathematical partial differential equations (PDEs) that depict the non-linear behavior of a flowing air parcel (*i.e.* a volume of air bounded by walls taken small enough with respect to the variation of the physical properties and not too big to allow a clear identification of this air volume within the atmospheric fluid). The space and time resolutions of the numerical climate model are forced by the particular time and length scales associated with the studied phenomenon and the aims of the model. It could be used for operational meteorological forecasting, climate change impacts assessment, air pollutant dispersion studies, and so on. As a result a broad set of numerical physically-based meteorological models exists.

- **Global climate models (GCM)**

  GCM models aim to forecast the global circulation at spatial resolutions of about 1° ($\simeq$100 km) to 5° ($\simeq$ 500 km) in latitude or longitude and time scale ranging from day to multi-century. Table 2.2 lists the current spatial resolutions adopted in the GCM models in latitude and longitude respectively. Altough many of them have already supported the IPCC's 21^{st} century projections on climate change, their coarse resolution prevents the simulation of the detailed flow field around

GCM models	Spatial resolution	References
NOAA's GFDL	2° and 2.5°	Delworth et al. [2003]
Hadley Centre's HadCM3	2.5° and 3.75°	Gordon et al. [2000]
NCEP's GFS	28 km to 70 km (according to the simulation length)	Environmental Modelling Centre [2003]
LMD's LMDZ4	2.5° and 3.7°	Houdin et al. [2006]

Table 2.2: Examples of GCM models and their spatial resolution.

buildings. Cities are besides often not represented as they represent a tiny fraction of the land-uses included in the grid-boxes. If there are, they are regards as a fraction of bare soil whose physical surface parameters (*e.g.* the heat capacity, the roughness, the albedo, the soil water content) are chosen to be adapted for cities. As a consequence, their influence on the atmosphere due to the resolution of the climate model is likely to be smaller than in reality [Best, 2005].

Nevertheless, improvements in the accuracy of the Earth land-cover-mapping by using high resolved satellite images [Friedl et al., 2002] and computational capacity have already allowed implementing advanced urban canopy parameterizations.

The Met Office Surface Exchange Scheme (MOSES) considers urban areas as an impervious warmer and rougher slabs composed of roofs and street-canyons whose physical parameters (*e.g.* the albedo, roughness and heat capacity) are walls and canyon floors averaged parameters [Best et al., 2006]. Although this surface scheme reproduces the capacitive effect of cities and roughness, it does not fairly reproduce the three-dimensional effects of the buildings on the wind, and the three-dimensional radiative and energy exchanges as well. Furthermore, MOSES does not include a building energy model to compute the building energy requirement. Several studies have, however, demonstrated the influence of anthropogenic heat on urban climate in particular during winter when the solar contribution in the surface energy budget is low [Kylski, 1996, Taha, 1997, Ichinose et al., 1999]. In particular Taha [1997] reported that the release of the anthropogenic heat in the atmosphere increases the air temperatures by about 2-3°C.

In a more complex parameterization, Oleson et al. [2008a] specified the urban areas with the help of three urban fabrics of increasing building density whose

typical canyon is supposed to be infinite long and form by a wall, a roof and a canyon floor that could be pervious or impervious. Shading, multiple radiation reflections and building drag effects due to the obstacle geometry are considered as well as canyon surfaces' separated energy budgets to compute a canyon specific air temperature and moisture. Anthropogenic heat from traffic and air conditioning are also modeled by imposing for the latter a room temperature comfort range and solving a specific room energy budget. Results indicate that the canopy parameterization qualitatively fairly reproduces the urban heat island features [Oleson et al., 2008b].

In conclusion, GCM have the capacity to consider long time scale and dynamical global climate changes. The entire Greece may cover 2 grid-boxes according to Giannakopoulos and Psiloglou [2006]. To date their low spatial resolutions, prevent the description in details of the urban areas and surface processes, but the implementation of much more sophisticated urban canopy parameterizations seems promising to address the climate feedbacks of the urban areas on the global climate.

- **Building energy micro-scale models (BEM)**

In contrast, micro-scale physically-based models that are often used to assess building energy efficiency and energy savings policies basically work at building scale by using grid boxes of few decametres and time scale of one hour.[Simpson and McPherson, 1998, Akbari et al., 2001]. Due to their fine resolutions, realistic buildings and surroundings site's characteristics are considered in the BEM models.
For instance, the windows and glazing systems include the description of the windows size and orientations, the glass radiative properties, and sun-control devices characteristics as well. The hourly sun positions, the sky cloud covers, as well as the shading of the exterior shading surfaces are other example of the surrounding details considered in the BEM simulations. As a consequence, BEM models constitutes a suitable tool for city planners and architects.
In the BEM models, the buildings are composed by thermally homogeneous spaces. The indoor temperatures are calculated by accounting for the thermal dynamic of the building envelop according to the outside weather conditions, the thermal dynamic of the building mass, the time varying building internal activity and heat gains, and the unintentional ventilation. The resulting thermal

loads, the differences in temperatures between the indoor and the outdoor of the building, are then used to compute the whole building energy demand. The more sophisticated BEM models such as EnergyPlus and DOE-2 of Birdsall et al. [1990] and Crawley et al. [2000] respectively consider in addition the dynamics of the activation of the Heat Ventilation and Air Conditioning (HVAC) system, its characteristics and its fuel requirements given the efficiency of the plant equipment.

While the fine resolution of BEM models allows simulating accurate building energy demands, the large amount of user-inputs for describing the building features and the miss-evaluation of the variations of the local climate limit their usages. Indeed the weather conditions are given by Typical Meteorological Year files (TMY). The TMY files issued from the averaging over 30 years of hourly meteorological observations that are considered to represent typical weather conditions of the study area. As a result, long meteorological campaigns are required to build suitable and statistical robust TMY files. Long time series are often documented by the fix-meteorological stations that are most of the time located out of the urban core. To such extent, Spitz [2012] estimated that the use of TMY files without considering the local climate and the heat island caused by the urban impervious areas leads to over-estimate the energy demand by up to +30%. A fortiori this scholars noticed that the averaging procedure smoothens the daily weather perturbations and hence, miss-evaluates the peak energy demand.

Therefore and during the last thirty years, several investigations have been carried out to improve the considerations of weather conditions in the BEM models. Some studies investigated the advantage of using CFD models (*i.e.* Computational Fluid Dynamics) like FLUENT or TRNSYS that resolve the whole length scales of the turbulent flows generated by the presence of an obstacle as in Bouyer et al. [2011], while others devised statistical downscaling approaches in which the outputs of the global atmospheric models are statistically interpolating to build station-scale meteorological TMY time series like in Loverland and Brown [1989], Richardson et al. [2013] and in Xu et al. [2009]. The fundamental assumption is then that consistent and stable empirical relationships between large scales and local processes can be established over an historical period and extended over years [Willby et al., 1998]. The latter assumption seems compromising with fast urban growth. Other approaches consist in dynamically downscaling the outputs of the global climate models by using intermediate climate models. Taha [1997]

for example used the outputs of the urban boundary layer model of [Bornstein, 1975] URBMET to dynamically downscale the global climate fields at the local levels. Other scholars preferred using mesoscale atmospheric models, which resolutions range between 1 km and 5 km, and which include a fortiori since the past 20 years sophisticated urban canopy parameterizations able to reproduce the urban heat island found at the building, neighborhood and city scales.

- **The mesoscale atmospheric model (MM)**

Conventionally, mesoscale atmospheric models are designed to provide a throughout knowledge on the climate at a regional scale, and in particular they investigate the energetic and dynamic processes that occur in the atmospheric boundary layer [Arnfield, 2003]. They account from the alteration of the atmospheric circulation due to the orography and the presence of built-up and non built-up areas. They usually consider study area (domain) of thousand kilometers and taken height enough in the vertical to account for the air ventilation of the urban areas by the countryside breezes induced by the contrasted urban-rural surface energy budgets, and the daily variations of the planetary boundary layer height. The domain is also taken not too much large for considering the changes in the shearing stress, the buoyancy intensity, and the contrasting surface energy budgets included by the mosaic of land covers at regional scale. Therefore, classical horizontal and time resolutions fall between 100 km to 1 km, and from 1 hour to a day. Hence, several studies showed that mesoscale atmospheric models due to their intermediate resolutions achieve to reproduce the dynamic of the urban heat island and the slow nocturnal cooling that occur above urban areas.

However, the increasing interests in the global warming and its impacts on the urban climate and the building cooling and heating energy requirements triggered new applications.
Some studies then, used mesoscale atmospheric models and their urban canopy parameterizations to dynamically down-scaling the meteorological outputs of the GCM models to study the interactions between the urban climate and the building energy requirements in the context of climate change. Seljom et al. [2011] for instance used a numerical climate modeling system consisting in the coupling of the Hadley Global Climate Model, the regional HIRHAM model and the building energy SolDat model from the UiO Norway meteorological Office. Hinkel et al. [2012] used the Colorado state University mesoscale model CSU-

MM to obtain the spatial and temporal distribution of the air temperatures over the Tokyo metropolitan area meanwhile the energy consumptions of commercial and residential buildings are deducted from empirical statistical models that link the energy consumptions and the air temperatures. Pigeon et al. [2014] proceeded with the same philosophy. These scholars coupled the Town Energy Budget urban canopy parameterization (TEB) of Masson [2000] with the simplified building energy model BEM of Bueno et al. [2011] to evaluate the cooling and heating building energy requirements considering successively the climate of Paris and Cordoba to simulate the effect of the global warming over the Paris urban region. The authors successively showed that the building energy simulations are particularly sensitive to the air infiltration and natural ventilation, and that the use of such type of climate modeling systems can provide more accurate building surroundings' climate conditions than traditional approach.

In parallel, other studies investigated the influence of the additional release of anthropogenic heat and water vapor due to human activities on the air temperatures and the formation of hydrometeors (*e.g.* clouds, liquid and solid precipitations). For this, the studies usually adopted encapsulated domains, which resolutions is successively increased, and which domains are two-way nested. In the two-ways nesting approach, the meteorological boundary conditions of the domains are inherited from the coarser domains (parent domains) meanwhile the finest domain provide the surface fluxes (the source) to its parent domain.
As an example and by adopting a two-way nesting approach, Kikegawa et al. [2003] proposed the use of a climate modeling system to assess the sensitivity of the cooling peak electricity demands with the air temperatures for a central business district of the great Tokyo. The system consists in coupling a mesoscale atmospheric model with a one-dimensional urban canopy model and a building energy analysis model. Doing so, they demonstrated that the use of more sophisticated urban canopy parameterizations improves the accuracy of the meteorological and indoor thermal condition simulations used to calculate the building energy requirements. They also found that the cutting-off of the air conditioning system may save up to +6% of the cooling energy. Salamanca et al. [2011] and Martilli [2014] by following such an approach used the urban canopy model BEP of Martilli et al. [2002], the box-type building energy model BEM of Salamanca et al. [2010], and the WRF/ARW mesoscale atmospheric model [Skamarock et al., 2008]. In particular Salamanca et al. [2011] determined the optimum degree of complexity that should be adopted in the urban canopy parameterizations and

evaluated some building energy conservation strategies. Their study that have been carried out over Houston demonstrated that the building energy and the meteorological simulations are considerably improved when using much more detailed informations on the urban morphology. They found that the use of more sophisticated urban parameterizations improves the simulations of the 2 m air temperatures. They also stressed that the use of such sophisticated urban parameterizations by considering the local climate and the urban heat island may produce differences in the building energy requirements by factor 1.7 and 2.2 compared to classical statistical bottom-up approaches in which the influence of the local climate on the building energy requirements is miss-evaluated.

In this study, we therefore took advantage of the intermediate resolution of the mesoscale atmospheric models and the results of such pioneer studies to design such a climate modeling system and dynamically assess the building energy requirements considering the complexity of the urban climate and the urban heat island effects.

2.3 Mesoscale meteorological models: promising tools to help urban planners?

The recent studies mentioned in the previous sections plaid in favor of designing climate modeling systems based on the use of mesoscale atmospheric models and sophisticated urban canopy parameterizations to dynamically assess the building energy requirements for space heating or cooling by considering accurate building surrounding thermal and dynamical conditions. With the reinforced roles of the local authorities in designing post carbon cities and mitigate the effects of the climate change, such tools is expected to provide interesting climate and energy knowledge that can serve guiding the energy and urban planning policies in the next decades. Indeed climate modeling systems, and the intermediate resolutions of the mesoscale atmospheric models allow considering the interactions between the urban morphology and hence the urban planning, the inherited physical properties of the surface and the physical processes that occur in the atmosphere at regional scale.

In this section, we first propose a description of the physical equations resolved by the mesoscale atmospheric models to simulate the variations of the meteorological

fields (*e.g.* wind, humidity, temperature, mass) over regional areas of thousand kilometers. Then we focused on the different urban canopy parameterizations that have been developed for mesoscale atmospheric models to consider the effect of the urban areas on the atmosphere. We secondly propose a discussion on the urban concept in both the meteorologist and urban planners communities in a second sub-section. Indeed, the increasing concerns on new urban environmental issues and the recognition of prevailing roles for urban planning raise questions on the representation of the complexity and heterogeneity of the urban areas in the mesoscale atmospheric models. More, the definition of the urban entities is showed to suffer from a lack of precision in the climatologist communities compared to the various existing definitions found in the urban planners communities. Nevertheless, the transfer of the climate and building energy knowledge between the two communities requires the adoption of common langage and concepts to create common understandings on the interactions between the urban climate and the building energy requirements. We, therefore, present at last a review of the existing research studies that attempt to bridge the gap between the two communities.

2.3.1 Mesoscale physical formulations

Mesoscale atmospheric models resolve the classical conservative equations for momentum, energy, mass and moisture that have been set by Navier and Stokes for describing the motion of any newtonian fluid. The effects of the surface on the atmosphere in mesoscale atmospheric model are introduced by the specific calculations of the surface skin temperatures, the thermal radiant energy restituted by the surface to the atmosphere, and the surface turbulent fluxes for momentum, energy and moisture by surface schemes. Because the physical properties of the surface differ from one land cover to another, it is a common approach to consider specific surface schemes or parameterizations for each land cover that represent the average effects of the surface on the atmosphere. Therefore this subsection is divided into two parts. The first one presents the atmospheric conservative equations while the second one presents the different surface schemes adopted to represent the effect of the urban areas on the dynamic and thermodynamic of the atmosphere.

2.3.1.1 The atmospheric conservative equations

The evolution of the meteorological field at a given place is given by the Navier-Stock conservative system of equations that is presented by the equations 2.6, 2.8, and 2.9. Note that the Einstein formulation, where $i = 1, 3$ is adopted for describing the three components of the vector variables in the equations. By convention the x direction is assigned to i=1, the y direction to i=2, and the z direction to i=3. Following the components of the wind vector $\vec{U}$ assigned to U_1, U_2, and U_3 refer respectively to the components U, V, and W. Note also that the air density is ρ (in $Kg.m^{-3}$). The wind velocity according to the chosen direction i or j is U_i or U_j (in m.s^{-1}), $p_i^{'}$ (in $Kg.m^{-1}.s^{-1}$) is the pressure perturbation from the hydrostatic pressure ρ_H, μ is the kinematic viscosity (in $m^2.s^{-1}$) that represents the ability of mixing of the fluid, S_{ij} the stress tensor that depicts the anisotropic deformations of the fluid, δ_{i3} the Kronecker delta, which represents a square matrix in which the Kronecker delta is equal to 1 for $i = j$ and 0 for the other cases. Θ (in °K) is the potential temperature, H is the hydrostatic potential temperature, g the universal gravitational constant set equal to 9.81 $m.s^{-1}$, f_c the Coriolis force, and at last, ϵ_{ij3} a unit tensor. Additionally T is the air temperature (in °C) and K the coefficient of heat conduction.

First in the system of conservative equations, we have the conservation equation for momentum. It is defined as:

$$\underbrace{\frac{\partial U_i}{\partial t}}_{\text{Term I.a)}} + \underbrace{\frac{\partial (U_j \rho U_i)}{\partial x_j}}_{\text{Term I.b)}} = \underbrace{-\frac{\partial p_i^{'}}{\partial x_i}}_{\text{Term II}} + \underbrace{\frac{\partial (\mu S_{ij})}{\partial x_i}}_{\text{Term III}} \underbrace{- \delta_{i3} \frac{\rho_H}{\theta_H} g(\theta - \theta_H)}_{\text{Term IV}} + \underbrace{f_c \epsilon_{ij3} U_j}_{\text{Term V}} \tag{2.6}$$

Then, we have the conservation equation for mass. It is:

$$\frac{\partial \rho}{\partial t} + \frac{\partial (\rho U_i)}{\partial x_i} = 0 \tag{2.7}$$

Equation 2.7 gives for incompressible fluid:

$$\frac{\partial (\rho U_i)}{\partial x_i} = 0 \tag{2.8}$$

And at last, we have the conservation equations for energy. It is written like:

$$\underbrace{\frac{\partial \rho\theta}{\partial t}}_{\text{Term I.a)}} + \underbrace{\frac{\partial U_j \rho\theta}{\partial x_j}}_{\text{Term I.b)}} = \underbrace{-\frac{1}{C_p}\frac{T}{\theta}\frac{\partial(K\frac{\partial T}{\partial x_i})}{\partial x_i}}_{\text{Term II)}} + \underbrace{S_\theta}_{\text{Term III}} \tag{2.9}$$

Equation 2.6 is used to describe the variation of the momentum.
The local variation of the wind speed *(term Ia)* of an air parcel and its advection *(term Ib)* is there showed to result from the actions of five unbalanced forces acting on the walls of the air parcel.
The pressure gradient forces *(term II)* may deform the fluid by compression or dilatation. The viscosity forces *(term III)* originated by the heterogeneities in the wind velocity within the fluid, cause anisotropic deformations of the parcel by shearing stresses and wind speed reductions as well. The buoyancy forces drive convective and uplifted motion within the fluid that the weight *(term IV)* counteracts by stratifying the fluid according to the mass of the air parcels. At last, the Coriolis force *(term V)* deflects the wind due to the rotation of the Earth.
Equation 2.8 is used to compute the local change in the density of the air parcels. The first term of the equation represents the variation in time of the density. This variation is only due to the ongoing and outgoing of momentum fluxes through the walls of the volume of air for which the budget is done. In our case, the atmospheric fluid is assumed incompressible meaning that the density and the volume of the fluid keep constant with time.
At last, to solve the momentum equations one should establish the additional conservative equation for energy (2.9). In equation 2.9 *term I.a* represents the the temporal variation of the temperature. It is driven by supplies or losses of energy provided by solar direct and diffuse radiations, water phases transformations, exothermal chemical reactions that constitute sources of energy *(term III)*. Advection *(term I.b)* and/or molecular convection *(term II)* may also modify the energy budget at a given site, and hence the air temperature.

As the fluid is moving, random perturbations within the fluid, which size can be millimeter up to meter can appear. Such flows are qualified to be turbulent. Precisely, a flow becomes turbulent when the inertia forces, which tend to bring closer heterogeneous fluid particles present in the moving fluid, overcome the viscosity forces, which tend to homogenize the fluid by opposing resistance to the motion. The relative strength of the two forces is given by the Reynolds number R_e. Thus, high Reynolds

number indicate high turbulent flow. However, if it is possible to observe the transition between a laminar flow that is characterized by well-organized and parallel streamlines into turbulent flow from the experimentation, the broad variety of initial conditions that causes the flow to become turbulent is not possible to predict. Nevertheless, a critical value that has been empirically determined is often mentioned to qualify the transition of a laminar flow into a turbulent flow. This value is equal to $R_e = 3500$ [De Moor, 1983].

The random perturbations within the fluid can be mechanically and/or thermally originated. The presence of shear strains within the fluid due to high velocity gradients, obstacles protruding from a surface or due to the contact of the flow with an opposite directed flow, cause mechanical perturbations. The relative strength of the buoyancy force compared to the weight may also produce micro-scale and macro-scale thermal perturbations, which famous form is represented by the convective cells.

Due to the broad diversity of turbulent flows and initial conditions at the origin of such flows, it is a common approach to characterize the flow with phenomenologic properties. As characterized by Tennekes and Lumley [1972] first, the *"Turbulence is a state of a flux not of a fluid"*. Because the perturbations are propagated and amplified throughout the fluid by the combined effects of swirls and their reverse currents (the eddies), turbulent flows are said highly diffusive. They are also qualified to be highly dissipative because the turbulent kinetic energy contained in the biggest eddies is successively dissipated by vortex stretching and tiling into smaller eddies of higher vorticity according to the Kolmogorov cascade until a certain eddy size, the Kolmogorov length scale $l\epsilon$. At the Kolmogorov length scale, the turbulent kinetic energy contained in the eddies is too low to counterbalance the molecular viscosity and the turbulent kinetic energy is then dissipated into heat. The turbulence spectrum that is sketched in figure 2.6 depicts the relationship found between the turbulent kinetic energy and the eddy size (in wavelength k).

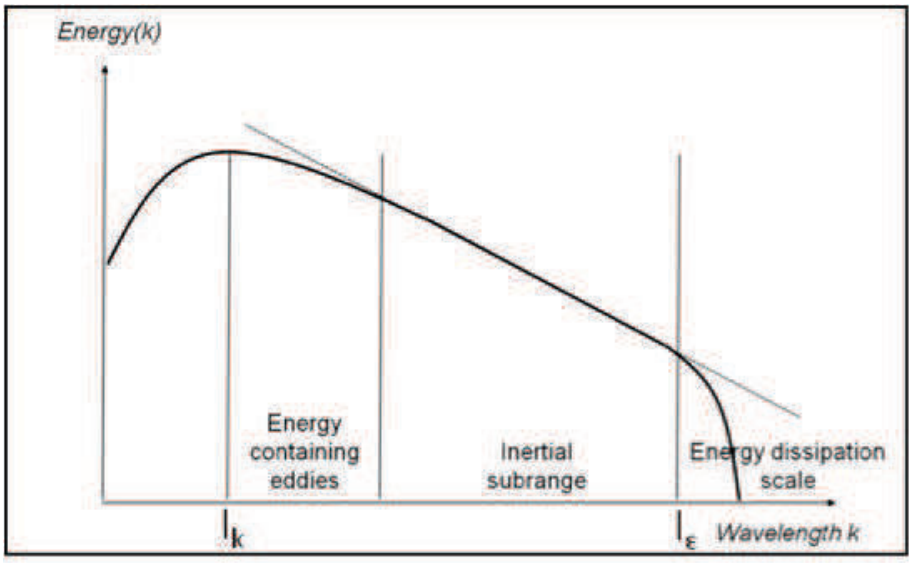

Figure 2.6: The turbulence spectrum (log-log scale) according to Rasheed [2009].

In figure 2.6, it is showed:
i) that large eddies of length scale l_k contains more E_k than small eddies;
ii) and that eddies quickly disappear below the Kolmogorov length scale.

It should be noted that the length scales $l\epsilon$ and l_k may vary according to the turbulence intensity. The latter is given by the turbulent kinetic energy budget set in equation 2.10 in which the time evolution of E_k is influenced by the mechanical shear stresses *(term IV)* that use to be always a source of turbulence, the buoyant production of turbulence *(term V)* that is positive during day and sink terms. The sinks are the gravitational force at night that tends to suppress the turbulent instabilities and cause the stratification of the fluid *(term V)* and the molecular viscous forces *(term VII)*.At last E_k could be transported by advection *(term II)* and by the turbulent flow itself *(term III)*. The contribution of the pressure perturbation *(term VI)* is often neglected.

$$\underbrace{\frac{\partial \rho E_k}{\partial t}}_{\text{Term I}} + \underbrace{\frac{\partial \overline{U_j} \rho E_k}{\partial x_j}}_{\text{Term II}} = \underbrace{-\frac{\partial \overline{\rho u_j' E_k}}{\partial x_j}}_{\text{Term III}} \underbrace{- \overline{\rho u_i' u_j'} \frac{\partial \overline{U_i}}{\partial x_j}}_{\text{Term IV}} + \underbrace{\delta_{i3} \frac{g}{\theta} (\overline{\rho u_i' \theta'})}_{\text{Term V}} \underbrace{- \frac{1}{\overline{\rho}} \frac{\partial \overline{\rho u_i' p'}}{\partial x_i}}_{\text{Term VI}} - \underbrace{\epsilon}_{\text{Term VII}} \tag{2.10}$$

Although the description of the turbulent flows remains one of the greatest challenges in physics, laboratory experimentations have proved that turbulent flows are

however predictable in average. Indeed, due to the high variability of the turbulent flow, diverse realizations of a turbulent flow cannot be qualified by a unique value taken at an identical point in the flow and time, but rather by a set of value that can be described by probability law. Hence, the average used for describing the turbulent flow is often associated to a statistical ensemble average of independent flow events. Nevertheless, because the the turbulent flow highly sensitive with the initial conditions and the initial conditions difficult to control even in experimentations, the ensemble average is then associated to a time average according to the ergodic theory. Indeed under stationary conditions, the events are like in the ensemble average independent [De Moor, 1983].

Thus, it is a common approach to split the instantaneous meteorological variables $U_{1,3}$ into an averaging predictable portion (indicated with an over bar $\overline{U_{1,3}}$) and a fluctuating one (with a prime $\overline{u'_{1,3}}$) when considering a stationary period, and by using the reynolds averaging decomposition procedure. The averaging predictable portion represents then the large scale motions in the flow, while the fluctuating portions refers to the small scale motions in the flow like in equation **??**.

Hence, by averaging the equations 2.6, 2.8 and 2.9, non linear terms, referred as the Reynolds stress tensors, emerge from the advection terms. Equations 2.11 and 2.12 and 2.13 present the stationary reynolds averaged (RANS) conservative equations for momentum, mass and energy.

Although the method is widely employed, the relying assumptions are questioned: the spectral gap between large scale motions and fast small scale motions is in doubt while steady conditions are unrealistic as synoptic forcing are uncontrolled [Rasheed, 2009].

For momentum:

$$\underbrace{\frac{\partial(\overline{U_j}\overline{\rho U_i})}{\partial x_j}}_{\text{Term I.b)}} = \underbrace{-\frac{\partial \overline{P_i}}{\partial x_i}}_{\text{Term II}} + \underbrace{\frac{\partial(\mu\overline{S_{ij}})}{\partial x_i}}_{\text{Term III}} \underbrace{- \delta_{i3}\frac{\overline{\rho_H}}{\overline{\theta_H}} g(\overline{\theta} - \overline{\theta_H})}_{\text{Term IV}} + \underbrace{f_c \epsilon_{ij3}\overline{U_j}}_{\text{Term V}} \underbrace{- \frac{\partial(\overline{u'_j \rho u'_i})}{\partial x_j}}_{\text{Term VI}} \tag{2.11}$$

For mass:

$$\frac{\partial(\rho\overline{U_i})}{\partial x_i} = 0 \tag{2.12}$$

For energy:

$$\underbrace{\frac{\partial \overline{U_j \rho\theta}}{\partial x_j}}_{\text{Term I.b)}} = \underbrace{-\frac{1}{C_p}\frac{\overline{T}}{\overline{\theta}}\frac{\partial(K\frac{\partial \overline{T}}{\partial x_i})}{\partial x_i}}_{\text{Term II)}} + \underbrace{\overline{S_\theta}}_{\text{Term III}} \underbrace{-\frac{\partial(\overline{u_j' \rho\theta_i'})}{\partial x_j}}_{\text{Term IV}} \tag{2.13}$$

The presence of the unknown non-linear terms requires additional equations that contain as much unknowns as the order of the system of equation. This is known as the turbulent closure problem. Hence, non-linear terms are often approximated in terms of known variables and parameters set in relation with the flow. Among turbulent closures, the "K-theory" is widely used. It is a local first order closure that considers the first prognostic equations of mean quantities and that approximates the non-linear terms in analogy with the molecular diffusion, so that:

$$\overline{u_i' N'} = \mu_{N,j} \frac{\partial \overline{N}}{\partial x_j} \tag{2.14}$$

With N any meteorological quantity, $\mu_{N,j}$, the eddy viscosity set in relation with the flow ability to exchange the quantity N.

Close to the surface the RANS equations are simplified and modified so as to consider with more accuracy the influence of the surface, and in particular the urban surface, on the airflow.

2.3.1.2 The surface schemes used for representing the effects of the urban areas in mesoscale atmospheric models

According to Voogt and Oke [1998] and Pielke and Niyogi [2011] surface properties are "critically important" as the surface, by exchanging momentum, heat, moisture and mass with the atmosphere, conditions the atmospheric turbulence structure. In the past, several approaches have been investigated to improve the representation of the urban areas and their influences on the air flow in mesoscale atmospheric models. Those approaches are presented in the following sections.

- **The surface layer scheme and the Monin-Obukhov similarity theory**

Close to the ground, in the surface layer, the effects of the surface become predominant. As the turbulent research has traditionally focused on flow other homogeneous and smooth surfaces, it is a common approach to consider a large and high enough layer, the boundary layer, that allows "seeing" the rough and heterogeneous terrain like the urban areas as an effective rough and homogeneous surface in which the spatial distribution of rough elements is assumed uniform [Rothach, 1999]. It is the boundary layer approximation.
By applying the boundary layer approximation, the vertical fluxes become relatively more important compared to horizontal fluxes. It allow the simplification of the conservative equations. Due to the boundary layer approximation, the equation 2.12 becomes:

$$\frac{\partial(\rho\overline{W})}{\partial x_i} = 0 \tag{2.15}$$

Since the wind speed is null at ground, the W-component of the mean wind speed is null everywhere. As a consequence, the *Term I.b)* in equation 2.11 falls.
More, other assumptions can be done in the boundary layer resulting in the simplification of the RANS equations. Such assumptions are listed here:
- the Coriolis acceleration is assumes to balance the horizontal pressure forces;
- the horizontal wind is considering to be not geostrophic;
- the vertical pressure forces may be given by the weight with the hydrostatic approximation;
- and at last the molecular viscosity force could be neglected compared to the turbulent diffusivity that is more efficient to mix the air [Stull, 1988].

Therefore the RANS equations can be simplified like in equations 2.16 and 2.17. This leads to consider constant vertical turbulent fluxes with height in the surface layer.

– for momentum:

$$-\frac{\partial(\overline{u_i'\rho w'})}{\partial z} = -\frac{\partial}{\partial z}(\mu_t \frac{\partial \overline{U_i}}{\partial z}) = 0 \tag{2.16}$$

– for energy:

$$-\frac{\partial(\overline{u_i'\rho \theta'})}{\partial z} = -\frac{\partial}{\partial z}(\mu_t \frac{\partial \overline{\theta}}{\partial z}) = 0 \tag{2.17}$$

In the classical formulation of Monin and Obukhov (the Monin Obukhov Similarity Theory or MOST) the wind velocity and temperature profiles within the surface layer are described by dimensionless functions using dimensional scales such as the friction velocity u_*, the temperature scale θ_* and the length scale z [Monin and Obukhov, 1954, Foken, 2006]. Accordingly, the surface fluxes for momentum is considered to be equal to u_*^2 and the surface fluxes for the energy is set equal to $u_*\Theta_*$.

More, the momentum and heat eddy diffusivity coefficients μ_t in equations 2.16 and 2.17 that have the dimension of a velocity scale time a length scale, are then defined as the product of the friction velocity u_* with the mixing length l, the size of the tallest eddies contained in the airflow. Those eddy sizes are assumed to freely and linearly increase with the height within the surface layer so that the mixing length is set equal to : $l = z$ or $l = kz$
Where k is the von Kármán constant that is often set equal to 0.35 or 0.40 [Högström, 1990, Businger et al., 1971] and z the height above the ground.

Therefore, the eddy diffusivity is:

$$\mu_t = \frac{u_* kz}{\Phi} \tag{2.18}$$

Where Φ could be Φ_M or Φ_H and represent statistical empirical functions that are used for considering the influence of the atmospheric stability on the momen-

tum and heat turbulent surface fluxes, respectively. For neutral conditions those functions are: $\Phi_M = 0$ *and* $\Phi_H = Pr$*. The Prandtl number Pr is then considered to be equal to 0.95 and represents the ratio between the momentum and the heat diffusion coefficients [Jacobson, 1999].*

By substituting all those parameters in the respective equations, the vertical profile for momentum is then given by equation 2.19 and for the energy by the equation 2.20 :

$$\frac{\partial \overline{U}}{\partial z} = \frac{u_*}{kz}\Phi_M \tag{2.19}$$

$$\frac{\partial \overline{\Theta}}{\partial z} = \frac{\Theta_*}{kzu_*}\Phi_H \tag{2.20}$$

given respectively,

$$\overline{U(z)} = \frac{u_*}{k} ln(\frac{z-d}{z_{0,M}}) - \Psi_M \qquad With \qquad \Psi_M = \int_z^{z_{0,H}} (1-\Phi_M)\frac{dz}{z} \tag{2.21}$$

$$\overline{\Theta(z)} = \overline{\Theta_S} + \frac{Pr\Theta_*}{k} ln(\frac{z-d}{z_{0,H}}) - \Psi_H \qquad With \qquad \Psi_H = \int_z^{z_{0,M}} (1-\Phi_H)\frac{dz}{z} \tag{2.22}$$

In the equations 2.21 and 2.22 it is showed that the dynamical effects of the surface are represented through the definition of a single length scale, the roughness length (*e.g.* $z_{0,M}$). The roughness length represents the maximum average resistance of the surface to the airflow and corresponds to the height at which the wind speed is null. This approach is sometimes referred as the roughness approach. Hence, from $z_{0,M}$ up to the top of the surface layer, the integration of equations 2.19 and 2.20 gives mean vertical profiles of wind speed and potential temperature. The profiles are then showed to be nearly logarithmic (as showed in 2.21 and 2.22) in the surface layer.

Because urban areas are among the roughest surfaces on the Earth, the pressure drag forces are much more pronounced than in rural flat areas, an increasing

$z_{0,M}$ is usually adopted in urban areas. Classical value of $z_{0,M}$ are of the order of 0.01 m for roofs and 0.6 m for urban canopy [Kusaka et al., 2001]. It could be determined by anemometric or morphometric methods [Maruyama, 1999, Grimmond and Oke, 1999a, Grimmond, 1998]).
More, in urban area where the RSL can amount for several tens meters [Rothach, 1999, Högström et al., 1982], a zero plane displacement d is considered in addition so as to fill in the domain of validity of the MOST. Indeed turbulent fluxes are constant with height in the inertial sub-layer. Therefore, the first layer of the atmospheric mesoscale model is often displaced at the height d and the wind speed is set null at $z_{0,M} + d$.

In the same manner, the heat turbulent fluxes over urban areas are represented by a gradient-flux relationships (equation 2.20) in which a roughness length for heat $z_{0,H}$ is adopted to represent the average effect of the surface. It is set bigger over urban areas compared to rural areas to represent the greatest heat capacity of the urban materials, ans represents the height at which the equivalent surface temperature T_S is equal to the ground temperature T_G. Additionally several physical parameters of the surface are adapted in the radiative and energy budgets for urban areas: *i)* a lower facets' averaged albedo is used for accounting to the interceptions of the radiations by vertical walls; *ii)* the soil water content is reduced or set null; *iii)* the heat capacity of the building fabric is at last increased so as to represent the building thermal inertia.

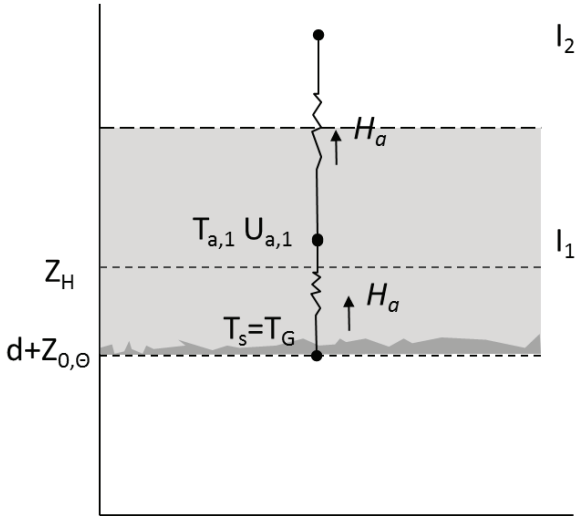

Figure 2.7: Slab model (adapted from Kusaka et al. [2001] T_a and U_a are respectively the air temperature and the wind speed of the mesoscale grid (I_1,I_2, and so on), the obstacle average height is z_H, d is the displacement height, $z_{0,\Theta}$ is the roughness length for heat. T_S is the equivalent surface temperature, and T_G of the ground. Then, H_a is the sensible heat flux from the canyon to the atmosphere.

However, the roughness approach is showed to be inadequate in urban areas where it tends to over-estimate the urban heat island intensity as well as the nocturnal cooling as Müller [2007] and Kusaka et al. [2001] highlighted.

- **Use of 1-dimensional canopy parameterizations**

Recent improvements of the computer power capacity and the regain of interest on processes that directly affect human living conditions within the urban canopy layer require direct simulations of the fluid dynamics and thermodynamics in and around urban structures. It triggered the development of sophisticated urban canopy parameterizations (UCPs). The effects of the different surfaces of the street-canyon on the atmosphere are explicitly taken into account by the re-calculation of the surface fluxes terms, f_S also called the source, that are directly inserted in the RANS conservative equations to force the meteorological conditions at the lowest level of the atmospheric domain (*e.g. term VII and V* of 2.23 and 2.24).

For momentum:

$$\underbrace{\frac{\partial U_i}{\partial t}}_{\text{Term I.a)}} + \underbrace{\frac{\partial(\overline{U_j \rho U_i})}{\partial x_j}}_{\text{Term I.b)}} = \underbrace{-\frac{\partial \overline{P_i}}{\partial x_i}}_{\text{Term II}} + \underbrace{\frac{\partial(\mu \overline{S_{ij}})}{\partial x_i}}_{\text{Term III}} \underbrace{- \delta_{i3} \frac{\overline{\rho_H}}{\overline{\theta_H}} g(\overline{\theta} - \overline{\theta_H})}_{\text{Term IV}} + \underbrace{f_c \epsilon_{ij3} \overline{U_j}}_{\text{Term V}} \underbrace{- \frac{\partial(\overline{u_j' \rho u_i'})}{\partial x_j}}_{\text{Term VI}} + \underbrace{f_U^S}_{\text{Term VII}} \tag{2.23}$$

For energy:

$$\underbrace{\frac{\partial \rho\theta}{\partial t}}_{\text{Term I.a)}} + \underbrace{\frac{\partial \overline{U_j \rho \theta}}{\partial x_j}}_{\text{Term I.b)}} = \underbrace{-\frac{1}{C_p} \frac{\overline{T}}{\overline{\theta}} \frac{\partial(K \frac{\partial \overline{T}}{\partial x_i})}{\partial x_i}}_{\text{Term II)}} + \underbrace{\overline{S_\theta}}_{\text{Term III}} \underbrace{- \frac{\partial(\overline{u_j' \rho \theta_i'})}{\partial x_j}}_{\text{Term IV}} + \underbrace{f_\Theta^S}_{\text{Term V}} \tag{2.24}$$

Like in the roughness approach the average effects of the obstacles that are immersed in an atmospheric grid is considered. Nevertheless, each of the street-canyon surfaces are treated separately to improve the computation of the skin temperatures, the canopy temperature, and hence the energy surface fluxes that are exchanged with the atmosphere. Therefore, the urban canopy parameterizations usually consider three dimensional and infinite long street-canyons composed by building walls and roofs and their afferent streets. Street-canyons are considered to be uniformly distributed in the atmospheric grid and separated by square horizontal cross-sections. The obstacle height can be assumed uniform and set equal to the average obstacle height [Masson, 2000] or heterogeneous. So far Kusaka et al. [2001] adopted a standard deviation of the obstacle height while Martilli et al. [2002] defined a vertical distribution function to account for the variations of the obstacle height.
The radiative energy budget is also modified to account for the three dimensional effects of the buildings on the shortwave and longwave radiations accounting for the shadowing and multiple radiative reflections that occur in the urban canopy layer.
By considering such an approach, two types of urban canopy parameterizations exist. They are referred as the single and multiple-layer urban canopy parameterizations. In the first one, the urban canopy layer is described by a single level while in the second urban canopy parameterization considers multiple vertical grid levels (respectively figures 2.8 (a) and 2.8 (b)).

(a) Single layer models (sketch (a) in figure 2.8) describe the urban canopy layer with a unique grid level in which the roof in the one hand, and the street-canyon floor and walls in the other hand are treated separately when computing the surface energy budgets. The street-canyon floor and wall surface energy budget permits to determine a canyon-system effective surface temperature that is used to compute accurate vertical heat fluxes according to the MOST formulation. In the same manner, a roof energy budget and a roof turbulent heat fluxes are computed according to equation

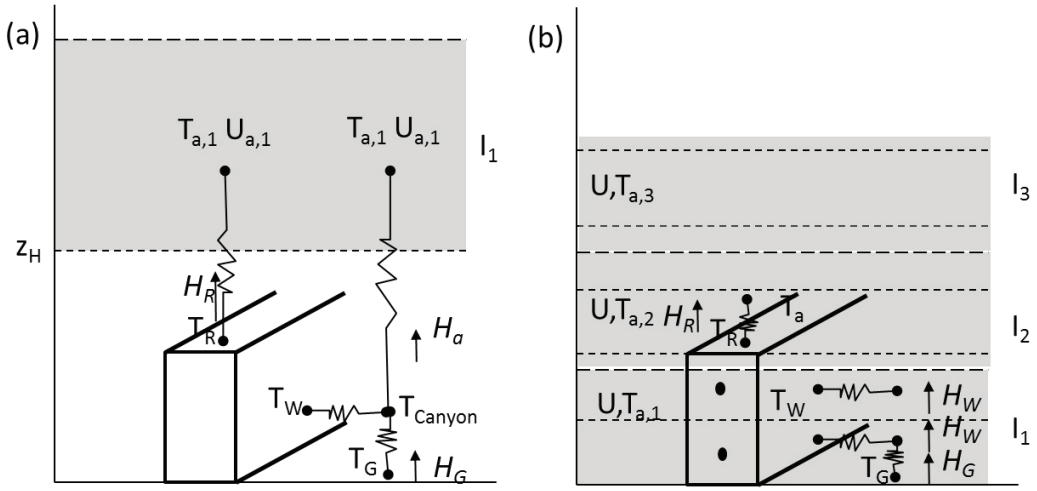

Figure 2.8: Distinction between single and multilayer canopy models (adapted from Kusaka et al. [2001] T_a is the air temperature of the mesoscale grid (I_1,I_2, and so on), the obstacle average height is z_H. T_R is the roof surface temperature, T_W the one of the walls, T_G of the ground. Then, H_a is the sensible heat flux from the canyon to the atmosphere, H_W and H_G are that from respectively the walls and the ground to the canyon, and H_R that from the roof to the atmosphere.

2.20 to represent the sensible heat exchanged between the roofs and the above lying atmosphere. The roof and street-canyon surface heat fluxes are then introduced in the conservative equation for energy as a source terms according to their respective coverage contributions to dynamically force the meteorological field in the lowest level of the mesoscale atmospheric grid. Note that the lowest level of the mesoscale atmospheric grid is usually displaced above the roof tops as showed in figure 2.8.

Usually, the surface fluxes for momentum is computed by using an appropriated roughness length and a zero-plane displacement height according to the MOST formulation. The surface wind speed is then set equal to zero. The reduction of the wind speed within the urban canopy layer and its influence on the thermal exchanges in the urban canopy layer is however consider in addition by interpolating the logarithmic vertical wind profile until the ground by using an exponential function.

At last, like other three-dimensional urban canopy parameterizations, sophisticated single layer models consider in addition the three-dimensional effects of buildings such as:

i) the radiation trapping and shadowing effects through three-dimensional radiative energy budget by using sky view factors or extinction functions to reduce the amount of solar energy that reaches the ground, and by accounting for various building orientations and the variations of the solar azimuth angles;

ii) the heat storage within the construction materials by solving the 1-dimensional heat conduction equations for each layers of a layered canyon facets;

and *ii)* the anthropogenic heat emissions caused by the use of the HVAC system, and the vehicles traffic in the canopy layer [Masson, 2000, Kusaka et al., 2001].

(b) In multilayer canopy parameterizations, the canopy layer is described through several vertical layers (canopy grid) that are immersed in the atmospheric mesoscale model (sketch (b) in figure 2.8). It means that the first level of the atmospheric model is located at ground. The additional source terms f_S, are computed for each level of the canopy grids each time the building interacts with the atmosphere. Contrary to the single layer canopy parameterization, the pressure and viscous drag forces induced by the obstacles are usually represented through a distributed drag force approach derived from the study of the airflow dynamic in tree canopies [Dupont et al., 2004, Uno et al., 1989, Ca et al., 1999, Otte et al., 2004, Martilli et al., 2002, Kondo et al., 2005, Hamdi and Masson, 2008].
It consists in computing at each canopy level and each time the airflow interacts with the obstacles, vertical and horizontal drag forces and friction forces respectively, as well as additional sources of turbulent kinetic energy (production or sink) induced by the obstacles. Indeed a $k - \epsilon$ turbulent closure is generally adopted in the canopy multilayer parameterizations so as to better consider the effect of the obstacles on airflow. It consists in parameterizing the turbulent diffusion coefficient by resolving the equation of turbulent kinetic energy and parameterizing the viscous forces. The reduction of the mixing length induced by the presence of the obstacles is reproduced by adapting the Kolmogorov and dissipation length scale. Like single layer canopy parameterization, separated energy budgets are computed for each canyon facets (walls, roofs and streets) and canopy grid levels to compute accurate surface heat fluxes and skin temperatures. Therefore, an average surface heat fluxes is at last computed for each canopy grid levels according to the coverage of each street-canyon surface as in Martilli et al. [2002]. Like in single canopy models, the radiative budget is 3-dimensional and a 1-D heat conduction equation is resolved for each layered of the canyon facets to simulate the storage of the energy in the building materials.

Recently, several simplified BEM models have been developed and implemented within the urban canopy parameterizations to address energy related urban environmental issues[Kikegawa et al., 2003, Ohashi et al., 2007, Kikegawa et al., 2003, Bueno et al., 2011, Salamanca et al., 2010]. Figure 2.9 sketches the climate modeling system forming by the MM, UCP, and building energy model.

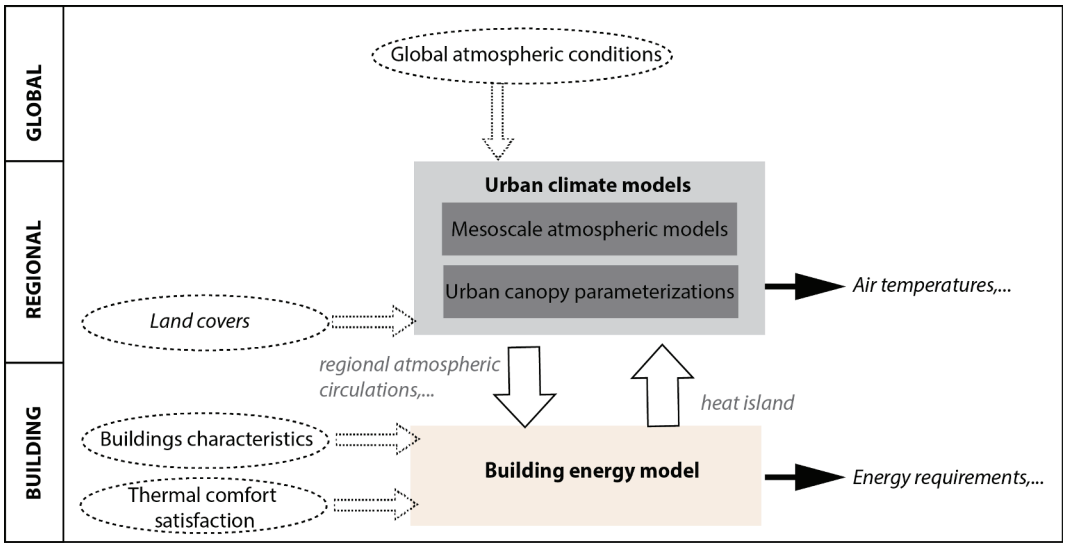

Figure 2.9: The climate modeling systems. The inputs of the models are surrounded by a circle and symbolized by dashed arrows. The outputs are symbolized by black arrows. The interactions between the building energy model and the urban climate models are symbolized by large arrows.

The building energy models usually consider the building as a box and compute either a unique indoor energy budget for the entire building or several indoor energy budgets for each floor of the building accounting for the solar heat gains through windows, the wasted from equipment and human metabolism, as well as the unintentional natural ventilation. Thermal and humidity loads are calculated and then compared to user-defined thermal and humidity comfort ranges for activating a heat pump model each time the comfort range is overpassed and for assessing the building heating or cooling energy requirements. The excess of heat and the wasted-heat generated by the heat pump are then directly ejected in the street. The coupling of the urban canopy parameterization with the building energy model is usually achieved by balancing the internal latent and sensible heat fluxes of the indoor and outdoor energy budgets through the resolution of a one-dimensional heat conduction equation for each layer of a layered wall system.

As a conclusion the MM+ UCP+ BEM climate modeling systems provide new cross-scale urban modeling capacity to address environmental urban issues. For some authors like Chen et al. [2011] the application of such urban modeling system will help bridging the gap between climatologists and urban planners. However, it is without counting on the retained physical approximations and the mismatch between the urban planners and climatologists in urban area definitions and representations.

2.3.2 Towards a better representation of the complexity of the urban areas in mesoscale meteorological models (MM)

2.3.2.1 A shift in the preoccupations of the urban climate community

A brief review of applicative studies that used MM+ UCP+ BEM climate modeling systems helps to identify a shift in the scientific preoccupations. To date, meteorological modeling systems have been widely applied on extended worldwide metropolitan areas of ten millions inhabitants or more (*e.g.* Beijing, Honk-Kong, New York city, Taipei according to Chen et al. [2011]) for assessing landscape and building adaptation strategies designed to cope with the climate change impacts. Salamanca et al. [2011] investigated the effects of some air conditioning energy conservations policies over the city of Houston (2.16 million people according to the US census). Kikegawa et al. [2003] and Ohashi et al. [2007] studied in particular the contribution of the anthropogenic heat on the local climate over the great Tokyo (37 million people according to the United Nations). Pigeon et al. [2014] studied the growth in the building energy demand in Paris (12 million people according to INSEE in 2011) considering the temperature rise induced by the climate change. Salamanca et al. [2012] simulated building energy demands over the great Madrid (6.5 million people).

In parallel, the number of projects that focus on one million, half-million or less populated metropolitan areas flourishes [Giovannini, 2012]. Although most of them are not directly commissioned by local authorities, they however, clearly assert providing materials for building energy and urban planning policies. In France, the ACCLIMAT (2010-2013) project of the CRNM laboratory aimed to study the effects of the urban development and climate change by 2100 on the urban climate and building energy requirements of the great Toulouse (1.2 million inhabitants in 2011). For this, the scholars coupled a system of urban growth models with the climate modeling system of Météo-France. The economic urban growth model NEDUM of Gusdorf et al. [2008] is used to model the residential development of the great Toulouse by taking into account mono centric urban areas, the cost of the lands and transportation, the household incomes and life style preferences. It provides the number of dwellings that should be built and the cost maps used by the urban growth cellular automata model SLEUTH* of Aguejdad et al. [2012] to constraint the built-up areas developments. The urban growth cellular automata model SLEUTH* simulate the development of the built-up areas considering four transition rules that prioritize either the development close to

the motorways, the existing built-up areas, or assumes spontaneous built-up areas development or new spreading centers. The GENIUS urban fabrics model of CNRM and LRA at last consist in an urban fabric database that allows specifying according to the number of dwellings and the cost of the lands the types of building and their physical features. The climate modeling system then includes the Météo-France meso-NH mesoscale atmospheric model, the TEB-Veg urban canopy parameterization that accounts for the presence of low vegetation in the street-canyons of [Lemonsu et al., 2012] and the BEM building energy model of [Bueno et al., 2011]. To provide accurate urban planning informations and represent accurately the surface heterogeneity, the resolution of the climate modeling system is set equal to 250 m. The scenarios that are used to constraint the residential development of the SLEUTH* model are co-imagined by various urban planners and stakeholders as well as architects. The MApUCE (2014-2018) project aims moreover to develop a building energy behavioral model and aims to develop quantitative microclimate and energy data that could be directly integrated in legal landscape planning instruments. Toulouse, Aix-en-Provence (nearly 141, 000 inhabitants) and La Rochelle (206,000 inhabitants) are the areas that are retained as study areas.

Other projects are more specifically dedicated to the study of the ecological amenities provided by the green areas at various scales (the building roofs, the neighborhood and the city scales) like in the VegDUD project (2010 to 2014). The ANR TVU (2009-2012) and CCTV2 (2011-2013) for instance, particularly investigated the biodiversity and local climate ecological services provided by the urban green areas over the Ile de France region and Strasbourg city council (nearly 450,000 inhabitants).
At last other projects aim to qualify and quantify the vulnerability of urban area to heat stress. The AMICA Interreg IIIC project (2005-2007) characterized the Urban Heat Island (UHI) patterns of the great Lyon (2.1 million people in 2011). The PhD work of Julita Dudek integrates in addition the analysis of the UHI patterns of the Grenoble (675,000 inhabitants in 2011) and Saint Etienne (506,000 inhabitants in 2011) agglomerations and compares the accuracy of several quantitative techniques in providing the UHI patterns. More recently, on the behalf of the Great Dijon, the climate laboratory CRC (CNRS/University of Bourgogne), and the laboratories of geography of ThéMa (CNRS/University of Franche-Comté and Bourgogne) and LIVE (CNRS/University of Strasbourg) collaborated for depicting the UHI patterns of the great Dijon so as to help designing the Plan Climat Energy Territorial of the Great Dijon city council. For this, those scholars performed a meteorological monitoring of the microclimate fields during an intensive observational period, and simulated the urban heat island intensity

by using the BEP+BEM urban canopy parameterization of Martilli et al. [2002] and Salamanca et al. [2010] included in the WRF American mesoscale atmospheric model of Skamarock et al. [2008]. For this, the atmospheric grid resolution is set equal to 150 m. Thus it can be stressed that more and more operational studies are performed to permit the transfer of climatologist and building energy knowledge in the urban planning documents of both large and medium-sized urban areas.

Nevertheless, one should be aware that the consideration of urban climate data in the urban planning instruments and policies is not a recent preoccupation. The Hygienist current in the 19_{th} century that could be illustrated by the Garden city of E. Howard, pleaded in favor of green open spaces and large streets to favor the natural ventilation of the urban areas. More, yet Thomas More in 1516 introduced climate principle in the urban area of Amaraute in Utopia. At last it could be stressed that since the late 1970's Germany particularly developed urban climate informations for urban planning by building urban climatic maps [Ren et al., 2011]. The region of Stuttgart, of the Ruhr (*e.g.* Dortmund, Essen, Bochum and so on) and the Bayern (*e.g.* Muenchen, Augsburg) were particularly studied [Matzarakis and Mayer, 2008, Beckröge, 1988]. Barlag and Kuttler [1991] and Kuttler et al. [1998b] particularly investigated the influence of regional and local winds on urban ventilation like in Cologne (Germany), while others scholars defined urban climatic maps. All this works give birth to city-scale and operational climatic maps. Climatic maps constitute evaluation tools that integrate both maps of urban climatic factors relevant for each land use and town planning considerations. Hence, the 10 to 100 m resolution local wind circulations (*e.g.* channeling effect, local winds types and directions), the thermal environment characterized by UHI intensity and heat or cold stress indices, as well as the air pollution level are captured to define Climatopes at pedestrian levels. The Climatopes are then type casted into climate sensitive class describing by planning recommendations (*e.g.* preservation of the thermal effect, modification of the channeling effect and so on) that could be visualized in the urban climatic planning recommendation map at district or city scales.

So finally what is new is the wide integration of quantitative climatic and energy data in prospective local planning policies and legal instruments [Godinot, 2011]. What is also new is the new capacity of mesoscale climate modeling systems to integrate the three dimensional effects of the buildings on the boundary layer dynamics and the interactions of the building energy with the microclimate. Although collaborative studies

emerged between scientific communities and urban planners, there is still some thematic limitations that arise from the difficulties in adopting the same urban definition in the urban planners and climatologist communities, and in representing the complexity of the urban ecosystem.

2.3.2.2 Representations of the urban areas in the MM models

In a climate perspective, the urban areas are considered as built-up areas that are mainly impervious in which human lives. This neutral definition is inherited from the land cover surveys and maps that are used in the climate modeling systems to define the static physical parameters of the surface. Those land covers issued from remote sensing images that are often provided at the global scale. To such extent, the US Geological Survey (USGS) dataset is commonly used to provide the surface properties and the land cover maps used in the climate modeling systems. Nevertheless, it comprises important limitations. The primary sources, the NASA high-altitude aerial photographs and the Advanced Very High Resolution Radiometer (AVHRR) satellite images are out-dated (respectively collected during the 1970's and the 1992-1993's). Therefore they are inaccurate to depict the periurban areas of the main built-up areas that are considerably and quickly grown during the pas decades. More, the classification of the USGS database is not based on surface morphological characteristics and therefore could not permit any distinction among urban fabrics (*e.g.* residential, commercial, or industrial estates) as stressed by Burian et al. [2004]. The second largest source is the International Geosphere-Biosphere (IGPB) land cover database. It is based on the analysis of the 2001 MODIS (MODerate resolution Imaging Spectroradiometer) satellite images that have a spatial resolution including between 250 m to 1 km [Chen, 2007]. Due to the use of 15 channels dedicated for land surface vegetation, the MODIS images allow better considering croplands and forested areas compared to the AVHRR radiometer. However, again solely a single class describes the built up areas.

In parallel, the sub-grid interactions between the different types of land cover included in a mesoscale atmospheric grid (*e.g.* the fetch effect, the oasis effect, the thermal plume and so on) are neglected in the atmospheric mesoscale model. Indeed, the spatial topology of the sub-grid elements is not considered. The presence of several types of land cover is either represented by the definition of average surface physical parameters: an average street-canyon albedo, heat capacity, and so on, or by the tile approach.

The tile approach consists in computing for each types of land-cover included in the atmospheric grid specific land cover vertical surface fluxes. The latter do not interact with each other before the first level of the atmospheric grid where they are weighted according to the respective coverage of the land cover types. the resulting average surface fluxes are then incorporated in the conservation equations as additional source terms [Essery et al., 2003]. Hence, the more the mesoscale atmospheric grid is resolved the more the sub-gridded advection is reproduced by the climate modeling system.
The increase in the horizontal atmospheric grid is, however, unrealistic as it leads to increase the computing power demand and may also question the boundary layer approximation.

Thus to date, it could be stressed that regional atmospheric models even through the implementation of sophisticated urban canopy parameterizations are not able to assess the retrofit of small scale urban planning actions on the urban climate and building energy requirements such as the microclimatic effects of green parks on the ventilation and thermal environment of the adjacent lanes or the effects of water pounds in public places because of the non-consideration of the spatial topology within the atmospheric grids. Such limit is particularly detrimental for representing vegetative areas in residential districts where a wide variety of vegetation categories and irrigated green areas are present [Grimmond et al., 2010] and significantly impacts the performance of the regional atmospheric model as stressed by Grimmond et al. [2011]. For such reason, several urban schemes recently incorporated vegetation effects within the urban canopy models [Dupont et al., 2004, Lemonsu et al., 2012]. Most of the time it consists in simple low vegetation located on the canyon floor or roof.

2.3.2.3 Representations of the urban areas in the urban planning

The concept of city and urban are somewhat new in the human evolution as the propensity of the society to become urbanized during the past century is striking [Frey and Zimmer, 2001]. The qualification of urban itself is fleeting and has changed through along the historical evolution of the city. Cities are first a social achievement of a group for a certain goal [Laborit, 1971]. The goal could be either political, economic or somewhat else. Hence the Antique city was political, the Middle Age city was commercial, the post-war city was industrial, and the nowadays city is global as stressed by Asher [1995] and Viard [1974] with their respective concepts of metapolis and archipelago

society. By chance and maybe the future city will be ecological and sustainable. Cities have become as much complex and emerges from actions of a so large set of agents (*e.g.* individuals, public authorities, associations and so on) that a unique definition or conception cannot serve [Gleau et al., 1996]. The definition of a city by a politician, an urban planner, an economist or a geographer may differ in various ways, so does their physical limits. Usually, a simple opposition to the rural countryside in a political (cities are then more complex social organization), demographic (cities are then qualified by high dense population) and socio-economical perspectives (cities are then depicts by the fact that the majority of the population not involved in the agricultural production) is used. But the dilution of the urban way of life in the rural countryside makes such definition out-dated. Hence, several criteria are used to define urban areas:

1. The population threshold as in Spain, Italy and Portugal in which a town is defined by the concentration in the administrative boundaries of the city of more than 10,000 inhabitants [Gleau et al., 1996]. Sometime an ecological criterion could be added like the population density as cities gather population and housings;

2. Spatial contiguity criteria. According to the French economic and demographic institute INSEE, an urban area is a continuous build-up unit with a distance threshold of less than 200 meters that contains more than 2,000 inhabitants which respectively represent more than 50% of the municipalities' inhabitants;

3. Sociological and economic criteria as urban areas gather population, educational, administrative and economical activities and favor innovation activities. The daily number of resident-to-work commuting, the accessibility to urban amenities and services (*e.g.* water pipe system), the diversity and level of expertise of the activities are some factors that are commonly used. Other sociological criteria could be added. Indeed although elderly people do not participate to the home-to-work trips they can however contribute to diffuse the urban way of life [Schmitt et al., 2000]. The *metropolitan area* defines a functional and continuously built-up area in which an urban pole offers more than 5,000 employments, attracts 40% of the population of the satellites towns for working, the hinterland;

4. Political decisions. In United Kingdom (UK), or United States (US) cities are legally assigned by monarchic or governmental decisions. The spatial extent is

then drifted by administrative boundaries where demographic and economic census data are driven.

To conclude, in an urban planning perspectives urban areas are regards as a complex socio-economic system which has material (population, buildings, transportation fluxes) and immaterial entities (information fluxes), and that polarize an area, the hinterland.

2.3.2.4 New representations of the urban areas and its complexity in the MM models

In a climatologist perspective, the urban area is rather confined to the built up environment that are extracted from remote sensing data whose resolution allow better considering the spatial heterogeneity of the landscape. Neverthless so as to bridge the gap between the two disciplines, recent efforts have been achieved for accentuating the representation of the heterogeneity of the built-up areas in the mesoscale atmospheric models and detailed land cover classifications have been devised for depicting a large panel of urban fabrics [Burian et al., 2004, Lemonsu et al., 2008]. Those classifications require the interpretation of a large panel of high resolved geospatial land cover informations, 3D digital building and vegetation provided by various sources (*e.g.* multispectral imagery, airborne LIDAR, orthophotographies) that are treated using Geographical Information System (GIS) geo-processing. The resulting geospatial databases usually provide geo-referenced land cover areas, predominant street orientations, building maximum and minimum height that could be interpolated for each node of a resolved mesoscale atmospheric grid (*e.g.* 250 m - 500 m horizontal resolution). The National Urban Database and Access Portal Tool (NUDAPT) project proposes for several US cities databases that include 1 km and 250 m aggregated building morphological features, and that can serve in climate modeling systems to provide accurate physical surface parameters [Ching et al., 2011]. However the management of such datasets appears difficult when dealing with the entire domain of the atmospheric mesoscale model and computational time expensive. Further sensitivity analysis of the urban canopy parameterization to input surface parameters are required [Burian et al., 2004].

Other authors focused on the definition of more relevant land cover classifications

based on relevant local climate site characteristics to avoid the use of the obsolete urban/rural distinction [Stewart and Oke, 2006]. Hence, the sky view factors, the built fraction, the soil moisture, the average building height and surface reflectivity and the anthropogenic heat fluxes as well, specify the single urban category into homogeneous urban terrain zones (UTZs). City are then described according to modern and old cores, compact housings, industrial processing, blocks, extensive low-rise, house and gardens and so on. There are then a broad variety of urban fabrics that is as much documented as in the urban planning documents.

At last, some authors took benefits of the resolution of the detailed airflow around a particular obstacle provided by classical CFD models (resolution of 1 m to 10 m). Thus, Tewari et al. [2010] and Miao et al. [2013] proposed using the climate outputs of the mesoscale atmospheric model WRF considering a resolution of 500 m as initial and boundary conditions for a CFD model. In their study, the mesoscale atmospheric model provides the boundary conditions to the CFD model each 5-15 minutes. Both authors showed that the coupling of a mesoscale model with a CFD model significantly improves the predictability of the urban plumes in the CFD model while the mesoscale model is showed to capture reasonably well the wind and temperature fields near the surface and in the boundary layer. Nevertheless, the complexity of the models are always inducing high computational requirements.

At last, urban areas are like a living organism that always recomposes. Some economical, residential, and commercial activities can decay meanwhile others could born or become attractive and quickly developed. This may trigger the development of new urban forms. In the geographer communities, a large branch of the research is focusing on the development of residential growth model based on the use of cellular automata model. The simplest ones use simple transition and neighboring rules to determine the state of a grid. The more complex ones integrate the economic and social factors that act on the household decision to settle down in a specific location and hence, the residential development. They are called the Land Use and Transport Integrated models. The agent-based MobiSim model developed at ThéMa (Besançon) is one such [Antoni and Vuidel, 2010]. It relies on the constitution of a synthetic population, the agents, characterized by socio-economic attributes (*e.g.* age, sex, income, and so on). Each agent can use a multimodal transportation infrastructure and occupy multifamily or single family dwellings by always following rational choices that are defined in the user settings of the model. For instance, the attractiveness of the green areas and the urban

services are considering in the choices of residential locations according to a ranking of the household preferences. The amount of new residential dwellings, the definition of the developable built-up areas, and the rules that are used to depict the home-to-work trips and mode of transportation of the agent rely on the geo-treatment of real urban planning documents. Thus, the complexity of the mechanisms behind the residential development and the mobility of the urban dwellers is step by step considered by sophisticated urban development models.
All those findings can serve improving the representation of the urban surface in the climate modeling system and the simulations of the building energy requirements by integrating in addition the behavior of the households in terms of residential locations and thermal stress and much more details building architectures and surface fluxes.

2.4 Discussion and conclusion

In the methods used for assessing the building energy performance and operating landscape and building strategies to cope with the impacts of climate change, systems of numerical and physically-based climate models receive more and more attention. They are based on the use of a mesoscale atmospheric model and urban canopy parameterizations that could include a simplified building energy model. The system of climate models considers the whole urban climate scales from the building up to the urban area. The mesoscale atmospheric model computes the evolution of the meteorological fields across a region discretized into 10 km to 1 km (recently 500 m and 250 m) atmospheric grids accounting for the presence of complex topography and built-up and non-built-up areas. The recent implementations of sophisticated urban canopy parameterizations permit to consider the sub-grid and average effects of a set of uniform buildings on the airflow thermodynamic in the urban boundary layer,as well as the urban heat island effect on the building energy requirements. To date the urge of designing climate change strategies and sustainable cities have led to develop a large set of quantitative meteorological and building energy indices that are integrated in the legal instruments and urban planning documents. It has fostered operational researches on the interactions between the building energy requirements and the urban climate that can be carried out also for 1 million or less populated metropolitan areas. Those new applications of the climate modeling systems increase at the same time the necessity of collecting high resolved spatial building and land cover informations to depict the heterogeneity of the urban areas and for considering accurate microclimate conditions when assessing the

building energy requirements.

Despite the increasing amount of high resolution urban databases, the application of the mesoscale atmospheric models seems however limited for urban planning issues. Indeed, the sub-grid heterogeneity is only partially accounting in climate modeling system: the sub-gridded advective processes are neglected, the vegetation is most of consider to be out of the street-canyon. More, the dynamics of the urban development is not taken into account. Nevertheless, some recent works proposed to benefit from the explicit resolution of CFD models of the airflow aerodynamic and thermodynamic properties around a single building or obstacle. Meantime others proposed using land cover-land-use classifications for specifying a large panel of urban fabrics in the mesoscale atmospheric domain and increasing grid resolutions (up to 500 m to 250 m). If the use of detailed land cover classification can found some echo in the urban planner communities, the adoption of high resolution may questioned the limits of the physical approximations adopted in the climate modeling systems. The next chapters are then dedicated to test the ability of the climate modeling systems to estimate the building energy demand and integrate urban planner preoccupations like the control of the residential development and the preservation of the green infrastructures.

Chapter 3

Fast methodology to assess building energy demand based on the use of the WRF/ARW-BEP+BEM climate modeling system

Abstract

With the reinforcement of the role of local authorities in designing operational climate change mitigation strategies, quantitative objectives of reductions of greenhouse gas emissions and energy consumptions largely penetrated most of the planning instruments. In this context, this study aims to develop a methodology capable of quickly assessing the building energy demand of any region taking into account the dynamic of the atmosphere, and in particular the effect of the urban heat island on the building energy requirements.

The methodology relies on the significant relationships found by previous studies between observed building energy consumptions and air temperatures, and their modeling through linear fittings (statistical model). The idea is to quickly reproduce for any surface conditions, study area or period such relationship by using the building energy and meteorological simulations of sophisticated climate modeling systems, in which the three-dimensional effects of the buildings on the atmosphere and the urban heat island are reproduced. The linear fittings permit to characterize the building energy performance of an area by using two parameters, the interception of the statistical model with the temperature axis or the base temperature, and the slope of the linear fittings or the sensitivity of the building energy requirement with the air temperature. Those two parameters are then used like in a degree-day method to quickly estimate the building energy requirements knowing in addition, the distribution of the air temperatures over a given period.

In this study, we simulated the air temperatures and the building energy requirements over the city council administrative limit of Strasbourg (France) by using the Weather Research and Forecasting (WRF) climate modeling system for 2010. It integrates the WRF mesoscale atmospheric model, the BEP urban effect parameterization, and the BEM building energy model.We gave particular attentions to reproduce in details the urban surface conditions. The simulations showed that the meteorological fields and the building energy requirements are well simulated by the WRF-BEP+BEM climate modeling system, and that such system is able in addition, to reproduce the significant relationships found between the building energy requirements and the air temperatures. Then, by simulating the impacts of current energy savings strategies, and building their corresponding statistical linear models, we showed that the climate modeling system is particular sensitive to the building intrinsic properties. It therefore encourages the development of sophisticate building energy behavioral models.

Keywords: *building energy, degree-day method, climate modeling system, energy conservation strategies*

3.1 Introduction

Energy savings in buildings and in particular residential buildings are regularly quoted in climate change mitigation strategies. Buildings represent about 40% of the end-use energy, in which more than the two third are dedicated for the residential housings. Accordingly, buildings represent 24% of the national greenhouse gas (GHG) emissions. Despite this, buildings represent a high potential of energy savings. Most of the consumed energy is dedicated for the thermal comfort. In France 62.1% of the 2011 end-use energy is dedicated for space heating according to ADEME [2012]. The thermal comfort in the buildings is influenced by the surrounding thermal environment, but also by the building intrinsic thermal properties. Thus, significant proportion of wasted energy due to defaults in the building construction and design can be save along with the building centennial life cycle with increasing thermal and energy performances. In France for instance, half of the national residential building stock dates before the adoption of the first thermal regulation (1974), and hence large energy savings can be achieve by improving the building energy performance of the residential buildings.

During the last years, quantitative statistical or numerical approaches have been increasingly used to assess the building energy requirements and help local authorities to implement energy efficient policies [Jones et al., 2007]. In the statistical approaches, the degree-day method produces fairly reliable statistical estimations of building energy demand for cooling (CDD) or heating (HDD) when building properties are relatively constant over time. The method relies on the strong linkage discussed by previous studies between the air temperatures and the heating/cooling energy consumptions [Thom, 1954, Quayle and Diaz, 1980]. The building energy requirement is estimated by using the building energy consumption sensitivity with the air temperatures P, and the statistical distribution of the gradients between the daily air temperatures and the base temperature. The base temperature represents the temperature at which the building energy needs is null. Usually, the building energy consumption sensitivity with the air temperatures P is obtained by linearly fitting the building energy consumptions-daily outdoor temperatures observations [Christenson et al., 2006, IEA, 2008]. The daily air temperatures issue from observational meteorological stations, while the base temperature, T_0, takes predefined values including between 10°C and 18°C. Recently Valor et al. [2001], Cartalis et al. [2001] and Amato et al. [2005] extended the degree-day method to estimate the electricity loads induced by the future climate change while Viejo-Garcia and Keim [2008] estimated the changes in the building energy use of the

Stuttgart metropolitan region (Germany) induced by its residential developments. In parallel, the increasing power capacity of the computers triggers new interests in microscale building energy models. Microscale building energy models are characterized by fine horizontal resolutions of few meters that permit to consider realistic building systems, and the surroundings site characteristics including the cloud covers and the shading of the exterior shading surfaces. Buildings are divided into homogeneous thermal rooms, in which the energetic dynamics of complex building envelop with the surrounding climate and the time varying building internal activity (*e.g.* the human occupancy patterns and the use of power equipment) are reproduced. A fortiori the most powerful codes such as Energy Plus and DOE-2 consider the dynamics and performance of Heat Ventilation and Air Conditioning systems used to meet predefined comfort temperature and humidity [Birdsall et al., 1990, Crawley et al., 2000]. Since the 1990's, several studies already took profit of such detailed building energy model for assessing the effect of cool roofs and tree shades on the building energy requirements of prototype buildings [Akbari et al., 2001, Rosenfeld et al., 1998]. Nevertheless, Spitz [2012] demonstrated that the use of standard climate (Typical Meteorological Year files) leads to over-estimate by up to +30% the simulated building energy demands. The TMY files are hourly meteorological files that are used to define the thermal environment of the buildings. They issue from 30 years averaged hourly meteorological variables taken out of the urban areas, and therefore, they miss-evaluate the local warming induced by the urban heat island.

Other studies took benefits of the numerical global or mesoscale atmospheric models [Christenson et al., 2006, Miller et al., 2008]. Despite their coarse resolutions (few kilometers), the mesoscale atmospheric models are able to reproduce the dynamics of the boundary layer, and in particular the urban heat island phenomenon. During the past 20 years, sophisticated urban canopy parameterizations (UCPs) that reproduce the three-dimensional effects of buildings on air dynamics and energetics (*e.g.* radiation and wind sheltering effects, heat trapping effects) have been implemented in many mesoscale atmospheric models. The SM2-U(3D) of Dupont et al. [2004] is implemented in the MM5 atmospheric model of Grell et al. [1994]. The Building Effect Parameterization BEP of Martilli et al. [2002] is coupled with the non-hydrostatic mesoscale model WRF of Skamarock et al. [2005] and the FVM mesoscale atmospheric model of Clappier et al. [1996]. The Town Energy Balance TEB of [Masson, 2000, Lemonsu et al., 2012] is implemented in the Meso-NH model of Météo France and so on. Recently and following the work of Kikegawa et al. [2003] and other scholars, the UCPs have been connected to simplified building energy models, which allow new application

studies on urban environmental issues (*e.g.* air pollution, anthropogenic heat, building energy requirement and so on). The simplified energy models are able to compute the energy dynamic of a floor considering internal heat gains due to the solar radiations, the presence of humans, the use of equipment and the activation of the Heat Ventilation Air Conditioning (HVAC) system. They have been widely employed to estimate the contribution of the anthropogenic heat in the urban heat island intensity.

3.2 Research objectives

Taken into consideration the recent improvements of the UCPs in the mesoscale atmospheric models and the observed relationship found between the air temperatures and the building energy requirements by previous studies, the objective of this study is to propose a new methodology able to quickly assess the building energy requirements over any part across the Globe and any period, and that is able as well to consider the dynamic of the atmosphere and in particular the urban heat island feedbacks on the building energy requirements.

For this, we used the Advenced Research Weather Research and Forecasting model WRF/ARW that integrates the Building Effect Parameterization of Martilli et al. [2002] and the Building Energy Model of Salamanca et al. [2010]. The system of climate models called the WRF/ARW-BEP+BEM allows investigating the dynamic of the atmosphere by considering the three-dimensional effects of the buildings on the atmosphere, as well as the building energy consumption feedbacks on the energetics and dynamics of the atmosphere. In addition the WRF/ARW-BEP+BEM climate modeling system enables us to consider any possible future depicted by changes in the surface and building properties.

In the following sections, section 3 describes the methodology used in this study. Section 4 presents the study case for which the methodology has been tested. At last, section 5 discusses in particular the building energy requirements and performance indexes obtained by using this new methodology.

3.3 The method

The building energy demand is highly sensitive to the weather conditions as discussed by Thom [1954], Quayle and Diaz [1980], Cartalis et al. [2001], Valor et al. [2001] and Amato et al. [2005]. Those scholars found a significant non-linear relationship between the air temperatures and the building energy consumptions over a year. In winter, the building energy consumptions are showed to decrease with the temperature rise. In summer, the building energy consumptions are observed to increase with the temperature rise. In between a plateau represents the building energy requirements that are non-temperature sensitive (*e.g.* cooking, lightening and so on). Commonly, the winter and summer branches of the building energy consumptions- air temperatures relationship are treated separately. This non-linear relationship is then summarized by a V-shape function for which distinct linear fittings (statistical model) of the summer and winter branches are performed. The slopes of the linear fits are the cold (or heat) building sensitivity with the air temperatures, while the interceptions of the linear fits with the axis of the air temperatures are the cold (or heat) base temperatures. Considering the cold sensitivity P and the base temperature T_0 it is possible to write the daily building energy demand at time i, noted EC_i (in Wh), like:

- For heating:

$$EC_i = P.min((T_i - T_0); 0) \tag{3.1}$$

- For cooling:

$$EC_i = P.max((T_i - T_0); 0) \tag{3.2}$$

In equation 3.1 and 3.2, the base temperature T_0 represents the temperature at which for a given internal temperature, the building energy budget is in thermal equilibrium with its surrounding. The base temperature T_0 is said to be influenced by the surroundings characteristics, non-temperature weather variables (e.g. humidity and wind), building design (*e.g.* insulating properties) and cultural preferences (*e.g.* comfort temperature) according to Valor et al. [2001] and Amato et al. [2005]. Usually, the base temperature T_0 is predefined and taken equal to nearly 18.33°C (*e.g.* 65°F) for heating and at 21°C for cooling. It should be acknowledged that other studies, even sociological studies [Crédoc, 2010], suggested higher (or lower) base temperature in winter (or summer). Valor et al. [2001] reported base temperature equal to 15°C when considering the space heating of the Spanish building stock while Christenson

et al. [2006] took the base temperature equal to 8°C, 10°C and 12°C for their Swiss study case.

In the same equations, the slope of the statistical model P could be physically interpreted as the cold (or heat) building energy sensitivity with the air temperatures (in Wh/°C). Hence, the cold (or heat) building energy sensitivity P can be influenced by the surrounding weather conditions such as the intensity of the Urban Heat Island as well as the building intrinsic properties.

At last, T_i (in °C) in equations 3.1 and 3.2 refers to the daily air (or outdoor) temperatures. According to Christenson et al. [2006] there are many definitions of degree-days and daily temperatures. The daily temperature could be the average of the 24 hourly outdoor temperatures, or the average of the maximum and minimum temperatures of the day. The latter is often preferred as it is assumed to better capture the peaks and valleys of the building energy requirements in a day [Valor et al., 2001].

Starting from the daily energy demand set in 3.1 for heating, the total energy requirement over a specific period J, Q_J could be expressed as an integral:

$$Q_J = P. \int_{j=1}^{J} min[(T_i - T_0); 0]dt \tag{3.3}$$

And hence,

$$Q_J = P. \sum_{j=1}^{J} min[(T_i - T_0); 0]dt \tag{3.4}$$

Assuming that D_J is the total degree-day over a period J, the total energy load becomes:

$$Q_J = P.D_J \tag{3.5}$$

If T_i keeps below T_0, it is possible to express 3.4 according to averaging quantities according to 3.6.

$$\overline{EC_J} = P.(\overline{T_J} - T_0) \tag{3.6}$$

With:

$$T_j = \frac{1}{n_j} \sum_{j=1}^{n_j} T_i \tag{3.7}$$

Following and considering that D can be easily computed, several cases can be considered:

- If T_0 is known and P is unknown, only one previous estimate of building energy load over a time period is needed to compute P by using 3.5.

- If P is known and T_0 is unknown, one previous estimate of the average building energy load over a time period and the corresponding average outdoor temperature are required so that:

$$T_0 = \overline{T_J} - \frac{\overline{EC_{J1or2}}}{P} \tag{3.8}$$

- If both T_0 and P are unknowns, two previous annual estimates of total building energy loads and outdoor temperature are needed to compute P and T_0 according to 3.9.

$$P = \frac{\overline{EC_{J_2} - \overline{EC_{J_1}}}}{\overline{T_{J2}} - \overline{T_{J1}}} \tag{3.9}$$

With J_1 and J_2 are two time periods.

As a consequence, it is possible to determine easily any parameters of the statistical model.

In the present study, the statistical models presented in equations 3.1 and 3.2 are expected to enable us to quickly estimate the building energy requirement for any period and region. The WRF/ARW-BEP+BEM climate modeling system is used to provide long time series of hourly-simulated air temperatures and its building energy requirements.

The WRF/ARW-BEP+BEM climate modeling system allows considering:

i) the influence of the non-temperature variables on the building energy requirements such as the wind speed and air moisture;
ii) the changes in the urban climate with changes in the surface and building properties;
iii) the influence of cross-scaled processes involved in the urban climate and their feedbacks on the building energy requirements.

The WRF climate modeling system consists in the non-hydrostatic Weather Research and Forecasting (WRF) model of Skamarock et al. [2005] and the BEP+ BEM urban canopy parameterization of Martilli et al. [2002] and Salamanca et al. [2010] that have been implemented since 2002 and 2012 respectively in the WRF mesoscale atmospheric system.

The WRF mesoscale atmospheric model is a terrain-following mesoscale atmospheric model that resolved the conservative Navier-Stock equations for the momentum, pressure, energy and mass. Several options for various physical processes are included in the WRF mesoscale atmospheric model (*e.g.* turbulence in the planetary boundary layer, water transfer soil models, and radiative budgets), but the WRF mesoscale atmospheric model has the particularities to account for the presence of the hydrometeors. Among the available land-surface models, the Noah LSM Chen [2007] is commonly used to compute the sensible and latent heat fluxes as well as skin temperatures of the surfaces. The Noah LSM also interfaces the BEP+BEM urban canopy parameterization with the mesoscale atmospheric model each time a built-up area is included in an atmospheric grid. The BEP+BEM urban canopy parameterization represents the sub-grid energetic and dynamic processes originated by the presence of buildings.

In particular, the Building Effect Parameterization BEP (Figure 3.1 a) computes the surface turbulent fluxes for momentum, kinetic energy, heat and humidity for refined vertical canopy grid immersed in the atmospheric grid each time the buildings interact with the atmosphere. A building is shaped with a roof and a wall, and a building and its bordering street form an urban canyon. In the BEP building effect parameterization, the urban canyons are oriented according to the North and considered as well, uniform and infinite long. Two urban canyon orientations are possible and the urban canyons are delimited only with square cross-sections. The vertical heterogeneity of the buildings in a given urban canyon is modeled with a height probability function. In the BEP building effect parameterization, the dynamical perturbations of the flow induced by the buildings are taken into account with the use of a distributed drag force

approach and a modified Bougeault and Lacarrère [1989] scheme where the turbulent length scales are adapted for accounting for the presence of the buildings. In addition, distinct energy budgets for plane (*e.g.* roofs and streets) and vertical (*e.g.* walls) surfaces of the street-canyons are resolved to better model the skin temperature of the buildings and the urban canopy heat fluxes. At last, the three-dimensional radiative budget is adapted to account for the multi-reflections of the longwave radiations and the shading in the urban canopy layer.

The Building Energy Model BEM (Figure 3.1 b) computes the energy budget for each floor of an occupied standard building and the way the resulting energy is exchanged with the building surrounds. The model represents internal heat and humidity gains by:
i) solving a 3-dimensional room radiative budget accounting for windows;
ii) solving a one dimensional conduction equation for each layer of a layered wall system, and by considering;
iii) the unintentional natural ventilation;
iv) the wasted heat generated by the occupants and the equipments.

User-defined humidity and temperature comfort ranges drive the model of the Heat pump and Air Conditioning system. The latter computes the building heating and cooling energy requirements and the amount of heat and humidity fluxes that have to be ejected in the atmosphere to maintain the floor in the temperature and humidity comfort ranges.

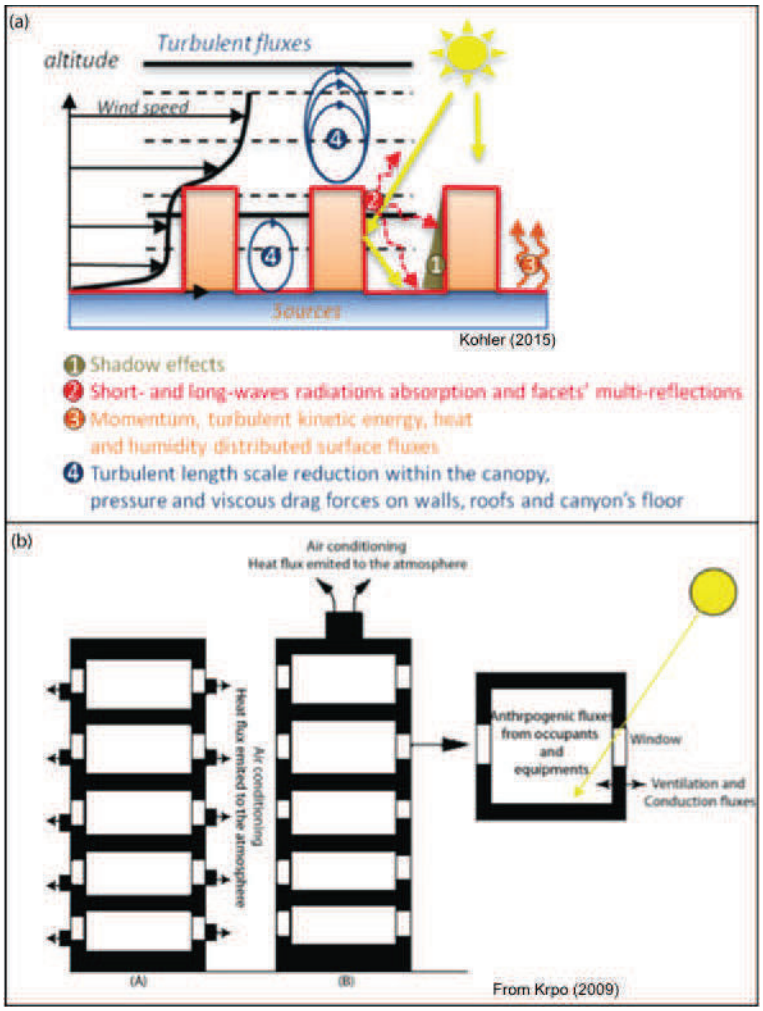

Figure 3.1: Presentation of the dynamic and thermodynamic processes taken into account by the BEP a) and BEM b) parameterizations.

Thus, like Salamanca et al. [2012], the total building energy loads EC over the atmospheric domain could be estimated for a period T according to:

$$EC = \int_0^T (\int \int_{domain} ec.dx.dy)dt \tag{3.10}$$

Where the grid dimensions are dx and dy and the time step is dt.

Given the building energy requirements and the outdoor temperatures simulated by WRF/ARW-BEP+BEM climate modeling system, the "building energy requirements-daily outdoor temperatures" relationship could be drawn to obtain the complying cold sensitivity P and the base temperature T_0 of statistical model. The latter can be used to rapidly estimate the heating and cooling energy performance of any urban region over any time period.

3.4 The study case

The method has been tested over the Strasbourg-Kehl urban region (France-Germany) for 2010. The building energy requirements for space heating are only considered since they represent in France more than the half of the residential building energy consumptions. A fortiori, the minister of Ecology reported in 2009 that only 3.6% of the residential buildings in France are equipped with individual AC for cooling.

3.4.1 The Strasbourg euro-metropolitan area and the ASPA energy consumption inventory

The Strasbourg great city (48°35'05"N and 7°4'02"E, elevation: 132-151m) is located in the flat area of the Rhine Graben in the Alsace Region (France). The climate is depredated oceanic according to the Köppen classification (type Cfb) with well defined seasons. The presence at West of the Vosges and at East of the Black Forest mountains shelters the area from mild and wet Westerlies as well as from the arrival of cold fronts. As a consequence the wind is low to moderate and often directed North-South. High frequencies of foggy days (56 days/year as much as Brest located close to the oceanic coasts) and snow (30 days per years in average that is more than some pre-alps cities) are singularities of the area. In particular, the study focuses on the 305.97 km^2 of the city council of Strasbourg (CUS). The CUS gathers 28 towns that are part of the metropolitan area of Strasbourg [CUS, 2005]. Figure 3.2 a) shows the innermost domain, the Urban Region of Strasbourg-Kehl (URSK) domain used in the WRF/ARW-BEP+BEM climate modeling system. It is centered on the Strasbourg city council (CUS). The largest domains are the parent domains. They provide the meteorological lateral and top conditions to the URSK domain are represented in figure 3.2 b).

As an attractive pole, the CUS represent 45% of the active population of the Bas-Rhin district ,which are mainly provided in the commercial and tertiary sectors (*e.g.* retailed trade, operational services, health and financial activities, restoration and hotel business). The proximity of the German frontiers fosters cross-borders daily commut-

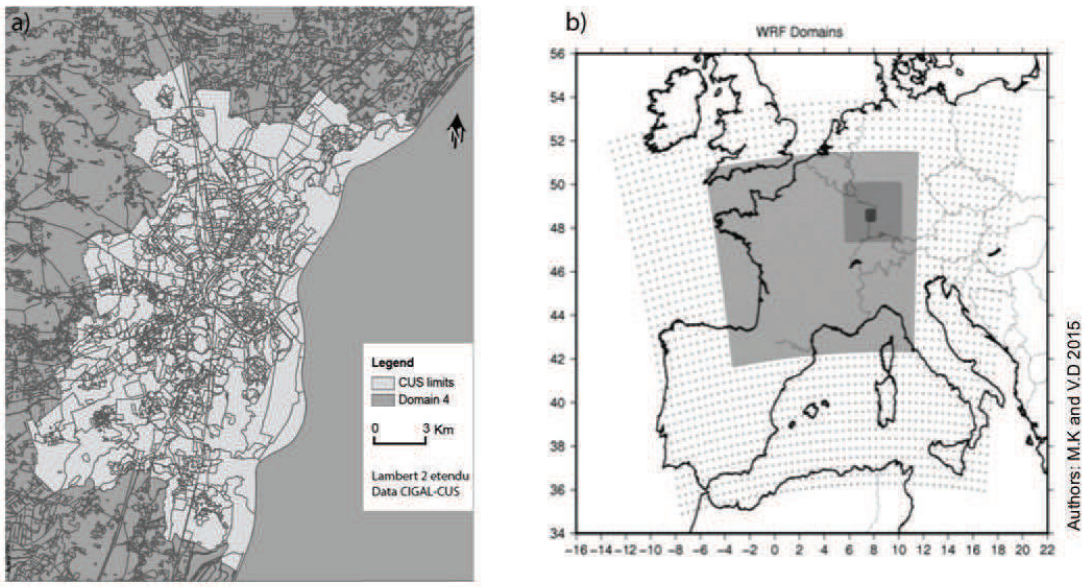

Figure 3.2: The URSK domain and the coverage of the WRF simulation domains.

ing and is part of the socio-economic regional dynamics. The CUS accounts for about 450,000 inhabitants in which 60% house in the urban main center, Strasbourg.
Likewise all French cities, which count more than 50 000 inhabitants, the CUS inventories its energy consumptions and greenhouse gases emissions in the framework of the "Plan Energy Climat Territorial". A reduction of 30% of the local GES emission and energy consumption is announced. Because the building stock of the CUS is mainly composed by renters (62%), it makes the objectives challenging [CUS, 2009]. It should be acknowledged that the classification of the center of Strasbourg in the UNESCO world heritage list can act as barriers to building renovations and improvements of the building energy performance of the neighborhood.

The local air quality agency (ASPA) is often mandated by the CUS city council to provide throughout atmospheric knowledge over the CUS territory. In 2006 and then in 2010, the ASPA characterized the CUS building energy consumption of the CUS territory following a bottom-up approach. The ASPA took benefits of the INSEE dwelling database and the building energy consumption intensities (in J/m^2) provided

for each prototype building of the national building stock by the CEREN. The INSEE dwelling database characterizes the building stock and include building energy performance related variables. The date of the end of the building construction according to milestone years (*e.g.* the adoption of thermal regulations), the type of dwellings (*e.g.* individual or collective), its category (*e.g.* main residence), the number and surface of the rooms, the type of the heating system (*e.g.* individual or collective) and the types of fuels (*e.g.* conventional domestic fuel, coal, natural gas, electricity, urban heating system, woods and LGP) are as much variables that can be used for describing the building energy performance. Thus this large dwelling database allows the segmentation of the building stock into coherent building energy performance segments for which a prototype building is assigned. Knowing the share of each building energy performance segment in the "îlot" statistical unit and the building energy consumption intensities of their prototype buildings, it is then possible to calculate the "îlot" overall building energy consumption. Figure 3.3 mapped the corresponding building energy consumption intensities considering in addition the building plan area fraction of the lot. In total the ASPA found an overall building energy consumption of 15,274,755 GJ over the CUS administrative area.

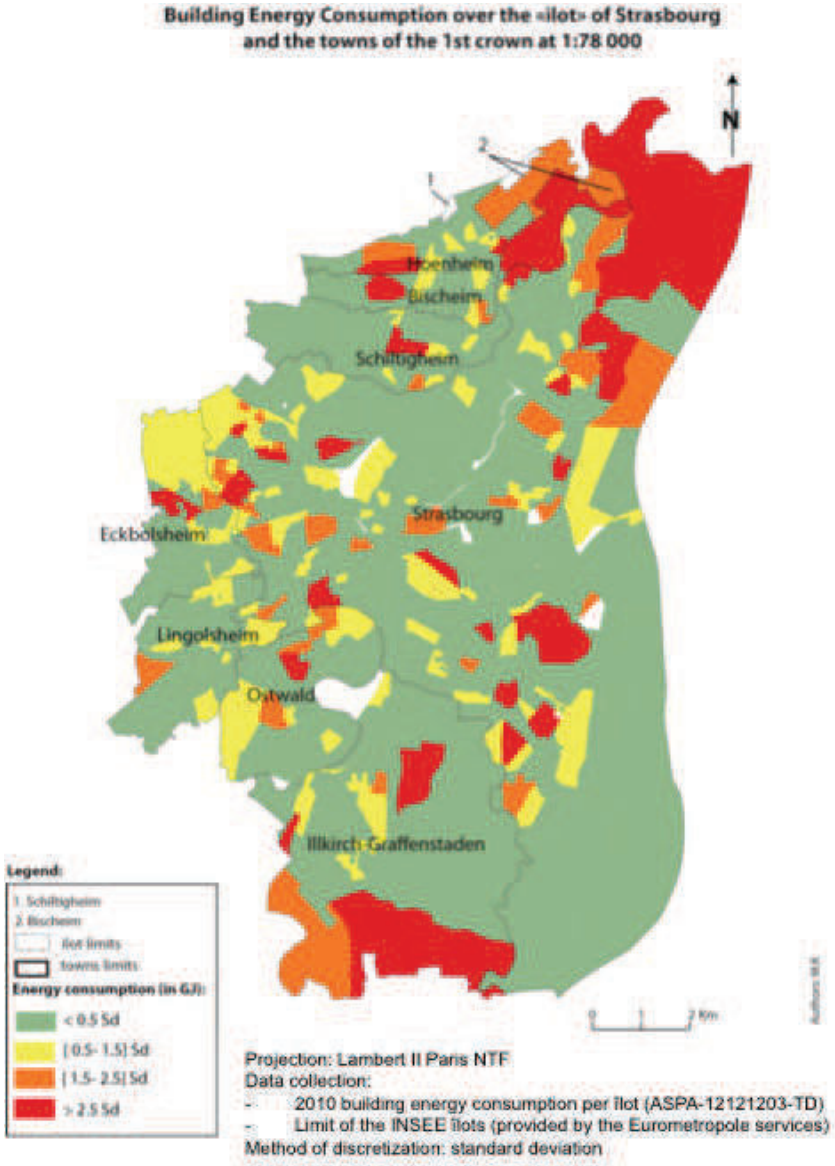

Figure 3.3: Mapping of the intensity of the building energy consumption over Strasbourg and the towns of the first crown. The energy consumption has been standardized by the building plan area density per "îlot".

Nevertheless, some limitations can be underlined:

- The socio-economical dimension of the energy consumption is neglected by considering a standard use of the housings included in a same building category.

- The approach miss-evaluates the dynamical changes in *1)* the building stock properties and the residential development, and *2)* the variations of the local climate.

1) The survey of the dwellings that is used to describe the building stock is up-dated each 4-5 years over the French metropolitan area. With rapid urban growth, the use of this dwelling database can produce discrepancies in the estimates of the building energy consumptions. Fortunately, the construction activity remains slow since the 2000's over the study area. The local development plan inventoried 8,874 new dwellings between 2003 and 2007 and 50, 681 new dwellings between 1985 and 2007 for the Strasbourg agglomeration [CUS, 2009].

2) The period of heating is defined by convention from 1^{st} October to 31^{st} May according to the petroleum comity neglecting the variations of the climate from one year to another.
One more, a climate stress factor calculated like the unified Heating Degree Day is considered. It is computed using a predefined base temperature set at 17°C and outdoor temperatures simulated by the mesoscale atmospheric model MM5 of Grell et al. [1994] over the AtmoRhena domain. The AtmoRhena domain covers the upper Rhine valley and includes the Alsace region and a part of Germany with an atmospheric grid resolution of 3 km. In the AtmoRhena simulations, the urban areas are represented like in the traditional roughness approach as warmer and rougher spots (referred as the roughness approach or MOST theory) in the region. No three-dimensional building effect parameterizations are considered and thus the urban heat island effect is neglected.
At last, an additional climate correction is applied to interpolate the 2006 building energy consumption in 2010. Then the ASPA used the ratio of the degree-days between a given "îlot" and a meteorological station of reference (here located at Entzheim airport). It is therefore assumed that the ratio does not change over years.

3.5 Settings of the climate modeling system

3.5.1 Settings of the mesoscale atmospheric model

The URSK domain atmospheric grid consists in 27x33 rectangular C-Arakawa grids of 1 km horizontal resolution and 28 stretched pressure levels according to a 5000 Pascal top pressure in the vertical. Its initial and lateral meteorological conditions are

provided by the other coarse resolution parent-domains, which atmospheric grid sizes range from 45 km to 3 km. The 2010 National Centers for Environmental Prediction meteorological global data reanalysis (NCEP-FNL) provides the meteorological conditions to domain 1 each 6 hours. The ARW core solves each 5 days fully compressible and non-hydrostatic Euler conservative equations for the wind velocity, the potential temperature perturbations, the surface pressure perturbation of dry air and the geopotential perturbation considering a third order Runge-Kutta scheme, a spin up time of 5 days, and a time step of 100 seconds for advection. As advised by Martilli et al. [2002] and Salamanca et al. [2012] the Bougeault and Lacarrre (Boulac option) k-ϵ turbulence model is adopted. The influence of water vapor on shortwave and longwave radiation processes is taken into account through the Dudhia [1989] shortwave radiation scheme and RRTM options respectively. The Thompson et al. [2004] scheme that explicitly resolves water phase's transformation is selected for the microphysics. At last, the NOAH Land Surface Model (LSM) computes the surface fluxes (latent and heat fluxes) as well as the skin temperature considering a roughness approach for non-urban areas while the BEP+BEM urban canopy parameterization does so for the urban areas.

Because surface coverage is critical for representing accurate land-surface exchanges and planetary boundary layer dynamics [Xiu and Pleim, 2001], the regional high resolution and multisource land use land cover CIGAL dataset (BdOcs_2008) is used for defining the 2010 land cover properties over the French part of the URSK domain. The correspondence between the different land cover classifications is found in figure 3.4 while the 2010 land cover map is presented in figure 3.5. The land cover database named BdOcs_2008 has a precision of 1:10,000 and shapes an up-to-date spatial land cover database obtained from multisource spatial informations such as: *i)* SPOT 5 satellite images taken in October 2007 and February 2008 with a spatial resolution of 2.5 m and several bands dedicated to vegetation; *ii)* orthophotographies with spatial resolutions of 50 cm provided by the IGN; *iii)* urban development plans provided by the CUS and so on. Finally, the MODerate resolution Imaging Spectroradiometer (MODIS) 2001 land cover dataset fills the no data in the URSK domain (German part). The MODIS land cover dataset (2001) is indeed more up-to-date than the USGS global land cover dataset (1997) [Chen, 2007].

The BdOcs_2008 provides, in particular, the dominant land cover types of each atmospheric grids and the ratio of the total built-up area included in each atmospheric urban grid on the atmospheric grid coverage (the urban fraction) over the French part of the URSK domain. The urban fractions enable us to determine whatever an atmo-

spheric grid is urban or not by considering an urban fraction threshold. We lowered the initial urban fraction threshold 0.5 to 0.2 for representing small urban settlements: the cumulated built up areas in an atmospheric grid should represent more or 20% of the atmospheric grid coverage. Then, the urban grids are describes by an urban and non-urban fractions. The remaining non-urban fraction is by default assigned to croplands and mosaic of natural vegetation types while one of the three available urban types of the climate modeling system can describe the urban fraction of the urban grids.The three urban types are high intensity residential buildings, low intensity residential buildings and commercial and industrial buildings. The latter are characterized by their functions, building density and vegetation areas.

Land cover classes	Descriptions CIGAL (CIGAL 2011)	Descriptions MODIS and BEP classifications (Friedl et al. 2010, Martilli 2009)
Urban classes		
Commercial & industrial estates	Built up infrastructures dedicated to production and services activities. Public institutions (University, cemetary are included in this class	Infrastructure where constructed materials represents more than 30% of the cover that is not considered as high or low intensity residential types.
High intense residential	Built up areas characterized by a high building and transportation network densities dedicated in particular to residential activities. Baren soils and vegetation are scarce.	Highly developped areas characterized by row of houses, complex appartments, vegetation cover < 20% and constructed materials > 80% of the cover, dense population.
Low intense residential	Building areas mixed with vegetation and bare soils. It includes as well collective buildings, parking lots and individual housings that are characterized by low building density.	Mixture of constructed materials and vegetation (construction materials 30-80%) lower population density than high intensity residential class, single family housings units.
Built up classes with no distinction between the classes mentionned above	Buildings and built-up areas (no distinction in the urban classes), transportation networks (motorways and airport runways)	Man-made structures
Other semi-natural classes		
Water bodies	Includes all the natural and artificial water bodies (lake, harbor bassins, rivers)	Ocean, seas, lake, rives that can be fresh or salt water
Croplands mixed with natural vegation mosaic	Family gardens, urban greens and linear tree plantations (hedges, treefarm)	Lands with mosaic of lands that represents each less than 60% of the land coverage. It includes crops, forests, shrubs, and grasslands.
Croplands	Intensive and annual agriculture (maize), greenhouses	Temprorary crops with bare soil periods
Grasslands	Meadows and lawns dedicated for farming activities	Herbaceous vegetation. Trees and shrubs represent less than 10% of the landscape covers.
Shrublands	Open areas characterized by reconquest low vegetation and small trees	Herbaceous vegetation and small woody vegetation (heigth<2 meters), canopy cover is 10 - 60% of the shrubland floors.
Mixed forest	Forests composed by half needleaves and half decideous broadleaves tree species	Mixture of forests types (none exceed 60% of the landscape), tree hight > 2 meters, forest canopy cover > 60% of the forest floor.
Decideous broadleafs forest	Forests composed by more than 75% of decideous trees species	Annual leaf-on and leaf-off cyclicity, broadleaf forest > 60% of the landscape coverage. forest canopy cover > 60% of the forest floor, tree height > 2 meters.
Evergreen needleafs forest	Forests composed by more than 75% of needleaves trees species	Evergreen foliage, forest coverage> 60% of the landscape. forest canopy cover >60% of the forest floor, tree height> 2 meters.

Figure 3.4: Table of equivalent land cover types for the three land cover datasets.

The resulting URSK land cover map (CIGAL) is qualitatively realistic as showed in figures 3.5 and 3.6. In figure 3.5 presents both the MODIS and CIGAL land cover maps. Figure 3.6 presents the maps of the three urban types in the study area considering solely the BdOcs_2008. At last table 3.1 provides the number of urban grids considered by the climate modeling system (n_{urb}) and building area (Ab) for both cases. The building areas are compared with the BdOcs_2008 building area obtained by GIS techniques.

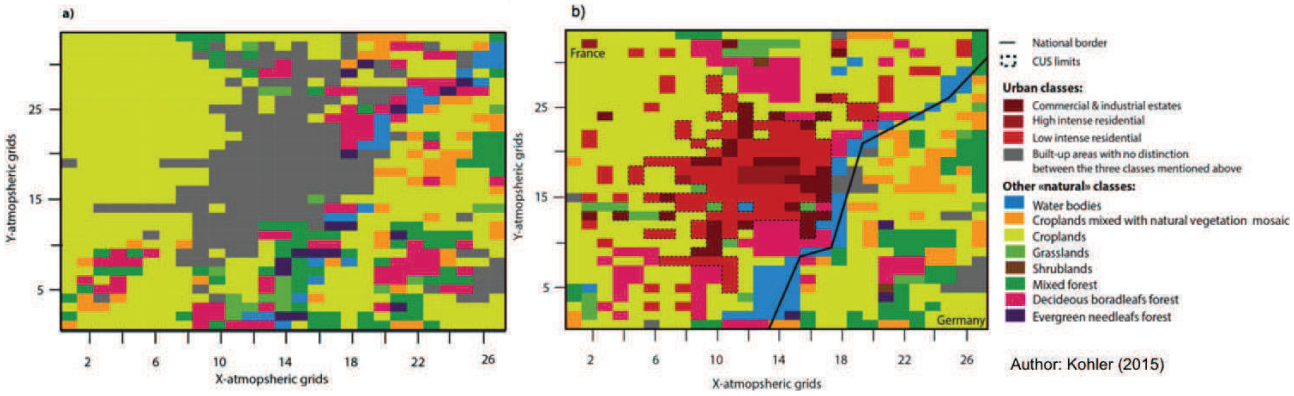

Figure 3.5: Comparison of the land cover maps provided by the WRF/ARW mesoscale atmospheric model using the MODIS (at left) and the CIGAL BdOcs_2008 (at right) datasets.

	BdOcs_2008	MODIS land cover	CIGAL land cover
A_b (in km^2)	85.49	187.15 (+74%)	68.64 (-21.86%)
n_{urban}	-	197	167

Table 3.1: Comparison of the built-up areas provided by the local development plan and the climate modeling system using, first, the MODIS land cover and urban types associated generic urban fractions, and second, the BdOcs_2008 land cover and corresponding built-up areas. Relative differences are calculated between the BdOcs_2008 land cover and respectively the MODIS land cover and the CIGAL land cover.

In table 3.1, the differences in the building area are the smallest in the CIGAL land cover datasets (-21.86%). The resolution of the spatial information explain the accuracy of the total built-up area. Nevertheless, it is showed that the building areas are under-evaluated. It could be an effect of the 20% rule. The MODIS land-cover shows the greatest differences with the BdOcs_2008 building area. Even with an urban fraction threshold set at 0.5, the building area is considerably over-estimated (+74%).

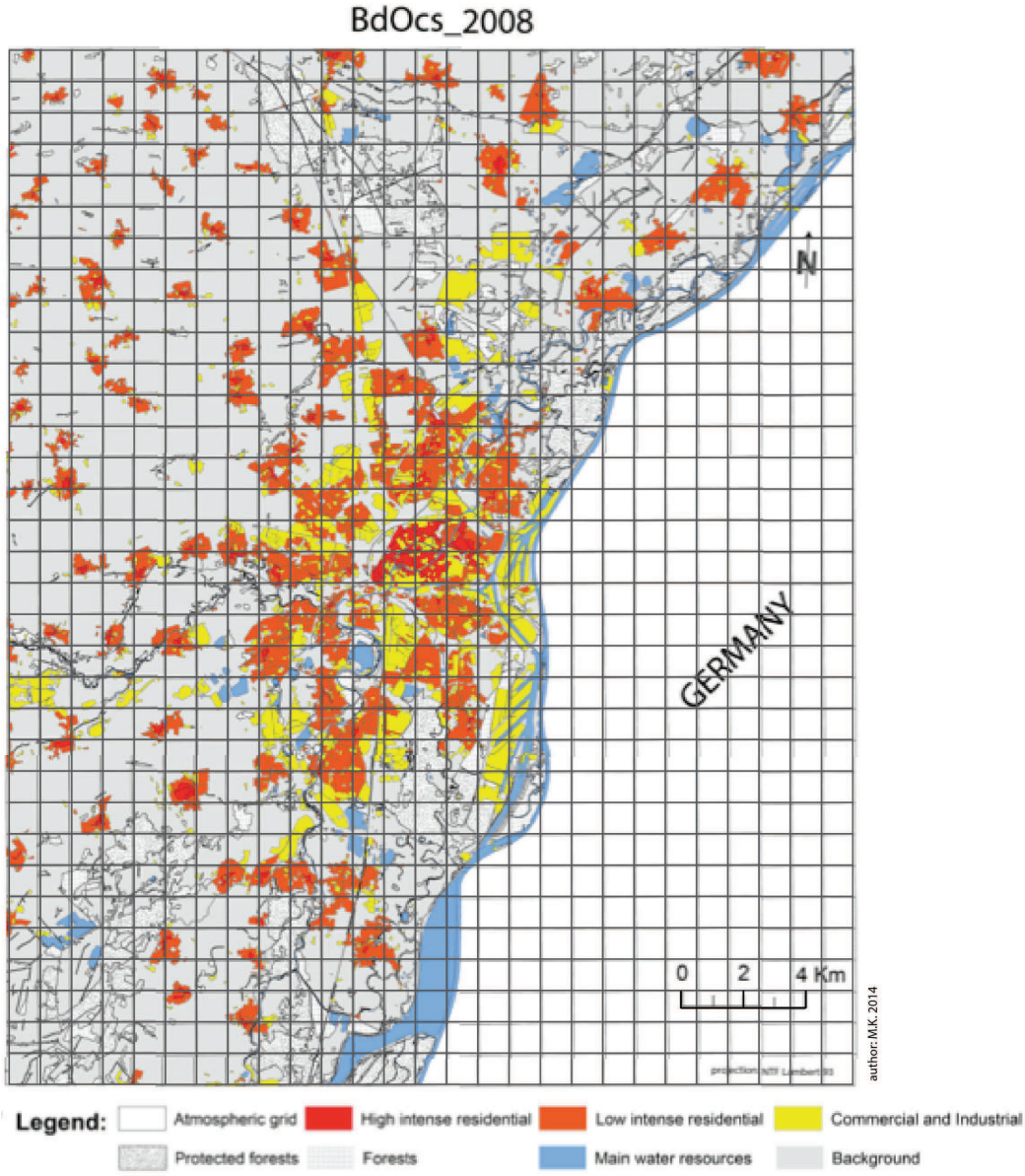

Figure 3.6: The BdOcs_2008 land cover.

It is due to the use of generic urban fraction for each urban type (here, 0.9) for assessing the building areas of each urban grid. Additionally, the number of urban grids is reduced in the CIGAL land cover compared to the MODIS land cover. This can be explained by the misclassifications of some lands in the MODIS land cover and to the higher accuracy of the CIGAL land cover compared to the MODIS land cover.

3.5.2 BEP and BEM selected parameters

The BEP + BEM considers that the urban areas are made up by three types of urban fabrics: the high intensity residential characterized by high population density and construction surface (*class 32*), low intensity residential (*class 31*) where constructed material is mixed with vegetation, and the commercial and industrial estates (*class 33*). In this study, transportation infrastructures are considered apart in the MODIS built-up class (*class 13*). The non-urban fractions of the urban atmospheric grids are defined as mosaic vegetation and croplands for reproducing the highly irrigated low urban vegetation. The American megacity urban parameters proposed by defaults are adapted for European urban areas. For this, we used several high resolution GIS spatial databases (*e.g.* Google earth satellite images, the 2012 BDtopo® of IGN, the 1999 population census of INSEE), scientific and grey literature and collaborative websites on building constructions. This permits to reproduce as real as possible the Strasbourg great city street-canyons' equivalent geometry (*e.g.* the canyon directions *dir.* counting 0° as the North, the building height H distributions, the building and street widths along with the North/South and West/East street-canyons respectively Bx, By, Wx and Wy in meters, and the ceiling height *dzcan*), as well as radiative and thermal surface properties and building's standard occupancy for each type of urban fabric (*Utype*).
Table 3.2 details the treatments adopted for each canyon parameters and urban type (Utype).

Parameters	Data	Treatments	Adopted parameters
dzcan	-	-	The vertical resolution of the BEP grid constrains the ceiling height. Thus the vertical resolution is set equal to 3 m.
dir.	Google Earth ®	Analysis of random samplings of prototype Utypes	class 31 (Palais Universitaire neighborhood): 45° N/S and 315° W/E ; class 32 (place Kléber neighborhood): 315° N/S and 45° W/E ; class 33 ("Port du Rhin" neighborhood) : 0° N/S and 90° W/E.
H	BDtopo ®	Building height distribution obtained by GIS geoprocessing.	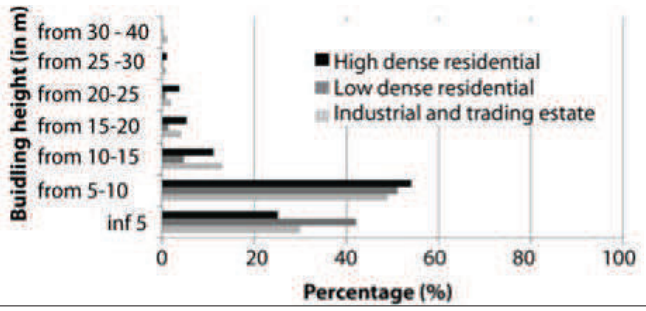
W	BDtopo ®	Adaptation of building's and street's widths (in the table for each Utype) to minimize the relative differences (in %) between the total building envelop and volume. We used the BDtopo ® (shallow grey) and assume cubic buildings.	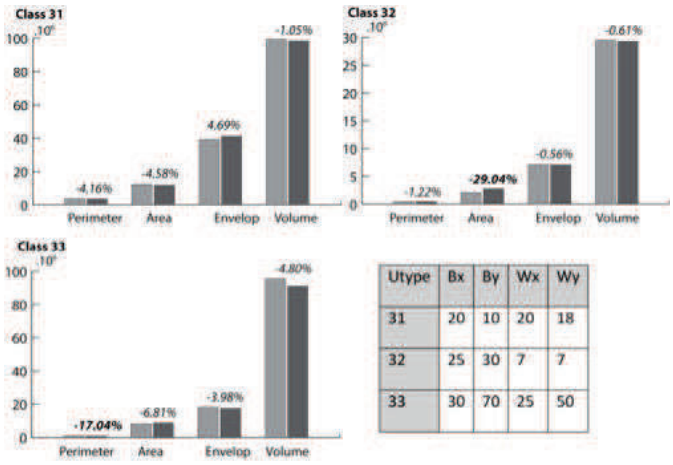

Utype	Bx	By	Wx	Wy
31	20	10	20	18
32	25	30	7	7
33	30	70	25	50

Table 3.2: Street-canyon morphological parameters.

The radiative and thermal proprieties of the layered building wall systems are presented in table 3.3 while figure 3.7 displays the material compositions and thickness for roofs, walls, floors and undergrounds that have been retained for representing the thermal behavior of the buildings.

For the BEM model other parameters such as the human metabolic heat rate, the heat wasted by the equipments, their daily use profile and the performance of the ventilation and HVAC systems have to be specified. Table 3.5 gives the BEM setting-up parameters. Unless floor population density and windows fraction, they are set by consulting scientific, official and building construction dedicated sources. The floor population density is obtained by setting proportional the 1999 IRIS (census unit) pop-

Building material	**Heat diffusivity** ($mm^2.s^{-1}$)	**Heat capacity** ($kJ.m^{-3}.K^{-1}$)
Roofs (Albedo: 0.1, Emissivity: 0.9, Roughness length: 0.01) from Krpo [2009] and weather.msfc.nasa.gov		
OSB	*0.13*	*982.08*
Air (1.2 kg/m^3)	*21.74*	*1.20*
Vapor check membrane	*7692.30*	*298.99*
Glass wool (18 kg/m^3)	*2.37*	*18.53*
AGEPAN	*1.29*	*58333.00*
Brown tile	*0.59*	*655.00*
Walls (Albedo: 0.2, Emissivity: 0.9, Roughness length: -) from Krpo [2009]		
Gypsum (BA13)	*0.30*	*831.60*
Air (1.2 kg/m^3)	*21.74*	*1.20*
Glass wool (18 kg/m^3)	*2.37*	*18.53*
Standard performed bricks	*0.59*	*655.00*
Roughcast in cement	*0.48*	*1642.00*
Undergrounds and floors		
Concrete	*1636.90*	*2167.20*
Glass wool (18 kg/m^3)	*2.37*	*18.53*
Air (1.2 kg/m^3)	*21.74*	*1.20*
Street (Albedo: 0.05, Emissivity: 0.95, Roughness length: 0.01) from Krpo [2009])		

Table 3.3: Radiative, thermal, and aerodynamic properties of buildings.

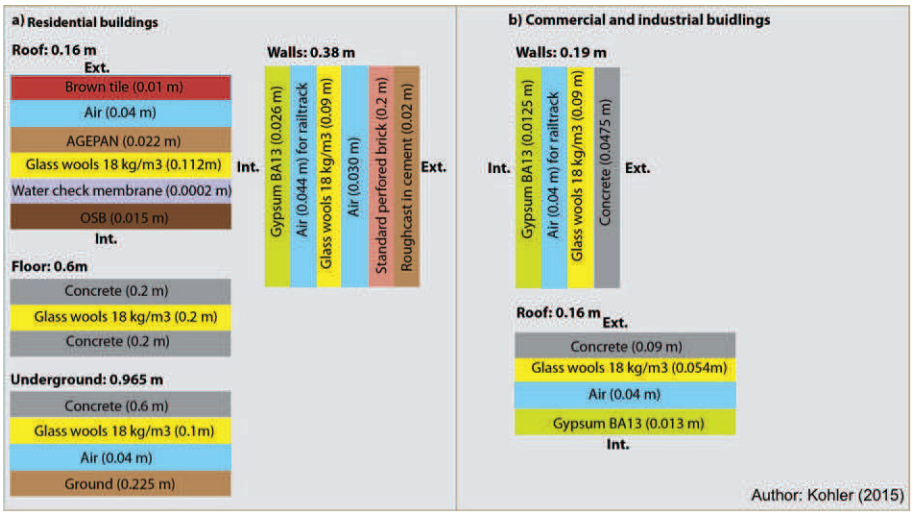

Figure 3.7: Composition of the building shell layers.

ulation census with the 1999 built-up area included in each atmospheric grid provided by the BDtopo®. A correction in applied on the resulting population to get the 2010 population census. The correction is done by considering a linear growth between 1999 and 2010 according to the 2005-1999 population growth issued from INSEE [2007]. The estimated 2010 population is showed to be slightly over-estimated (+1.22%) for the CUS limits and the Strasbourg center (+0.77%) when assuming a linear growth

between 1999 and 2010 and when comparing with the official population census. Table 3.4 shows the population in 1999 when setting proportional the 1999 IRIS (population census with the BDtopo®, the estimated population in 2010, the floor area considered by the BEP model and finally the population floor density considered in the BEM model.

Urban class	**Utype 31**	**Utype 32**	**Utype 33**
Population in 1999 (in inhab.)	315,873.0	63,533.2	89,556.9
Population in 2010 (in inhab.)	334,608.0	67,0288.1	94,587.0
Total floor area (in m^2)	32,787,972.0	9,767,846.0	30,353,366.0
Population floor density (in inhab/ 100 m^2)	1.02	6.86	0.31

Table 3.4: Estimated population, floor area and population floor density for each urban type.

At last, the windows fraction on each building wall is defined by considering a prototype residential buildings.

Parameters	Chosen settings	Literature review
Windows -to-wall fraction	15% for residential and 20% for commercial & industrial buildings	$1/6^{th}$ of the building living space [IAURIF, 2008] ; 0.2 [Salamanca et al., 2012]
Population density	1.02 ind. for 100 m^2 (Utype 31), 6.86 ind. for 100 m^2 (Utype 32) and 0.31 ind. for 100 m^2 (Utype 33)	2 individuals for 100 m^2 [Salamanca et al., 2012]
Metabolic heat rate	80 Watts	A man of 75 Kg emits 75W (at rest) and 100-200W (extreme activity) [Sailor, 2011]; An adult emits 63W (asleep) and 90W (in activity) (MEDDTL 2012); An individual emits 75W (at rest) and175W (at maximum) [Allen et al., 2011] ; An individual emits 54.7W [Kikegawa et al., 2003]
Peak heat generated by equipment	Pk=36 W/m^2	Pk=36 W/m^2 and 20 W/m^2 for commercial/industrial buildings and for residential respectively [Salamanca et al., 2012] ; Pk=5.58 W/m^2 for a typical Hausmannian building and an internal heat generation of 38.61 W/m^2 and 193.05 W/m^2 plan area respectively for residential and offices [Bueno et al., 2011]; Pk=5.7 W/m^2 the day and 1.1 W/m^2 at night [CSTB, 2012]
Ventilation rate	$\beta = 0.75$	$\beta = 0.43$ in Paris and $\beta = 0.5$ in Toulouse[Bueno et al., 2011] ; $\beta = 0.75$ [Salamanca et al., 2012] ; $\beta = 0.6$ [Kikegawa et al., 2003]
Humidity target	0.005 kg/kg	[Salamanca et al., 2010]
Humidity gap	0.005 kg/kg	[Salamanca et al., 2010]
Temperature target	T_{targ}=293°K +/- 0.5°K (19.85°C)	T_{targ}=[19 ; 24°C] for Toulouse [Bueno et al., 2011] ; T_{targ}= [24 ; 26°C] for Madrid in summer [Salamanca et al., 2012] ; T_{targ}=19°C in average [CSTB, 2012]; T_{targ}=20°C or more [Crédoc, 2010]
COP heat	0.9	COP heat=0.9 [Bueno et al., 2011] ; COP heat=0.75 [Salamanca et al., 2012]

Table 3.5: Settings of the building energy model parameters

3.6 The meteorological validations

The national meteorological institute Météo France freely provided the hourly 2 m air temperatures (in °C), and the 10 m wind speeds (in m.s^{-1}) and directions (in ° from the North). We used those monitoring time series to validate the meteorological fields simulated by the climate modeling system. Three stations, which locations are showed in figure 3.9, are showed to be included in the URSK domain. Note, however, that the wind field is only monitored at Entzheim and La Wantzenau.For the meteorological validation of the simulations, we excluded the no data from the analysis.

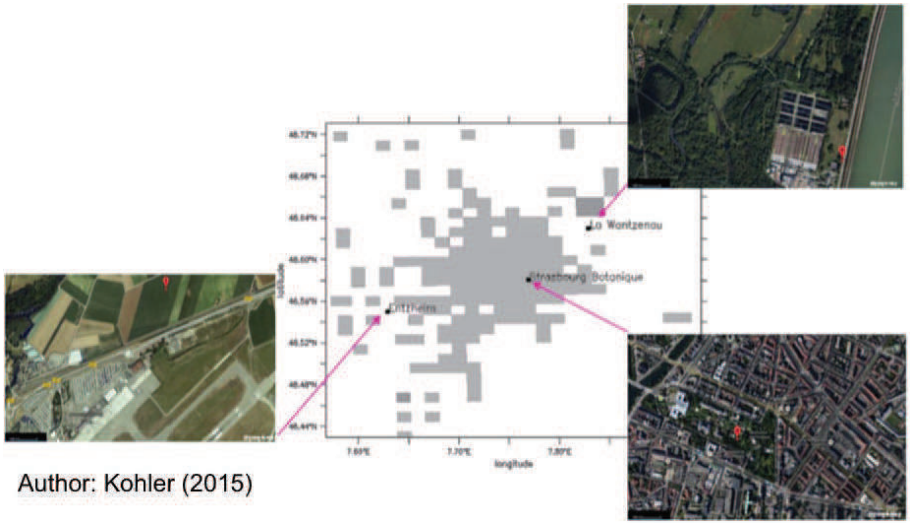

Figure 3.8: Location of the meteorological stations in the urban grids (in grey) and their surroundings.

- The Entzheim station managed by Météo France is located at the airport, South-West at the outskirt of the urban area (150 m, 48°33'N and 7°38'E) in a homogeneous flat terrain.

- The Strasbourg-Botanique station is located in the core of the urban area (139 m, 48°35'N and 7°46'E). Nevertheless, the station behaves as a cool island due to the presence of water pounds and vegetation in the nearby of the station.

- La Wantzenau station is located North-East from the urban area (135 m, 48°38'N and 7°50'E) and North from the Robertsau forest (area 493 ha) in a flat terrain

bordering the Rhine river.

Ohashi et al. [2007] recommended the use of several observational points in a grid to compute an equivalent spatially averaged near surface temperature. Nevertheless, due to the availability of the data, the 2 m simulated averaged air temperatures of the grid that includes the stations are directly compared with the 2 m observed temperatures of the stations assuming that the air is well mixed near the stations. In addition the high vertical resolution of the atmospheric grids near the ground allows the differences between the lowest level of model and the 2 m observed temperatures to be small according to Martilli [2010]. Table 3.6 gives the temperature monthly biases (in °C), the monthly RMSE (in °C), and the annual correlation coefficients for each station.

3.6.1 The air temperatures

	MBs			RMSEs		
*P*eriod	*E*ntzheim	*B*otanique	*W*antzenau	*E*ntzheim	*B*otanique	*W*antzenau
*Y*ear	-0.78	1.71	0.01			
*J*anuary	-0.45	2.03	0.31	1.78	2.78	1.86
*F*ebruary	-0.47	1.79	0.15	1.86	2.60	1.95
*M*arch	-1.17	0.76	-0.69	2.42	2.31	2.30
*A*pril	-1.61	0.81	-1.02	2.73	2.40	2.45
*M*ay	-0.91	1.70	-0.19	2.14	2.61	1.85
*J*une	-1.25	1.90	-0.44	2.29	2.82	1.89
*J*uly	-1.03	2.13	-0.18	2.64	3.29	2.44
*A*ugust	-0.91	2.20	0.32	2.28	2.99	2.00
*S*eptember	-1.98	0.54	-0.77	2.82	2.40	2.07
*O*ctober	-0.28	1.59	0.84	2.33	2.90	2.57
*N*ovember	-0.22	2.16	0.47	1.54	2.71	1.74
*D*ecember	-0.94	2.85	1.33	2.23	3.53	2.38
	R			RMSE		
*Y*ear	0.96	0.96	0.96	2.29	2.80	2.15

Table 3.6: Hourly temperature monthly mean biases (MBs), Hourly temperature monthly root mean square errors (RMSEs), and the annual correlation coefficients (R) obtained from the hourly temperatures (R) for each of the three stations.

The linear coefficients of correlation are close to 1 meaning that the climate modeling system reproduces well the variability of the temperatures over the year. Never-

theless, the RMSEs indicate a dispersion of the simulated temperatures equal to nearly 2°C compared to the instrumental observations for all the meteorological stations. The RMSEs are the highest at Strasbourg-Botanique, and are lower at Entzheim and La Wantzenau. No clear seasonality is found in the RMSEs.

Analyzing the MBs, we found the lowest MBs at La Wantzenau and the highest MBs at Strasbourg-Botanique. As showed in table 6, the MBs are negative at Entzheim, positive at Strasbourg-Botanique, and positive and negative at la Wantzenau. The air temperature over-estimations at Strasbourg-Botanique can be due to the cooling effect of the botanic garden (Fisher 2001). In addition, the MBs follow seasonal patterns. The MBs are the highest: i) from March to September at Entzheim; ii) in winter and in plain summer at Strasbourg-Botanique, and iii) positive during the winter and negative in spring and summer at La Wantzenau.
Figures in the appendix of this chapter plot the annual profiles of maximum and minimum temperatures for the three stations. The seasonality of the minimum and maximum temperatures are well reproduced by the climate modeling system. The climate modeling system tends to underestimate the minimum and maximum temperatures at Entzheim and La Wantzenau, but in contrast over-estimates the minimum and maximum temperatures at Strasbourg-Botanique, the "urban" meteorological station.

Giovannini [2012], Giannaros et al. [2013], Garcia-Diez et al. [2013] reported systematic over-estimations of the minimum temperatures and under-estimations of the maximum temperatures. Unless at La Wantzenau, this patterns is not found in the maximum and minimum temperatures. At Entzheim, the climate modeling system tends to under-estimate both the daily maximum and minimum temperatures (respectively -1.47°C and -0.72°C in average over the simulation period). At Strasbourg-Botanique, the climate modeling system over-estimates both the maximum and minimum temperatures (restively +1.94°C and +1.10°C in average over the simulation period). It seems that the climate modeling system neglects the cooling effect of the botanic garden at Strasbourg-Botanique [Fischer, 2001].

3.6.2 The wind speeds and directions

We compared the simulated and observed wind fields at Entzheim and at La Wantzenau using the 10 m wind speeds and the wind directions from the North. Table 3.7 shows the hourly mean biases (MBs), the Pearson coefficient of correlations (R) and the root

mean square errors (RMSEs) over the whole year 2010. The wind speeds are well simulated. The MBs reveal that the simulated wind speeds are slightly over-estimated at La Wantzenau station and quite well appreciated at Entzheim. The linear correlations are quite good for the two stations (respectively, R=0.67 and R=0.61) . The RMSEs, however, indicate high variations of the simulated wind speeds compared to the observed wind speeds. The RMSEs are the highest at La Wantzenau compared to Entzheim (respectively 4.82 m/s and 2.80 m/s). The greatest RMSEs at La Wantzenau could be explained by the precision of the wind monitoring sensor that is not as accurate as the one that is used at Entzheim.

*S*tatitical parameters	*E*ntzheim	*L*a Wantzenau
MBs	0.16	1.38
R	0.67	0.61
RMSEs	2.80	4.82

Table 3.7: Annual mean biases (MB), root mean square errors (RMSE), and correlation coefficients (R) of hourly wind speeds for the two stations

To deepen the analysis, we then considered only moderate wind speeds (U> 2.5 $m.s^{-1}$). We found that the RMSEs and the MBS are higher than in table 7. In particular, the RMSE is the highest at La Wantzenau. The RMSEs are respectively 6.10 m.s^{-1} at La Wantzenau and 3.46 m.s^{-1} at Entzheim. Identically, the MBs are the highest at La Wantzenau. The MBs are 3.35 m.s^{-1} at La Wantzenau and -0.22 m.s^{-1} at Entzheim.
Considering then light wind speeds, the RMSEs are lower than in table 7. They are at La Wantzenau and Entzheim respectively 4.10 m.s^{-1} and 2.19 m.s^{-1}. The MBs at La Wantzenau are also slightly decreasing. The MBs are 1.33 m.s^{-1} at La Wantzenau and 0.52 m.s^{-1} at Entzheim. Thus, the errors are more important at La Wantzenau and for moderate wind speeds.

The North/South wind channeling effect of the Rhine Graben reported by Najjar et al. [2004] is present in the wind field observations, and especially at Entzheim. There, North and North/East winds and South/South-West winds are prevailing winds (about 18%). Frequent wind speeds are included between 2.4 m.s^{-1} and 3.9 m.s^{-1}. Strongest wind velocities (>10 m.s^{-1}) are also recorded for North-/East and South/West winds. At La Wantzenau, calms winds (< 1.4 m.s^{-1}) are more frequent. Wind speeds are mainly included between 1.9 m.s^{-1} and 2.4 m.s^{-1}. Wind directions are scattered compared to Entzheim but South and South/West prevailing winds could be outlined.

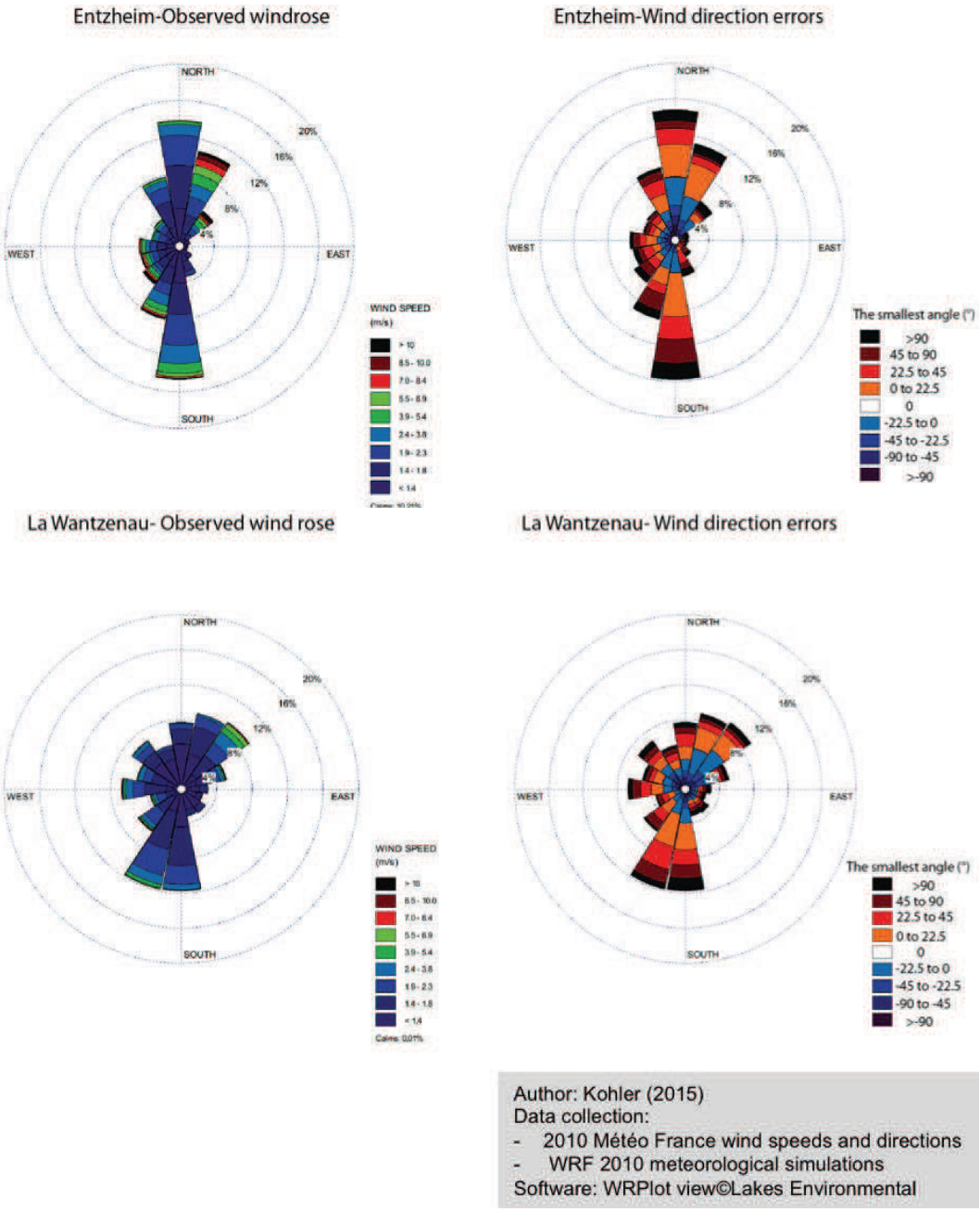

Figure 3.9: Frequency of monitored wind directions with respect to the wind speeds at Entzheim and La Wantzenau (at left) and frequency of simulated wind directions errors with respect to the angle of the errors. The smallest error angle is considered (or azimuth). The head of the arrows indicates the direction of the wind vector. The simulated wind is at the right (or left) of the observed winds when the azimuths are positives (or negatives).

Strongest winds are less frequent than at Entzheim but are also observed from the North/East sector. As a conclusion, La Wantzenau station is under the plume of light South/West winds and seems influenced by local surface conditions. Entzheim,

is showed to be rather influenced by the synoptic circulation.

When comparing the observed wind directions with the simulated wind directions, one can state that simulated wind directions are quite in accordance with the observations. The angle errors are usually included between +45° and -22.5°. The errors are mainly positive and more frequent in the prevailing wind directions. At Entzheim, the errors are highly positives. At La Wantzenau, positive errors are identified in prevailing wind directions while negative errors are observed in the wind direction sectors. As a conclusion, the climate modeling system tends to systematically deflect the wind at the right of the observed winds. The errors are more frequent and higher for the prevailing winds. The errors seem to be less systematic at La Wantzenau compared to Entzheim: negative errors are more frequent than at Entzheim and are presents for all the wind directions.
As a conclusion, the absence of a dense observational network over the domain, and in particular in the urban core, refrains the significancy of the validation of the simulated meteorological fields. The station located in the urban core behaves like a cool island and therefore it is difficult to conclude on the accuracy of the simulations of the climate modeling system. At Entzheim and La Wantzenau, the temperature fields seem to be well simulated (in particular in wintertime).
The wind fields is quite well reproduced by the climate modeling system as witnessed the correlation coefficients (R=0.60) and the mean biases. In particular, the climate modeling system tends to produce more discrepancies for moderate wind speeds.
Moderate wind speeds are not accurately reproduced by the climate modeling system. The channeling effect of the Rhine graben is, however, well reproduced at the two stations, and a systematic easterly wind deflection of the simulated winds is observed. In the stations, La Wantzenau shows higher errors in the wind speeds and variable direction errors. It is possible that the station exhibits local wind patterns. In contrast, Entzheim shows more frequent high wind speeds. The direction errors are mainly found for the prevailing wind speeds. Entzheim seems to represent the synoptic conditions.

3.7 Results and discussion

3.7.1 The simulated building energy requirements over the CUS area for 2010

The total 2010 heating energy requirements for space heating simulated by the WRF/ARW-BEP+BEM climate modeling system over the CUS area (EC_{2010}) is 12,055,372.6 GJ. By considering, then, the simulated outdoor daily temperatures, computed as the 24h average of the hourly 2-m temperatures, and the building energy consumption taken as the sum of the simulated hourly building energy requirements for space heating in a day, we drew the building energy requirement-outdoor temperature function of the CUS area. Figure 3.10 presents the resulting building energy requirement-outdoor temperature function. It is showed that the building energy requirement-outdoor temperature function is non-linear. The building energy requirements, first, decrease with the outdoor temperature rise. The building energy requirements are then close to zero for outdoor temperatures included between 9°C and 15°C, and equal to zero above 15°C. More, for a given outdoor temperature, the building energy requirements vary of +/− 10 000 MWh. It can be due to the insulating properties of the buildings and their thermal inertia according to air temperature variations. By considering, days for which the building energy consumption is non-null, we then considered the linear fitting (the statistical model) of the simulated building energy requirements-outdoor temperatures function, and obtained the statistical model (the straight line in figure 3.10) representative for the study area.

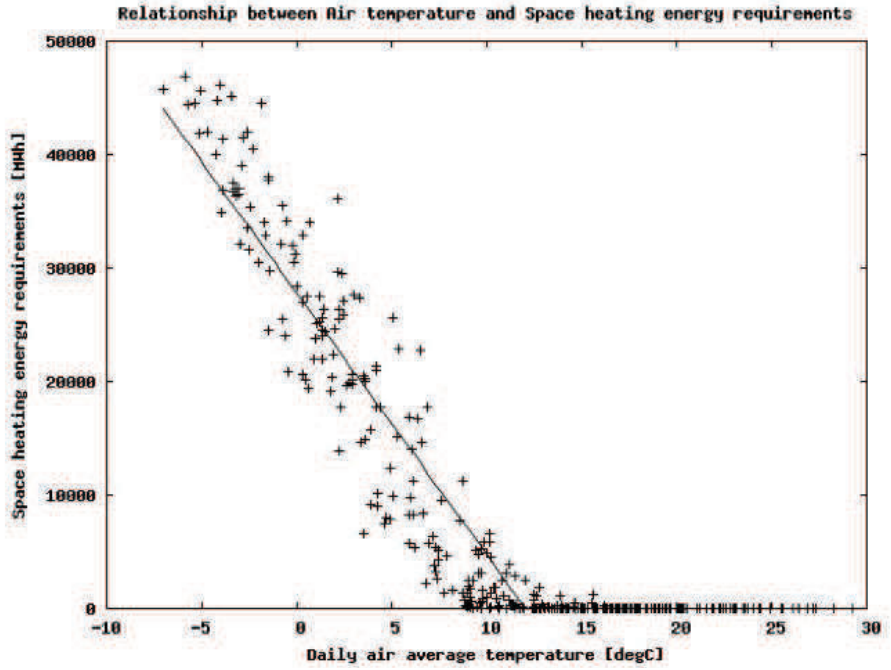

Figure 3.10: The daily building energy requirements (in MWh) as a function of the daily outdoor temperatures (in °C) over the CUS area.

The Pearson correlation coefficient of -0.93 indicates a high negative correlation between the two variables. A Student hypothesis test has been conducted by using an uncertainty α of 5%. With a calculated t statistics larger than the critical t (*e.g.* |-37.86| compared to 1.96) the Student test concludes that the linkage between the two variables is significant.

We then, reconstructed the building energy requirements by using the cold sensitivity and base temperature of the statistical model and the distribution of the CUS outdoor temperatures according to equation 3.5. We found an overall 2010 heating degree-day $D_{12.05}$ of -1520.05°C days. By using those degree-days and the slop of the linear fits, we then obtained an estimated building energy requirements (Q_{2010}) equal to 12,675,785.7 GJ. The discrepancies between the simulated building energy requirements and the estimated building energy requirements by using the statistical model are then equal to -5.01%. Valor et al. [2001] by using such kind of statistical model to predict the electricity consumption found an error in the estimates of +/- 4%. The error in the estimates is then in agreement with their study and acceptable.
Using equation 3.8, we then computed the base temperature from the knowledge of the average outdoor temperature and building energy requirements over a given period, and the cold sensitivity P. Assuming that we didn't know the number of day

where EC_i>0, we took the average of the 365 daily outdoor temperatures present in the dataset. We then found a base temperature of 14.44°C and a correspondent error of +18.04%. The base temperature is then highly sensitive to the size of the daily outdoor temperature dataset.

3.7.2 Comparison with the ASPA estimates of the building energy consumption

The ASPA estimated the building energy consumption of the CUS area to be 15,274,755.00 GJ in 2010. The simulated building energy requirement for 2010 by using the climate modeling system is 12,055,372.6 GJ. The difference in the estimates is then -21.07%. The discrepancy could arise from:

(1) The non-consideration of building areas that cover less than 20% of the atmospheric grid;

(2) Differences in the base temperatures and the cold sensitivities;

(3) The building energy settings of the climate modeling system;

(4) Differences in the definitions of the daily outdoor temperature.

(1) The non-consideration of built-up areas that represent less than 20% of the atmospheric grid area (< 20% urban grids) leads to neglect the contribution of small built-up area in the total 2010 building energy requirements. Besides, those small built-up areas are expected to be high energy intensive: no wind shielding effects and local warming are expected with low building densities. We considered 5-days simulations using the WRF/ARW-BEP+BEM climate modeling system and an energy intensive period (started from 06/01/2010). The land cover provided to the WRF climate modeling system is presented in figure 11. From the 5-days simulations we found that the < 20% urban grids contribute to 43,887.6 GJ when the other urban types represent 846,536.4 GJ by their own. The difference between the ASPA estimate and our estimate is not due to the non-consideration of the small built-up areas.

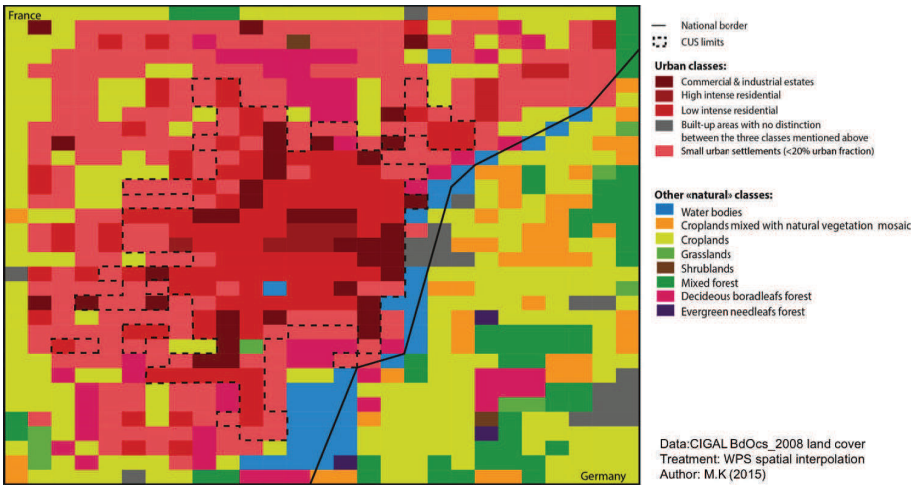

Figure 3.11: Land cover of the URSK domain with the representation of the small urban settlements (urban fraction of the atmospheric grid<20%).

(2) The ASPA defines by convention the heating period from October to May and set the base temperature at 17°C. It results in a degree-day D_{17} equal to -1701.31°C days. Our statistical model deduced a base temperature equal to 12.05°C leading to a difference of -34.07% in the base temperatures. Taken the same heating period and the base temperature provided by our statistical model (12.05°C) we found a degree-day $D_{12.05}$ equal to -1445.64°C days. The differences with the ASPA degree-day are then equal to-15.02%.

We computed the equivalent cold sensitivity P of the ASPA study using equation 3.9. We found a cold sensitivity P that is equal to -2493.94 MWh/°C. The relative difference between the two cold sensitivities P is nearly -7.11%. The cold sensitivity is slightly enhanced in the ASPA study.

The differences in the base temperature explain a large part of the differences in the building energy requirements. A review of the literature dedicated to the degree-day method pointed out that the base temperature is correlated with the building types and characteristics. Amato et al. [2005] mentioned that well-insulated homes and commercial buildings due to internal heat gains from office machinery and occupants have relatively low base temperature. In contrast, Giannakopoulos and Psiloglou [2006] reported that well-ventilated homes in USA need almost no space-heating energy when outdoor temperatures are between 12.8°C and 18.3°C. It is thus possible that the consideration of the internal heat gains lowers the base temperature.

(3) We investigated the sensitivity of the building energy requirement with the in-

ternal heat gains and losses. We performed successive 5-days simulations over a domain of 19x19 atmospheric grids of 45 km width considering the atmospheric conditions of the Strasbourg urban region, and a single urban grid placed at the center of the domain. We successively removed the heat generated by the occupants, the wasted heat due to equipment, considered opaque buildings (no windows) and cut off the natural ventilation.
The windows fraction influences the radiative budget of the floor by allowing solar radiation penetration in the room and permit longwave radiation losses. The ventilation rate quantifies the fraction air that is renewed each hour considering the temperature gradient between the building and its surroundings. The wasted heat due to the use of equipment is an additional source of heat in the buildings room as well as the heat emitted by the human being due to the human metabolic activity.

	Contribution in the building energy requirements
Base case	49,320,518 MWh
Heat generated by the equipment	+58.82%
Heat generated by the occupants	+1.20%
Air ventilation	-8.18%
Windows	-8.49%

Table 3.8: Sensitivity of the building energy requirements with the BEM settings.

In table 3.8, it is showed that the heat gains induced by the equipment highly impact the building energy requirements and contribute for a large part to the internal heat gains. Windows and the natural ventilation are showed to contribute to the building energy losses. Thus, the consideration of no-ventilated and opaque buildings decreases the building energy requirements. The consideration of the internal heat gains due to the equipment can lower the base temperature and explain the differences in the estimated building energy requirements found by the two studies.

To more deeply stress the sensitivity of the building energy requirement with the equipment settings, we changed successively the intensity of the peak heat emission due to the use of the equipment and the daily profile of the heat emissions. We firstly considered the peak heat intensity and profile recommended in the technical report of the French scientific and technical center for buildings

used to calculate the standard building energy consumption (Th-C-E method of the thermal regulation) [CSTB, 2012]. The peak heat intensity is 5.7 W/m^2. The daily profile is set at 100% between 7 a.m. and 11 a.m. and between 6 p.m. and 11 p.m. The heat generated by the equipment corresponds to one fifth of the maximum peak heat intensity for the remaining hours. Then we considered that the equipments are used all the day (daily profile equal to 100% all the day) and increased the peak heat intensity at 36W/m^2 like Kikegawa et al. [2003]. We found that the maximum use of the equipment all the day decreases the building energy requirement by -18.68%. Further decreases in the building energy requirements of -19.82% are reported when increasing the peak heat generated by the equipment. Hence, the modeling of the internal heat gains due to equipment (especially the peak heat intensity) is a key point in the building energy model set-up.

(4) Differences in the definitions of the daily outdoor temperature.
Several definitions of the daily outdoor temperatures exist. The *Tminmax* (equation 3.11) is commonly used to determine the daily temperature. Wallace [2012], however, demonstrated that the Tminmax method may over-estimate or under-estimate the true daily average temperature depending on the location and season. In our study the use of the *Tminmax* contributes to increase the degree-days by up to +30.78% compared to the use of the average of the hourly temperatures over the day (average method). Indeed, the *Tminmax* method gives lower daily outdoor temperatures compared to the average method. The mean bias is -3.68°C when considering the annual scale. It seems that the *Tminmax* method overestimates the variations of the temperature during the day and is highly sensitive to the minimum temperatures.

$$T_i = \frac{T_{max} - T_{min}}{2} \tag{3.11}$$

We considered the *Tminmax* and the base temperature deduced by the linear statistical model (12.05°C). The degree-day becomes $D_{12.05}$ -3159.34°C days. The degree-days are then over-estimated by up to +118.54%. This suggests that our *Tminmax* are cooler than the ASPA *Tminmax* and more frequently below the base temperature threshold.
Thus, either the maximum temperatures are under-estimated or the minimum temperatures are over-estimated (or both) by the climate modeling system com-

pared to the ASPA study. A roughness approach is used in the ASPA study for modeling the urban effects on the atmosphere. This approach is acknowledged to not fairly reproduce the urban heat island effect by over-estimating the air temperatures (especially during the day) and the nocturnal cooling rate over urban areas [Müller, 2007, Kusaka and Kimura, 2004]. It can trigger over-estimations of the maximum temperatures (warmer) and over-estimations (cooler) of the minimum temperatures. Unfortunately, we have not the minimum and maximum temperatures used in the ASPA study at our disposal to conclude on this point.

To deepen the analysis, we decompose the differences in the building energy requirements considering equation 2.4. We called ΔE the difference in the building energy requirements considering our study and the ASPA study (noted with the over script A), and as the same respectively, ΔP the differences in the cold sensitivities P, and ΔD the differences in the degree-days computing by using the statistical model and the degree-days provided by the ASPA. The latter can be decomposed into $\Delta D^{\Delta t}$ the difference in the degree-days caused by the different period of heating that are considered (October to May in the ASPA study, and all the year in our study), caused by the ΔD^{T_0} that is the difference in the degree-days due to the consideration of deduced base temperature or predefined base temperature, $\Delta D^{T_{avg}}$ the difference in the degree-day due to the method used to computate the daily outdoor temperature (average of the hourly temperature, or average of the daily extreme temperatures). At last the $\Delta \widetilde{D}$ is the differences between the degree-days calculated by using the parameters of the statistical model deduced from the linear fitting, and the degree-days calculated by using the statistical model, the parameters of adopted in the ASPA study, and the WRF/ARW-BEP+BEM simulated hourly minimum and maximum temperatures according to equation 2.1.
The relative differences in the simulated building energy requirements is then:

$$\frac{\Delta E}{E^A} = \frac{\Delta P}{P^A} + \frac{\Delta D}{\Delta \widetilde{D}} . \frac{\Delta D^{\Delta t}}{\Delta D^A} + \frac{\Delta D}{\Delta \widetilde{D}} . \frac{\Delta D^{T_0}}{\Delta D^A} + \frac{\Delta D}{\Delta \widetilde{D}} . \frac{\Delta D^{T_{avg}}}{\Delta D^A} + \frac{\Delta P}{P^A} . \frac{\Delta D^{\Delta t}}{\Delta D^A} + \Delta_{inter} \tag{3.12}$$

First the interaction terms Δ_{inter} that represent the differences due to the combination of the other terms of the equation 3.12 are positive and are equal to +7.2%. For simplification we consider that the problem is linear. Nonetheless, further investigations are required to explain this term.The differences due to the

differences in the cold sensitivities P and the base temperatures T_0 simultaneously are small (+1.1%). The differences in the building energy requirements due to the cold sensitivities represent -7.1%. At last, the differences in the building energy requirements caused by the degree days represent -15.02%. The discrepancies are mainly caused by the differences in the base temperatures (-9.3%) and the use of the *Tminmax* method (-13.1%). As a conclusion, the method used to calculate the daily outdoor temperatures account for the largest differences in the degree-days, and in the building energy requirements.

3.7.3 Assessment of building energy saving strategies

The statistical model enables us to quickly estimate the building energy requirements over any time period. We therefore choose to take advantage of this method to assess some well-known energy saving strategies. In addition, the cold sensitivity and the base temperature can be used as new building energy performance indexes for assessing the building energy conservation strategies. For this, we first optimized the methodology to save computational time, and then performed the meteorological and building energy simulations of each scenario by using the WRF/ARW-BEP+BEM climate modeling system.

3.7.3.1 Presentation of the scenarios

We considered three types of building energy conservation strategies. The first type represents the building energy conservation strategies that attempt to lower the air temperature in the context of global warming. Cool surfaces and shade trees are acknowledged to participate to such types of strategies. In this study we considered the effect of high reflective roofs on the building energy performance. The roofs represent more than 25 millions square meters in France, and exposed at the solar radiations, those dark surfaces become particularly hot (about 65.55°C in summer according to EPA [2013]). Nevertheless, the adoption of reflective coatings can lower the skin temperatures up to 100°F (10°C), and hence, lower the air temperature. Hence, several studies like Rosenfeld et al. [1995] found that increasing urban albedos (0.13 to 0.26) can limit or reverse the urban heat island and that reflective roofs can reduce around 40 to 50% the cooling energy use and the peak cooling demand. The second type of

building energy conservation strategy reduces the permeability of the building sensitivity to the exterior thermal environment by improving the building shell properties and takes benefits of the windows apertures. At last, the third type of energy conservation strategies acts on the behavior of the building occupants. In particular studies reported that the turning down of the thermostat is a behavioral strategy often adopted by the household in a context of increasing price of energy to save money [Desjardin et al., 2011, Herring and Roy, 2007]. The potential of energy savings are high: it appears that most of the building rooms are over-heating compared to the recommended 19°C [Crédoc, 2010].

3.7.3.2 Optimization of the methodology

A simulation over a whole year is expensive in computing time. So we shorten the period on which the methodology could be based. For this and so as to preserve the quality of the statistical model we calculated and compared the cold sensitivity P and the base temperature T_0 for each combination of three months possible in a year. We chose the combination that minimizes the relative differences in P and T_0.The three selected months are February, March and September. The cold sensitivity is -2316.7 MWh/°C and the base temperature is 12.14 °C. The discrepancies in the cold sensitivity P and base temperature T_0 are respectively +0.01% and +0.74%. The simulated building energy requirement by using the climate modeling system for those three months ($EC_{3months}$) is equal to 3,859,534.1 GJ. The estimated building energy requirement obtained by using the statistical model Q_{3month} using the $P_{3months}$ and the $T_{0,3months}$ obtained from the three months is 3,985,090.6 GJ. The discrepancies are then +3.2% over the three months. Over the year, we obtained a building energy requirement equal to 12,824,277.6 GJ. The relative error is then +6.18%. It is hereby possible to calculate the annual building energy requirements computation by using only the three selected months.

3.7.3.3 Results and discussions

- **High reflective roofs**

We designed three scenarios in which we successively increased the roof albedo from 0.1 (*Case A0*) to 0.3 (*Case A1*) and finally like in Akbari et al. [1999] to 0.7 (*Case A2*). Firstly, we analyzed the influence of the changes in the roof albedos on the outdoor temperatures. Table 3.9 sums up the statistical distribution of the outdoor temperatures while figure 3.12 presents the distributions of the outdoor temperatures. It is showed that in average the outdoor temperatures slightly change when considering increasing roof albedos. In particular and as showed in table 3.9 the maximum temperatures decrease with the rise of the albedo while the minimum temperatures become colder compared to the case A0.The distribution shows two modes, which characterize in the one hand the contribution of the cold months (February and March) in the time serie, and in the other hand the contribution of September (the warmest of the three months) in the time serie.

	Case A0 albedo=0.1	Case A1 albedo=0.3	Case A2 albedo=0.7
Tmin	-5.73°C	-5.74°C	-5.76°C
Tmax	17.93°C	17.89°C	17.73°C
Tmean	7.45°C	7.13°C	7.44°C
T median	9.15°C	8.97°C	9.11°C
q_1	1.91°C	1.79°C	1.87°C
q_3	12.59°C	12.52°C	12.57°C

Table 3.9: Statistical description of the distributions of the outdoor temperatures over the CUS area (computed using the three months: February, March and September) with changes in the roof albedo. *Tmin* is the minimum temperature, *Tmax* is the maximum temperature, *Tmean* is the temperature average, Tmedian is the median of the temperature dataset and at last q_1 and q_3 are the first and third interquartile, respectively.

Then, we investigated the effect of cool roofs on the daily profiles of the air temperature. We considered February and September for accounting for wintertime and summertime seasons, and an urban grid assigned to high intense residential type that is characterized by a high building density. Figure 3.13 displays the daily profiles for each scenario.

Few differences are observed in the daily temperature profile in February. The differences in the air temperatures are at maximum equal to 0.2°C during the day and below 0.1°C at night. When comparing the air temperatures of the high-reflective roofs (scenario A2) and dark roofs (scenario A0), one found cooler temperatures during the day (after 9 a.m. and until 1 p.m.) and warmer air temperatures at night and in the

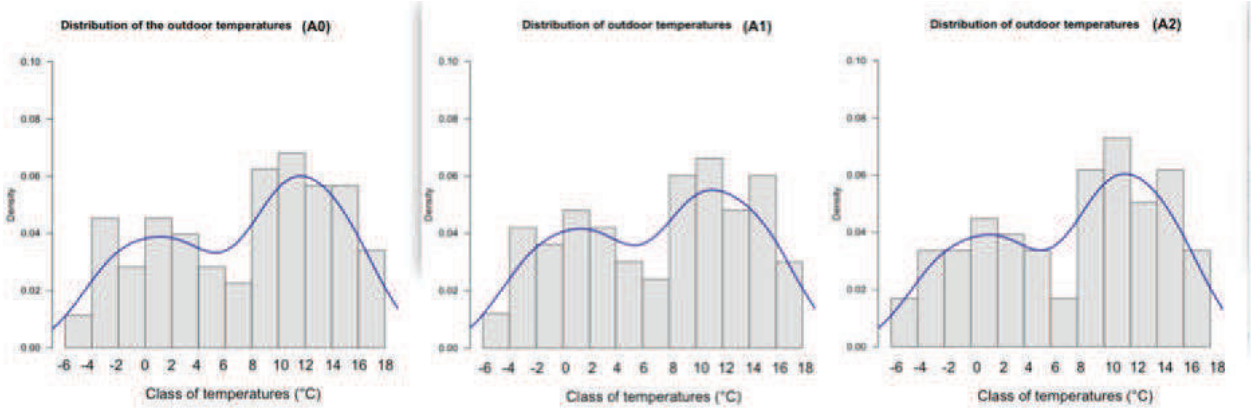

Figure 3.12: Distributions of the urban outdoor temperatures over the CUS area for the roof albedo scenarios. The solid lines are the probability density functions.

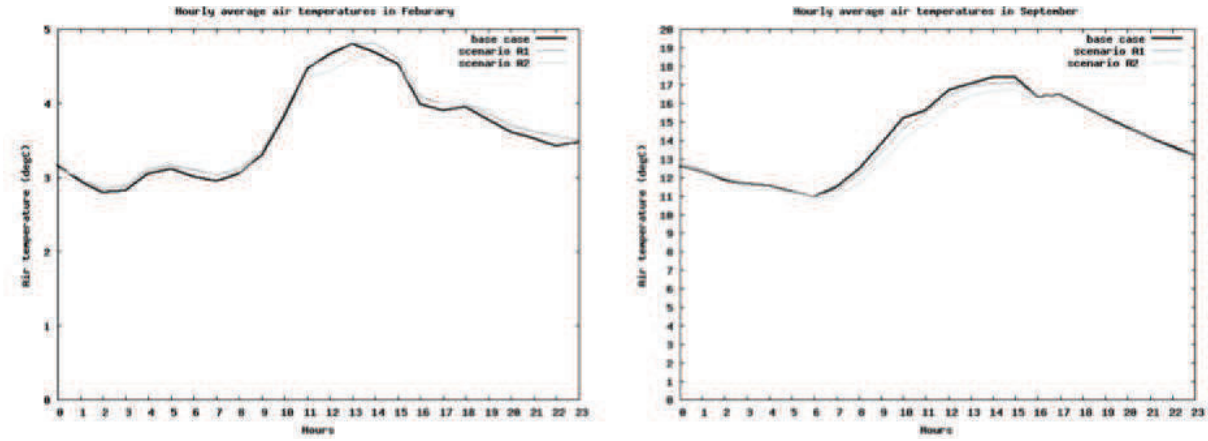

Figure 3.13: Average profiles of the daily air temperatures for February and September considering the roof albedo scenarios. Be careful, the two plots have not the same scales to account for the slight differences in the temperatures between the scenarios found in February.

morning in the scenario A2. In contrast, high-reflective roofs considerably impact the air temperatures in September. The dark roof scenario exhibits the warmest air temperatures during the day (between 6 a.m. and 5 p.m.). The air temperatures are then decreasing with the roof albedo rise. The differences in the air temperatures between the scenarios A0 and A2 are at maximum equal to -1°C (at 2 p.m.) and are increasing from the morning up to the late afternoon. After 5 p.m. the temperatures of the three scenarios are nearly equal.

Our results are consistent with Rosenfeld et al. [1995] that found changes in the simulated hourly temperatures at noon equal to -2°C and at maximum equal to -3°C in

the early afternoon (3 p.m.) with increasing urban albedos by using the CSCUMM mesoscale atmospheric model. Thus, high reflective roofs rather impacts summertime and daytime air temperatures that are characterized by high solar radiation forcings. As a conclusion high-reflective roof strategies may improve the summer and have moderate effect on the winter thermal comfort as they contribute to warm the air up at night in winter but also contribute to cool the air during day.

	$EC_{3months}$ (in GJ)	P (in MWh/°C)	T_0 (in °C)	$Q_{3months}$ (in GJ)	Q_{2010} (in GJ)
Case A0	3607156.1	-2316.7	12.14	3,985,090.6 *(+3.2%)*	12,823,834.8
Case A1	3861728.6 (+10.23%)	-2248.0 (-2.99%)	12.44 (+2.52%)	3995561.7 *(+3.40%)*	12,917,744.8 (+0.72%)
Case A2	4045404.8 (+11.45%)	-2233.6 (-3.65%)	12.79 (+5.29%)	4216217.8 *(+4.13%)*	13,404,022.6 (+4.42%)

Table 3.10: The building energy requirements and statistical model parameters for each roof albedo scenario. The building energy requirements outputted from the climate modeling system are $EC_{3months}$. The building energy requirements calculated from the cold sensitivity P and the base temperature T_0 using the statistical model are $Q_{3months}$. The differences with the case A0 are written in (%) while the errors committed in the building energy requirement by using the statistical model are written in *(%)*. The building energy requirements and statistical parameters are always computed by considering the three selected months (February, March and September).

Then, table 3.10 provides the total building energy requirements simulated by using the climate modeling system and the three months ($EC_{3months}$), the statistical model parameters (the cold sensitivity P and the base temperature T0), and the building energy requirements estimated by using the statistical model and the three months ($Q_{3months}$) or the entire year (Q_{2010}).

It is showed that the building energy requirements for space heating increase with high-reflective roofs by about +10%. Our results are in agreements with Conner [1985] cited in Taha et al. [1988] that reported energy savings including between -5% and -25% for well-insulated buildings and from -7% to -16% for no insulated buildings when lowering the wall and roof albedo from 0.7 to 0.3 of prototype residential buildings in several US cities. The rise in the building energy requirement is non-linear as pointed out in figure 14. An albedo threshold is found for albedos that are equal to 0.4 and 0.5.
In parallel, the cold sensitivities and the base temperatures of the scenarios slightly

vary (less than 5%). The cold sensitivity decreases with the roof albedo rise meaning that the buildings are less sensitive with the cold temperatures. Like the building energy requirements, the cold sensitivity P shows a non-linear relationship with the rise in the roof albedo. In contrast, the scenarios A1 and A2 are characterized by distinct base temperatures (T_0). According to figure 3.14, the base temperatures linearly increase with the roof albedos.

It is well acknowledge that cool roofs can contribute to save energy in summer [Taha, 1997, Salamanca et al., 2011]. In this study and like Kuttler [2012], we found in contrast that cool roofs have controversial and moderate effects in winter on the building energy requirements. Like Conner [1985] (cited in Taha et al. [1988]), we found that the increase in the roof albedo increases the heating energy requirement by about 10% other the three simulated months. This is mainly because highly reflective walls do not help to achieve a solar radiation energy gain for the building, and thus the increase in the building energy requirements can be attributed to the lowering of the air temperature during daytime when using cool roofs. From the statistical model it is showed that the base temperature, that represents the temperature at which the buildings is at thermal equilibrium, is slightly more influenced by higher roof albedos than the cold sensitivity. This can be due to the decrease in the internal heat gains. It is also possible that our buildings are well insulated. Akbari et al. [1999] indeed reported that the effects of cool roofs on the building energy savings are reduced for well-insulated buildings.

Over the study area, such measures is not really feasible. Historically, the pitched roof are covered by brown- red tiles made in clays. A large modification of the roof properties seems unrealistic, and in particular in historical centers for which drastic building codes are imposed to preserve the regional vernacular architecture. The replacement of the red-brown tiles by high reflective materials seem more realistic in new constructions located out of the historical centers. However, clay tiles despite their cost are now preferred to concrete tiles due to their long life cycle even in new constructions. More, some studies like Akbari et al. [1999] reported that high reflective roofs, and more high reflective pitched-roofs can dramatically make the car traffic dangerous due to the reflection of the solar radiations at street levels.

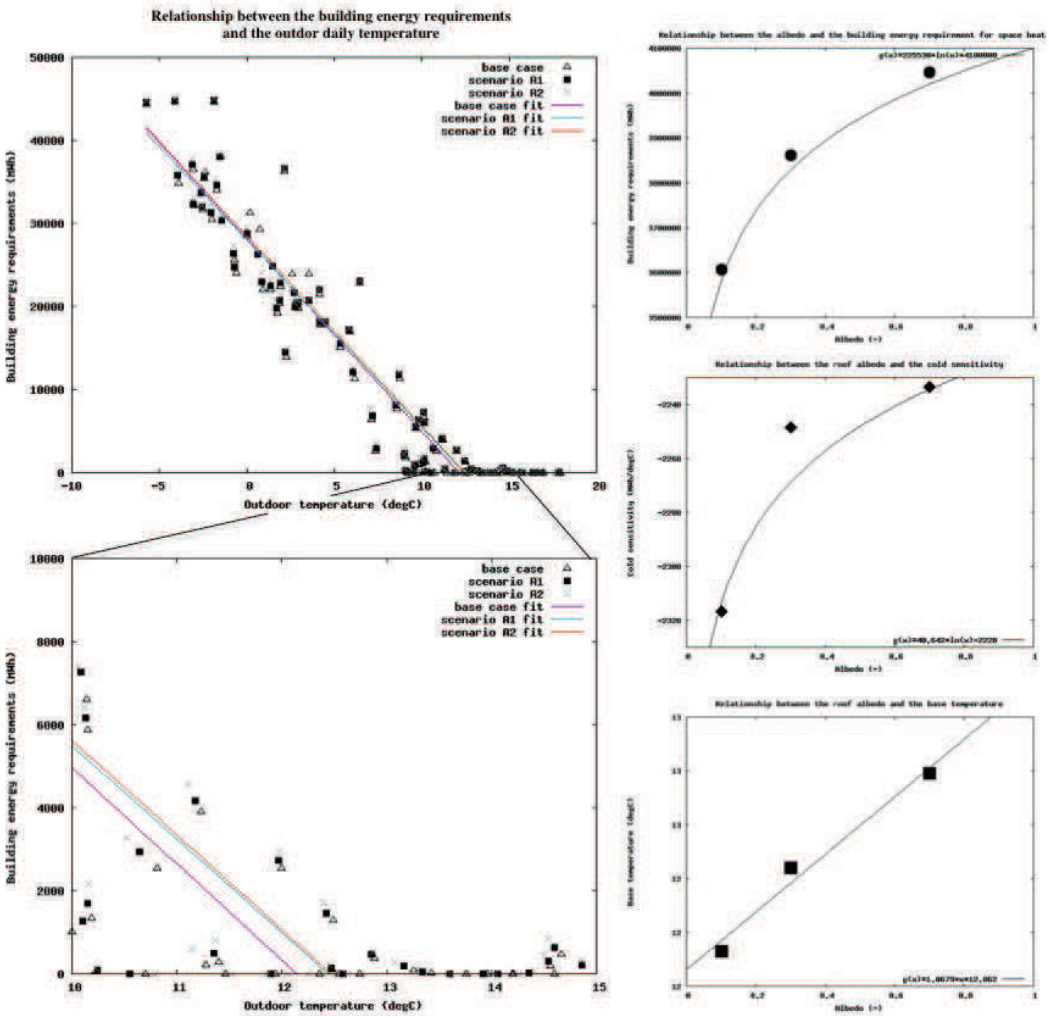

Figure 3.14: At left, sketch of the relationship between the building energy requirements and the outdoor temperature. At right, figures plot the relationships between the roof albedo, and in one hand the building energy requirements, and in other hand the cold sensitivity and the base temperature, respectively.

- **Improvement of the building wall insulating properties**

We designed three scenarios and focused on the building walls. The first scenario considers massive walls composed of 20 cm bricks. In the second and third scenarios a 20 cm insulation layer of glass wools is added in the wall envelope that faces either the room indoor wall (the interior insulation scenario) or the room outdoor wall (the exterior insulation scenarios), respectively.

Table 3.11 and figure 3.15 provides the statistical descriptions of the distributions of the outdoor temperatures. No differences are found in the statistical distributions of the outdoor temperatures. Again the two modes represents the variation of the outdoor

temperatures due to the use of two contrasted sub-sets in the three months (February and March in the one hand, and September in the other hand). The building insulating properties seem to have no direct effects on the outdoor temperatures.

	Scenario No insulation	Scenario Interior insulation	Scenario Exterior insulation
Tmin	-5.84°C	-5.90°C	-5.89°C
Tmax	17.79°C	17.49°C	17.57°C
Tmean	7.42°C	7.38°C	7.39°C
Tmedian	9.00°C	9.04°C	9.09°C
q_1	1.89°C	1.79°C	1.88°C
q_3	12.49°C	12.47°C	12.66°C

Table 3.11: Statistical description of the distributions of the outdoor temperatures over the CUS area (computed using the three months: February, March and September) with changes in the building envelop properties. *Tmin* is the minimum temperature, *Tmax* is the maximum temperature, *Tmean* is the temperature average, Tmedian is the median of the temperature dataset and at last q_1 and q_3 are the first and third interquartile, respectively.

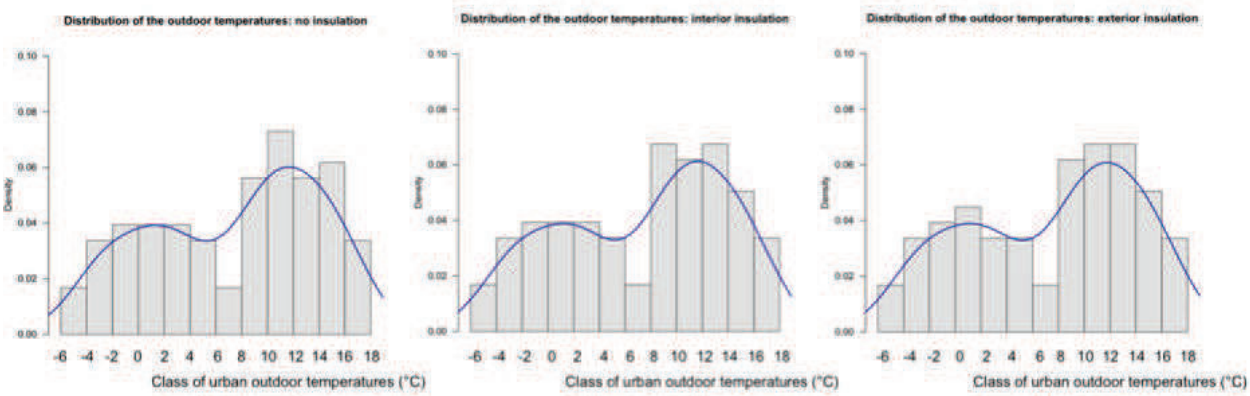

Figure 3.15: Distributions of the urban outdoor temperatures for the three building insulation scenarios.

When deepen the analysis and considering average daily profiles of air temperatures (figure 3.16), we observed little differences in the air temperatures between the scenarios that are even greater in February compared to September. The air temperatures when wrapping the building interior or exterior walls with insulating materials are always cooler in February and at night by -0.1°C compared to the no-insulation scenario. Few differences in the air temperatures are found between the insulation scenarios. The exterior walls insulation scenario is a bit warmer at noon compared to the interior walls

insulation scenario both in February and September. Grossiord [2009], indeed, when simulated the air temperature and the buildings temperatures considering the Finite Volume Model (FVM) mesoscale model of Clappier et al. [1996] and the BEP+BEM urban parameterizations observed that the external insulation raises the outdoor temperature during daytime.

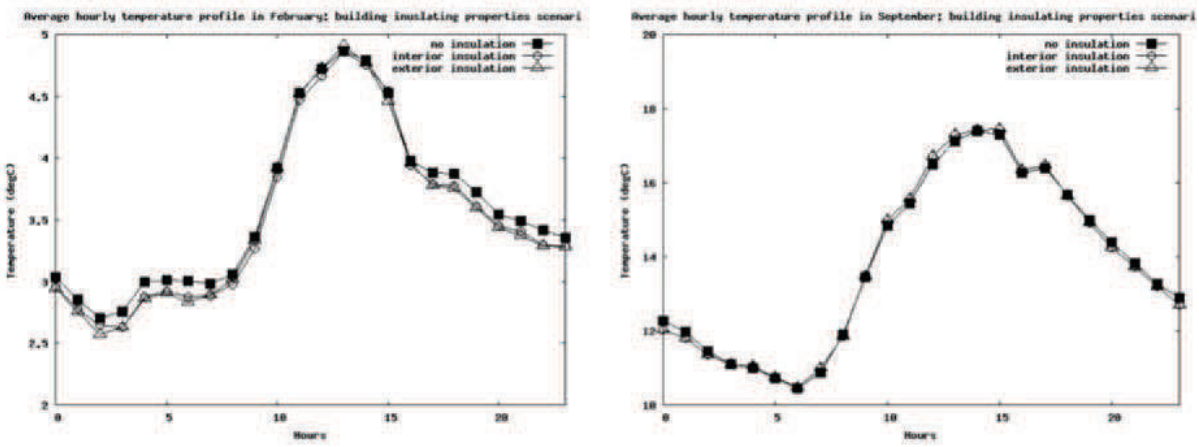

Figure 3.16: Average daily temperature profiles for February and September when changing the building insulating properties. Be careful the scales are changed to account for the slight differences in temperatures in February.

In the building energy perspectives, construction system with no insulation layer is characterized by the highest simulated building energy requirements as showed in table 18. Indeed the bricks are characterized by a higher thermal conductivity than the insulating materials. It enhances the heat exchanges between the buildings envelope and its surroundings, in particular when the wall thickness is reduced to 20 cm. Then, the simulated building energy requirements considerably decrease when increasing simultaneously the walls thickness and when adding building insulating materials (nearly -155%). The position of the insulation layer in the layered wall has no effects on the building energy requirements as showed in table 3.12 and figure 3.17. Aste et al. [2009] found, however, slight differences in the heating energy requirements when considering insulation that faces either the outside or inside walls. The annual heating energy requirements are 421 kWh, 415 kWh respectively. Bojic et al. [2001] found that indoor and outdoor insulation wall systems have quite equal building energy performance. The insulation materials has a heat capacity set at 22.08 kJ/m^3/°K and the heat conductivity is 0.034 W/m/°K. Another study, however, stressed high differences in the building heating and cooling energy requirements according to the position of the insulation layer in the construction system. Kossecka and Kosny [2002] pointed out

that insulation outside the massive wall composed by concrete materials has the best performance. They set the wall heat capacity at 19.36 kJ/m^3/°K and the wall heat conductivity at 0.036 W/m/°K. The wall thickness is, however, kept constant (25.4 cm). The annual difference in the heating requirement between outdoor and indoor insulation wall system is about 586 to 1025 kWh. At last, Salamanca et al. [2012] simulated the impacts of wall insulation on the cooling demand of the Madrid great area. The addition of an insulation layer of 6 cm reduces the cooling energy load by -3.59% compared to the simulation in which a massive wall with no insulation layer is considered. The heat capacity is 0.38 J/m3/°K and the heat conductivity is 0.09 W/m/°K.

Considering the heat capacity and conductivity magnitude (we adopted a heat conductivity of 0.04 W/m/°K and a heat capacity is 16.48 kJ/m^3/°K), we concluded that the considerable energy saving found in this study is induced by the wall thickness. It is also possible that the wall thickness (40 cm) hides the differences in the building energy requirements induced by the wall insulation position.

	$EC_{3months}$ (in GJ)	P (in MWh/°C)	T_0 (in °C)	$Q_{3months}$ (in GJ)	Q_{2010} (in GJ)
Case No insulation	2,577,515.0	-1886.7	10.56	2,658,612.8 *(+3.09%)*	8,449,517.7
Case Indoor insulation	322,232.1 (-155.55%)	-347.4 (-147.83%)	7.66 (-31.83%)	327,952.5 *(+1.75%)*	1,017,849.5 (-156.99%)
Case Outdoor insulation	316,730.9 (-156.22%)	-353.3 (-147.07%)	7.36 (-35.71%)	319882.6 *(+0.99%)*	985,284.6 (-158.22%)

Table 3.12: The building energy requirements and statistical model parameters for each building wall insulation scenario. The building energy requirements outputted from the climate modeling system are $EC_{3months}$. The building energy requirements calculated from the cold sensitivity P and the base temperature T_0 using the statistical model are $Q_{3months}$. The differences with the case "no insulation" are written in (%) while the errors committed in the building energy requirement by using the statistical model are written in *(%)*. The building energy requirements and statistical parameters are always computed by considering the three selected months (February, March and September).

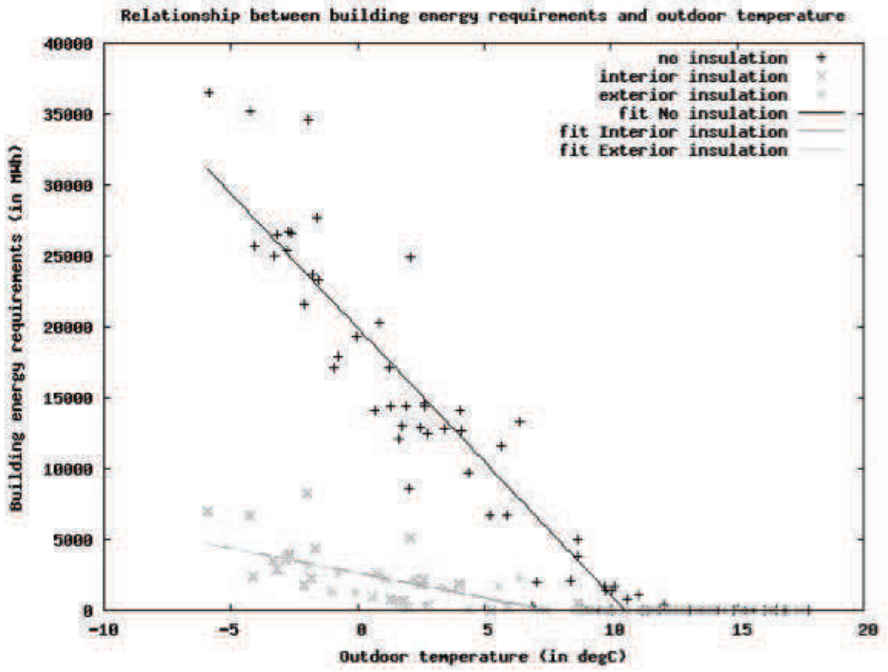

Figure 3.17: Relationship between the building energy requirements and the urban outdoor temperatures with changes in the insulation properties of the building walls.

Like the building energy requirements, the building cold sensitivities are considerably reduced (by -147%) when wrapping either a home's exterior or interior walls. The base temperature change also considerably (-30%). Insulated buildings are therefore less sensitive to the cold temperatures meantime the building thermal inertia is enhanced as witnessed by the lower base temperatures.

In conclusion the enhancement of the buildings insulating properties has slight effects on the air temperatures. The building energy requirements are showed to be considerably higher for no insulated buildings. This result can be induced by the wall thickness. It is also showed that the changes in the buildings insulated properties impact both the cold sensitivity and the thermal equilibrium of the buildings. At last, no differences in the building energy performance are found with the relative location of the insulating materials layers in the walls.
Although the improvement of the building insulating properties produces considerable energy savings, the measure is expansive and sometime not technically feasible. Wrapping an interior wall with an insulating layer contributes to reduce the living space, and contributes to create thermal bridges between the building indoor and outdoor. As highlighted by Desjardin and Llorente [2009], the investment is often done once at the arrival of the new households in the dwelling. As a consequence, the measure is

expected to produce large energy savings in areas where the the residential migrations is intense. In the urban region of Strasbourg-Kehl, the residential migration is intense in the old city center for the young population (between 20 and 30 years old). This category of population are usually students and renters. Thus, the ownerships of the buildings are divided between several stakeholders and constitute a barrier to the building refurbuishments. At reverse, the 30 years and family population that have larger purchasing power migrate at the periphery of the CUS territory and farthest out of the limit of the metropolitan area in new dwellings [INSEE and ADEUS, 2012]. Thus, the impact of such measure on the building energy saving is moderate. In contrast, wrapping the outdoor wall with an insulating layer is often cited as an efficient energy loss counter-measures as it prevents the formation of thermal bridges. However, like in the study area, most of the dense city center in European countries are old and some part classified in the UNESCO world heritage list. Thus, the modifications of the outdoor walls is often limited and drastic building codes have prohibitive effects. As a consequence, such measure seems more adapted for new buildings for which the energy performance is though at the design phases. Since the 2000's, the Strasbourg urban center follow a voluntarist construction policies. In 2012 the CUS territory (Eurometropole) represents 40% of the new constructions of the Bas-Rhin district. The new dwellings are for the largest share located in multi-family housings built in hollow teeth, and brownfields. Thus, the improvement of the building energy performance over the CUS territory is particularly driven by those new constructions, for which the building codes and standards are particularly strict in terms of envelop energy efficiency. However, INSEE [2013] reported an overall slow down in the construction intensity.

- **Increase in the windows size**

We considered three scenarios in which the windows-to-wall fraction is increasing by +25% (*Scenario P2*) and +50% (*Scenario P3*) compared to the scenario A0 (here, recalled *Scenario P1*). Firstly, we investigated the changes of the windows-to-wall fractions on the outdoor temperatures. Table 3.13 and figure 3.18 highlight that the changes in the windows-to-wall fraction have few impacts on the temperature fields. Scenarios P2 and P3 that are characterized by increasing windows-to-wall fractions are quite warmer than the reference scenario P1. Nevertheless, the differences are small. The distribution of the outdoor temperature again show two modes. Sharper peak characterized the scenarios P2 and P3.

	Scenario P1	scenario P2	Scenario P3
Tmin	-5.84°C	-5.90°C	-5.89°C
Tmax	17.79°C	17.49°C	17.57°C
Tmean	7.42°C	7.38°C	7.39°C
Tmedian	9.00°C	9.04°C	9.09°C
q_1	1.89°C	1.79°C	1.88°C
q_3	12.49°C	12.47°C	12.66°C

Table 3.13: Statistical description of the distributions of the outdoor temperatures over the CUS area (computed using the three months: February, March and September) with changes in the windows-to-wall fractions. *Tmin* is the minimum temperature, *Tmax* is the maximum temperature, *Tmean* is the temperature average, Tmedian is the median of the temperature dataset and at last q_1 and q_3 are the first and third interquartile, respectively.

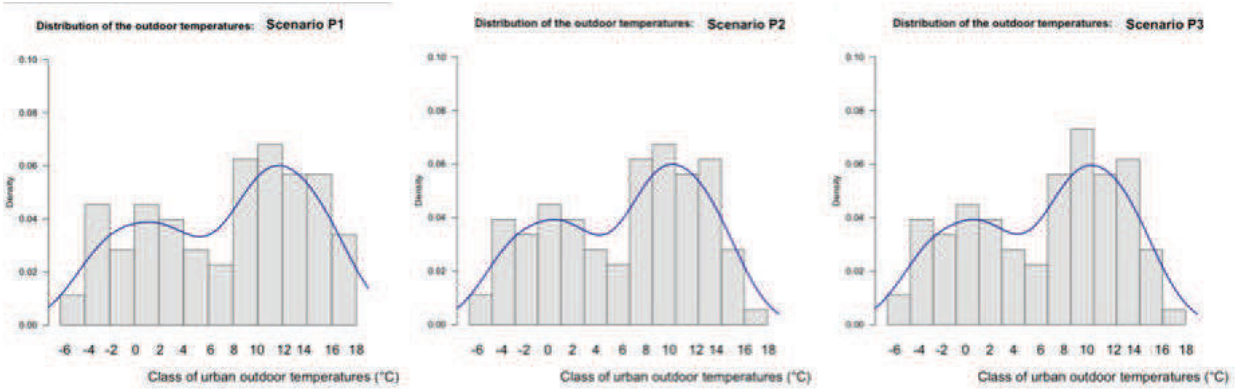

Figure 3.18: Distributions of the urban outdoor temperatures for the three windows-to-wall fraction scenarios.

To deepen the analysis, we took into account a single urban grid located at the center of the main urban center. We plotted the average daily profiles of the air temperatures for each scenario (figure 3.19). The differences in the near surface temperatures are small between the scenarios. They are even greater in February compared to September. In February, the temperatures of the scenarios P2 and P3 are warmer compared to scenario P1 through along the day. Nevertheless, the magnitude of the warming is low (+0.2°C). No differences are found in the average daily profiles of air temperatures of the scenarios P2 and P3 except in the evening (from 4 p.m. until midnight). The scenario P3 is then the warmest, and P1 the coldest. In September, no significant differences are found between the scenarios.

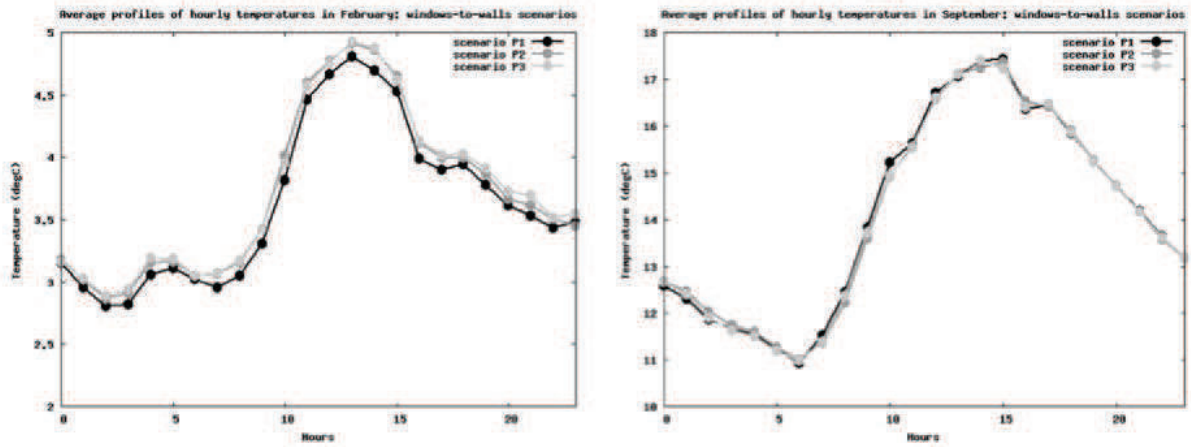

Figure 3.19: Average daily temperature profiles for February and September when changing the windows-to-wall fractions. Be careful the scales are changed to account for the slight differences in temperatures in February.

Secondly, we calculated the building energy requirements and the parameters of the statistical model (the cold sensitivity P and base temperature T_0). They are presented in table 3.14.

	$EC_{3months}$ (in GJ)	P (in MWh/°C)	T_0 (in °C)	$Q_{3months}$ (in GJ)	Q_{2010} (in GJ)
Case P1	3,607,156.1	-2316.7	12.14	3,985,090.6 *(+3.2%)*	12,823,834.8
Case P2 (+25%)	3,936,384.1 (+8.72%)	-2326.8 (+0.43%)	12.32 (+1.47%)	4,092,019.8 (+3.87%)	13,173,869.9 (+2.69%)
Case P3 (+50%)	4,177,445.4 (+14.65%)	-2474.7 (+6.59%)	12.31 (+1.39%)	4,348,580.0 (+4.01%)	13,993,813.5 (+8.72%)

Table 3.14: The building energy requirements and statistical model parameters for each building windows-to-wall fraction's scenario. The building energy requirements outputted from the climate modeling system are $EC_{3months}$. The building energy requirements calculated from the cold sensitivity P and the base temperature T_0 using the statistical model are $Q_{3months}$. The differences with the case P0 are written in (%) while the errors committed in the building energy requirement by using the statistical model are written in *(%)*. The building energy requirements and statistical parameters are always computed by considering the three selected months (February, March and September).

The building energy requirements and the windows-to-wall fractions are positively correlated like in Arasteh et al. [2006]. Those scholars estimated that the increase in the windows-to-wall fractions contributes to increase by +30% of the annual building heating of several US study cases. They attributed the loss of energy to the heat conductivity of the glazing system. It is possible that the radiative losses of the buildings contribute to warm the air up. The buildings cold sensitivities (P) are increasing with the windows-to-wall fractions. The cold sensitivity is the highest in the scenario P3 meanwhile the cold sensitivities of scenarios P1 and P2 are quite equal. In contrast, the base temperatures (T_0) increase slightly between the scenarios, and no differences are found between the scenarios P2 and P3. The rise in the windows-to-wall fractions modifies the buildings energy exchanges with its surroundings but does not change the building thermal equilibrium.

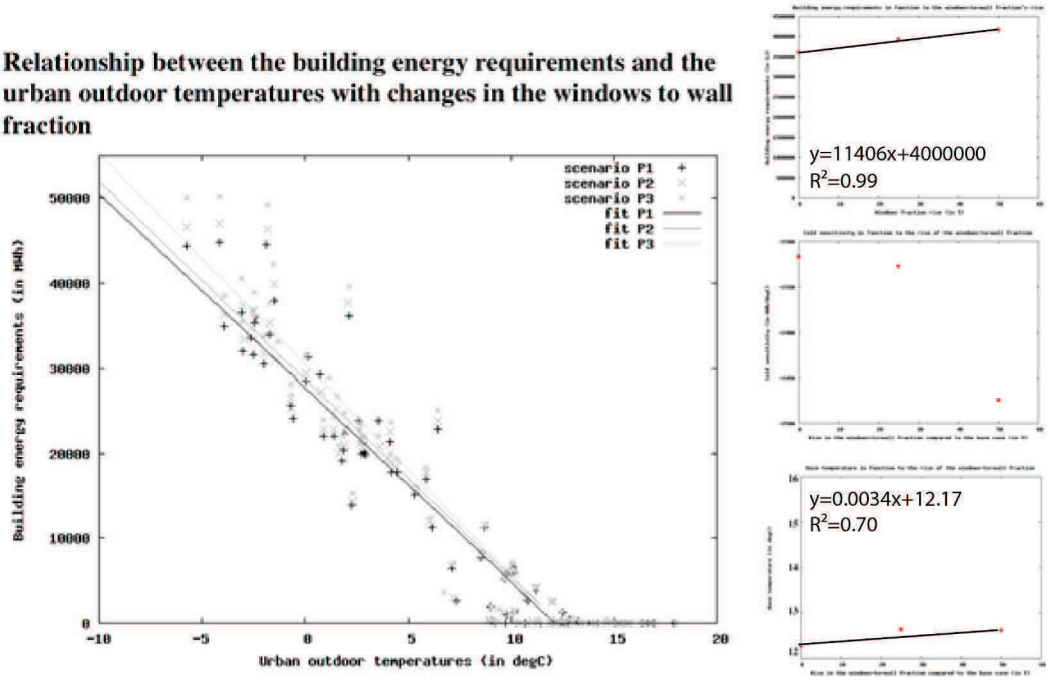

Figure 3.20: At left, sketch of the relationship between the building energy requirements and the urban outdoor temperatures with changes in the window-to-wall fractions. At right, the figures plot the relationships between the building energy requirements EC, the cold sensitivity P, and the base temperature T_0.

Figure 3.20 displays the relationships between the windows-to-wall fractions, and *1)* the building energy requirements, *2)* the base temperatures, and *3)* the cold sensitivities, respectively. Building energy requirements and base temperatures are showed to have linear relationships with the rise in the windows-to-wall fraction unlike the cold sensitivities. A threshold effect is found for windows-to-wall fraction rises included between +20% and +30%.

In conclusion, the change in the windows-to-wall fraction slightly changes the air temperature. It increases the building energy requirements and rather impacts the cold sensitivity. The latter is showed to have a non-linear relationship with the rise of the windows-to-wall fractions. Across the study area, the changes in the windows size seem only possible for new constructions for which the details of the building morphology is already though at the design phases.

- **Management of the thermostat set point temperature**

We simulated three scenarios by using the climate modeling system, in which we successively increased the thermostat set point temperature of the room by +1°K. The three scenarios are referred as scenario T1, T2 and T3, respectively. In the scenario T1 the thermostat set point temperature is 19.85°C. In the scenario T2 it is equal to 20.85°C. Finally in the scenario T3 it is equal to 21.85°C.

Firstly, we investigated the impacts of the steady changes in the thermostat set point temperature on the outdoor temperatures. The statistical description of the outdoor temperature dataset is presented in table 3.15. The scenario T3 is the warmest scenario when taking into account for the maximum, minimum and mean temperatures given in table 3.15. The warming is, however, limited and equal to +0.43°C for the mean temperature compared to scenario T1. With the increasing thermostat set point temperatures, the minimum temperatures are getting warmer, while the maximum temperatures are getting warmer, but at a lesser extent between scenario T1 and T2 compared to scenario T3.

	Scenario T1 (T1=293°K)	Scenario T2 (T2=294°K)	Scenario T3 (T3=295°K)
Tmin	-5.73°C	-5.72°C	-4.12°C
Tmax	17.93°C	17.81°C	18.18°C
Tmean	7.45°C	7.55°C	7.88°C
Tmedian	9.15°C	9.08°C	9.30°C
q_1	1.91°C	1.92°C	2.15°C
q_3	12.59°C	12.90°C	13.12°C

Table 3.15: Statistical description of the distributions of the outdoor temperatures over the CUS area (computed using the three months: February, March and September) with changes in the thermostat set point temperature. *Tmin* is the minimum temperature, *Tmax* is the maximum temperature, *Tmean* is the temperature average, Tmedian is the median of the temperature dataset and at last q_1 and q_3 are the first and third interquartile, respectively.

Clear differences in the distributions of the outdoor temperatures are evidenced in particular for the T3 scenario as showed in the probability distributions of the outdoor temperatures 3.21. The variation of the cold and warm temperatures is the highest in the scenario T3 compared to scenarios T1 and T2, and the maximum temperature is the highest in the scenario T3 compared to the other scenarios.

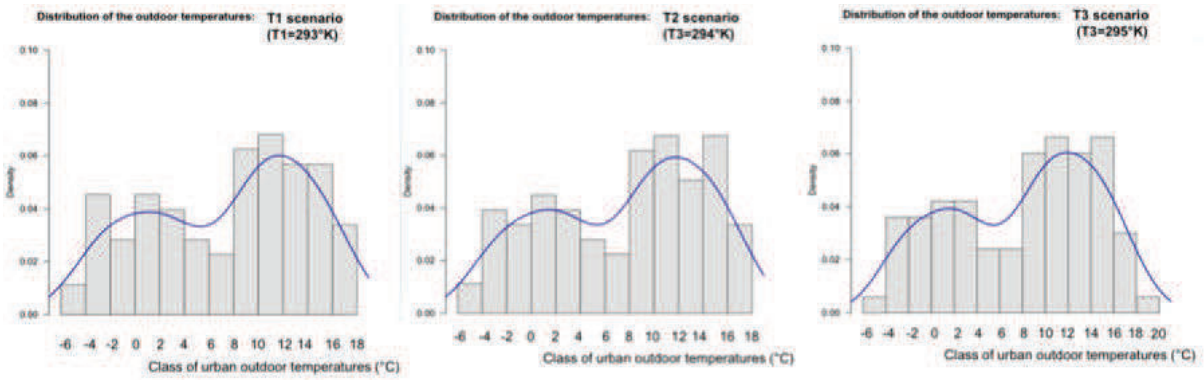

Figure 3.21: Distributions of the urban outdoor temperatures for the three thermostat set point temperature scenarios.

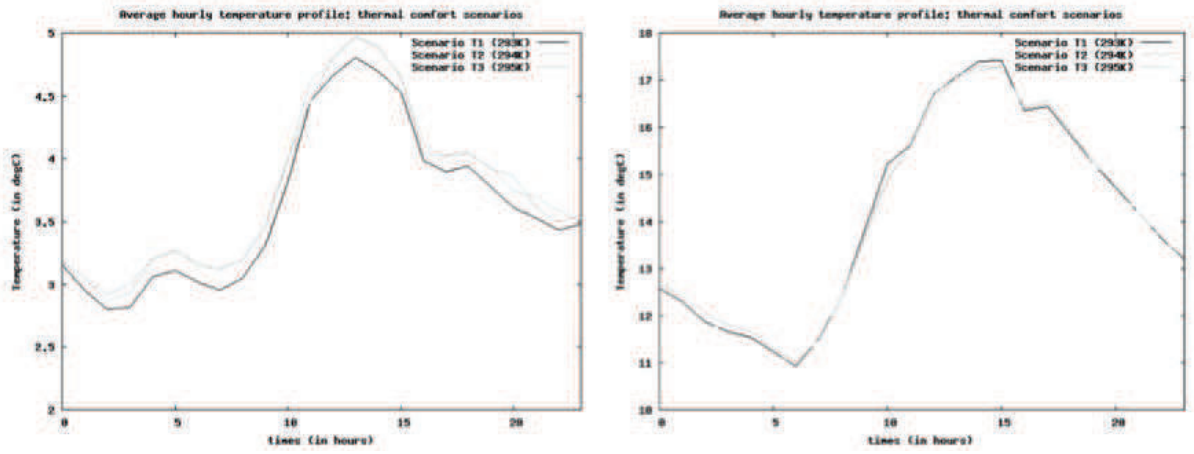

Figure 3.22: Average daily temperature profiles for February and September when changing the building thermostat set point temperature. Be careful the scales are changed to account for the slight differences in temperatures in February.

We then plotted the average daily profiles of the air temperature for each scenario considering a single urban grid located in the dense urban core of the main urban center. The hourly average profiles of the air temperatures slightly vary between the scenarios in February and in September.

In February, the air temperatures are always warmer (+0.2°C) in scenarios T2 and T3 compared to scenario T1. The average daily air temperature profiles of scenarios T2 and T3 are, however, quite similar. In September, the scenarios T2 and T3 have similar averaged daily air temperature profiles: their hourly air temperatures are warmer for scenarios T2 and T3 at night, and cooler in the morning compared to scenario T1. The rise of the thermostat set point temperatures can increase the amount of anthropogenic heat released in the atmosphere, which contributes to warm the air up in particular at

night when the solar forcing is absent.

Secondly, we simulated the building energy requirements for space heating and calculated the statistical model from the "building energy requirements-outdoor temperature" relationship. The building cold sensitivities P and the base temperatures T0 for each scenario are also given in table . The latter are then used to estimate the building energy requirements for the three selected months and the annual building energy requirements for 2010. In addition, table exhibits the changes in the building energy requirements with the changes in the thermostat set point temperatures. It is showed that the changes in set point temperature and the building energy requirements are positively correlated. Nevertheless, the building energy requirements between the T2 and T3 scenarios are quite equals when considering only the three months and quite higher in scenario T3 when considering the whole year. The increase in the building energy requirements with respect to the rise of the thermostat set point temperature is thus, non-linear.

	$EC_{3months}$ (in GJ)	P (in MWh/°C)	T_0 (in °C)	$Q_{3months}$ (in GJ)	Q_{2010} (in GJ)
Case T1 (T1=293°K)	3,607,156.1	-2316.7	12.14	3,985,090.6 *(+3.2%)*	12,823,834.8
Case T2 (T2=294°K)	4,334,957.9 (+18.32%)	-2352.89 (+1.55%)	13.01 (+6.91%)	4,515,435.3 *(+4.07%)*	14,508,175.3 (+12.32%)
Case T3 (T2=295°K)	4,341,546.9 (+18.47%)	-2489.26 (+7.18%)	13.51 (+10.68%)	4,528,714.0 *(+4.22%)*	16,305,759.8 (+23.88%)

Table 3.16: The building energy requirements and statistical model parameters for each building windows-to-wall fraction's scenario. The building energy requirements outputted from the climate modeling system are $EC_{3months}$. The building energy requirements calculated from the cold sensitivity P and the base temperature T_0 using the statistical model are $Q_{3months}$. The differences with the case T1 are written in (%) while the errors committed in the building energy requirement by using the statistical model are written in *(%)*. The building energy requirements and statistical parameters are always computed by considering the three selected months (February, March and September).

In addition, one can observe in table 3.16 that the cold sensitivities of the buildings are increasing by +1.55% and +7.18% respectively for the T2 and T3 scenarios. In parallel, the base temperatures considerably increase (by +10%). The base temperature is

the highest in the scenario T3. It is the lowest in the scenario T1. The change in the set point temperature considerably influences the thermal equilibrium of the buildings as well as the dynamical thermal behavior of the buildings with its surroundings.

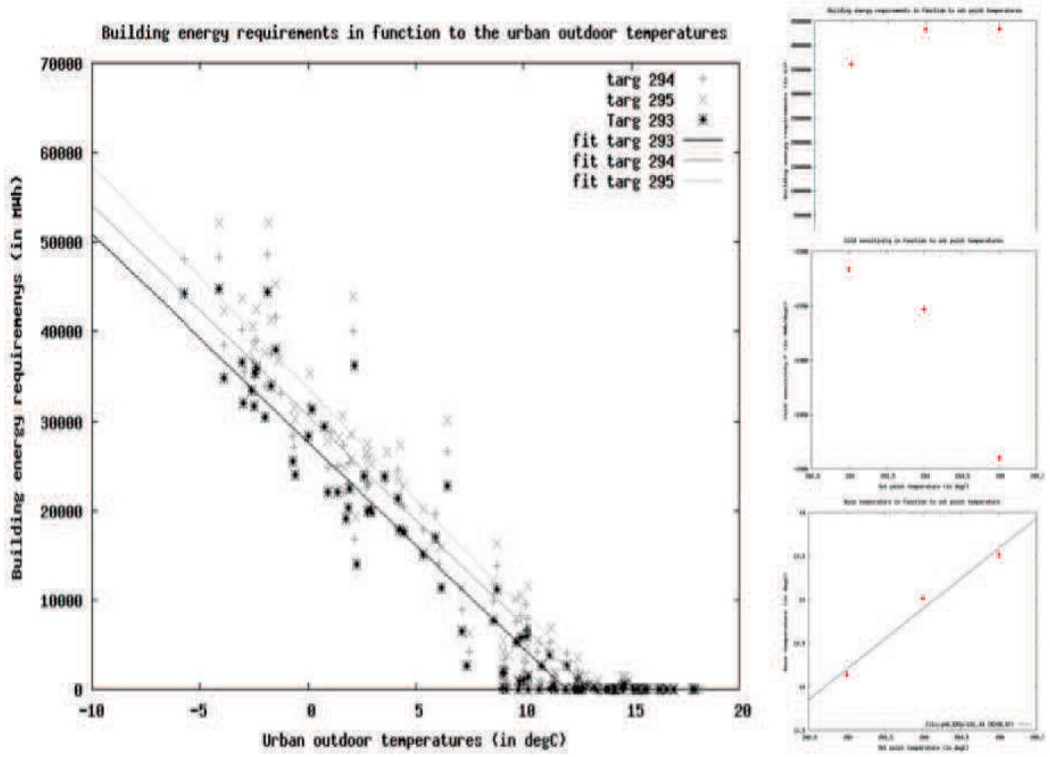

Figure 3.23: At left, sketch of the relationship between the building energy requirements and the urban outdoor temperatures with changes in the thermostat set point temperatures. At right, the figures plot the relationships between the building energy requirements EC, the cold sensitivity P, and the base temperature T_0.

Figure 3.23 displays the relationship between the building energy requirements and the urban outdoor temperatures as well as the relationships between the thermostat set point temperatures and *1)* the building energy requirements, *2)* the cold sensitivities, and *3)* the base temperatures.
The relationships between the thermostat set point temperatures and *1)* the building energy requirements and *2)* the cold sensitivities respectively, are non-linear. In contrast, the base temperatures and the thermostat set point temperatures are linearly increasing.

As a conclusion, the changes in the thermostat set point temperature have moderate impacts on the air temperatures. More, it considerably modifies the building cold sensitivity and building thermal equilibrium. The building energy model is then highly sensitive to the thermostat set point temperatures. Possible improvements in the modeling of the thermal comfort in building energy model have been discussed in Peeters et al. [2009]. These scholars proposed introducing behavioral variables to define the thermal comfort range like the predicted mean vote of Fanger that set in relation the thermal behavior of an environment with the metabolic heat activity and the clothing insulation. The efficience of such measure is mainly controlled by the building occupants behavior, their social and economical characteristics, and their environmental concerns awareness.

3.8 Discussions and Conclusion

In the present study, we aim to test the ability of the WRF/ARW-BEP+BEM climate modeling system to provide urban planners guidelines in terms of building energy requirements. For this, we simulated the 2010 annual building energy requirements and meteorological fields across the Strasbourg-Kehl urban region by using the WRF/ARW-BEP+BEM climate modeling system. The BEP urban canopy parameterization enables us to integrate the effects of the buildings on the local climate while the BEM model computes the building energy requirements for room acclimatization. To consider the feedbacks of the surface on the atmosphere, we set up four two-way nested domains, which finest atmospheric grid resolution is 1 km. In addition, we took benefits of the high-resolved regional land-use land-cover and dwelling databases to provide accurate surface physical parameters to the climate modeling system and to design as much as possible real building properties.

We then compared the simulated meteorological conditions obtained over the finest atmospheric grid with meteorological records taken at three stations located in the URSK domain. Despite the low density of the meteorological stations, the simulated air temperatures are in relative good agreement with the 2-m observed temperatures: the correlation between the two temperature datasets is highly positive and the mean biases are included between 0°C and -1°C. More, the simulated wind field is fairly reproduced by the climate modeling system. In particular, the regional channeling effect of the Rhine Graben is well reproduced by the climate modeling system. Nevertheless, further validations of the meteorological conditions are required to conclude on the accuracy of the climate modeling system to reproduce the observed meteorological conditions.

In an energy outlook, the regional air quality association (ASPA) provided the annual estimated heating energy consumption of the city council of Strasbourg [ASPA, 2012]. The ASPA used a building stock approach considering fixe period of heating and a climate severity index to introduce the effect of the climate variations in the building energy consumption. The climate severity index is based on the definition of the degree-days over the period of interest. The base temperature is the outdoor temperature at which buildings are in thermal equilibrium and do not need heating energy. It is predefined and set at 17°C in the ASPA study. The ASPA simulated the outdoor temperatures using a 5x5 km resolution atmospheric grid over the study area and a mesoscale climate model that does not include sophisticated urban canopy parameterizations (AtmoRhena simulations).
The comparison of the simulated building energy requirements with the ASPA estimates revealed differences in the estimated annual heating energy equal to about -23.55%. Since the ASPA used regional delivery energy census to correct their estimates, we admit that their estimates are the closest from the real building energy requirements of the study area.
Considering the whole physical assumptions and the numerous setting parameters, the discrepancies between the studies are found acceptable. The system of climate models gives good estimates of the building energy requirement over the study area. We, nonetheless, identified two possible sources of discrepancies in the results: the non-consideration of the urban canopy effects on the air temperatures, and the predefinition of the base temperature.
First, the daily temperatures are more frequently cooler than the base temperature in our study compared to the ASPA study. It suggests that our climate modeling system simulates either lower maximum temperatures or minimum temperatures compared to

the AtmoRhena simulations of the ASPA. The roughness approach used in the ASPA study is, however, acknowledged to overestimate the temperature during the day and not fairly reproduce the nocturnal cooling rate at night, hence, the urban heat island effect. Unfortunately the details of the degree-day calculation (the minimum and maximum temperatures) used in the ASPA study are not at our disposal to conclude on this topic. Further comparison analyses are needed.
Second, a large discrepancy is found in the base temperatures chosen in the two studies. Reviews of the scientific literature over the degree-day method pointed out that this parameter is sensitive with the building characteristics and internal heat gains. We then performed several sensitivity tests using the climate modeling system by successively removing the sources of internal heat gains. It seems that the building energy requirements are highly sensitive to the modeling of the wasted heat due to the use of equipment. It could be then assumed that the lower base temperature of our study compared to the ASPA study can be due to the consideration of the internal heat gains in the BEM building energy model.

From the simulations provided by the climate modeling system, we drew the outdoor temperature-building energy requirement relationship found by former studies [Thom, 1954, Valor et al., 2001, Amato et al., 2005]. In particular, we used the simulated air temperature and building energy requirements. This relationship is then sum up by applying a linear regression (the statistical model). The statistical model is showed to provide the fundamental building energy performance parameters: the cold sensitivity P and the base temperature T_0. The first measures how sensitive are the buildings energy requirements with the temperature variations (the slope of the linear fit). The second is the temperature at which the energy gains offset the energy losses (interception of the linear fit with the temperature axis). Our method has the advantage to not define a priori the base temperature that may vary according to location on the Globe, fuels and building types [Amato et al., 2005].

The statistical model is found to well appreciate the building energy requirements. The discrepancies in the estimates of the building energy requirement are less than 5%. We, therefore, explored the potentiality of the climate modeling system and statistical model to assess some building energy conservation strategies. Indeed, compared to other methods, numerical physically-based methods allow testing possible future by considering one by one the changes in the one hand in the built-up patterns, and in the second hand in the surrounds and building radiative, thermal, and aerodynamic prop-

erties. We optimized the computational time required to draw the statistical model by testing the sensitivity of the statistical model with the number of simulated months. We then successively used the systematic combination of three months in a year. It is therefore showed that the daily simulations of air temperature and building energy requirements over three months (February, March and September) are enough to compute the parameters of the statistical model and the building energy requirements of a study area for any period (here, a year).

Among the conservation energy strategies, we simulated the effect of cool roofs, enhancing wall insulation properties, increasing windows size, and the effect of increasing thermostat set point temperatures on the building energy requirements. Urban greenery and urban extension were excluded from the analysis. Most of the studies consider systematic additions of green areas in urban grids that do not allow considering realistic planning strategies. Moreover, the tile approach that considers distinct tiles in each urban grid and distinct land surface models for each tiles prevents the assessment of urban greenery strategies. Grimmond et al. [2010] and Grimmond et al. [2011] concluded the intercomparison program of the urban energy balance model by stating that the latent flux is the least well modeled fluxes in climate modeling systems. In the tile approach, each land surface models indeed calculated the skin temperature and the surface heat fluxes (latent and sensible heat), but the two surfaces do not interact before the first vertical level of the atmospheric grid. Hence, it is not possible to account for the shading of the buildings walls by tree canopies, and cooling effects of vegetative surfaces that act in a radius of 50 m to 100 m downwind the green areas. The effects of the urban development and greening strategies will be, however, investigated in the two next chapters.

For the whole scenarios, the urban outdoor temperatures remain unchanged, unless each scenario shows local changes in the near-surface temperatures. In contrast, the building energy requirements change with the considered scenarios. Building energy savings are reported when adding an insulation layer in the construction system of massive walls whatever the position of the insulation layer in the walls. In opposition, other types of scenarios reported building heating energy increase. The increase in the building energy requirements is the greatest when changing the thermostat set point temperatures and the lowest when increasing the roof albedo. The cold sensitivity P of the statistical model is showed to be always more sensitive to changes in the buildings properties than the base temperature T_0. The cold sensitivity is positively correlated with the building energy requirements except for the wall insulation and roof albedo

scenarios, for which the building sensitivity with the air temperature is reduced. The cold sensitivities P also show non-linear responses to steady changes in the building properties. We proposed that this threshold effect is due to the building insulating properties and internal heat gains. In contrast, the base temperature (T_0) is less sensitive to changes in the buildings properties unlike the changes in the building insulating properties and thermostat set point temperatures. Those two set of scenarios act on the internal heat gains. The first influences the heat transmitted and stored in the building materials. The second influences directly the activation of the heating system. Unlike the cold sensitivity, the base temperature shows linear relationship with steady changes in the building properties.

In conclusion the climate modeling system is able to estimate realistic building energy requirements. It is showed to be more sensitive to internal buildings characteristics than external buildings properties (*e.g.* albedo, windows system). The climate modeling system therefore insists on two energy conservation strategies: the design of passive energy buildings with low heat transmittance and high heat admittance, and behavioral strategies that reduce the thermostat set point temperature. The thermostat set point temperature is often showed to be in relation with the socio-economic characteristics of the household. Desjardin et al. [2011] found higher thermostat set point temperature in aging households (more than 65 yr.) and family. Other studies also found that the thermostat set point temperatures is well correlated to the price of the fuels and household income. However, building energy models implemented in mesoscale atmospheric model such as the BEM model often neglect the socio-economical dimension of the building energy requirements. Further improvements could be achieved by considering adaptive thermostat set point temperatures and windows opening algorithms.

Appendices

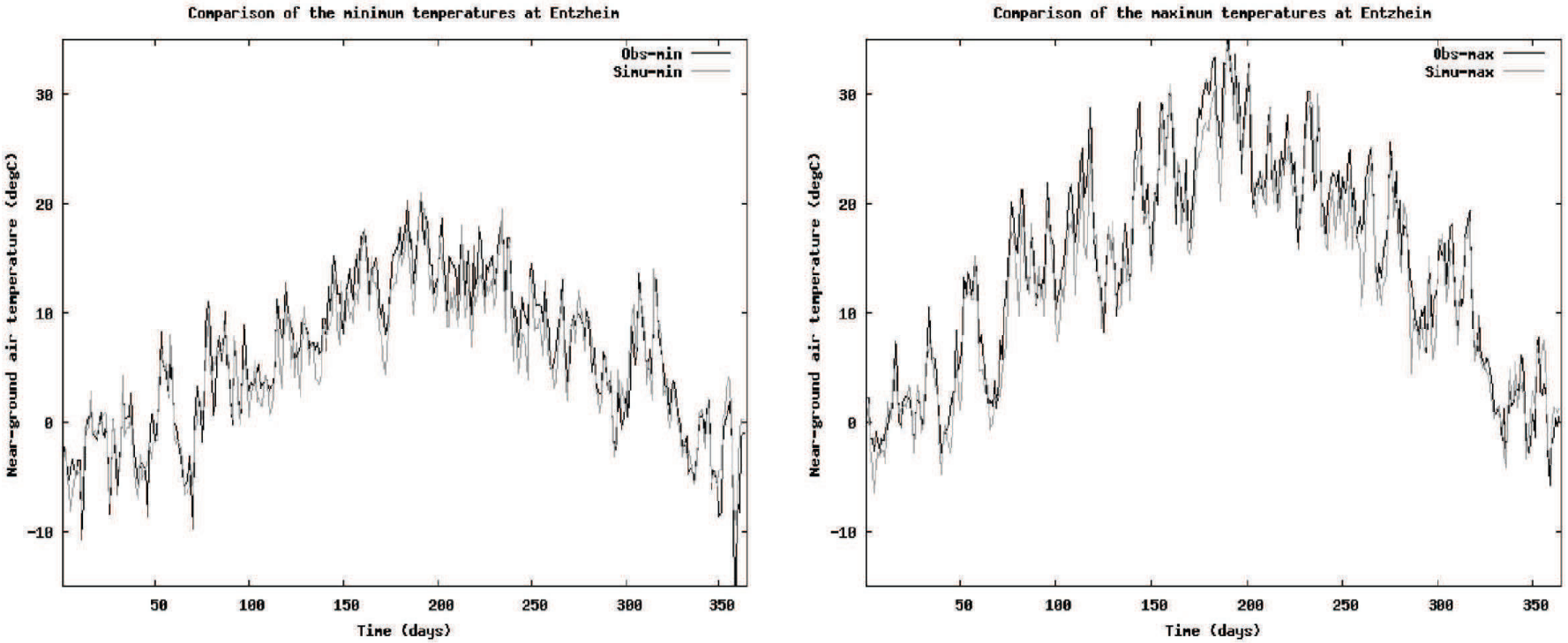

Figure 24: Maximum and minimum temperatures over the simulation year at Entzheim.

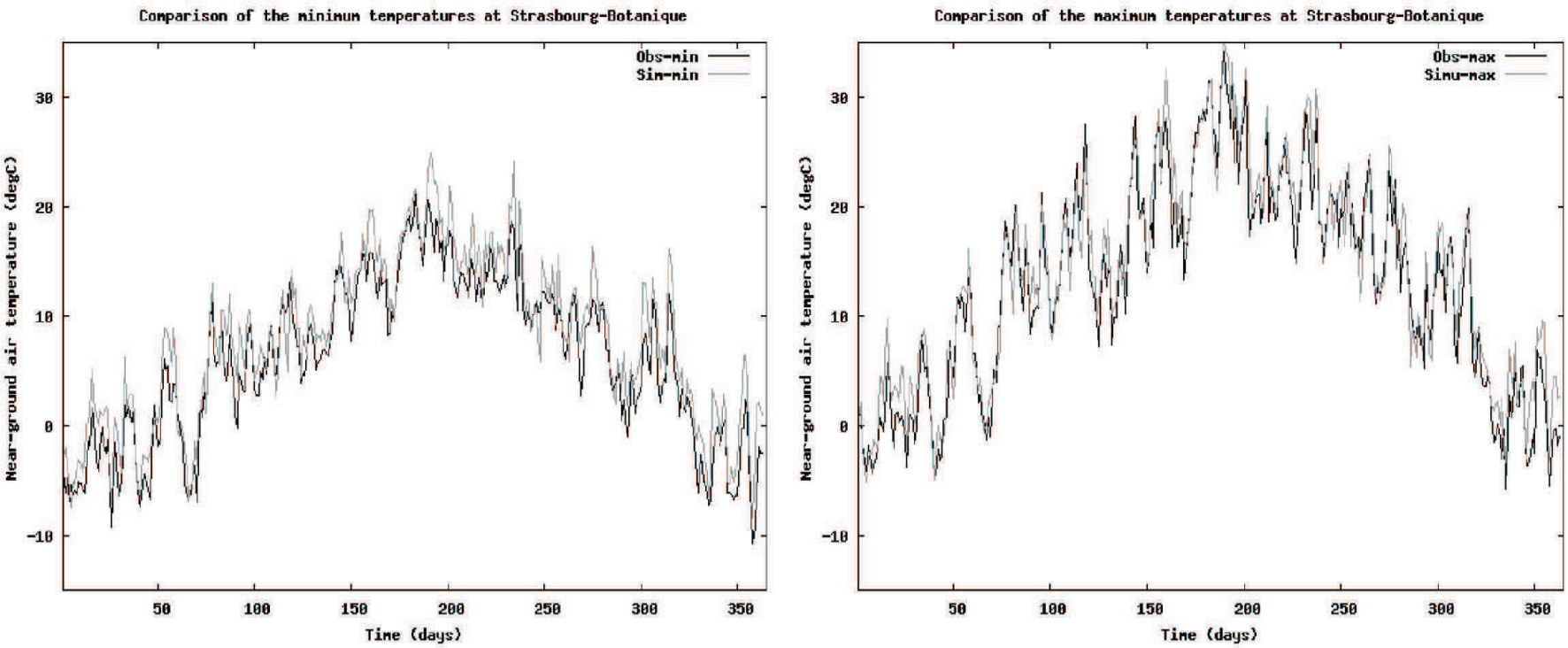

Figure 25: Maximum and minimum temperatures over the simulation year at Strasbourg-Botanique.

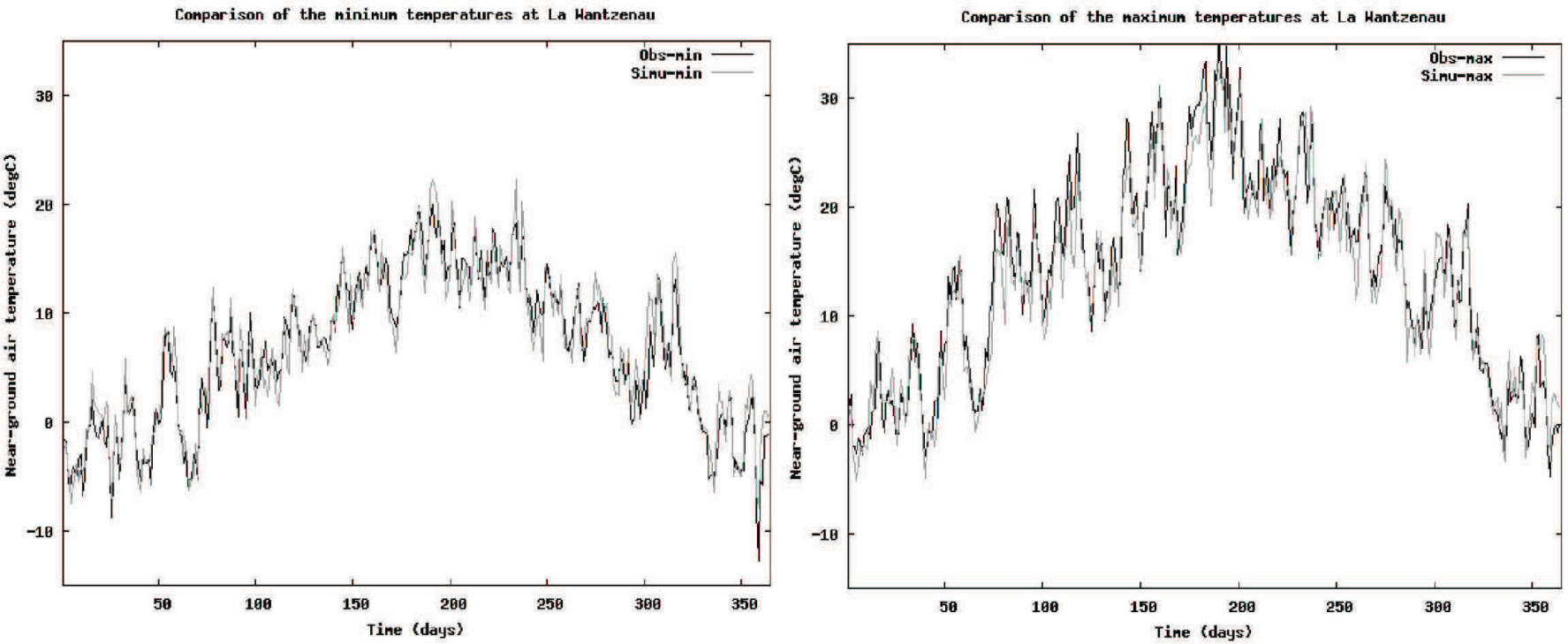

Figure 26: Maximum and minimum temperatures over the simulation year at La Wantzenau.

Chapter 4

Impacts of urban development policies on building energy requirements-Part I

Abstract

Urban sprawl is recognized as the most land consuming urban form [Haines, 1986]. It is also acknowledged to weaken the biological diversity and enhance the city-scale Urban Heat Island phenomenon. With climate change, the latter is expected to harsher the biological thermal stress and modify the building heating or cooling energy use pattern [Hunt and Watkiss, 2011]. The control of residential developments and the preservation of green lanes are measures often proposed to counter these negative effects. The aim of this study is twofold: *i)* quantify the influence of those land planning policies on the urban climate and the building energy requirements; *ii)* assess the ability of the numerical physically-based urban climate modeling systems to provide guidelines for urban planning. A modified version of the urban growth American cellular automata SLEUTH* is used to simulate six contrasted archetypal urban development scenarios. The MorphoLim and Graphab software applications developed at ThéMA laboratory (Besançon, France) help translating the urban planning policies into SLEUTH* through the creation of maps of non-developable lands. MorphoLim delineates morphological built clusters. Graphab determines forested areas essential for ensuring the ecological network connectivity. Afterwards, the six simulated built-up patterns provide the surface boundary conditions of an urban climate modeling system that includes the WRF American fully compressible and non-hydrostatic mesoscale atmospheric model of Skamarock et al. [2008], the building effect parameterization BEP of Martilli et al. [2002], and the box-type building energy model BEM of Salamanca et al. [2010]. The study is carried on over the Strasbourg-Kehl urban region. The construction of the urban development scenarios and the resulting built-up maps are presented in this part I.

Keywords: *Urban climate modeling-Urban planning-Urban growth scenarios-Building energy*

4.1 Introduction

In France after the World War II the urban growth has been rapid. Since the 80s, it has been accompanied by the deconcentration of a large share of the urban dwellers to the nearby less dense suburbs and periurban areas [Bessy-Pietri, 2000]. The spatial extension of urban agglomerations has increased several times faster than the population. Even if this phenomenon is nowadays slowing down, the renewal of traditional values and activities that are associated with the rural way of life, the desire of nature, and the household wish for a periurban detached family housing, still contribute to urban sprawl [Charmes et al., 2009, Desjardin et al., 2011, Bailly and Bourdeau-Lepage, 2011, ADEUS, 2012c]. As a consequence, new built-up areas represent about 610,000 km^2 each 7 years according to the 2006-2009 Agreste study [Agreste, 2011]. Besides the land consumption for housing and due to the built-up areas discontinuities, transportation and services infrastructures are the most land consumers. Such landscape fragmentation dramatically weaken the ability of the landscape to support ecological flows and hence, the biological diversity [Forman, 1995].

Altough the biodiversity conservation was initially a supra-national issue and only concerned remarkable flora and fauna, a change in the paradigm is operating [Franchomme et al., 2013]. Urban sprawl induced intermeshed types of land-uses where human activities and natural lands cohabit. In such a hybrid nature, generalist species that provide ecological services for the humans receive more and more recognitions. They have a concrete reality as part of the urban dwellers every-day environment [Blanc, 2008]. Moreover, according to Sizling et al. [2009] and Gaston and Fuller [2008], they are much better correlated with the overall spatial patterns of species richness than are other species. As a consequence, the role of small reserves in the functional ecological networks is pointed out: scholars assume that they provide a large scale offer for species migrations and land diversity [Forman, 1995]. Meantime the role of local authorities, in particular urban local authorities, in the ecological preservation issues is increasing [Lepart and Marty, 2006]. Bryant [2006] and Bergès and Avon [2010] concluded that urban ecological greenways certainly contribute preventing from landscape fragmentation and preserving biodiversity. They are supposed to act as a source or sink of species and abiotic matters for the ecological background as well as a path between two disjointed habitats. Selmi et al. [2013] pointed out other ecological services provided by the urban green areas in their review of the scientific literature of the 1990-2011 periods. Mehdi et al. [2012] portrayed the evolution of the green areas

in the French urban context. For these authors, the Grenelle 2 marks a milestone in this evolution of the role of green areas in the urban context: green and blue infrastructures are considered as a complete urban planning instrument. The biodiversity preservation concerns in the Agenda 21 and the PADD (spatial planning guidelines for sustainable development), achieve completing the set of urban planning instruments at disposal of the local authorities [Bonin, 2006, CERTU, 2010, Godet, 2010]. One of the main urban sprawl countermeasures is the control of the residential growth. Two spatial planning policies get the upper hand among all possible policies: urban renewal and urban densification. Urban renewal consists in a land redevelopment program. It involves city-initiated re-localization of economic activities and population, as well as urban fabrics demolition/reconstruction. Since 2000, the French SRU law assists the urban renewal operations. It abolishes the minimal threshold size of building lots for sale and encourages the social and urban diversity within renewed urban fabrics. In the other hand, urban densification policies spur the development of new urban areas at the vicinity of existing constructions. The postulate is that an increased density may favor the use of public transport services, soft vehicles, and provide a good access to a larger offer of urban services and amenities. In such policies, particular attention is paid to the articulation of the built-up and natural ecosystems to facilitate the flows of persons, soft vehicles and species and provide access to natural amenities [ADEUS, 2012a].

In parallel, the forthcoming fossil fuel depletion and climate change issues have highlighted the interactions between the fossil fuel combustion, human activities and the global climate. The magnitudes of climate change impacts are such that adaptation policies are required. Local authorities, as they have a thorough knowledge of the land, are expected to play a key role. Particular focuses are given to the buildings sector (about 40% of the total final energy consumption mainly used for space conditioning [ADEME, 2012]) and the urban areas (70% of the total world energy production, more than 50% of the world population [IEA, 2008]). A fortiori urban areas experience a particular macro-scale phenomenon known as the urban heat island (UHI). It consists in the presence of a warm and fully developed turbulent boundary layer downstream the dense built-up urban core that could be about +10°C warmer than the nearby vegetative surfaces. Hence, the UHI may modify the building energy consumption patterns both in time and space and harsher the thermal stress induced by heat waves [Smith and Levermore, 2008]. By sealing through pavements and buildings more and more natural lands, urban sprawl is expected to enhance such a phenomenon.
Therefore the question is: in which extent the urban sprawl countermeasures (*e.g.* urban densification, preservation of the ecological network) can modify the local climate

and hence, the building energy consumption patterns? Are such policies a way to build more sustainable cities?

4.2 Research objectives

The first objective is to dynamically assess the retrofits of urban sprawl countermeasures on local climate and building energy requirements in the context of urban development. During the past decades with climate change, local authorities are more and more asking for quantitative indicators on building energy efficiency, greenhouse gas emissions, air quality, and so on. Accordingly, climate modeling systems developed within the scientific communities are often viewed as appropriate tools to dynamically address complex urban environmental issues [Chen et al., 2011]. They include a regional atmospheric model that provides the meteorological field over a region of about ten thousand square kilometers, an urban canopy parameterization that represents the effects induced by the buildings on the dynamics and thermodynamics of the lower layers of the atmosphere (the canopy, the atmospheric layer extended from the ground up to the roof tops). In addition the urban canopy parameterizations are coupled with simplified building energy model that compute the building energy requirement for space heating or cooling induced by the activation of the Heat Ventilation Air Conditioning system, and provide the influence of the building energy budget on the regional atmospheric energy budget. The climate modeling system requires two sorts of data: the atmospheric conditions at the border of the region, that are often provided by global climate models, and the specification of the surface thermal and aerodynamic properties (*e.g.* roughness, surface skin temperatures, albedo, emissivity, and so on) inherent to each and land cover type present within the domain. The land cover types are usually provided by satellite images. Thus the surface properties only vary according to the up-to-date of the land cover databases, and is not in concordance with the dynamic of the land cover changes, and urban growth. The idea is then , like in 4.1 to couple an urban growth model to the climate modeling system so as to consider the dynamic of the residential development.
The second objective of this research is then to test the ability of such climate modeling systems to consider sub-grid scale changes of land-surface properties that are of same order of magnitude than the scales of planning practices. Indeed, the land cover type of a grid is usually assigned by determining the dominant land cover type of the lowest atmospheric grids according to a predefined urban cover threshold. This urban cover threshold is here set equal to 20%, meaning that a grid is considered as urban if more

than 20% of its surface is of urban nature.

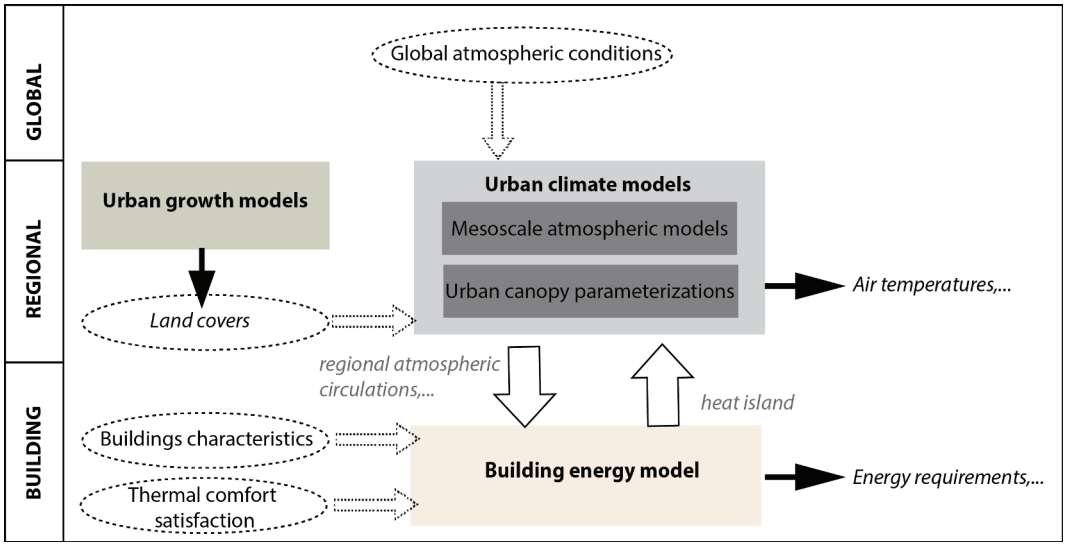

Figure 4.1: Scheme of the chain of models used to assess the effect planning policies on the building heating energy requirements. The inputs of each system of models are surrounded by a dashed circle, the outputs are written in black italic fonts and can be spotted by the black arrows. Building, regional and global represent the different scales involve in the resolution of this complex issue.

We divided the chapter in two parts. The first one is dedicated to the construction of urban development scenarios that integrate urban sprawl countermeasures The second is more specifically dedicated to the climate modeling system's settings and building energy requirement simulations.

4.3 Method and tools

A numerical approach is adopted in this study. It allows testing dynamically, by taken into account several scales, the incidences on local climates and building energy requirements of 6 archetypal and contrasted urban development scenarios. For this, a set of geographical computer-based models was consecutively used.

4.3.1 Presentation of the archetypal urban development scenarios

According to Galster et al. [2001] five types of urban sprawl exist: compact, diffusive, linear, poly-nucleated sub-units, and stepping path urban sprawl patterns. The current study focuses on the diffusive (no control of the residential growth) and compact types of urban sprawl. Two types of compact urban development that represent two current urban policies are distinguished. First, the urban renewal promotes the densification of the inner core of the agglomerations (*e.g.* hollow teeth, vacant lands). Second, the urban densification favors the developments close to the existing built up areas at the fringe of the agglomerations or at the vicinity of transportation infrastructures and services. The resulting archetypal urban development scenarios then come in two versions. Each of them corresponds to the preservation or not of the ecological habitat. Table 5.1 summarizes the main characteristics of the six simulated urban planning scenarios.

During the past, land use change models have played an important role for understanding the mechanisms creating land use changes. They are now expected to provide a broad opportunity to evaluate land use policies and help visualizing alternative futures [Chaudhuri and Clarke, 2013]. Cellular automata (CA), a type of mechanistic models, are the most used. As Batty et al. [1999] pointed out, despite their simplicity CA models achieve to capture the whole uncertainties and complexity of real urban systems. They contain both the spatial and time dynamics. The global form emerges from local actions with no hidden hand directing the macrostructure: like urban systems, CA models are self-organizing systems. Thus, a CA model has been used in this study to simulate the spatial extension of the built-up surfaces over a domain of interest. The simulation period covers few decades. The Doukari et al. [2013] modified version of the American cellular automata SLEUTH* model [Clarke, 2008, Clarke et al., 1993] was selected for the sake of reinforcing the collaborations between two research teams of the LIVE laboratory of Strasbourg.

As the six archetypal urban growth scenarios should reflect the actual urban development control policies, two geographic software applications have been successively used to map the non-developable areas. The ThéMA Laboratory of Besançon has developed these two software applications. First, MorphoLim is a geographical software dedicated to the identification of the morphological boundary of built clusters [Tannier et al., 2011]. The second software application, Graphab [Foltête et al., 2012], is a

Scenarios	No Preservation of the ecological network	Preservation of the ecological network
Spontaneous development	Except non-developable lands that are included in the local development plan, urban sprawl is totally uncontrolled. New urban settlements are spread over the territory to the detriments of the ecological landscape. **(Sc1)**	Urban sprawl is totally uncontrolled. New urban settlements are spread over the territory. However the forested areas that ensure the ecological network connectivity are preserved from the urbanization. **(Sc2)**
Compact development	Except lands that are included in the urban planning instrument, new urban units fill the hollow teeth of the morphological agglomerations to the detriments of natural areas. No refurbishment, demolition and construction phases are assumed. Constructions close to existing built-up areas and transportation infrastructures represent the fact that the urban growth is well controlled. **(Sc3)**	New urban units fill the hollow teeth of the morphological agglomerations No refurbishment, demolition and construction phases are assumed. The urban growth is well controlled and urban densification policies are assumed. New urban units settle down close to the existing built-up area and transportation infrastructure. Forest areas essential to ensure ecological flows over the ecological network are preserved from the urbanization. **(Sc4)**
Moderately compact development	Except non-developable lands that are included in the local development plan, the urban sprawl is concentrated close to the existing built-up areas and transportation infrastructures at the fringe of the morphological agglomerations. **(Sc5)**	New constructions are located at the fringe of the morphological agglomerations close to the existing built-up areas and transportation infrastructures. Forested areas that are relevant for the connectivity of the ecological network are preserved from the urbanization. **(Sc6)**

Table 4.1: Description of the six urban planning scenarios

landscape graph-based software dedicated to landscape networks characterization. It allows the identification of ecological patches that are relevant for ecological functional flows and that should be preserved from urbanization.

4.3.2 The SLEUTH* model

The SLEUTH* version of Doukari et al. [2013] is a modified version of the American SLEUTH Urban Growth Model [Clarke, 2008, Clarke et al., 1993] , an open source and collaborative cellular automata model. It has been adapted and used by Aguejdad et al. [2012] and Masson et al. [2013] for the behalf of the ACCLIMAT project to perform urban growth pattern simulations over the Toulouse great city. Recently, SLEUTH* has been install in the LIVE laboratory for developing new expertise in urban modeling simulations. Unlike the version of Clarke [2008] that has been applied to almost 66 different cities and regions, this version has few validation cases. In the author knowledge it has only been applied over the Toulouse great city. It aims to simulate the urban growth according to a fully controlled mode that can be spatially allocated in terms of quantity and patterns according to predefined contrasted prospective scenarios. Opposite to the SLEUTH model that relies on the use of two or more historical urban maps for calibrating the growth rate and the transition rules [Gazulis and Clarke, 2006, Dietzel and Clarke, 2007], the SLEUTH* model requires directly as inputs the amount of constructible lands and the definition of five calibration coefficients (each of them ranging from 0 to 100) that influence the degree to which each of the four growth rules influences the simulated urban growth. The four urban growth rules are: the dispersed urban growth where urban settlements are spontaneous, the new spreading center, the road-influenced growth, and the edge growth. It thus enables us to design scenarios of urban development in a fully-control mode. As the Clarke [2008] version, SLEUTH* requires five maps as inputs. The existing built-up map represents the actual extension of the urban areas. The exclusion layer inventories lands unlikely to be built up (*e.g.* water bodies, protected area, roads and so on). The slope map acts as a supplementary constraint. The road map, as well, is used to consider transportation integrated urban planning policies. The hill shade maps is only used for representing the results of the urban development simulations. Unlike the precedent version, SLEUTH* does not differentiate the types of roads according to their attractiveness for the urban development. Furthermore it considers an additional layer that represents socio-economic factors' influences (the housing rent, the land prices, the transportation time-distance or other socio-economic cost-distances). Like in other CA models, SLEUTH* does not

allow the simulations of the urban renewals rules.
As in any cellular automata model, the land use is divided into grid cells whose behaviors and characteristics are determined by their own state and transition rules that depend on the state of the neighboring grid cells. Each run, an iterative Monte Carlo process is firstly applied for selecting a set of cells on which the transition rules are then applied. No preferential urban growth directions (unlike the SLEUTH-3r version of Jantz et al. [2004]) are considered. For each scenario, different combinations of transition rules are applied and defined according to parameters, which values range between 0% and 100%. Those parameters allow users to set the percentage of land that will be developed according to each transition rule (*i.e.* the spontaneous urban growth, new spreading centers, road-influenced growth, edge growth).

4.3.3 MorphoLim

The identification of the boundary of urban agglomerations is challenging. No general consensus exists on the definition of cities' limits. It usually depends whenever geometrical, functional or operational criteria are considered. Geometrical criteria methods compared to others present the advantage to be transferable from one country to another, as they are not influenced by socio-economic criteria. According to the literature, the GIS dilution and erosion method seems the most employed [CERTU/URB, 2008, Loriot, 2007]. It consists in applying successively predefined distances threshold over 2D vector built elements. First the built elements are aggregated together. Then, a second distance threshold is applied to make the building envelop be closer to the buildings. The Direction Régionale de l'équipement [DRE, 2008] and the CERTU/URB [2008] advocated a distance threshold of 50 m /50 m that could be adapted according to the nature of the buildings (*e.g.* commercial and industrial: 100m/100m). Other methods rather utilize the maximum distance between buildings to identify the spatial building continuity. Meanwhile the INSEE imposes a distance threshold set by definition at 200 meters. However, as Tannier et al. [2011] stressed, such methods are questionable for European cities that are rather characterized by irregular patterns at their fringes. Overall they questioned the existence of the same distance threshold for all the cities. As a consequence the authors proposed the use of fractal geometry to identify a distance threshold specific to each city.

To identify the distance threshold, an iterative dilation process is applied on the 2D vector building elements of the BDTOPO ®of IGN. At each dilation step, the size of

the dilation buffer increases geometrically (*e.g.* Minkovski dilation). Each built element represents first a single cluster that is surrounded by a buffer zone of a certain diameter. After a while, each cluster is grouped together until only one cluster remains and gathers the whole building elements of the study area. In the fractal mathematics the number of built clusters N is linked to the size of the dilation buffer ϵ according to a power law 4.1.

$$N = a\epsilon^{D} \tag{4.1}$$

On a log-log plot the relationship defined in 4.1 results in a straight line whose slope D is the fractal dimension. It translates how invariant across scales are the built-up patterns. For real patterns, one should identify the point at which the dilatation curve drifts the most from the straight line to define the distance threshold that allows the identification of coherent built clusters. For this, the dilatation curve is modeled by a polynomial fitting.

4.3.4 Graphab

The functional connectivity measures the ability of a landscape structure to facilitate the species movements across landscape patches or to support other ecological flows [Taylor et al., 1993]. The common postulates are that flows of organisms between subpopulations of a metapopulation are proportional to the size of the reserve patches and to the inverse distance between two patches. Large reserve patches provide space for numerous individuals and species' varieties (abundance). Recently, Kindelmann et al. [2005] demonstrated that the landscape between two reserves also plays a significant role on the population flows by favoring the species motions or by inhibiting it (*e.g.* roads) while Forman [1995] pointed out that intermediate and smaller patches may optimize the population flows by connecting two disjoint reserves. As a consequence, the structure of both the habitat matrix and the ecological background are important. In this context graph theory became establishing as a promising way to analyze landscape connectivity [Cantwell and Forman, 1993, Urban et al., 2009b, Minor and Urban, 2007, Bunn et al., 2000, Urban and Keitt, 2001, Urban et al., 2009b] compared to population dynamics models that require mortality, fecundity and other various biological

parameters for a single focal species. A graph defines a set of nodes connected by links. In landscape ecology, nodes represent a discrete element of a landscape (*a habitat patch*) that provides space for a single focal species. Basically, habitat patches are characterized by the geographical position of their barycenter and their area. Other ecological information such as the abundance of species, the species capacity of the reserve could be added to give more ecological richness to the graph. Links represent functional connections between a pair of habitat patches. They could be directed (*edges*) and weighted. Non-directed links mean that the population fluxes are symmetric from a patch i to a patch j. The weight could be the Euclidian distance between two habitat patches meaning that the ecological background is isotropic, or least cost path distance when the landscape mosaic is assumed to be more or less permeable to the species motions. The degree of human disturbance (*e.g.* noise, road traffic and s.o.) on the landscape is one such. A sequence of nodes and links defines a path when nodes are crossed only once. The path length is the sum of the weight of all the links of the path and the maximum length defines the diameter of the graph. This diameter can be adapted to the focal species behavior by accounting for a threshold distance that represents the maximum dispersal distance of a focus species.

Graphab 1.1 software [Foltête et al., 2012] is a GIS integrated application that helps analyzing the ecological network and its connectivity using landscape graphs. It computes several connectivity indexes that qualify the degree of relationship between a pair of nodes. The global Probability of Connectivity Index (PC) is one such (4.2). It has been first designed by Pascual-Hortal and Saura [2007] and then used in the ecological network studies of Tannier et al. [2012] and [Saura and Rubio, 2010] for instance. It quantifies the probability of two randomly located individuals to be connected.

$$PC = \frac{\sum_{i=1}^{n} \sum_{j=1}^{n} a_i a_j p_{ij}^*}{A^2} \tag{4.2}$$

The subscripts i and j refer to habitat patches among a total n of patches. The area of the habitat patches is a while A is the area of the whole studied area. At last, p_{ij}^* is the maximum probability of all possible paths between patches i and j. It is 0 for an isolated patch, 1 for i=j and p_{ij} for other cases. The probability of dispersal for individuals between to patches i and j is inversely proportional to the distance d_{ij} between patches i and j that can be computed with an exponential function like: $p_{ij}e^{-\alpha d_{ij}}$.
Where α is an extinction coefficient included between 0 and 1 computed by Graphab

setting the p_{ij} at a given probability (5%) and considering the least cost distance between i and j. It expresses the intensity of the decrease of the dispersal probabilities.

The process used for identifying the patches or edges that ensure the connectivity of the network is called prioritization. We only consider patches in this study. To prioritize habitat patches Pascual-Hortal and Saura [2007] proposed the dPCk index 4.3, which corresponds to the variation of the PC index when iteratively removing each patch k from the graph and analyzing its decomposition 4.4.

$$dPC_k = \frac{PC - PC_{removek}}{PC} * 100 \tag{4.3}$$

The dPCk could be then decomposed into a dPC flux (term I in 4.4), a dPC intra (term II in 4.4) and a dPC connector (term III in 4.4) [Saura and Rubio, 2010].

$$dPC_k = \underbrace{dPC_{flux,k}}_{\text{Term I}} + \underbrace{dPC_{intra,k}}_{\text{Term II}} + \underbrace{dPC_{connector,k}}_{\text{Term III}} \tag{4.4}$$

With:

- $$dPC_{flux,k} = \sum_{i=1}^{n}\sum_{j=1}^{n} a_i a_j p^*_{ij} \tag{4.5}$$

  For $i \neq j$ and i=k or j=k

- $$dPC_{intra,k} = \sum_{i=1}^{n}\sum_{j=1}^{n} a_i a_j \tag{4.6}$$

- $$dPC_{connector,k} = \sum_{i=1}^{n}\sum_{j=1}^{n} a_i a_j p^*_{ij} \tag{4.7}$$

  For $i \neq k$ and $j \neq k$ and when k is part of the maximum probability path

The *term I* in 4.4 and described in 4.5 corresponds to the area-weighted dispersal

flux from a patch i to all other patches j in the landscape where k could be either the starting or the ending patch of that flux. This fraction measures how well the path is connected to the others assuming that large patches provide space for a higher ecological diversity and hence, individuals more often cross them [Saura and Rubio, 2010]. The *term II* in 4.4 and presented in 4.6 measures the intra-patch connectivity when i=j=k. It is only due to the patch area and no links are considered. Note that the dPC_k is $dPC_{intra,k}$ when k is an isolated patch. At last the *term III* in 4.4 and defined in 4.7 measures the contribution of patch k to link other habitat patches as a connecting elements. This fraction depends on the topological situation of the patch k in the graph and how the patch is located on a "best" path for dispersal.

4.4 The case study

4.4.1 Presentation of the study area

The study area is focused on the French part of the urban region of Strasbourg-Kehl (URSK). Figure 4.2 shows the study area also called the URSK domain. The URSK is located in the flat area of the Rhine Graben and is mainly influenced by the urban pole of Strasbourg (48°35'05"N and 7°45'02"E, elevation: 132-151m).

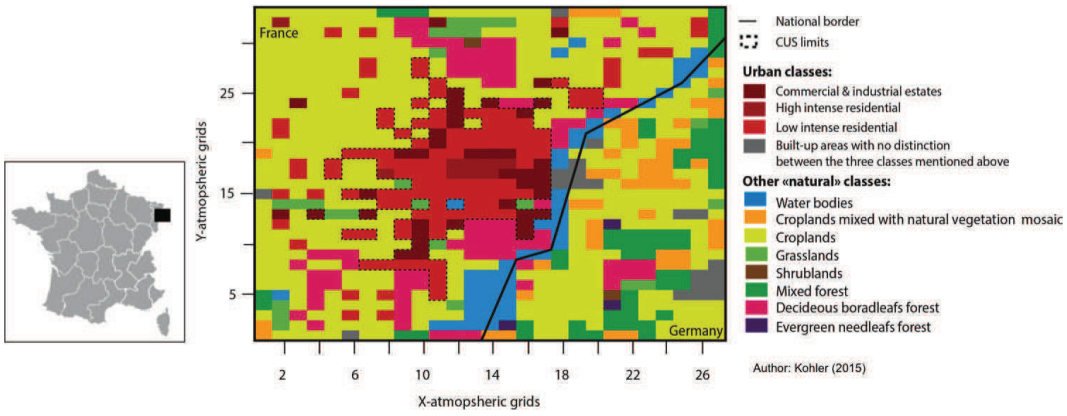

Figure 4.2: The Strasbourg-Kehl urban region "URSK domain" and its location in France

The Strasbourg municipality represents about 60% of the population of the Strasbourg

city council (CUS), an attractive tertiary and industrial urban community. The CUS gathers 28 municipalities and accounts for 43% of the Bas-Rhin district population and 45% of its active population [CUS, 2005]. Even though the CUS population increases (+10% between 1990 and 2006 according to "ASPA" [2006]), the migratory balance is negative. Among migrants, the 18-24 years olds represent a large share of the incoming fluxes while the 30-40 years old dwellers' outward migrations grab the deficit in the migratory balance. Home property is the main motivation for those young families. In residential locations, towns at the periphery and owning to the Strasbourg SCOT are the most attractive but the major share of those new migrants continues commuting every day to the CUS area for working [ADEUS, 2012a] nourishing the urban sprawl. For practical reasons and even if 85% of the CUS population and in particular the Strasbourg population commutes at least once in a year to the nearby Germany [ADEUS, 2011], the German part of the studied area (27,500 ha or about 30% of the URSK domain) is out of the urban sprawl considerations. Planning policies, administrative limits and non-spatial variables like behavioral ones indeed differ drastically between France and Germany.

Over the French part of the URSK, one third of the lands are built up (source: CIGAL BdOcs_2008). In built up areas, transportation infrastructures, retail services and production units account for 71 % of the built-up areas while buildings and urban green areas account respectively for 22% and 7%. The remaining available lands are mostly used for speculative and intensive agriculture (*e.g.* maize, hops, and vineyards). At last, agricultural and the natural lands represent respectively 47% and 16% of the URSK area. Approximately 29% (∼18,590 ha) of them are protected by the 1992 international Ramsar convention on water resource and ecosystem preservation, the 1971 Bern convention on the wild life protection, and the European commission directives Bird, Habitat and Water (79/409/CEE, 92/43/CEE and 2000/60/CE). Thus, with the presence of the Rhine River at the East, the cultivation of vast fertile loess soils at the West of the Strasbourg agglomeration (*e.g.* Kochersberg) and the protection of vast areas, the urban development is drastically restrict originating in turn a high human pressure on the developable natural areas.

The climate of the region is a depredated oceanic one with well-defined seasons according to the Köppen classification (type Cfb). The region is also characterized by particular high frequency of foggy days and snow. Wind velocities are low to moderate ($<3\text{m}.s^{-1}$) and the winds are often channeling by the Rhine Graben oriented North/South [Fischer, 2001]. The intensive field campaign of Fischer [2005] carried on

in August 1999 on 26 meteorological stations stressed the presence of a summer urban heat island effect over the Strasbourg agglomeration particularly intense between 5 pm and 10 pm. Urban stations were about +7.5°C higher than the rural station of Hegeney (40 km from Strasbourg) when low North-Eastern wind speeds (>2m.s^{-1}), clear sky and stable atmosphere conditions were observed.

4.4.2 Settings of the urban growth model SLEUTH*

4.4.2.1 Quantification of the urban growth

The CIGAL cooperation gathers a broad set of public stakeholders that produce and treat the spatial information over the Alsace region. They produce in particular a very detailed land use land cover maps named BdOcs for the year 2000 (BdOcs_2000) and 2008 (BdOcs_2008) that can be exploited at scale 1:10,000. The maps are available for the years 2000 and 2008. The BdOcs_2000 is the result from the IRSS Indian satellite images interpretations. The resolution is 23 m in the multispectral bands and 5.8 m in the panchromatic. Due to its low quality, the spatial information has been corrected with the 1997 orthophotographies database of the IGN which issued from the LANDSAT ETM+ satellite image (15 m) when no land mutations have been stated. When land changes are observed only mutations of 2,500 m^2 are reported (SIRS 2011). The BdOcs_2008 is more accurate. It combines the 2.5 m resolved SPOT 5 satellite images treatments (taken in October 2007 and February 2008) with the 2007 orthophotographies of IGN (spatial resolution of 50 cm) and local land registries. Since the BdOcs_2008 is more precise, the BdOcs_2000 has been made coherent with the BdOcs_2008 so as to build a 2008-2000 lands' mutations database over the region Alsace. During the process, the finest levels of information on the land use of the BdOcs_2008 have been lost. The built land mutation database only inventoried land changes of more than 2,500 m^2 according to the CIGAL technical note of 2011. A GIS extraction of the 2008 and 2000 built up areas per municipalities that are included or intersect in/by the URSK domain has been done. In total 745.75 ha have been converted into built-up area in 8 years (yr.) leading to a land change rate of 93.22 ha/yr. For comparison the Toulouse metropolitan built up area gains +1400 ha/yr according to Aguejdad et al. [2012]. The land conversion is particularly intense at the North-West of the second crown of the Strasbourg metropolitan area. For instance, Wiwersheim (+44.59%), Innenheim (+34.63%), Oberschaeffolsheim (+18.95%) and Eckbolsheim

(+15.9%) municipalities are characterized by a rate of change of more than 10%. This result is in accordance with the DATAR publications (www.datar.gouv.fr) that report land changes of about 890 ha between 2000 and 2006 using the Corine Land Cover European database (the database reports built up area of more than 25 ha and linear elements of more than 100 m width). The results also correspond with the 2002-2007 period average urban growth rate reported by the Strasbourg local planning agency that is 120 ha/yr. for the SCOTERS area [ADEUS, 2012a]. Considering this, 1864 ha are expected to be built by 2030.

4.4.2.2 Input maps of the SLEUTH* model

Basically the SLEUTH* model requires 6 input maps: the existing built pattern, the non-developable land, the transportation networks, the hill shade, the slope in percentage and the socio-economic cost map. The socio-economic factors are not considered in this study while the hill shade map is used for representing the SLEUTH* outputs. The BdOcs_2008 is used to map the existing built pattern and the transportation infrastructure. All built-up lands in the BdOcs_2008 land cover are included in the map of the existing built-pattern except motorways and railroads that are included in the transportation map, and urban green areas and brownfields that are part of the non-developable land maps. The 2.5 m resolved regional digital terrain provides the slope in percentage of the studied area. To such extent, the little fraction of no data present in the South East part of the studied area was corrected iteratively by taking the 8 neighboring pixels average elevation. To preserve a high level of spatial details the whole maps were rasterizing at a resolution of 20 m and then converted into .gif files. For the six scenarios, existing built pattern and transportation infrastructures are non-developable. The German part of the domain that represents almost 27,500 ha ($\sim$30% of the URSK domain) is not considered in this study. The 2012 local development plan of the CUS region determines other non-developable areas over the CUS territory. It includes agricultural and natural areas defined as A, Nc, N, NB, ND, NDL and NDir in the local development plan terminology. The natural and artificial hydrological networks are also out of the developable lands as well as the natural area that are preserved by biodiversity protection national and European legal instruments (RAMSAR convention, Birds and Habitat Directives, ZNIEF "Zone naturelle d'intérêt écologique, faunistique et floristique" and so on). The resulting map corresponds to the non-developable maps for scenarios 1 that is the less restrictive one. For the others

scenarios the Graphab and MorphoLim computing programs were successively used to translate the landscape planning rules in order to introduce additional non-developable areas.

- **Graphab**

  Forested zones are relevant and suitable ecological habitat for several mammal species. In this study they are of particular interest for local and European stakeholders as part of the old Rhine river floods rainforests.

  The selected target species is the Red Squirrel (*Sciurus vulgaris*), a common and abundant rodent species in Eurasia who homes in mature coniferous and deciduous forests. The red squirrels have the following characteristics: (1) they preferentially use forested landscape elements; (2) they have difficulties moving in nonforest landscapes; and (3) they are threatened by the extension of built areas [Tannier et al., 2012]. Although the European Hamster (*Cricetus cricetus*) is highly considered in the planning and ecological policies in the study area, several arguments incite to consider here a more common species. First, the more a generalist species is affected by landscape changes, the more the ecosystem is revealed to be endangered. Second, the more a species population is below a threshold size the more the species could be affected by other extinction factors (gene diversity losses, illness propagation). In the case of the European Hamster, the threshold size of the species estimated at 1,500 individuals is overpassed. The authorities and the associations estimate a population size of 161 to 174 individuals in 2007 (Le Monde 10/12/2012) and 319 individuals in 2013 (L'Alsace 07/12/2013) that are mainly located in enclaves. Third, the lowest is the maximal dispersal distance and the more the habitat species are separated, the more the species is affected by landscape changes resulting from landscape fragmentation. Red Squirrel is characterized by short displacements that are often dedicated for feeding while displacements in unfavorable habitats are scarce. Hence the largest is the home range (*i.e.* the area traversed by individuals in its normal activities for food gathering, mating and earing for young) the more the probability of a subpopulation to become extinct decreases. From survey Verboom and Van Apeldoorn [1990] found a home range size of 0.5 ha while others reported sizes included between 1.52 and 13.4 ha. The daily maximal dispersal distance is set at 61 m in winter and 107 m in summer by Verboom and Van Apeldoorn [1990] while it is set at 1.5 km in open space by Hall et al. [2001] using a loci

gene analysis.

The maps of red squirrel habitat and the ecological background issue from the BdOcs_2008. They are entered into the software application Graphab in the form of a raster land cover map of 10 m resolution. The species habitat patches are built using an 8-nearest neighbor interpolation while the Thiessen-Voronoï polygons method is used for drawing the links between two disjointed patches using the barycenter of each of the habitat patches and selecting the least path cost distance. The costs are attributed to each land covers in the ecological background according to the permeability of the ecological background to support the movements of red squirrels. Contrasted costs are adopted: 1 for the species home and other tree surfaces favorable to movements (tree rows), 10 for habitat patches favorable to movement, and 100 for unfavorable landscape patches characterized by a high level of anthropogenic perturbations. The land cover classification according to the human perturbation cost is found in the cost table presented in the appendices of this chapter.

The maximum dispersal distance allows truncating the planar graph of the red squirrel. As Urban et al. [2009a] found, the number of isolated components of a graph is particularly sensitive to the dispersal distance threshold: a low maximum dispersal distance disconnects the elements of the graphs and a high maximum dispersal distance tends to join together pairs of disjoint and far patches. As evidenced in Figure 4.3, the graph exhibits four components with the use of a 1.5 km maximum dispersal distance: two isolated habitat patches, one simple graph (I) and a bigger one (II). For computing the $dPC_{flux,k}$ and $dPC_{connector,k}$, the probability p_{ij} is set to 0.05 meaning that the probability to cross distances larger than 1.5 km is small. With such parameters, the Graphab computing program identifies a set of nodes particularly relevant for preserving the north-south components of the subset II of the graph in regard to the $dPC_{connector,k}$ and a single node that ensures the connectivity between the south-east and south-west part of the subset II (in black on the Red Squirrel graph 4.3).

The log-log plots (figure 4.4) permits selecting relevant nodes for preserving the ecological network connectivity considering the first visual major break in the slopes of the ranked dPC. Ten forest patches are selected with regard to $dPC_{flux,k}$ characterized by a minimum home range size of 239.52 ha and twelve forest patches with regard to $dPC_{connector,k}$. The latter are characterized by threshold

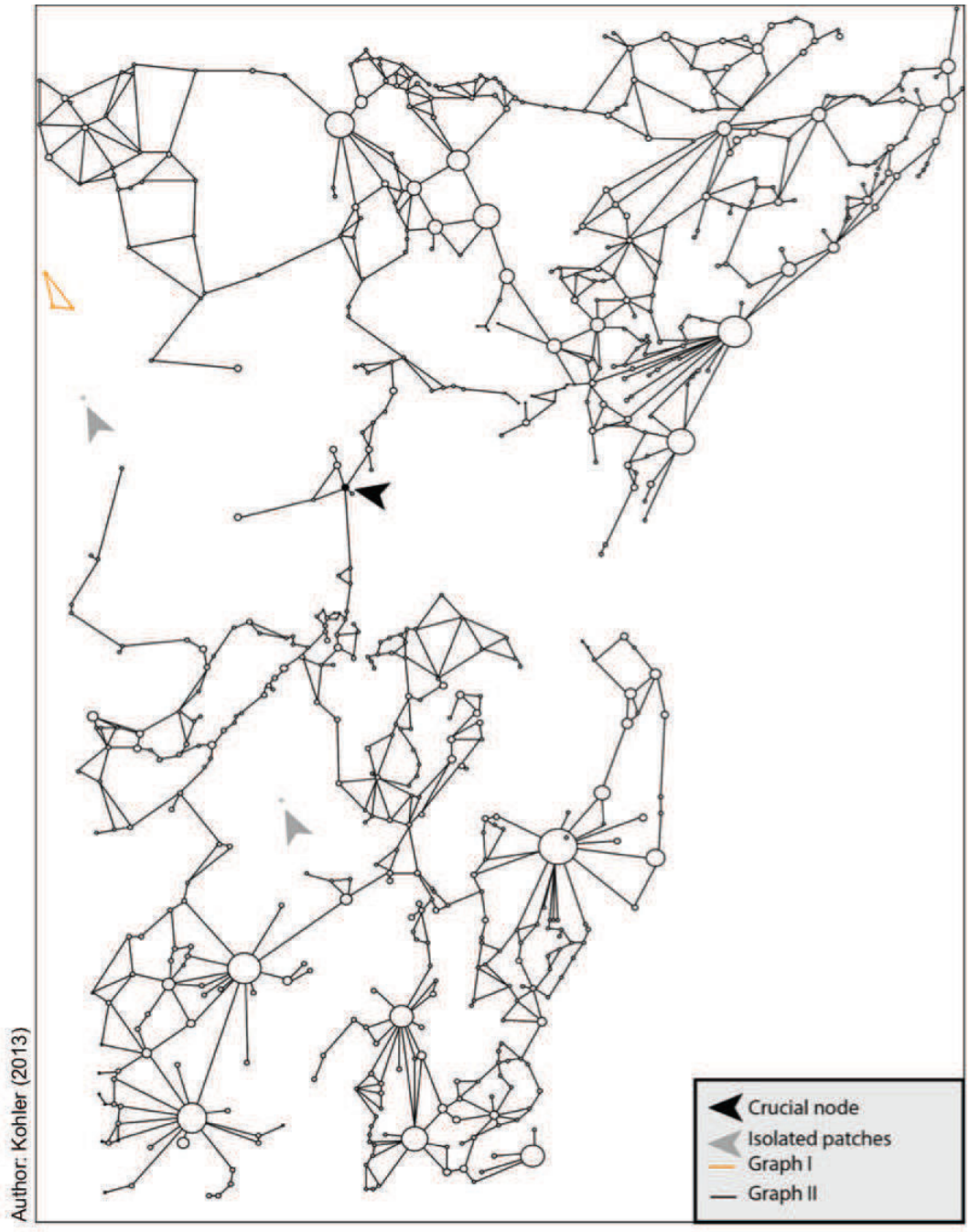

Figure 4.3: The Red Squirrel graph over the URSK domain. The circles represent the habitat patches and are set proportional to the forest areas and lines are the least path distances between two disjointed patches

sizes of 20.88 ha for the biggest one and 0.58 ha for the smallest one. The corresponding forested patches are mapped in figure 4.5.

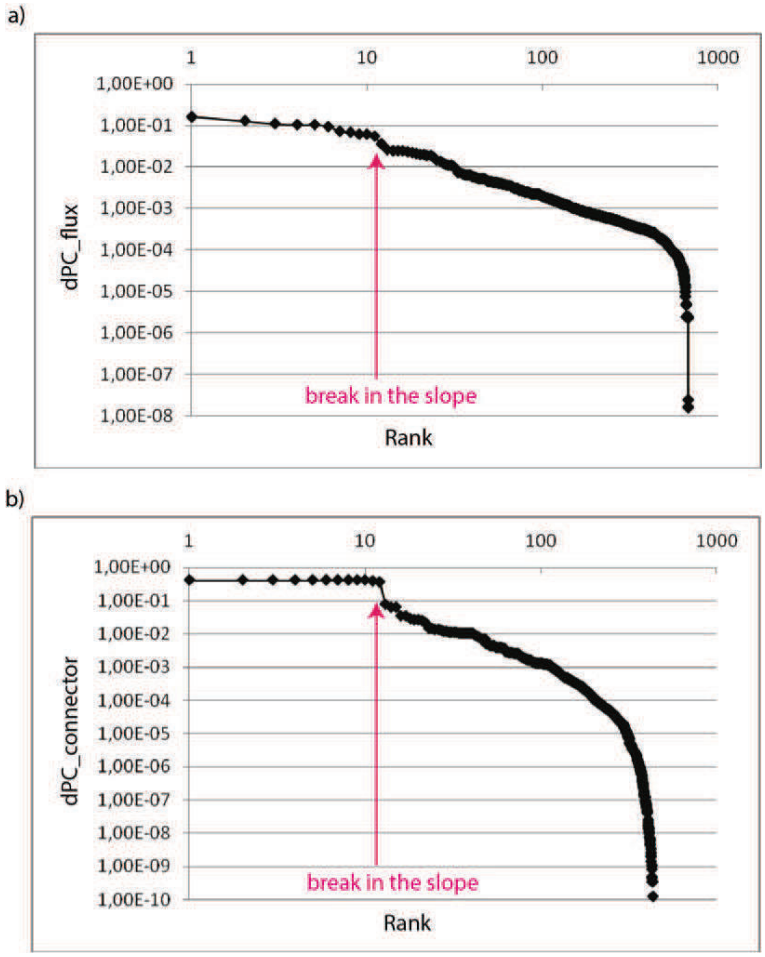

Figure 4.4: The log-log plots of the ranked dPC metrics. In figure a) figures the $dPC_{flux,k}$ and in figure b) are the $dPC_{connector,k}$. Breaks in the slope are identified and are highlighted by the pink arrows.

The results highlight some well-known forested zones that are considered in the local development map (PLU) and already protected. The massive forests of La Robertsau, Neuhof, Illkirch-Graffenstaden, the Plobsheim water plan and the Rohrschollen Island are identified by the $dPC_{flux,k}$. Others wooded areas are mentioned as ecological major axis like the Erstein wood and the Brüche de l'Andlau. We can notice that the small size hardwood forests identified by the $dPC_{connector,k}$ for connecting the north and south part of the graph-component II are located on the future "Grand Contournement Ouest" (GCO) highway axis as showed in the schemes of the study area issued from the local development plan and found in the appendices of this chapter.

- **MorphoLim**

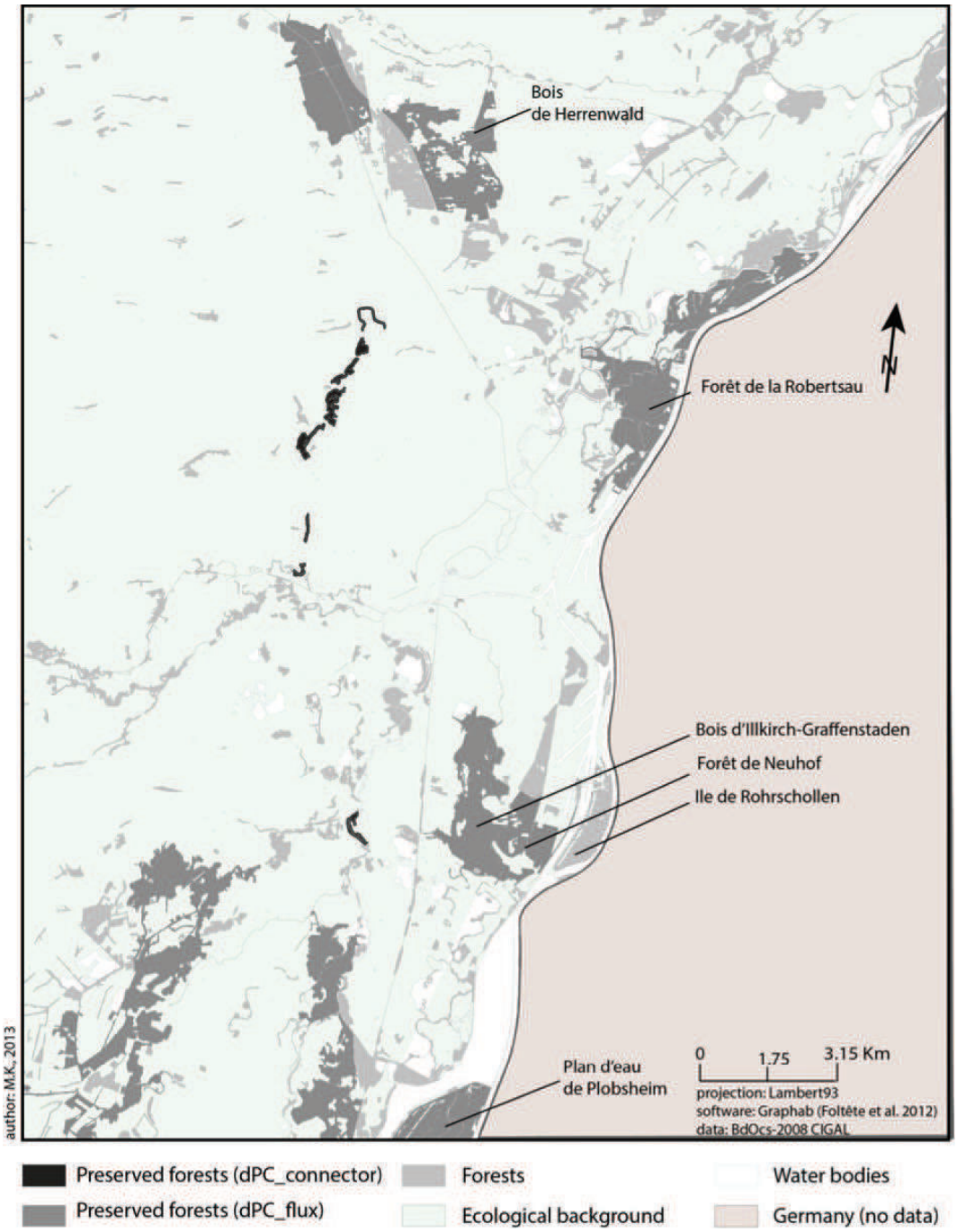

Figure 4.5: Relevant forested habitats for preserving the ecological network connectivity.

The MorphoLim software was applied to delineate the urban boundary of all built clusters including the morphological agglomeration over the URSK domain. Used data is the vector 2012 IGN BDTOPO®database that provides the 2D built elements over the metropolitan area of Strasbourg. By construction, all

built elements larger than 1 m^2 are mapped in the database and qualified by attribute information (nature of the built element, elevation and so on). The BIC (Baysesian indicator criterion) indicates that the number of built clusters-buffer dilation size curve (dilation curve) is well estimated by a 6^{th} order polynomial.

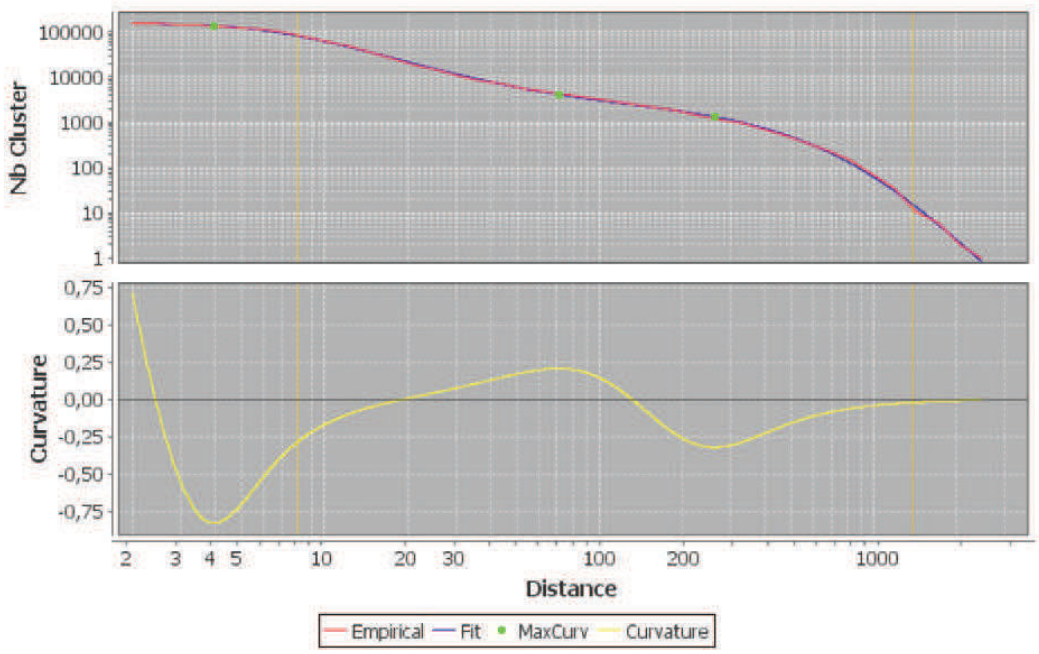

Figure 4.6: The first plot shows the log-log plot of the number of clusters with respect to the size of the dilation buffer. The observed dilation curve is colored in red while the fitting curve is in blue. If the built pattern would be fractal, the dilatation curve would be a straight line. The second graph evidences the relation between the size of the buffers and the curvature of the dilation curve at each point.

Figure 4.6 displays the empirical and the estimated dilation curves, and the associated curvature function given by MorphoLim. The curvature plot presents three maximum curvature values for buffer diameters taken at 4 m, 70 m and 266.10 m. Since the 4 m-buffer diameter is as large as the building dimension it is neglected. As a result we retain the buffer size with the highest curvature value that is 266.10 m leading to a distance threshold of 133.05 m.The delineations of the built clusters over the URSK domain are presented in figure 4.7.

In total we retained the 44 biggest built clusters to constraint the urban development within and close to the urban agglomerations in the compact and moderately compact development scenarios. With the compact development scenario the urban development is possible only within each of the 44 built clusters.

With the moderately compact scenario the urban development is not possible within each built cluster but is possible in their vicinity. The width of which is set proportional to the size of each built cluster. The size of each vicinity buffers are approximated by the 2012-2030 differences in the built clusters radius assuming that the relative size of each morphological agglomeration in the total set of morphological agglomerations is steady during the investigation period.

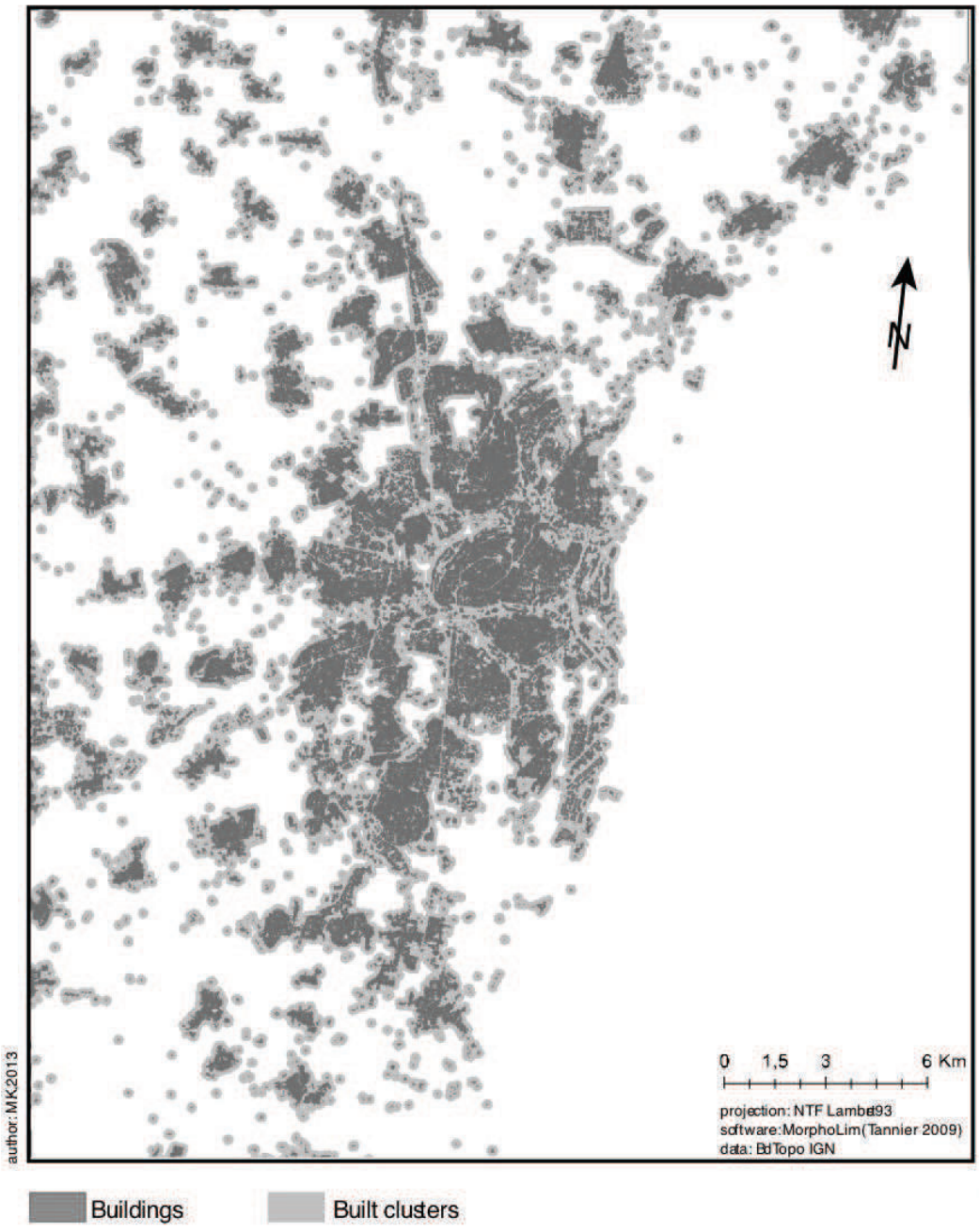

Figure 4.7: Built clusters identified over the French part of the URSK domain.

4.4.2.3 Urban growth parameters

The combination of each urban growth types is controlled according to parameters that range from 0 to 100 and by setting road attractiveness and slope constraint. The slope on the URSK domain varies from 0% and 99.6%. Only slopes higher than 90% are consider to be critical for urban development. Slopes in-between 2% and 18% characterize more than the half of the domain area. It results that the major part of the domain is considered to be flat and that slope exerts few constraints on the urban growth. Roads and other transportation infrastructures influence the choice of residential locations. It could act as a barrier or attract urban settlements along the transportation lanes. The influence of the transport infrastructures has been set according to the literature and urban planning documents. ADEUS [2012b] reported that although the motorization rate tends to decrease in the Bas-Rhin district and 71% of the interviewed households claimed prefer living at 500 m from local services, the residential location choice is still related for 36% of them to the accessibility to public transportation services, motorways and parking lots. Hence the automobile even though in depreciation, continues to have a significant role in the population movements especially when the work and population basins are disconnecting [ADEUS, 2012d]. In 1975, 84% of the working people that work in the CUS lived there. To date, it represents 72%. Thus the distance threshold that is attributed to the road attractiveness is 100 m.

Prior 1990, a depreciation of the new constructions within the main urban poles of the urban region of Strasbourg is observed [ADEUS, 2012d]. However since 2010, it seems that the urban region of Strasbourg supports a new dwelling construction dynamics. Between 2002 and 2007, half of the 7,163 dwellings built in the SCOTERS regions are located within the Strasbourg agglomeration, and villages represent only 20% of the new constructions. In parallel a polarization of the activity centers is observed. It represents 28% of the SCOTERS urban expansion [ADEUS, 2012a,d]. To such extent ADEUS-AURM and DRE [2007] reported a pace of surface growth for activity centers that is 2.5 fold faster than the one of the whole morphological agglomeration.
The largest urban extensions are in villages and small local centers in which urban renewal or brownfield developments are the main figures of the SCOTERS region urban development. In the future, urban planning instruments mention the reinforcement of the metropolitan position of the Strasbourg agglomeration. Development of mixed activity areas close to the main axes of transit, enhancement of the level of the local services and major facilities, preservation of lands for future social collective housing constructions are some of the announced measures. Out of the metropolitan area, local

urban poles that have a good accessibility to the metropolis by public transport and that have a high level of services and infrastructures are privileged for new constructions. For all of those urban poles, urban renewal (in the agglomeration of Strasbourg and in its vicinity) and the urban densification at the urban fringe are urban growth rules. For the other communities, the control of residential development consists in reducing the size of the building lots.
In matters of agricultural and natural lands preservations, particular attention is paid to the ecological network. Natural buffer zones between two urban settlements should be preserved and some protected areas are identified (*e.g.* Natura 2000, hillsides and the humid areas). At last the local periurban agriculture should be maintained.

In the SLEUTH* system four main growth rules are defined. There are: *i)* the spontaneous growth (the space is isotropic); *ii)* the new spreading centers; *iii)* the edge growth, *iv)* the road-influenced growth. Urban development in scenarios 1 and 2 rather corresponds to spontaneous built-up development out of the existing built-up areas. Thus, scenario 1 and 2 are qualified with 100% spontaneous growth. In contrast scenarios 3 to 6 are characterized by 50% road-influenced growth and 50% edge growth.

4.4.3 Conclusion

Six urban development scenarios that integrate urban development and ecological network preservation policies have been designed (three urban types scenarios and two-subsets that account for ecological preservation policies). For each of the six scenarios corresponds a SLEUTH* simulations setup which is given in table 4.2 and a non-developable map that is presented in figure 4.8. The spontaneous urban development scenarios (1 and 2) correspond to the quasi-absence of urban development policies. Solely areas that are already preserved by the local development plan are excluded from the urban development and the spontaneous growth contribution is set at 100%. The compact urban development scenarios (3 and 4) and moderately compact urban development scenarios (5 and 6) tied better with the future urban plan of the region and promote urban density. For such scenarios, the growth rules do not change according the urban type scenarios. Half of the developable areas in 2030 should follow road-influenced growth rule. The other half follows the edge growth rule. Thus, only the non-developable maps ensure the distinction between the scenarios. For compact scenarios the urban development is restricted in the built clusters. For the moderately compact scenarios the urban development is restricted at their vicinity.

We used the MorphoLim computing program to identify coherent built clusters. We consider the 44th biggest built-up clusters over the URSK domain and buffer zonings around each of them to constrain the compact and moderately compact development scenarios. Then the Graphab computing program enables us considering the impact of the red squirrel ecological network preservation policies on the urban development for each urban development types (scenarios 2, 4 and 6). As stressed by the developable areas of each scenario there are slight differences when preserving or not the red squirrel habitat network connectivity for scenarios 3 to 6. This result could be partly explained by the integration of most of the major forest areas in non-developable and protected area in both the local development plan and European Natura 2000 network. Unlike scenarios 3 to 6, scenarios 1 and 2 show that the developable area is reduced by -19.19% when considering ecological network preservation rules. For scenarios 5 and 6 slight differences could be notice in the South part of the non-developable maps.
Finally, since the developable area is always greater than the amount land that is expected to be built for each scenario, it results that the maps of developable areas do not restrict the urban development. Only the CA growth rules reduce more or less the possibility to develop new residential areas.

Scenarios parameters			
2010-2030 expected urban development	*1864 ha*		
Slope	*90 %*		
Socio-economic maps	*No*		
Scenarios	**Developable areas**	**Ecological Preservation**	**Growth rules**
Scenario 1	*34,126.68 ha*	*No*	*Diffusive growth: 100%* *Road-influenced growth (100 meters): 0%* *Edge growth: 0%*
Scenario 2	*27,577.32 ha*	*Yes*	*Diffusive growth: 100%* *Road-influenced growth (100 meters): 0%* *Edge growth: 0%*
Scenario 3	*2,474.80 ha*	*No*	*Diffusive growth: 0%* *Road-influenced growth (100 meters): 50%* *Edge growth: 50%*
Scenario 4	*2,407.32 ha*	*Yes*	*Diffusive growth: 0%* *Road-influenced growth (100 meters): 50%* *Edge growth: 50%*
Scenario 5	*2,918.84 ha*	*No*	*Diffusive growth: 0%* *Road-influenced growth (100 meters): 50%* *Edge growth: 50%*
Scenario 6	*2,748.00 ha*	*Yes*	*Diffusive growth: 0%* *Road-influenced growth (100 meters): 50%* *Edge growth: 50%*

Table 4.2: Settings of SLEUTH* for each development scenario.

4.5 Results and discussions

4.5.1 Maps of simulated urban development

We obtained three series of six scenarios. Maps are presented in figures 4.9. Figure 4.10 shows the corresponding local urban development patterns. The resulting 2010-2030 built up areas extension correspond to the urban development area (1864 ha between 2010 and 2030) define in the inputs of the SLEUTH* simulations for almost all the scenarios except for scenarios 3 and 4 where only about 63% of the urban development area is achieved due to the growth rules constraints. A brief analysis of the land cover change reports that more than 20 ha croplands, meadows and deciduous forests permute into built-up area by 2030. For scenario 1 to 2 and 5 to 6, croplands are the most depredated landscape following by the meadows and the deciduous forests. The compact urban development scenarios exhibit a different pattern of land cover change. Although annual croplands, meadows represent the main land cover changes, the changes of deciduous forests into built-up area are as intense as the changes of the familial cultivated lands, horticultural and greenhouse areas, brownfields and embankments into built-up area. Hence, nearly 86 ha/59 ha of familial cultivated lands, 30 ha /29 ha of horticultural and greenhouse areas, 43 ha /27 ha of brownfield as well as 34 ha /26 ha of embankments turn off into built-up areas respectively for scenarios 3 and 4.

Six morphological indexes allow us to characterize the built pattern resulting from each scenario: the 2010-2030 urban development area Ab in hectar, the number of built clusters (Nb_b), the area of the biggest cluster or morphological agglomeration (A_{MA}) in m^2, the distance threshold (d) in m, and the fractal dimension of the built surface (D) over the urban region. For this we used the same fractal box counting dimension calculation process as used by Tannier and Thomas [2013]. It enables us to easily distinguish built-up patterns characterized by a high diversity in the size of the built clusters (D close to 1.5) and the distance separating each of them from uniform built-up patterns (D close to 2). The primate index (P_i) is also given as well as the rank-size distribution of built clusters (Figures 4.11 and 4.12). The primate index corresponds to the ratio of the area of the largest built cluster (MA) on the second largest built cluster.

	A_b(in ha)	Nb_b	A_{MA}	d	D	P_i
Initial case	No	346	140,900,000	133.05	1.54	25.15
Scenario 1	1,864.00	127,791	74,390	No	1.6266	1.93
Scenario 2	1,864.00	126,172	74,390	No	1.6261	1.93
Scenario 3	1,185.24	367	145,200,000	118.34	1.5771	19.84
Scenario 4	1,182.48	367	144,400,000	119.16	1.5771	20.16
Scenario 5	1,864.00	148	260,500,000	188.24	1.6000	20.27
Scenario 6	1,864.00	155	254,700,000	186.94	1.5990	19.86

Table 4.3: Morphological characteristics for the six scenarios and the initial case (2008). Note that D, the box-counting fractal dimension is calculated with significance level controlled by an R^2 (>0.99) and a p-value << 0.01.

The initial case is characterized by an intermediate number of built-clusters compared to the compact and moderately compact development scenarios. It outlines a polarization of the past development in the main agglomerations of the URSK domain. The primate index is the biggest of the whole set of scenarios indicating a hierarchical urban framework that could also be observed in figure 4.11. A sharp slope is observed between the area of the two first built-up clusters following by a plateau and a moderate slope in the rank-size distribution. The distance threshold is lower than for the compact development scenarios but higher than for the moderately compact development scenario meaning that the urban development is concentrated in the main agglomerations but not as much as in the compact development scenario. At last, the fractal dimension indicates a high diversity in size of built clusters as showed by the rank-size distribution.

It appears in this study that each morphological index gives complementary and no redundant information on the simulated built up patterns. The fractal dimension however close to 1.6 for the whole scenarios is a less discriminating index compared to the rank-size distributions. It indicates built-up patterns that are connected according to the scales (no isolated aggregate) and characterized by a high diversity in the size of the built clusters and distance thresholds. A higher fractal dimension as observed in scenarios 1 and 2 and at lesser extent in scenarios 5 and 6 stresses a tendency for such scenario to create more uniform built up patterns compared to scenarios 3 and 4.

Hence, the analysis on the morphological indexes presented in table 4.3 clearly evidences differences in the three types of built-up patterns meaning that the resulting 2030 land covers are as much contrasted as the urban development policies. The introduction of forest preservation rules does not modify the simulated built-up patterns. The spontaneous urban development (scenario 1 and 2) is characterized by: *i)* a very large number of built clusters; *ii)* the smallest morphological agglomeration area; *iii)* a loss of primacy of the largest built clusters with nevertheless a dominant morphological agglomeration as indicating by the primate index that is 13 time lower than the one of the initial case. No distance threshold between built clusters could be identified. The presence of thousands of built clusters reveal a scattered built-up pattern. The moderately compact scenarios (5 and 6) exhibit: *i)* the lowest number of built clusters; *ii)* the biggest morphological agglomeration area; *iii)* and a fractal dimension slightly lower than for the other scenarios. Scenarios 5 and 6 generate concentrated built-up patterns characterized by a more hierarchical polycentric built pattern as revealed by the weak rank-size distribution's slope. At last the compact development scenarios (3 and 4) show the smallest distance threshold, the smallest fractal dimension (close to 1.5) meaning that the built-up pattern is characterized by high diversity in the sizes of built clusters. The rank-size distribution shows several plateaus where built-clusters have the same built area. Because the number of built clusters is higher and the area of the morphological agglomeration is smaller than in the moderate development scenarios (5 and 6), it seems that the simulated compact planning policy generates more fragmented built patterns than the moderately compact planning policy.

4.5.2 Integration of the 20x20 m resolved simulated urban development in the 1x1 km resolved atmospheric grid

Land cover types are static data assigned for each atmospheric grid of the mesoscale climate model. It permits specifying the physical radiative (*e.g.* albedo), thermal (*e.g.* skin temperature) and aerodynamic (*e.g.* roughness) surface properties in each atmospheric grid that are then used for computing the surface forcings (momentum, heat and moisture fluxes at the surface-atmosphere interface) used as boundary conditions of the partial differential governing equations at the surface interface.

In the WRF-ARW model dominant land cover types are used. It requires the definition of an urban fraction threshold corresponding to the fraction of built-up area included in each atmospheric grid. This urban fraction threshold initially set at 50% was lowered to 20% meaning that more than 20% of the land covers that are included in a given atmospheric grid should be of urban nature (*20% rule*). The remaining part is considered as non-urban and a uniform natural land cover type is attributed for each remaining non-urban fractions of the considered urban grids over the whole domain. This process is referred as the atmospheric grid's urban classification. It is usually automatically fulfilled in the geoprocessing step of an atmospheric simulation during which initial and boundary conditions are assigned for each atmospheric grid of a simulation domain using various institutional datasets (MODIS and USGS land cover and topography datasets). In this study the land cover types and urban fractions were provided by the resolution BdOcs_2008 land cover datasets. We aggregate in each atmospheric grid of 1km width the area of each type of urban land uses for determining the proportion of urban land uses present within each 1km grid (urban-fraction). Then the 20% rule is applied to classify the atmospheric grids into urban or non-urban grids.

To study what is really "seen" by the WRF-ARW mesoscale atmospheric model, we have compared the distribution of the urban land uses in each atmospheric grid before and after the application of the 20% rule. Several descriptors have been computed to analyze the effect of this rule (dominant land cover approach) on the modeled land covers. They are presented in table 4.4. The median (μ) indicates the center of the urban fraction distributions. The interquartile range shows the variance of the distributions. The kurtosis measures the "peakedness" of the probability distribution of a set of data compared to a normal distribution (average=0, and standard deviation=1) and the skewness indicates the asymmetry of the probability distribution compared

to the median. A negative skewness indicates a distribution that is decentered at the right of the median, while a positive skewness indicates a decentered distribution at the left of the median.

Statistical parameters	**Spontaneous development**		**Compact development**		**Moderately compact development**	
	After the 20% rule	Before the 20% rule	After the 20% rule	Before the 20% rule	After the 20% rule	Before the 20% rule
Median	44.91	12.68	48.22	14.60	43.77	18.10
Interquartile	30.36	27.97	34.23	39.03	32.51	38.12
Kurtosis	-0.73	0.77	-0.92	-0.18	-0.74	-0.23
Skewness	0.54	1.31	0.40	0.97	0.51	0.89

Table 4.4: Statistical distribution of the amount of urban fraction in each atmospheric grid.

From table 4.4, one notice that the median is the same for the whole scenarios but it is four times higher after the atmospheric grids classification indicating a re-centering of the urban fraction distribution. The interquartile ranges slightly vary between the scenarios before and after the atmospheric grids classification. The deviations are larger after the atmospheric grids classification in compact and moderately compact scenarios and conversely slightly smaller in the spontaneous scenario. The negative kurtosis become larger pointing out a larger spreading of the urban-classified fractions compared to the normal distribution after the atmospheric grids classification. This feature is particularly obvious in the spontaneous development scenario in which the positive kurtosis becomes negative after the classification of the atmospheric grids indicating a spreading of the urban-classified fractions. At last, the skewness is showed to dramatically vary for the spontaneous development scenario after the atmospheric grids classification.
Thus, larger modifications of the urban fraction distribution function are reported in the case of the spontaneous development scenario using the dominant land cover assignment approach.

Then we compute the total built-up area and the corresponding number of urban grids (table 4.5) considered in the urban climate modeling system using the 20% rule. It can be showed that the urban climate modeling system considers a larger total built-up area compared to the spontaneous urban development scenarios although the

SLEUTH* simulated built-up area was the lowest (only 63% of built up developed area) in such scenario.

Urban development scenarios	Number ofurban grid	Corresponding urban grids' built-up areas (in Km^2)
Scenario 1	188	87.24
Scenario 2	188	87.06
Scenario 3	184	89.83
Scenario 4	185	90.18
Scenario 5	210	98.00
Scenario 6	209	97.68

Table 4.5: Urban grid counts and corresponding built-up areas taken into account in WRF/ARW.

Thus as showed in table 4.4 and 4.5 the dominant land cover methods is inappropriate for studying scattered built-up patterns. As a consequence, scenario 1 and 2 will not be considered in the WRF/ARW scenarios comparison analysis.

4.6 Conclusion

Like previous study we attempt to explore the effect of two planning rules (control of urban development and preservation of ecological habitats) on the 2030 urban morphology and urban climate [Tokairin et al., 2010, Aguejdad et al., 2012, Masson et al., 2013, Stone et al., 2010]. The latter is set in relation with the space heating building energy requirements. The intermediate time lapse (20 years) is in accordance with the time horizon of planning strategies. The planning rules and mechanisms behind the urban development are explicitly taken into account through the design of non-developable lands' maps that are integrated in the SLEUTH* urban growth cellular automata model. For this we use the MorphoLim and Graphab geographical computing program. MorphoLim permits distinguishing three contrasted urban type scenarios: the compact, moderately compact and spontaneous urban development scenarios. Each of them corresponds to different planning policies and residential development con-

trol intensities. The first corresponds to the densification of the existing built pattern within each existing built cluster. The second scenario corresponds to the reinforcement of the main urban centers by concentrating the development at the periphery of the middle-sized built clusters. The third type of scenario considers no control of urban development except the zoning set in local development plans (PLU).

It has been showed with the morphological indexes that the compact scenarios do not produce necessarily connected built-up patterns. More built-up clusters, smaller morphological agglomeration are reported in the compact development scenarios despite the shortness of the threshold distance compared to the moderate compact development scenarios. Moreover compact development scenarios do not permit to construct all the expected urban development area meaning that the compactness of the urban form may be too constraining in a context of high urban development intensity in particular in the Strasbourg-Kehl region where a large part of the vacant lots in the existing built clusters are zoned as non-developable lands in the local development plan. However it is without counting on the urban renewal policies, an option that is not available in SLEUTH* that only considers the non-urban to urban land changes and does not distinguish residential built-up clusters from the commercial and industrial ones. Actually few CA model are able to consider urban renewal and efforts have to be pursuit in this way. In the author knowledge only the inspired Dynamic Urban Evolutionary Modeling approach used for instance in the Batty et al. [1999] cellular automata accounts for life-cycle mechanisms and activities for residential, manufacturing and industry, services and commercial-retail-shopping and so on. Like it was expected, the analysis of the resulting SLEUTH* 2030 built-up patterns using morphological indexes confirms that the following method achieve reproducing three contrasted urban types scenarios that are characterized by different rank-size built-up clusters distributions, fractal dimensions and morphological agglomeration distance thresholds. Nevertheless, the SLEUTH* urban development simulations could be improved by distinguishing different types of roads according to their attractiveness for the residential development. Residential development is more intense far away from main roads than secondary roads. The CA model could also be improved by considering changes in other types of land uses (parking lots and commercial malls) and other transportation modes such as rail or other public transportation services (bus, tramway) as recommended in urban densification strategies.

Then, for each scenario we distinguished two sub-scenarios that consider or not the preservation of the forest ecological network using the graph-based Graphab computing

program. This approach permits considering more realistically the ecological network planning policies than other approaches that are currently proposed in "green and ecological friendly" scenarios. Masson et al. [2013] for instance considered a green belt strategy to refrain the urban development and added to each new dwelling a steady garden fraction that is thus unable to slow down the urban sprawl. Several studies like Mehdi et al. [2012] however outlined that green belt strategies in the ecological preservation policies make no more agreement. As the determination of the regional ecological network of the Strasbourg urban region was not the main scope of this study, we produced only one focus species graph. The red squirrel species was selected. Its population abundance and relatively low maximal dispersal distance motivated the selection of this mammal common species. Indeed as Urban et al. (2009) demonstrated, the maximal dispersal distance threshold has non-negligible impacts in the resulting graph diameter and therefore a low maximal dispersal distance permits highlighting the role of small reserves in the regional ecological network. One limit of this approach is that it suffers from the subjective and generalization attribution of human disturbance costs for each land cover type of the ecological background that in turn influence the least cost path and the graph diameter. The costs are given to a type of land and do not account for local specificities such as the human frequentation or the noise level. After the morphological analysis of the outputted SLEUTH* macro-scale built-up patterns, it appears that the ecological network preservation policies have few impacts on the future 2030 built-up patterns.

As the six 2030 built up maps are then provided to the WRF-BEP+BEM climate modeling system for specifying lower boundary conditions such as the gridded urban fraction, the gridded dominant land-cover, skin temperatures, roughness length and so on, a sensitivity analysis on the atmospheric grid resolution was performed. It results that the integration of the 20x20m resolved built up pattern in the 1x1km atmospheric horizontal grid resolution raises some difficulties. In particular the dominant land cover methods that is usually used in mesoscale atmospheric model obviously fails to reproduce scattered built-up patterns. As a consequence, only two of the six urban development scenarios were finally integrated in the urban modeling system to answer to the initial research objectives.

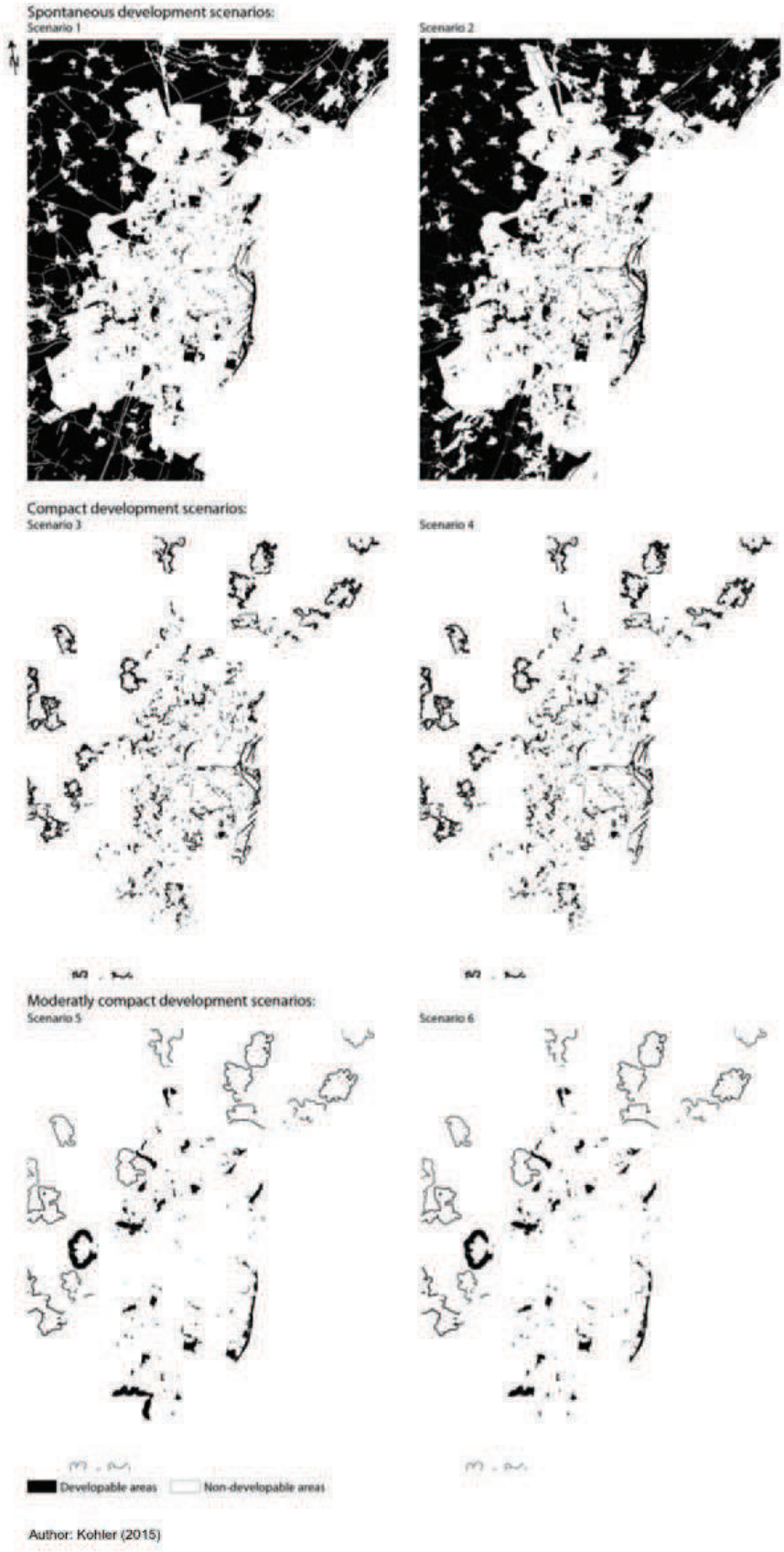

Figure 4.8: Non-developable lands for the six scenarios (SLEUTH* Inputs)

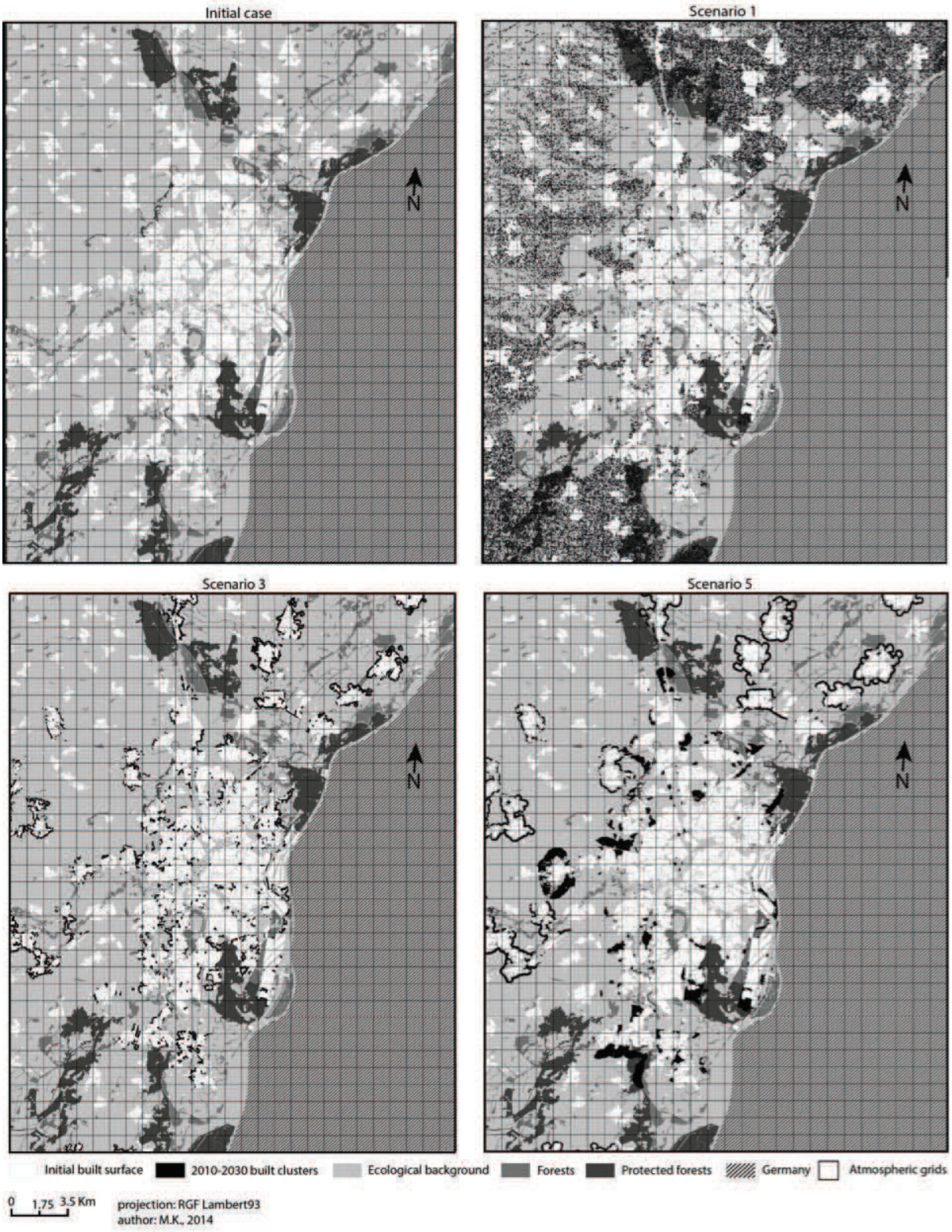

Figure 4.9: The initial case maps and the three urban development types maps.

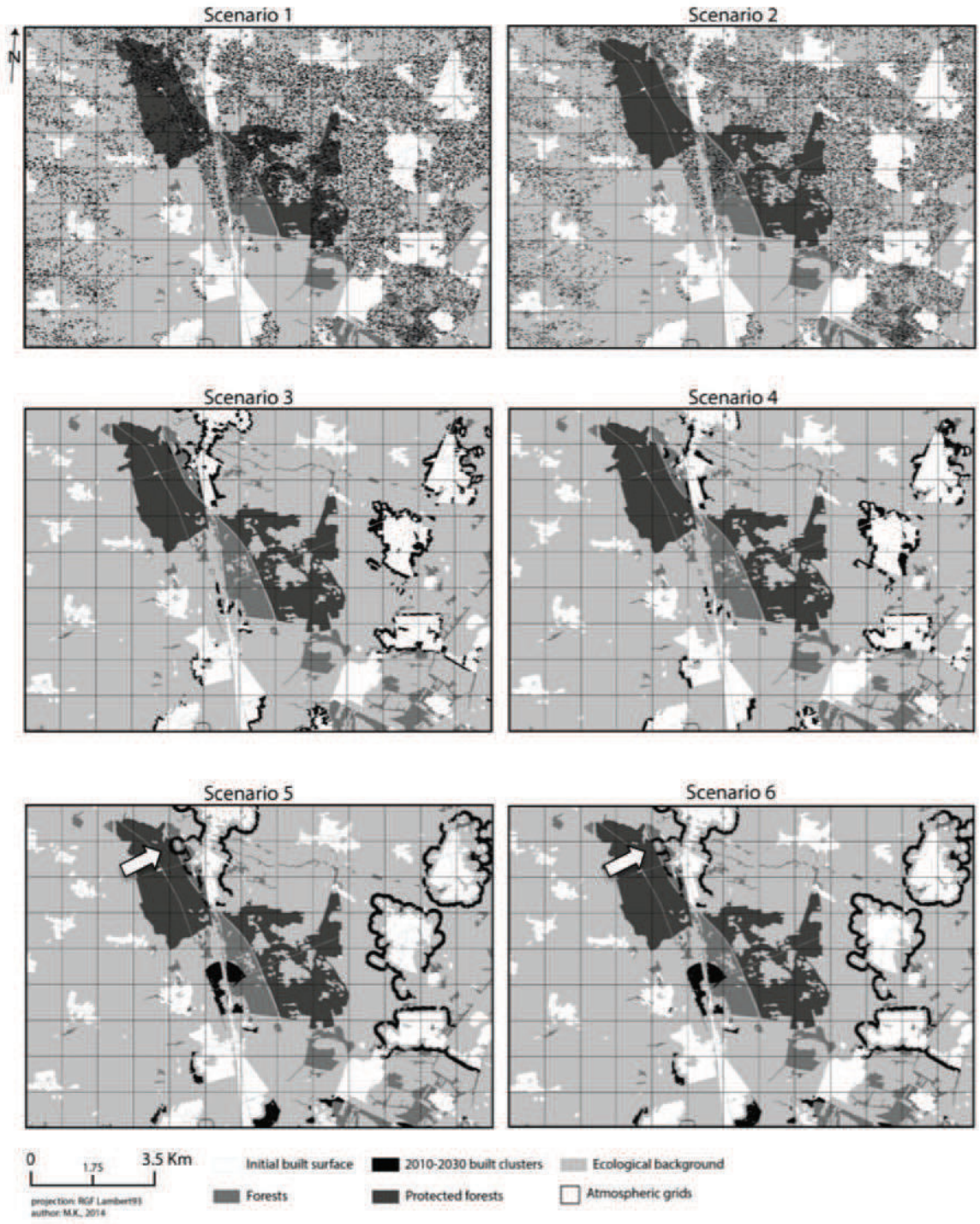

Figure 4.10: The local built up patterns generated by simulation-focus on a 3532.10 ha zone north from the Strasbourg agglomeration. The arrows in scenarios 5 and 6 focus on the differences in the developed areas between the two scenarios.

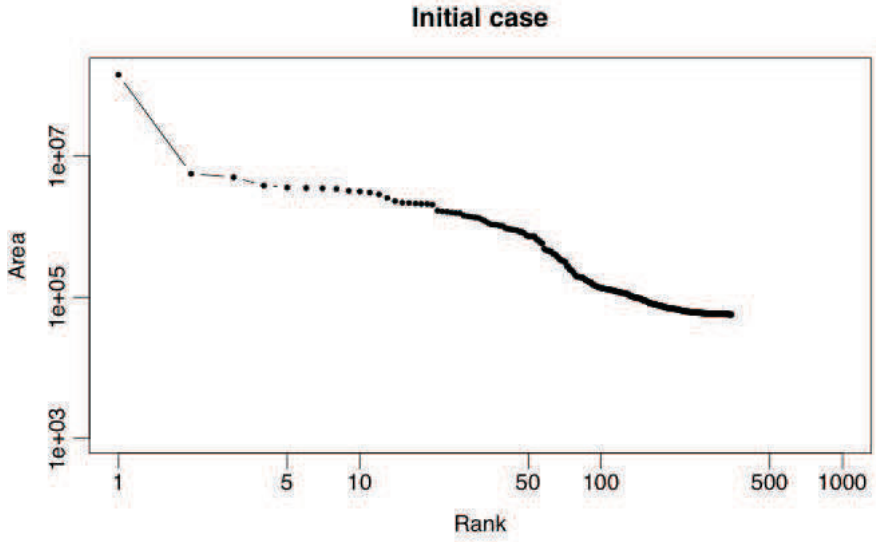

Figure 4.11: The rank-size distribution of the initial case built-clusters (log-log plot).

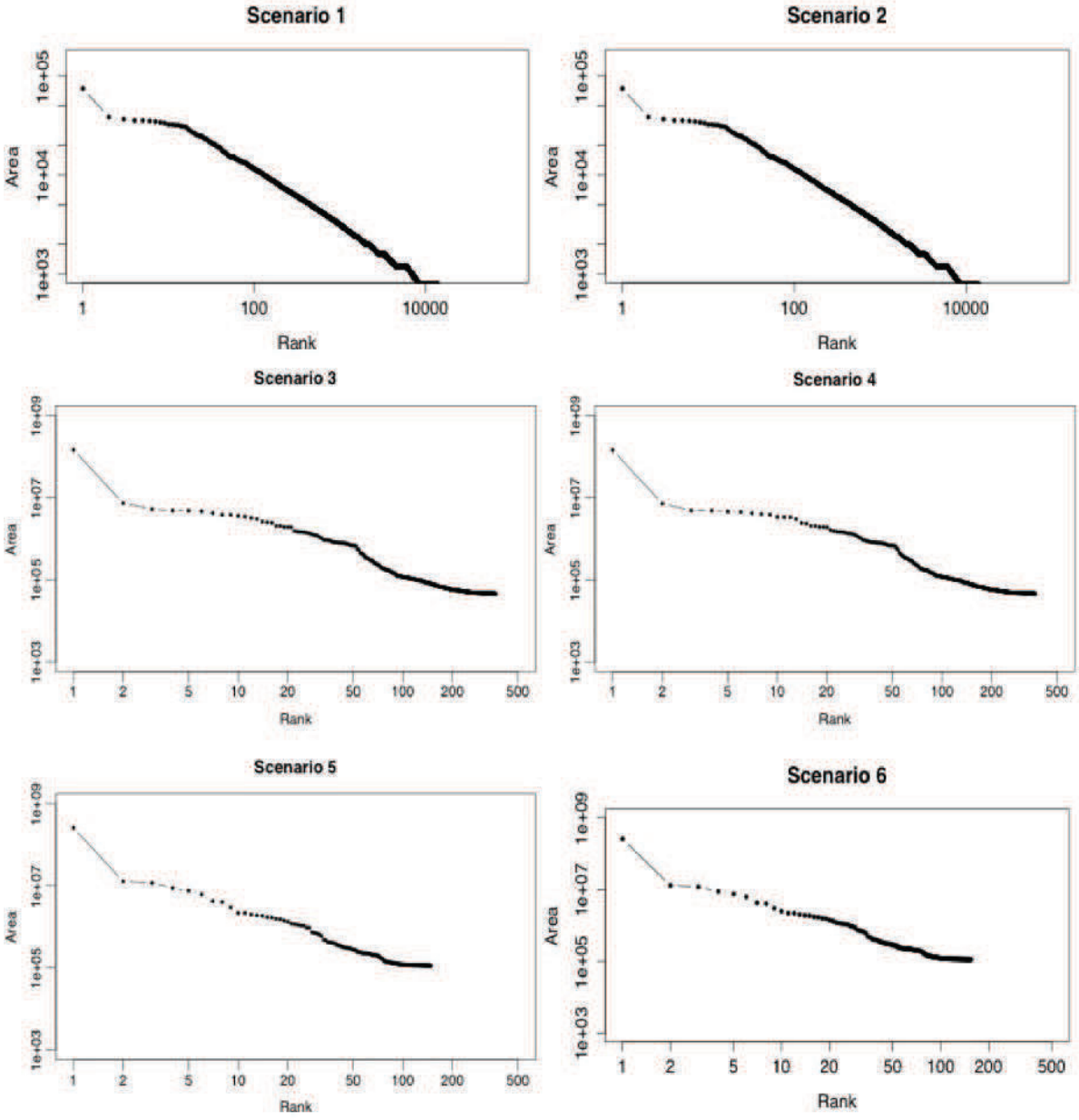

Figure 4.12: Rank-size distributions of the delineated built clusters. Be careful the scales differs from scenarios 1 and 2 to the others.

Appendices

Land cover classes	Descriptions	BdOcs-2008 classes	Costs
1	Habitat patches : needleaves, broadleaves, mixed and hardwood flood forests	311,312,313,315	1
2	Built up area	11,121,122,123,131,132,133,1351, 1361,1372,1310,13112,13111, 1312,1313	100
3	Artificial green areas with no man-management (brownfield, railroads, and so on)	151,152,139,13113,134	10
4	Open green areas	1412	10
5	Green areas dedicated to leisure	142,1411	10
6	Green areas considered as equipment (cemetery, sport infrastructure)	143,125,124	100
7	Artificial water bodies	412,414	100
8	Natural water bodies	411,413	10
9	Intensive crop lands	21, 221, 222, 226	100
10	Orchards	223	10
11	Meadows	224	10
12	Agricultural green (edge)	324, 314, 225	1
13	Marshland	322	10
14	Moor	323	10
15	Barren soil exploited by humans	1352, 1362, 1371, 138	100

Table 6: Human land use's perturbation costs

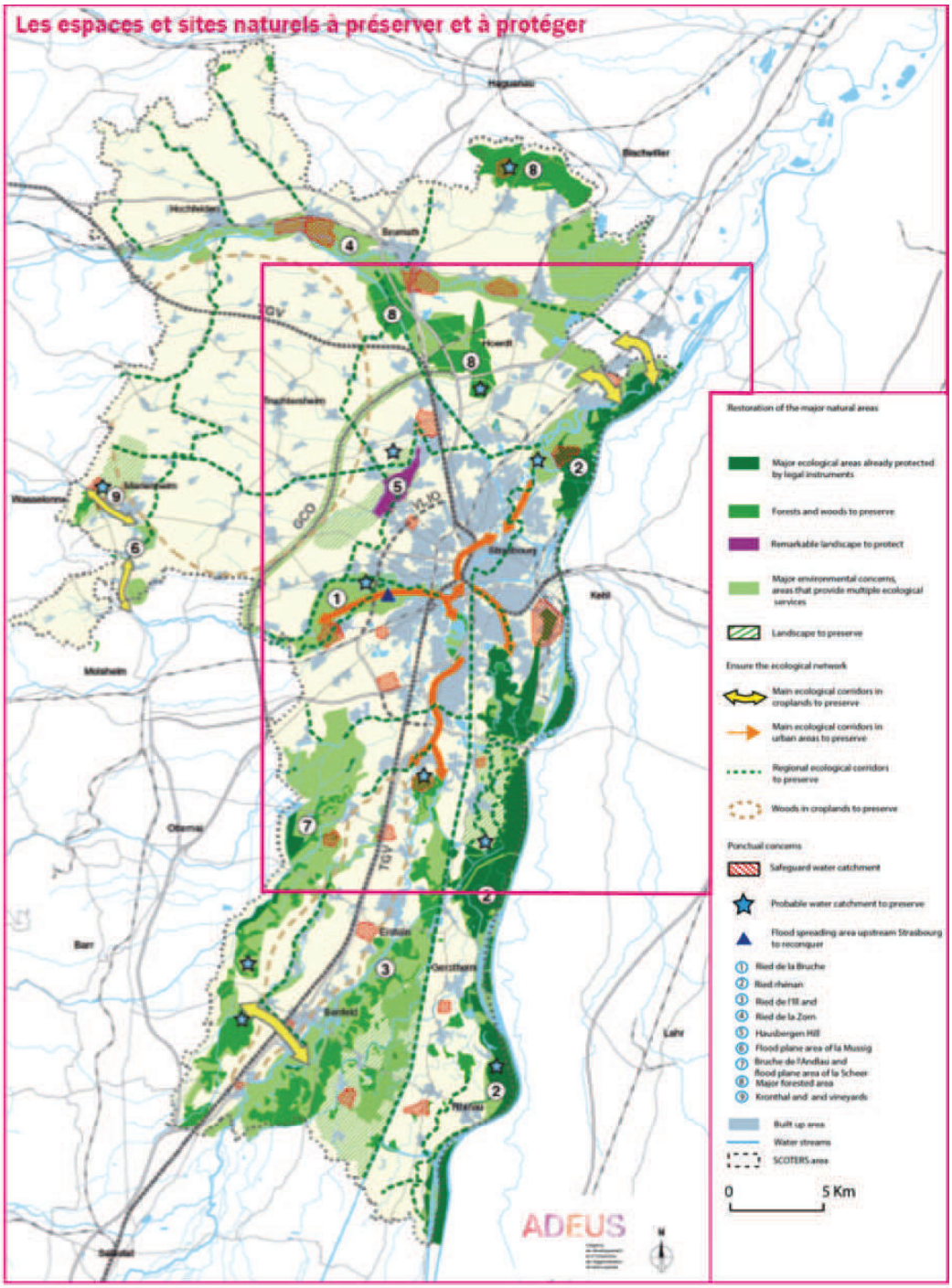

Figure 13: Protected areas to preserve (after the urban planning agency ADEUS and extracted from the Document d'Orientation Général, 5/11/2013). The square indicates the URSK domain.

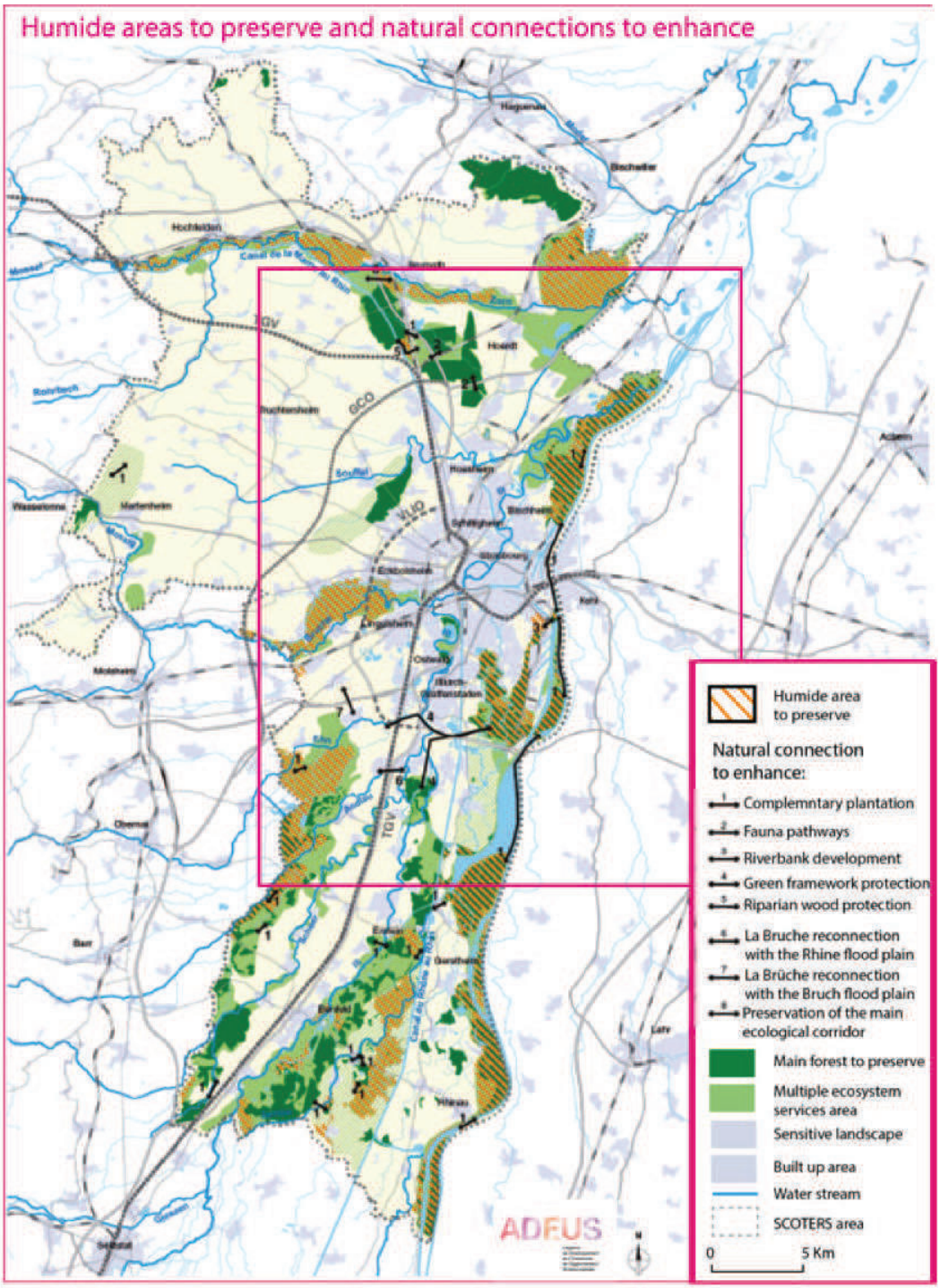

Figure 14: Humid areas and ecological corridors to preserve and enhance (after the urban planning agency ADEUS and extracted from the Document d'Orientation Général, 5/11/2013). The square indicates the URSK domain.

Chapter 5

Impacts of urban development policies on building energy requirements-Part II

Abstract

Urban sprawl is recognized to be the most land consuming urban form. It is also acknowledged to weaken the biological diversity and enhance the city-scale Urban Heat Island (UHI) phenomenon. The latter plays a significant role in the urban dwellers thermal stress and modifies the space heating/cooling building energy needs. The control of residential developments and the preservation of green lanes are measures often proposed to counter negative effects of urban sprawl. But what are their feedbacks on the UHI intensity and building energy needs? The aim of this study is twofold: *i)* quantify the influence of the residential development policies on urban climate and building energy requirements; *ii)* assess the ability of the numerical physically-based climate modeling systems that simulate the building energy needs like the WRF/ARW-BEP+BEM system Salamanca et al. [2010] to provide urban planning guidelines. In part I (chapter 4), the SLEUTH* model, a modified version of the American SLEUTH urban growth and land use change model of Clarke [2008], has been used to simulate six contrasted and archetypal built-up developments over the Strasbourg-Kehl urban region (three built-up types and two ecological preservation subset scenarios). It has been showed that ecological preservation policies do not produce large differences in the simulated built-up patterns and that scattered built up patterns are incorrectly consider in the WRF/ARW+BEP+BEM system. Finally only two simulated built patterns (compact and moderately compact) have been selected for applications with the WRF/ARW-BEP+BEM system. The simulated built patterns provide information on the atmospheric grids surface static physical parameters (albedo, heat capacity, roughness) used to compute the surface forcings in each lowest atmospheric grid. Results show that the WRF/ARW-BEP+BEM system well captures differences in energy requirements according to different built-up patterns. However the differences are rather due to an increase in the volume of the building to be heated than to a modification of the temperature field. Those results scale back the role of WRF/ARW-BEP+BEM systems in assessing building energy requirements changes regarding changes in built-up patterns over the study area.

Keywords: *urban climate modeling, urban planning, urban growth scenarios, building energy*

5.1 Introduction

In France after the World War II and since the 80's the urban growth has been accompanied by the migration of a large share of the urban dwellers to the less dense periurban areas [Bessy-Pietri, 2000]. It results in the sealing of vast lands for building and transportation infrastructures at the origin of the landscape fragmentation. It also triggers changes in the local climate. Landscape fragmentation dramatically weakens the ability of the landscape to support ecological flows [Forman, 1995]. The enhancement of the city-scale urban heat island intensity (UHI), caused by the differential in warming of the impervious built-up area and the rural surrounds, affects both the human heat stress and the building heating and cooling loads. Taha [1997] found that urban areas due to urbanization and urban heat island effect are characterized by more cooling degree-days (i.e. the cumulative temperature differences between the air temperature and a base temperature set in relation with the thermal comfort in the building) and fewer heating degree-days with respect to rural surrounds.
The recent urban planning strategies to cope with the negative effects of the urban sprawl promote compact cities in which the development of built-up areas is limited at the vicinity of existing built-up areas, in brownfields, vacant lots or as part of urban renewals strategies. By enhancing the UHI intensity, compact urban forms are expected to save building energy and thus, enhance the building energy performance [Haines, 1986]. Nevertheless the issue is still under debate. Green lane preservations are also part of urban sprawl counter-measures. Green areas by shadowing the surface and through evapotranspiration fluxes contribute to less warm the air compared to impervious areas.
Some studies investigated the linkage between local climate, urban form and building energy loads for cooling and heating. Urban heat island is rather complex and dependent on local spatial configurations. However the following common assumptions are commonly admitted:

i) Sprawl built-up areas have less concentrated sources of heat (buildings) and are characterized by higher tree canopy covers that lessen the temperature in summer and weaken the wind in winter, hence reducing the building cooling and heating loads [Heisler et al., 1986, Stone et al., 2010]. Family detached houses are also characterized by higher unoccupied and floor areas per inhabitant and hence they family detached houses are characterized by a greater building volume to

be heated per inhabitant.

ii) In contrast because of an enhanced UHI intensity, compact urban forms are expected to increase the building cooling loads but, with respect to the population density and occupied areas, compact forms appear to be more energy efficient than less concentrated forms. Recent studies have showed, however, that the population density per floor square meters has decreased in the past decades with the decreasing of the size of the household (ageing people, students, single parent families).

This suggests that the choice of residential and building stocks properties as the buildings material insulating properties, the household structures and the building dimensions are a key issue in enhancing the building energy efficiency in urban area more than the UHI intensity [Owens, 1992, Haines, 1986, IAURIF, 2008]. Three approaches are usually adopted for studying the relationship between urban forms and building energy loads. The climate approach investigates the indirect effects of the urban form on the building energy loads by considering the influence of the meteorological conditions on the building energy loads. The building stock approach focuses on the direct effects of the building characteristics (*e.g.* insulating, age of the building structure and so on) on the building energy loads. At last, since the last decades a third approach emerges. It relies on the use of climate modeling systems that consider simultaneously the complexity of the urban climate and important features of the buildings in the building energy performance (*e.g.* insulating properties, anthropogenic internal heat gains).

- **The climate approach**

  Several studies have stressed the linkage between local temperatures and residential energy consumptions. The relationship is showed to be non-linear. First the relationship is characterized by a decrease in the space heating energy load with temperature rise due to building space-heating requirements. Second, a plateau where the building loads are no more sensitive to climate conditions is observed. Finally, an increase in the building energy loads with temperature rise is observed due to the use of the air conditioning for cooling purpose. The degree-day method takes advantage of this significant linkage and proposes to estimate the building energy loads over a period through the air temperature

distributions. Due to the plateau it is possible to distinguish the winter and the summer branches of the temperature-building energy requirements relationship and linearly fit each of them. The resulting slopes of the two linear fits are the buildings cold and heat sensitivities. They represent how much the buildings are sensitive to local temperatures. The interception of the linear fits with the air temperature axis defines the base temperature. The base temperature represents the thermal equilibrium of the buildings with their surroundings thermal zones. It is assumed to be representative of the building energy efficiency and is often taken at 65°F (18°C).
The degree-days represent the cumulative differences over a given period of the air temperatures and the predefined base temperature when the air temperatures are cooler (or warmer) than the space heating (or cooling) base temperature. The air temperatures distribution over a period gives the correspondent building energy consumption knowing the cold or heat sensitivity of the area. Thom [1954], Amato et al. [2005], Valor et al. [2001] developed such methods and found an air temperature-energy use functions sensitivity varying with respect to the type of fuels (electricity shows increasing sensitivity with the air temperatures) and urban types (residential, commercial).

- **The building stock approach**

This approach investigates the relationship between the building stock characteristics and the building energy consumption but miss-considers the influence of the local climate [ANAH, 2008, ASPA, 2012]. The knowledge of the energy use intensity (*e.g.* energy losses, energy consumption, theoretical energy loads) of a standardize building of a given building stock segment and the proportion of the latter in the whole building stock gives the overall building energy consumption over a study area. The segments of the building stock are depicted according to energy related variables such as the floor areas, the types of fuel, the size of households, the type of buildings and so on. It requires the collection of large dwellings databases and regular up-date so as to consider the effect of additional dwellings in the building stocks of the considered study area. The energy consumption intensity can also be determined empirically through intrusive energy consumption sub-metering, analyze of thermal radiant emissions on thermal images or through the constitution of building prototype in numerical physically-based building energy models.

- **The climate modeling system approach**

Recently the integration of a large panel of climate models in a unique climate modeling system allows researchers to dynamically resolve climate processes from synoptic up to building scales. Those climate-modeling systems explicitly consider the climate feedbacks on building space heating and/or cooling energy requirements. The climate modeling system usually includes: *i)* a regional atmospheric model that provides the meteorological fields over a region of about thousand square kilometers discretized into atmospheric grids of 5-1km horizontal resolution; *ii)* an urban canopy parameterization that represents the surface dynamics and thermodynamics effects induced by the streets and the buildings on the lowest atmospheric layer; and *iii)* a simple building energy use model that computes the building energy requirements for space heating or/and cooling considering the building occupancy and the Heat Ventilation Air Conditioning (HVAC) system activity. Climate modeling systems, thus, are envisaged tools for integrating climate knowledge and building energy efficiency guidelines in future urban planning policies given their ability to test several probable future [Chen et al., 2011].

Ohashi et al. [2007], Kikegawa et al. [2003], Kondo et al. [2005], Bueno et al. [2011] and Salamanca et al. [2010, 2012] carried on simulations over megacities using climate modeling systems. They found that the wasted anthropogenic heat by the HVAC systems could warm the air up by +1°C to +2°C, hence, enhancing the UHI phenomenon. Meanwhile Salamanca et al. [2010], Salamanca et al. [2012] and Martilli [2012] investigated the impacts of some of the energy savings and urban heat island mitigation strategies (light roof, improved insulating properties). Masson et al. (2013) focused on the impacts of urban planning strategies on the air temperature and building energy requirements over the Toulouse urban region by 2100. In this last study, scholars considered abrupt changes in the urban development and planning strategies, changes in the building stock energy efficiency properties and increase in the urban green areas. Masson et al. [2013] tested green belt strategies as urban sprawl counter-measures. However, greenbelt makes no more consensus in the scientific and urban planners communities. They added systematically garden fraction to each new developed built-up area to test the effects of urban green areas on urban climate with respect to urban areas cooling strategies. This further contributes to the spatial extension of the urban areas, which seems in discordance with the current urban density

promotions. Masson et al. [2013] also proposed changes in the building insulating properties and types in accordance with the population and dwelling density thresholds computed through the NEDUM2 dynamic economic land use transportation interaction model [Viguié and Hallegatte, 2011, Gusdorf et al., 2008] and the GENIUS model [Bonhomme, 2013]. NEDUM2 simulates residential private housing developments accounting for the trade-off of the accommodation offer and demand market, future transportation policies and demographic growth. It provides the population and housing densities to the GENIUS model for a 250x250 m resolution grid. The GENIUS model characterizes the building morphology and insulating performance of the new constructions according to seven pre-defined construction types (*e.g.* commercial buildings, old center, detached houses and so on) using spatial contiguity rules as well as housing and population densities thresholds. The changes in the building types and energy performance even if operating in one century (the time horizon is 2100) seem unrealistic considering the hysteresis of the building stock. Indeed today 55% of the French dwellings have been built before 1975 [ADEME, 2012]. In addition Bailly and Bourdeau-Lepage [2011] estimated that 70% of the buildings that will exist in 2050 are already built. Finally the study of Masson et al. [2013] does not allow investigating if either the local climate or the building stock characteristics influence the building energy performance as several parameters vary simultaneously.

5.2 Research objectives

The aim of the study is to assess the impact of urban planning policies on urban heat island and building energy requirements. Particular efforts have been done for integrating realistic urban planning policies in the urban development scenarios simulations and only land-use changes are considered (no changes in the building energy efficiency properties are modeled). This permits investigating the climate indirect and building stock direct impacts on building energy loads.

5.3 Method and tools

In this study we investigate the effect of six archetypal and contrasted urban development scenarios on building energy requirements and urban heat island intensity. We simulated the urban development by using successively the SLEUTH* [Doukari et al., 2013] cellular automata model, the MorphoLim [Tannier et al., 2011] and Graphab [Foltête et al., 2012] computing programs. We analyze the building energy requirements of two urban development scenarios using the WRF/ARW-BEP+BEM modeling system. The method has been applied on the Strasbourg-Kehl urban region (URSK) North-East France. Since space heating counts for 50% of the residential housings energy requirements according to a preliminary work of ASPA on the Climate Energy plan of the CUS territory we only consider the winter branch of the air temperature-building energy function. A short memory of the urban development scenarios characteristics and previous results is given below but for more information on the case study and urban development scenarios, please refer to part I (see chapter 4).

5.3.1 Urban development scenarios: results of part I

Among the five types of urban development identified by Galster et al. [2001], the current study focuses in particular on the diffusive and compact urban development types. The first refers to the absence of control of the residential growth. The second type of urban development corresponds to the densification of the inner core of the agglomerations (e.g. hollow teeth, vacant lands). The third type of urban development favors the developments at the vicinity of existing built-up areas and transportation infrastructures. Each of those three types of urban development is considered in this study. They further come in two versions. Each of them corresponds to the preservation or not of the ecological habitat. The six simulated urban development scenarios are presented in table 1.

We used the modified version SLEUTH* [Doukari et al., 2013] of the american SLEUTH urban growth model [Clarke, 2008, Chaudhuri and Clarke, 2013] to simulate the urban development for each scenarios over the Strasbourg-Kehl urban region (France). The urban development policies were integrating in the SLEUTH* cellular automata model through the definition of non-developable land maps using the MorphoLim [Tannier

Scenarios	No Preservation of the ecological network	Preservation of the ecological network
Spontaneous development	Except non-developable lands that are included in the local development plan, urban sprawl is totally uncontrolled. New urban settlements are spread over the territory to the detriments of the ecological landscape. **(Sc1)**	Urban sprawl is totally uncontrolled. New urban settlements are spread over the territory. However the forested areas that ensure the ecological network connectivity are preserved from the urbanization. **(Sc2)**
Compact development	Except lands that are included in the urban planning instrument, new urban units fill the hollow teeth of the morphological agglomerations to the detriments of natural areas. No refurbishment, demolition and construction phases are assumed. Constructions close to existing built-up areas and transportation infrastructures represent the fact that the urban growth is well controlled. **(Sc3)**	New urban units fill the hollow teeth of the morphological agglomerations No refurbishment, demolition and construction phases are assumed. The urban growth is well controlled and urban densification policies are assumed. New urban units settle down close to the existing built-up area and transportation infrastructure. Forest areas essential to ensure ecological flows over the ecological network are preserved from the urbanization. **(Sc4)**
Moderately compact development	Except non-developable lands that are included in the local development plan, the urban sprawl is concentrated close to the existing built-up areas and transportation infrastructures at the fringe of the morphological agglomerations. **(Sc5)**	New constructions are located at the fringe of the morphological agglomerations close to the existing built-up areas and transportation infrastructures. Forested areas that are relevant for the connectivity of the ecological network are preserved from the urbanization. **(Sc6)**

Table 5.1: Description of the six urban planning scenarios

et al., 2011], and Graphab [Foltête et al., 2012] computing programs. MorphoLim identifies coherent built-up areas using the fractal theory and permits to constrain the urban development either within the main built-up areas (compact scenarios) or in the periphery of the main built-up areas (moderately compact scenarios). Graphab is a software dedicated to graph-based landscape modeling. It is used to identify non-built patches that are essential for ensuring the ecological network connectivity for a target species. The target species selected here is the red squirrel (*Sciurus vulgaris*), particularly sensitive to landscape fragmentation due to its short dispersal distance. The setup of the SLEUTH* model and the simulated built-up patterns for each development scenarios are presented in part I (see chapter 4). The description of the simulated built-up patterns by morphological indexes revealed slight differences in the built-up patterns between scenarios that preserve the ecological network connectivity and scenarios that do not. Furthermore it has been showed that the integration of the simulated built-up areas in the 1x1 km climate modeling systems grids prevents the consideration of dispersed built up patterns due to the climate modeling system limitations. Thus among the six scenarios, we only retain the compact and moderately compact scenarios for further investigations with the climate modeling system.

5.3.2 Description of the WRF/ARW-BEP+BEM climate modeling system

We use the WRF/ARW-BEP+BEM urban climate modeling system [Skamarock et al., 2008], which consists in:

i) The WRF/ARW mesoscale regional atmospheric model

The WRF mesoscale model is a fully compressible terrain following non-hydrostatic regional atmospheric model that provides the meteorological fields over a region of thousand kilometers. The model offers various physical options for radiation and soil energetics processes and takes into account the presence of hydrometeors (*e.g.* cumulus, precipitation and graupels) and their interactions with the short-wave and long-wave radiations. Due to its coarse spatial resolution, the model does not represent explicitly the effects of the surface. Sub-grid atmospheric dynamical and energetic processes induced by the surface are parameterized through a roughness approach in which a roughness length is attributed for representing

the average gridded effects of the obstacles on the airflow. The surface model that computes specifically the surface sensible and latent heat fluxes as well as the skin temperature is the Noah LSM of Chen [2007].

ii) The BEP urban canopy parameterization

For urban areas, where most of the adopted physical assumptions (flat uniform terrain, constancy of turbulent flux with height) fail [Rothach, 1999, Kusaka et al., 2001, Müller, 2007] other urban canopy parameterizations have been introduce in the climate modeling system.
For specifically taking into account the urban canopy vertical structure in the surface fluxes calculation, several urban parameterizations of higher sophistications have been introduced in the WRF/ARW atmospheric model. They reproduce the 3-dimensional radiative, thermal and aerodynamic effects induced by buildings facets (*e.g.* walls, street, roof) on the atmosphere, like the shadowing effects, the walls radiation trapping, the wind sheltering effects as well as the turbulent kinetic energy production induced by the presence of obstacles in the airstream path.

The Building Effect parameterization (BEP) of Martilli et al. [2002] is one such. Urban areas are made up of three urban types (the high intensity residential, the low intensity residential, and the commercial, industrial and transportation). In each grid cell, infinite long canyons (*i.e.* the spatial unit composed of a building and its adjacent street) are uniformly distributed. Two equiprobable canyon orientations are considered with square cross-sections. The canyon geometry consists in a building and street width, and a building height probability function for representing the building heterogeneity. Distinct energy and radiative budgets resolutions for plane (*e.g.* roofs and streets) and vertical (*e.g.* walls) facets of the canyon achieve reproducing the radiation shadowing and trapping effects while a distributed drag force approach derived from vegetation schemes is used for computing the airflow momentum losses induced by the buildings walls. Those momentum, energy and humidity surface fluxes are computed each time the buildings interact with the airflow for each layer of a refined 1-dimensional canopy grid that is immersed in the mesoscale atmospheric. The surface fluxes are later weighted according to the canyon facets areas and interpolated in the mesoscale 3-dimensional atmospheric grid. At last, a modified Bougeault and Lacarrère [1989] turbulent scheme that solves the turbulent kinetic prognostic

equation is adopted to take into account the dynamical perturbations of the atmospheric flow induced by the buildings.

iii) The BEM building energy use model

Since few decades, urban canopy parameterizations have been coupled to simplify building energy models. Since 2002, the Building Energy Model (BEM) of Salamanca et al. [2010] is coupled with the BEP model. In BEM, the building shell is described according to four oriented walls characterized by finite dimensions, layered buildings materials and uniformly distributed windows' wall fraction. Each building is divided into floors or rooms according to the canopy grid resolution. Each floor in BEM corresponds to a box in which a simplified heat budget is calculated considering an occupied standard building. The heat budget takes into account: *i)* the room indoor radiative budget accounting for the windows fraction; *ii)* the heat conduction through layered buildings materials, *iii)* the unintentional natural ventilation; and *iv)* the heat generated by occupants and wasted by equipments. The regulation of the air temperature and humidity is modeled through a heat pump system driven by the imposed thermal and humidity comfort ranges, the thermal and humidity loads, and the efficiency of the HVAC system. The coupling with the BEP model is done through the balance of the indoor and outdoor energy budgets, and the resolution of 1D heat conduction equation through the layered buildings materials. Finally, BEM reproduces accurately the surrounding building thermal ambient conditions. It considers the building wasted heat due to human activities ejected in the street. Moreover it provides to BEP accurate building facets skin temperatures.
Salamanca et al. [2011] and Kikegawa et al. [2003] used such improvements for assessing building energy conservation strategies.

5.4 Settings of the climate modeling system

A previous study on the space heating building energy requirement over the URSK domain has been performed and validated over the 2010 year (see chapter 3). This is the initial case. The same climate modeling system configuration is adopted to simulate the building energy requirements for the two urban development scenarios. Only the built-up pattern changes for considering the influence of the compact and moderately

compact urban development policies on the building energy requirement and urban heat island intensity.

5.4.1 The WRF atmospheric model grid and physical configurations

Four nested meteorological domains (figure 5.1) centered on the administrative limits of the Strasbourg city council (CUS) (figure 5.2) are drawn. The innermost domain is the URSK domain.

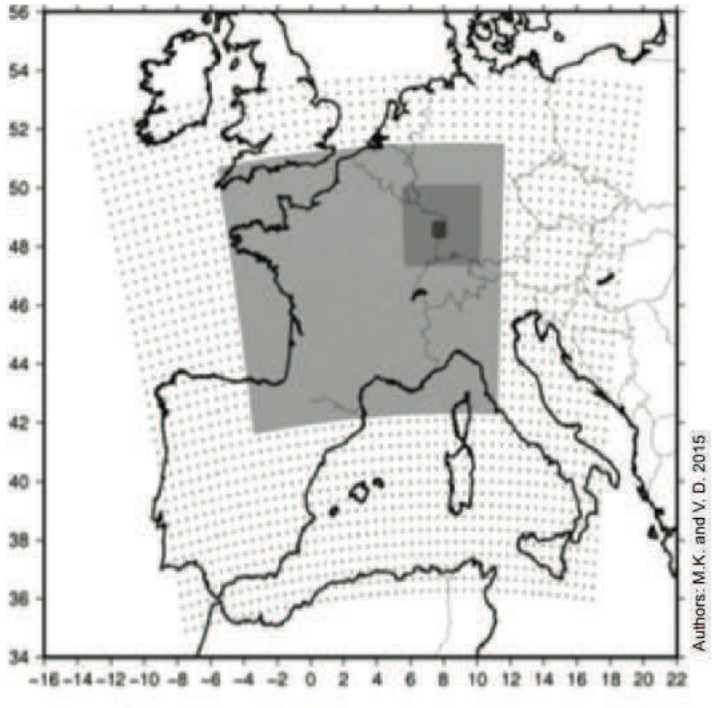

Figure 5.1: Coverage of the WRF nested climate simulation domains (from larger to finer): the West part of Europe (domain 1), over France (domain 2), Upper-Rhine Region (domain 3), and the Strasbourg-Kehl urban region (URSK domain).

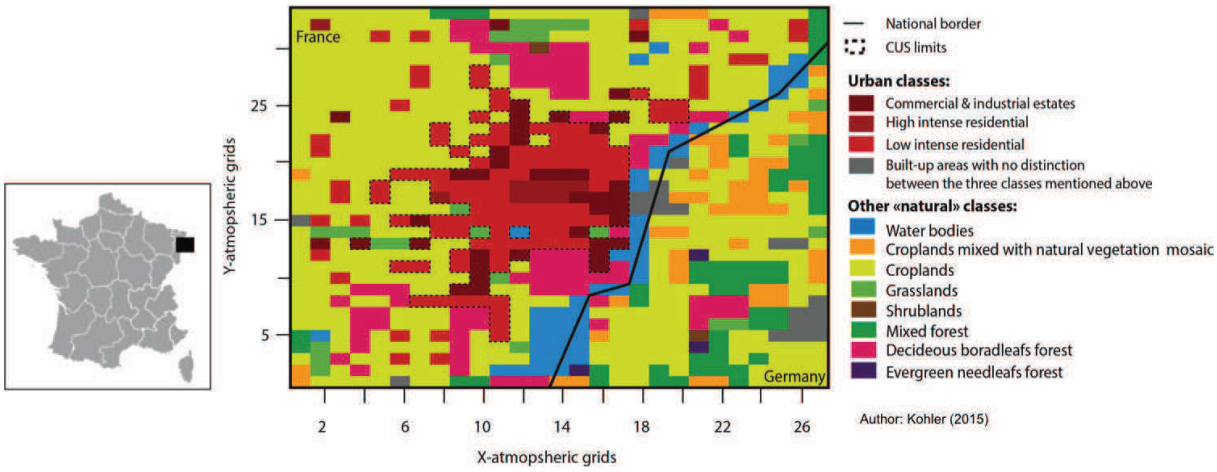

Figure 5.2: The URSK domain.

The URSK domain atmospheric grid consists in 27x33 rectangular C-Arakawa grids of 1 km horizontal resolution and 28 stretched pressure levels according to a 5000 Pascal top pressure in the vertical. Its initial and lateral meteorological conditions are provided by the other coarse resolution parent-domains, which atmospheric grid sizes range from 45 km to 3 km. The FNL- National Centers for Environmental Prediction meteorological global data reanalysis provides the meteorological conditions to domain 1 each 6 hours. The ARW core solves fully compressible and non-hydrostatic Euler conservative equations for the wind velocity, the potential temperature perturbations, the surface pressure perturbation of dry air and the geopotential perturbation considering a third order Runge-Kutta scheme. As advised by Martilli et al. [2002] and Salamanca et al. [2012] the Bougeault and Lacarrre (Boulac option) k-ϵ turbulence model is adopted. The influence of water vapor on shortwave and longwave radiation processes is taken into account through the Dudhia [1989] shortwave radiation scheme and RRTM options respectively.
The Thompson et al. [2004] scheme that explicitly resolves water phase's transformation is selected for the microphysics. At last, the NOAH Land Surface Model (LSM) computes the surface fluxes (latent and heat fluxes) as well as the skin temperature considering a roughness approach for non-urban areas while the BEP+BEM urban canopy parameterization does so for the urban areas.

Because surface coverage is critical for representing accurate land-surface exchanges and planetary boundary layer dynamics [Xiu and Pleim, 2001], the regional high resolution and multisource land use land cover CIGAL (BdOcs_2008) dataset is used for

defining the 2010 land cover over the French part of the URSK domain. The correspondence between the different land cover classifications is found in figure 5.3 while the 2010 land cover maps is presented in figure 5.2. The MODerate resolution Imaging Spectroradiometer (MODIS) 2001 land cover dataset fills the no data in the URSK domain (German part).

For the scenarios, the WRF/ARW 2030 land cover maps are issued from the combination of the BdOcs_2008 land cover dataset and the SLEUTH* simulated 2030 built-up areas maps. A random algorithm permits to assign, for each 20x20 m developed built-up cell, an urban type with respect to the proportion of each urban type in the initial case's overall urban areas. It is assumed that developed built-up areas could either be low intense residential or commercial and industrial. The areas of each of the urban types including in each atmospheric grid are then aggregated, which allows a dominant land cover type to be assigned to each grid according to an urban fraction threshold set at 20%. When urban areas count for more than 20% of the atmospheric grid coverage, the atmospheric grid is urban and the BEP+BEM models are activated. The remaining part is necessary of croplands or mosaic vegetation type as proposed by the climate modeling system. The resulting compact and moderately compact WRF/ARW land cover maps are given in figure 5.4.

Figure 5.3: Correspondence between the land cover types classifications.

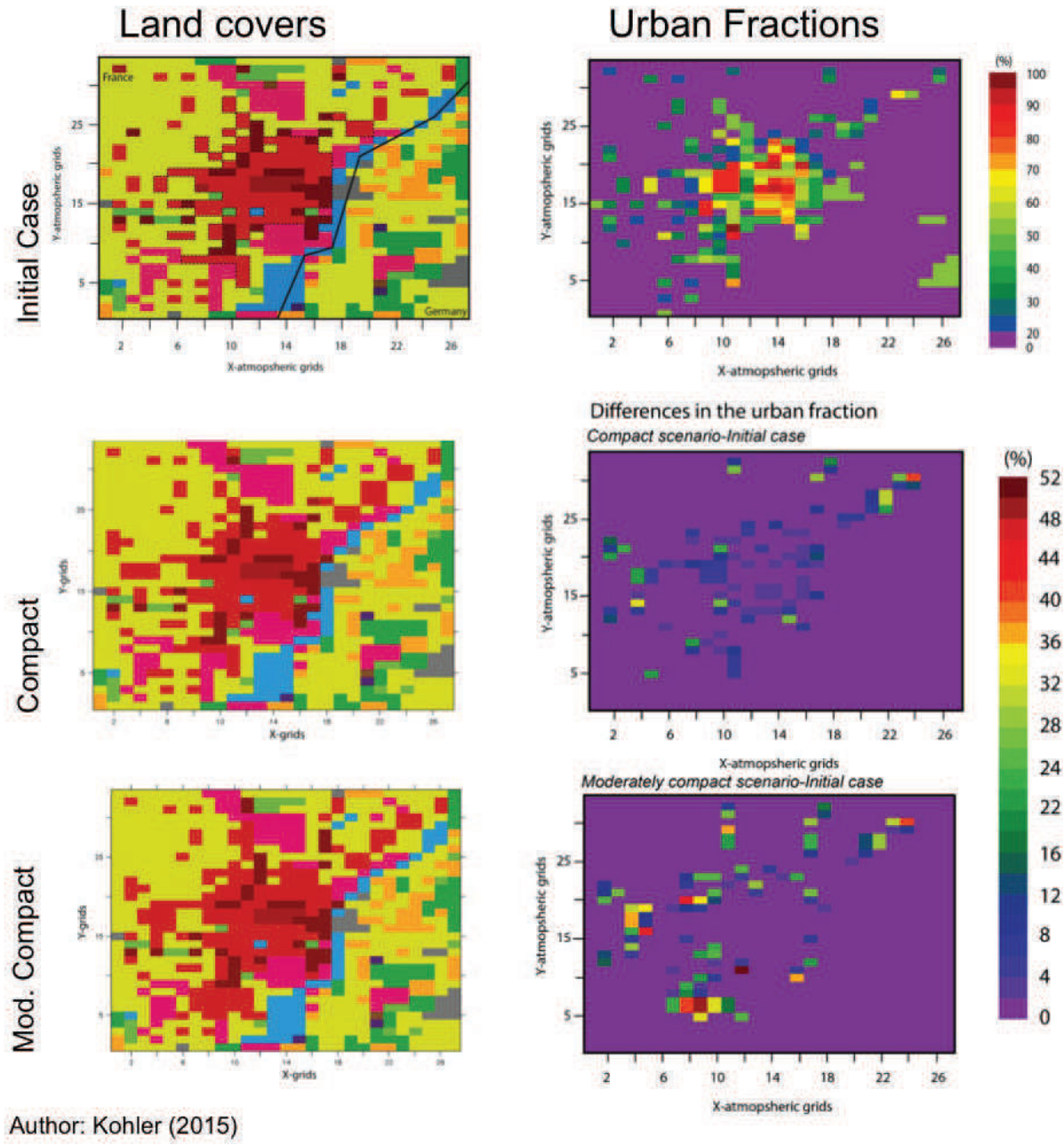

Figure 5.4: The WRF/ARW land cover maps for the compact (scenario 3) and moderately compact (scenario 5) scenarios.

5.4.2 BEP and BEM selected parameters

The BEP + BEM urban canopy model distinguishes three types of urban fabrics: the high intensity residential characterized by high population density and construction surface (*class 32*), low intensity residential (*class 31*) where constructed material is

mixed with vegetation, and the commercial and industrial estates (*class 33*). In this study, transportation infrastructures are considered apart in the MODIS built-up class (*class 13*). The non-urban fractions of the urban atmospheric grids are defined as mosaic vegetation and croplands for reproducing the highly irrigated low urban vegetation. In this study, the American megacity urban parameters proposed by defaults are adapted to better correspond to European cases. For this we use several high resolution GIS spatial databases (*e.g.* Google earth satellite images, the 2012 BDtopo® of IGN, the 1999 population census of INSEE), scientific and grey literature and collaborative websites [Sellé, 2011]. This permits to reproduce as real as possible the Strasbourg great city street-canyons' equivalent geometry (the canyon directions *dir.* counting 0° as the North, the building height H distribution, the building and street's widths W along with the North/South canyon and West/East canyons respectively Bx, By, Wx and Wy in meters, and the ceiling height *dzcan*), as well as radiative and thermal surface properties and building's standard occupancy for each type of urban fabric (*Utype*).

The layered radiative and thermal proprieties of materials for each canyon facets are presented in table 5.3 while figure 5.5 displays the material compositions and thickness for roofs, walls, floors and undergrounds that have been retained for representing the thermal behavior of the buildings.

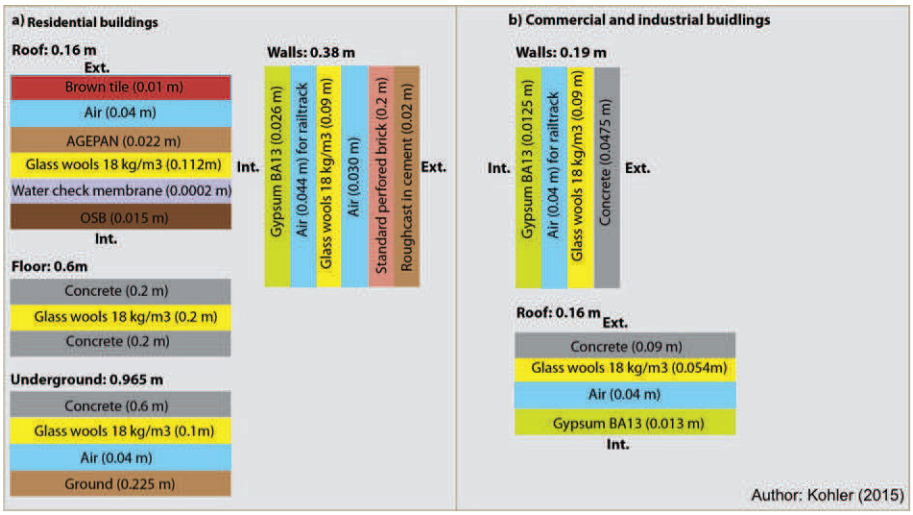

Figure 5.5: Composition of the building shell layers.

For the BEM model other parameters such as the human metabolic heat rate, the heat wasted by the equipments, their daily use profile and the performance of the ventilation

Parameters	Data	Treatments	Adopted parameters
dzcan	-	-	The vertical resolution of the BEP grid constrains the ceiling height. Thus the vertical resolution is set equal to 3 m.
dir.	Google Earth ®	Analysis of random samplings of prototype Utypes	class 31 (Palais Universitaire neighborhood): 45° N/S and 315° W/E ; class 32 (place Kléber neighborhood): 315° N/S and 45° W/E ; class 33 ("Port du Rhin" neighborhood) : 0° N/S and 90° W/E.
H	BDtopo ®	Building height distribution obtained by GIS geoprocessing.	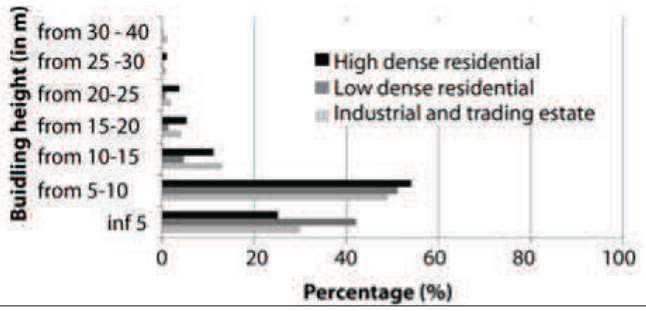
W	BDtopo ®	Adaptation of building's and street's widths to minimize the relative differences (*in %*) between the total building envelop and volume. We used the BDtopo ® (shallow grey) and assume cubic buildings.	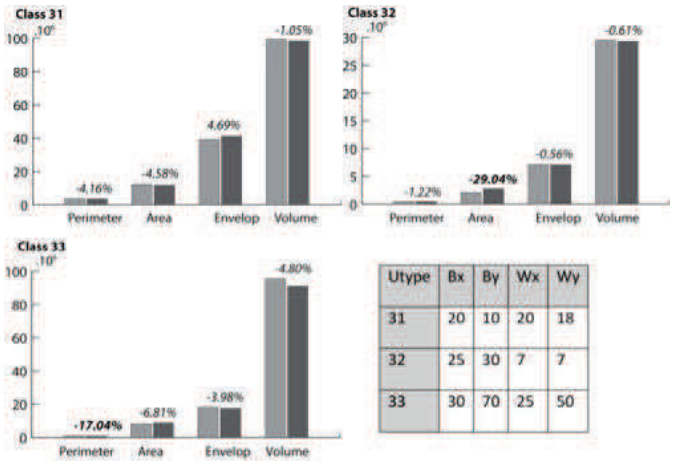

Utype	Bx	By	Wx	Wy
31	20	10	20	18
32	25	30	7	7
33	30	70	25	50

Table 5.2: Canyon morphological parameters.

and HVAC systems have to be specified. Table 5.4 gives the BEM setting-up parameters. Unless floor population density and windows fraction, they are set by consulting scientific, official and building construction dedicated sources. The floor population density is obtained by setting proportional the 1999 IRIS (census unit) population census data corrected by a 2010-1999 population growth issued from the literature [INSEE, 2007] with the BDtopo® built-up area included in each atmospheric grid. The windows fraction on each building wall is defined by considering typical prototype of residential buildings.

Building material	**Heat diffusivity** ($mm^2.s^{-1}$)	**Heat capacity** ($kJ.m^{-3}.K^{-1}$)
Roofs (Albedo: 0.1, Emissivity: 0.9, Roughness length: 0.01) from Krpo [2009] and weather.msfc.nasa.gov		
OSB	*0.13*	*982.08*
Air (1.2 kg/m^3)	*21.74*	*1.20*
Vapor check membrane	*7692.30*	*298.99*
Glass wool (18 kg/m^3)	*2.37*	*18.53*
AGEPAN	*1.29*	*58333.00*
Brown tile	*0.59*	*655.00*
Walls (Albedo: 0.2, Emissivity: 0.9, Roughness length: -) from Krpo [2009]		
Gypsum (BA13)	*0.30*	*831.60*
Air (1.2 kg/m^3)	*21.74*	*1.20*
Glass wool (18 kg/m^3)	*2.37*	*18.53*
Standard performed bricks	*0.59*	*655.00*
Roughcast in cement	*0.48*	*1642.00*
Undergrounds and floors		
Concrete	*1636.90*	*2167.20*
Glass wool (18 kg/m^3)	*2.37*	*18.53*
Air (1.2 kg/m^3)	*21.74*	*1.20*
Street (Albedo: 0.05, Emissivity: 0.95, Roughness length: 0.01) from Krpo [2009])		

Table 5.3: Radiative, thermal, and aerodynamic properties of buildings.

5.5 Validation of the meteorological fields and space heating energy requirements

The mean biases MBs, the root mean square errors RMSEs and the Pearson correlation coefficient R are computed for the 2-m air temperatures and the wind speeds using the Météo France hourly meteorological datasets of three experimental stations. Wind roses are analyzed for comparing the observed and simulated wind directions. It should be retained that wind speeds and directions are only available at Entzheim and La Wantzenau stations.

The absence of a dense meteorological observation network over the URSK domain, in particular in the dense urban core, does not allow a correct validation of the simulated meteorological field. Indeed, the single station located in the urban core (Strasbourg-Botanique) is surrounded by large vegetation and thus may behave as a cool island [Fischer, 2001, Ringenbach, 2009].

Parameters	Chosen settings	Literature review
Windows -to-wall fraction	15% for residential and 20% for commercial & industrial buildings	$1/6^{th}$ of the building living space [IAURIF, 2008] ; 0.2 [Salamanca et al., 2012]
Population density	1.02 ind. for 100 m^2 (Utype 31), 6.86 ind. for 100 m^2 (Utype 32) and 0.31 ind. for 100 m^2 (Utype 33)	2 individuals for 100 m^2 [Salamanca et al., 2012]
Metabolic heat rate	80 Watts	A man of 75 Kg emits 75W (at rest) and 100-200W (extreme activity) [Sailor, 2011]; An adult emits 63W (asleep) and 90W (in activity) (MEDDTL 2012); An individual emits 75W (at rest) and175W (at maximum) [Allen et al., 2011] ; An individual emits 54.7W [Kikegawa et al., 2003]
Peak heat generated by equipment	Pk=36 W/m^2	Pk=36 W/m^2 and 20 W/m^2 for commercial/industrial buildings and for residential respectively. [Salamanca et al., 2012] ; Pk=5.58 W/m^2 for a typical Hausmannian building and an internal heat generation of 38.61 W/m^2 and 193.05 W/m^2 plan area respectively for residential and offices [Bueno et al., 2011]; Pk=5.7 W/m^2 the day and 1.1 W/m^2 at night [CSTB, 2012]
Ventilation rate	$\beta = 0.75$	$\beta = 0.43$ in Paris and $\beta = 0.5$ in Toulouse[Bueno et al., 2011] ; $\beta = 0.75$ [Salamanca et al., 2012] ; $\beta = 0.6$ [Kikegawa et al., 2003]
Humidity target	0.005 kg/kg	[Salamanca et al., 2010]
Humidity gap	0.005 kg/kg	[Salamanca et al., 2010]
Temperature target	T_{targ}=293°K +/- 0.5°K (19.85°C)	T_{targ}=[19 ; 24°C] for Toulouse [Bueno et al., 2011] ; T_{targ}= [24 ; 26°C] for Madrid in summer [Salamanca et al., 2012] ; T_{targ}=19°C in average [CSTB, 2012]; T_{targ}=20°C or more [Crédoc, 2010]
COP heat	0.9	COP heat=0.9 [Bueno et al., 2011] ; COP heat=0.75 [Salamanca et al., 2012]

Table 5.4: Settings of the building energy model parameters

Despite this, the climate modeling system qualitatively reproduces well the meteorological field over the study case. The R coefficients show a good adequacy between the simulated and observed temperatures (R=0.96) for each meteorological station. Nevertheless, the MBs reveal different patterns for each station. Moreover biases change according to the season. At Entzheim the MBs show that the average, maximum and minimum temperatures are systematically underestimated by about -1°C during the leaf-on period and -0.20°C during the leaf-off period. The slight MBs in winter help to conclude that the temperature biases have little incidence on the heating building energy loads. At Strasbourg-Botanique, the model systematically over-estimates the

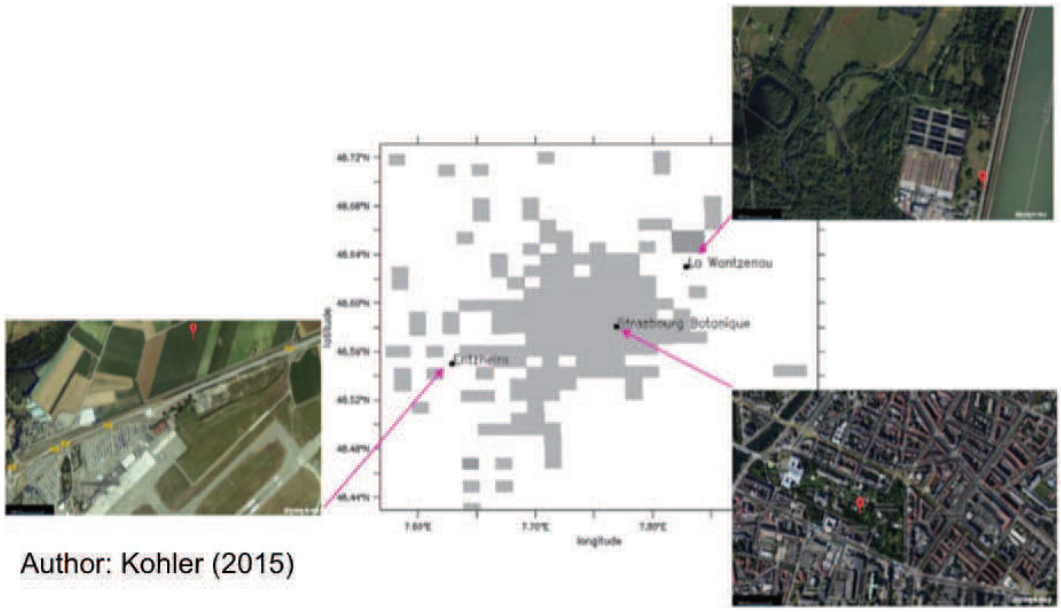

Figure 5.6: Location of the meteorological stations over the URSK domain.

air temperatures by about +2°C. It could be a result of the cool island effect recorded in the observations as reported in Fischer [2001]. At last at La Wantzenau station, the MBs are low showing a good agreement with the observations. Hence, the climate modeling system fairly reproduces the synoptic meteorological stations but no conclusion could be addressed on the urban air temperature and adequacy of the setup of the BEP+BEM models.

The wind field is accurately reproduced by the climate modeling system. The R coefficient is significant for each of the two available stations: R is equal to 0.60. The RMSE and the MBs highlight that the wind speed is more accurately reproduced at Entzheim, the synoptic station of Météo France for the region, than at La Wantzenau. According to the wind roses, the Entzheim station represents well the synoptic conditions with a channeling North/North-East and South/South-West wind effect caused by the Rhine graben. Systematic easterly wind deflections in the Entzheim simulated winds are found. More frequent high winds are reported at Entzheim compared to La Wantzenau where calm winds and low winds are more frequent. The location of the station close to the forests may indeed shelter the station from synoptic circulations. The higher RMSE and MBs at La Wantzenau indicate that the climate modeling system does not achieve to reproduce calm winds. Wind directions are as scattered as errors. Easterly wind deflections as well as westerly wind deflections are observed.

In conclusion, the meteorological field is quietly reproduced by the climate modeling system. However the scarcity of instrumental observation sites prevents the generalization of the latter findings.

For validating the building energy requirements for space heating, we used the energy census data provided by the regional air quality association ASPA [ASPA, 2012]. They followed a building stock approach using the INSEE dwellings database over the CUS area. In the dwellings database, each building type is depicted according to the age of the structure, the number of rooms, the size of households, the building type (residential or commercial) and so on. Then the CEREN gives the energy consumption intensity for space-heating for each of the prototype buildings. The energy datasets are provided by public or private electricity, oil and gas delivery companies, thermal images, surveys and building energy simulations. ASPA computed the heating building energy requirements for the CUS area in 2010. We found a 2010 building energy requirement of 11,802,994.6 Giga Joule (GJ). The relative difference between our case study and the ASPA study is about -25.64%. This difference is found acceptable with regards to all the physical simplifications and building parameters that are included in the climate modeling system.

5.6 Results and Discussions

For each scenario of urban development, we made a simulation with the WRF/ARW-BEP+BEM climate modeling system over a time period that covers three non-consecutive months. We took into account the 2030 WRF/ARW land cover maps and the 2010 meteorological conditions. The year 2010 represents at the global scale the warmest global land and ocean surface temperatures above the 20th century according to the National Oceanic and Atmospheric Administration (NOAA) with +0.62°C compared to the 20^{th} century average that is 13.9°C. In France and according to Météo France, the 2010 winter ranks among the coldest of the century period (it was as cold as 1996) but, however, it does not represent unusual winter conditions. The meteorological conditions of 2010 are also characterized by a warm summer: it is the 10^{th} warmest summer since 1950. As a conclusion, the meteorological conditions observed in 2010 display the influence of the climate change in the global surface temperatures. This year presents also the advantage to show that despite the global warming, the variability of the climate system continues to produce cold winters. More, according to

the meteorological simulations performed to regionalize the climate change across the French territory, the climate change will induce in average slight changes in the annual temperatures. By 2050, the warming is included for the region between +1.26°C to +1.44°C (www.drias-climat.fr). The selected months for the simulations are February, March and September. They have been showed in chapter 3 to give good estimates of the building cold sensitivity and base temperature of the statistical model for the studied area.
The sealing of natural surfaces through pavements, parking lots, and buildings triggers changes in the near surface temperature fields and urban heat island intensity [Oke, 1987].

Usually, the difference of the air temperatures between two stations or two atmospheric grids is used to assess the urban heat island intensity. One is chosen being representative of the countryside thermal environment, and the other is considered being representative of the urban thermal environment. We use the temperature averages of all the urban area considering that the average temperatures are representative of the urban thermal environment. We also use the temperature averages of all the rural considering that the average temperatures are representative of the rural thermal environment. We argue that average temperatures over a domain are more representative of the local climate than the consideration of two temperatures datasets. On this basis we defined the average UHI intensity (ΔUHI) as the difference over the three months of the daily urban and rural simulated temperatures. The urban (or rural) temperatures are taken as the daily average temperature of all the urban (or rural) atmospheric grids. We calculated the nocturnal (ΔUHI_night) and daily (ΔUHI_day) urban heat island. The nocturnal temperatures are the average of the hourly temperature over the 6 p.m to 8 a.m. period of all the urban (or rural) grids of the domain. The daytime temperatures are the average of the hourly temperature over the 8 a.m. to 6 p.m period of all the urban (or rural) grids of the domain.

Scenarios	ΔUHI	ΔUHI_night			ΔUHI_day		
		Feb.	March	Sep.	Feb.	March	Sep.
Initial Case	0.62°C	0.57°C	0.83°C	1.15°C	0.32°C	0.24°C	0.37°C
Compact scenario	0.59°C	0.55°C	0.79°C	1.09°C	0.30°C	0.22°C	0.33°C
Moderately compact scenario	0.56°C	0.52°C	0.77°C	1.05°C	0.29°C	0.22°C	0.33°C

Table 5.5: Urban heat island intensity for each simulated built-up pattern (February is Feb. and September is Sep.)

Table 5.5 shows that the average and nocturnal urban heat island intensities are weak. The UHI is frequently less than 1C. Cantat [2004] used a network of meteorological stations and observed an UHI of nearly +3°C and +1°C over the Paris agglomeration at night taking the minimum temperature and during the day taken the maximum temperatures, respectively. Ketterer and Matzarakis [2014a] reported from the 2000-2011 meteorological survey of Stuttgart (Germany) using four urban stations and a single reference station, an average annual UHI intensity equal to 0.3°C in the suburbs of Stuttgart that could rise up to +2°C in the city center. Szymanowski and Kryza [2012] by analyzing urban and rural temperatures measured respectively at urban and rural stations found that the UHI phenomenon rises the temperature of the city center of Wroclaw (Poland, 293 km2 and 640,000 inhabitants) by +1°C. Mayer in 1987 found an UHI intensity of +1.9°C in Munich (Germany) that could reach up to +8.2°C [Ketterer and Matzarakis, 2014a]. Finally, Hamdi and Schayes [2008] reported measured UHI intensity of +5°C at night and of +2°C at noon in Basel (Switzerland).

Over the Strasbourg agglomeration, the RECLUS field campaign permits outlining a nocturnal UHI of +6°C for the August 1^{st} and 2^{nd} 2002 and considering 10 p.m. to 6 a.m hourly temperature average [Kastendeuch et al., 2000]). This scholar simulated the temperature field of the Strasbourg urban area using the Meso-NH mesoscale model of Mto-France and TEB urban canopy parameterization [Masson, 2000]. He found a nocturnal UHI of +4°C that is approximately null during the day considering two atmospheric grids, the first taken in the city center (Place Kléber) and the second at the airport (Entzheim). Taken the same method, we found over the three months a simulated UHI intensity of +1.97°C at night for the initial case. The averaging procedure smoothes the local differences in air temperatures and could explain the weak intensity of the UHI calculated in our study.

Second, the urban heat island intensity is higher at night compared to the day. The UHI is indeed usually more intense few hours after sunset when the differential in cooling between urban impervious surfaces and the rural surrounds is the highest and when the air mixing is reduced. Meanwhile it is negative or quasi null in the morning due to the higher contribution of the heat storage term in the urban surface energy budget [Oke, 1987]. Because the simulated UHI is higher at night compared to daytime, one can conclude that the climate modeling system achieves reproducing the UHI diurnal pattern.

Third, the monthly UHI intensity at night is the highest in September and the lowest

in February. This seasonal behavior of the nocturnal UHI is also well acknowledged in the researcher communities. Cantat [2004] highlighted that 34% of the highest UHI phenomenon occurs in summer while it concerns only 6% of the case in winter. Ketterer and Matzarakis [2014a] mentioned that monthly UHI intensities are higher in summer or spring and lower in winter. Physically, the solar forcings on the surface is more intense in September than in February or March. As showed in table 5.6, the average, minimum and maximum air temperatures are the warmest in September and the lowest in February. Moreover, the shadowing effects are reduced in summer when the solar elevation in the sky is high. In urban areas, the presence of tall obstacles may favor shadowing effects with low sun elevations. Hence urban surface absorbs more energy in summer than in winter. Other studies also pointed out the higher frequency of clear-sky and calm wind meteorological conditions in summer that favor the occurrence of the urban heat island phenomenon. In our study the frequency of simulated high winds (above 5 $m.s_{-1}$) at the three stations, which may hide the local effects of the surfaces in the temperature fields, are scarce over the simulated period. In parallel, the evapotranspiration fluxes are higher during the summertime leaf-on period, which contributes to lower the rural surface temperature [Schatz and Kucharik, 2014]. Besides as showed in table 5.7, the diurnal thermal gradient increases during the year in both rural and urban areas. They are the lowest in February and the highest in September. The low differential in solar energy absorption and the absence of evaporative cooling could also explain that the UHI intensities at night and during the day are equal in February.

In contrast, the daytime monthly UHI is more intense in September and February. No explanation are given but the highest Bowen ratio in March compared to February and September, that measures the contribution of the sensible heat flux compared to the latent heat (humidity) flux in the surface energy budget, could give insight on the phenomenon. Note that the Bowen ratio is computed using average rural latent and heat fluxes over the three months at 2 p.m and that the Bowen ratio is above 1 all over the period meaning that the simulated latent heat fluxes are very low.

At last, table 5.5 shows that the differences in the UHI intensity between the scenarios are weak. Moreover the differences fail in the ranges of the climate modeling system error.
Seaman et al. [1989] reported a surface temperature rise of +0.2°C with the tripling of the Saint Louis urban area, a shift of UHI center 6 km downwind, and a reduction

In °C	*Initial Case*			*Compact scenario*			*Moderately compact scenario*		
	Feb.	March	Sep.	Feb.	March	Sep.	Feb.	March	Sep.
Average urban temperature	2.87	5.62	13.48	2.76	5.90	13.39	2.77	5.91	13.43
Average rural temperature	2.43	5.06	12.69	2.34	5.36	12.59	2.37	5.38	12.65
Min. urban temperature	0.75	2.83	9.70	0.67	3.09	9.67	0.68	3.11	9.66
Min. rural temperature	0.28	2.12	8.69	0.21	2.40	8.73	0.24	2.42	8.82
Max. urban temperature	4.94	8.73	17.24	4.79	8.98	17.17	4.81	8.97	17.23
Max. rural temperature	4.48	8.60	17.09	4.35	8.85	17.03	4.38	8.85	17.10

Table 5.6: Urban and rural air temperature for each simulated built-up pattern: daily average, minimum (Min.) and maximum (Max.) for each month (February or Feb., March and September or Sep.).

Months	*Thermal amplitude in urban areas*	*Thermal amplitude in rural areas*
February	4.12°C	4.14°C
March	5.89°C	6.45°C
September	7.50°C	8.30°C

Table 5.7: Thermal amplitude in urban and rural areas.

of the wind convergence at the surface. Atkinson [2003] reported an increase in the temperature by +0.2°C when the urban area radius of an ideal city located at 50° N goes up from 6 km to 20 km. Tokairin et al. [2010] found a temperature increase equal to about +0.6°C and +0.9°C in average due to the extension of the Jakarta urban area between the 1970s and the 2000s. The largest difference in temperature is equal to +3.5°C and occurs in the South and West parts of the old city. Aguejdad et al. [2012] found differences in the UHI intensity of +22% and -24% at midnight and 6 a.m between compact and sprawled urban development scenarios over the Toulouse great city. They took an annual built-up area increase of 1300 ha/yr that is about 1.5 times higher than the annual built-up area increase adopted in our study. They also used a grid size of 250 m and forced the climate model by using ideal meteorological conditions (an idealized anticyclonic summer situation). The urban temperatures are taken as the horizontal average of the atmospheric grids contained in a line of 5 km length centered at the city core (considered in the middle of the domain). The rural conditions are

taken as the horizontal average of the atmospheric grids contained in a line of 5 km width and located 17 km upwind of the city center. Therefore the influence of the surface on the local climate and the UHI intensity are enhanced in their simulations compared to our results.

In our study it also appears that the correlations between the air temperature and the urban fraction are not significant (R=0.52 and R=0.49 for the compact and moderately compact scenarios, respectively). It means that the local effects of built-up area on the climate do not contribute to explain a large share of the temperature field. The temperatures seem to be well influenced by the synoptic conditions.

In order to deepen the analysis we analyzed the statistical distributions of the daily urban temperatures to point out some changes in the temperature fields between the scenarios. Table 5.8 sums up the different analyzed parameters while figure 5.7 depicts the frequency distributions of urban daily temperatures for each scenario.
We can observe that the daily urban temperatures are not affected by the urban development and that the slight differences observed in the statistical parameters fail in the error range of the modeling system. For comparison Aguejdad et al. [2012] found differences in the maximum and minimum temperatures between their urban development scenarios equal to about 1°C.

Scenarios	*Initial case*	*Compact*	*Moderately compact*
Mean	7.45°C	7.44°C	7.46°C
Median	9.09°C	9.08°C	9.04°C
Minimum	-5.77°C	-5.76°C	-5.78°C
Maximum	17.79°C	17.92°C	17.73°C
Standard deviation	6.39°C	6.40°C	6.41°C
Skewness	-0.29°C	-0.30°C	-0.30°C
Kurtosis	-1.16	-1.15	-1.15

Table 5.8: Characteristics of the statistical distributions of urban average daily temperatures.

Figure 5.8 displays the 3 months-averaged temperatures for the initial case and the differences in the 3 months-averaged temperatures considering successively *1)* the initial case and the compact development scenario, and *2)* the initial case and the moderately compact development scenario. The warmer surfaces in figure 5.8 are water tables. One can notice a concentric temperature gradient over the main urban centers. The

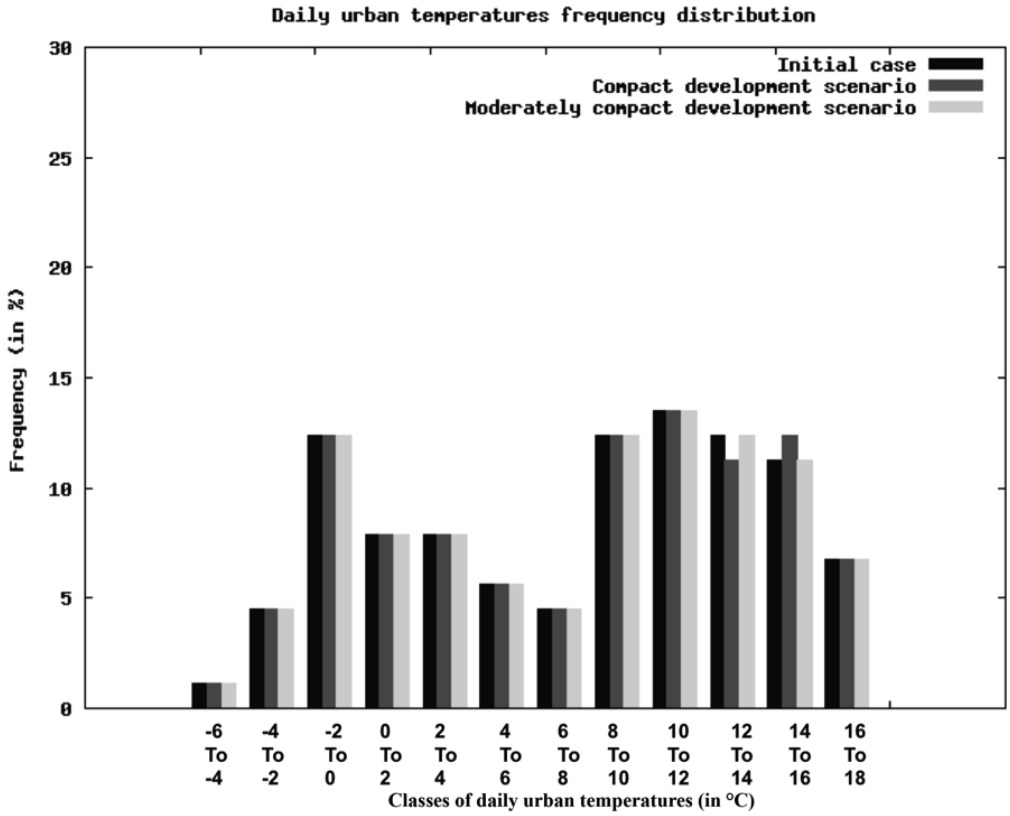

Figure 5.7: Frequency distributions of urban daily temperatures.

temperatures over the morphological agglomeration decrease from a linear temperature gradient of about -0.4°C from the warmest urban grids up to the periphery of the urban agglomerations. The highest differences between the scenarios and the initial case are in-between +0.7°C and +0.9°C for the compact development scenario and +1°C and +0.7°C for the moderately compact scenario. In case of compact urban development, punctual locations of warming can be identified. They correspond to the grids for which the urban fraction difference is greater than 20% with respect to the initial case. In case of moderately compact development scenario, punctual locations and extended areas of warming are identified. They also correspond to the grids for which the urban fraction difference is greater than 20% with respect to the initial case and grids where the urban development concerns several contiguous grids.

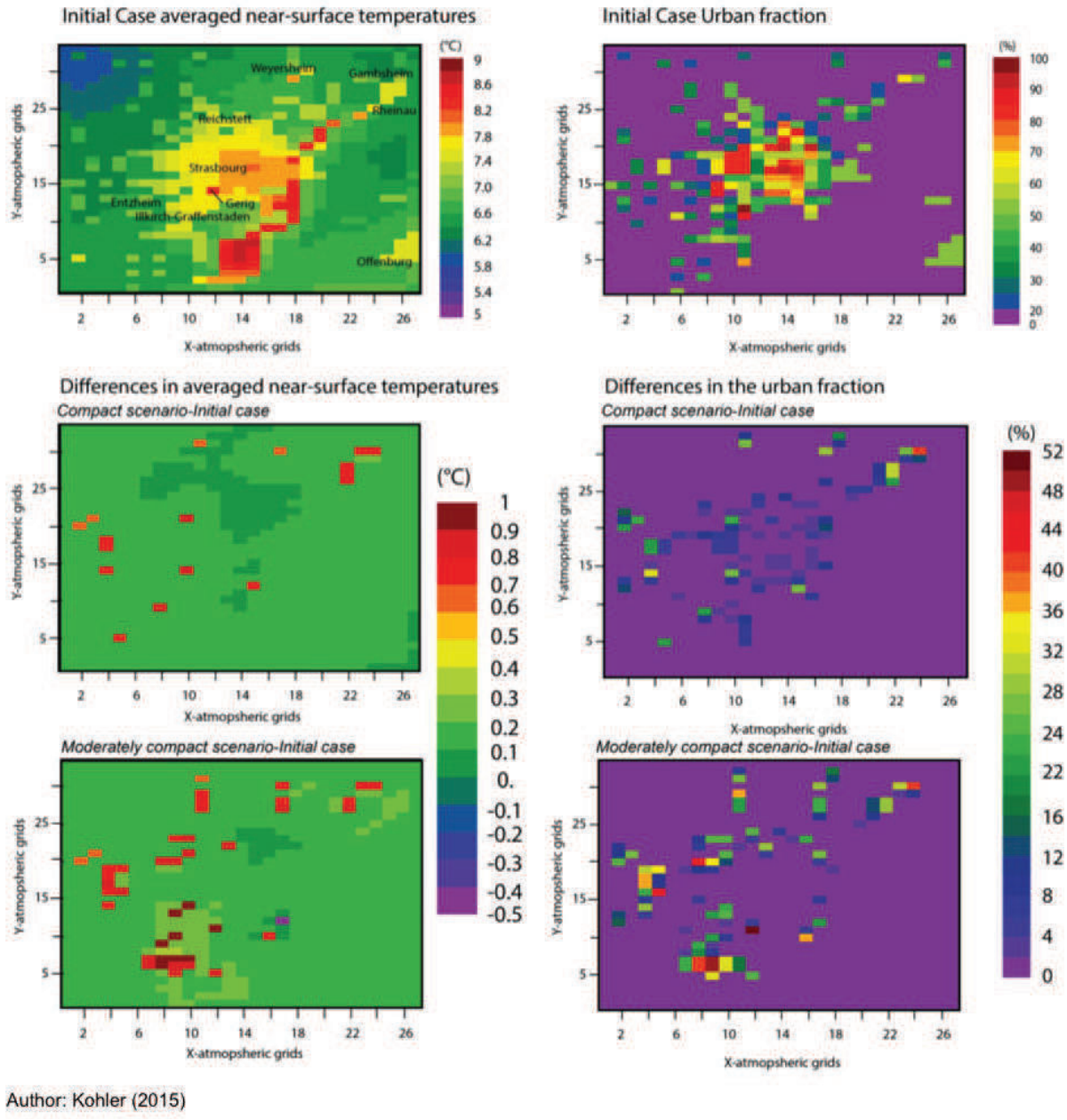

Figure 5.8: Maps of average daily air temperatures and urban fractions in the initial case, and average daily temperature differences between the initial case and the compact and moderately compact development scenarios, respectively (outputs from WRF/ARW modeling system).

As a conclusion the temperature fields seem unaffected by the urban development in average. When introducing a change of the built pattern, the average daily temperatures locally change. The warming is slightly more pronounced in the moderately compact scenario than in the compact development scenario in particular in areas where the urban development concerns several contiguous grids.

The climate modeling system by providing the building energy requirements and outdoor temperatures permits to build the "building energy requirements-daily outdoor temperatures" relationships found by previous study. A linear fitting allows taking out the cold sensitivity P which quantifies how sensitive are the building energy requirements with temperature rise. It also provides the base temperature T_0, which is the temperature at which there are no more building energy requirements for space heating. The first corresponds to the slope of the winter branch of the building energy requirements-air temperatures function. The second corresponds to the interception of the linear fits with the daily outdoor temperature. Such relationship (linear model) is sketched in figure 5.9.

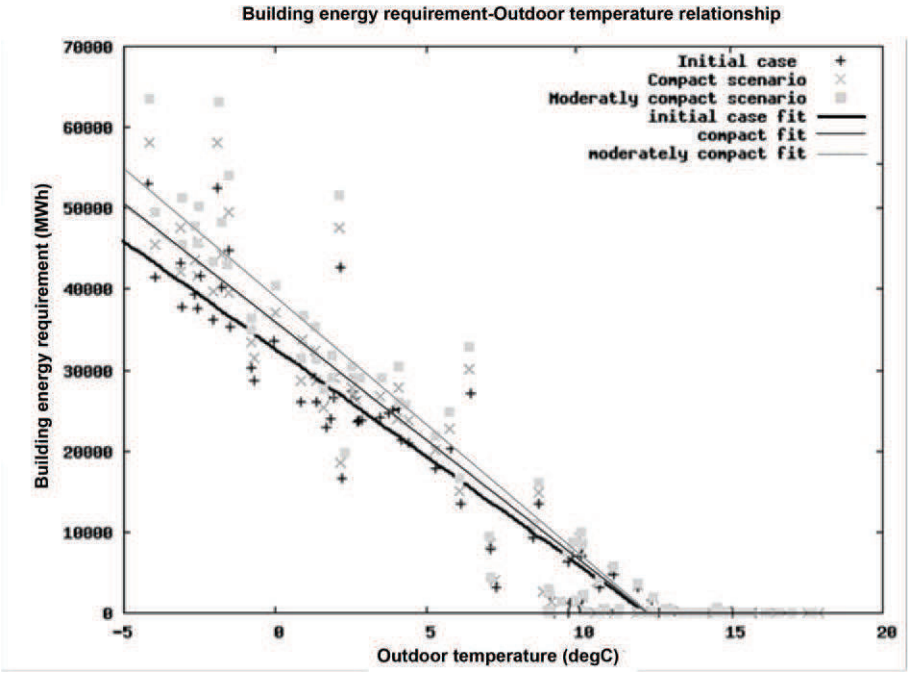

Figure 5.9: Building energy requirement as a function of the daily outdoor temperature for each scenario.

Table 5.9 provides the linear fittings parameters P and T_0 for each urban development scenario. The cumulated space heating building energy requirements outputted from the climate modeling system is $EC_{3months}$, and the corresponding building energy requirement estimations using the linear model parameters is $Q_{3months}$. Finally, we calculated the 2010 entire year building energy requirements. For this we used the cold sensitivity P and base temperature T_0 estimated with the linear model for each scenario for the three considered months. We also use the daily air temperatures simulated in the initial case for the whole year. It is referred as Q_{2010}.

Scenarios	EC_{3month} *(in GJ)*	Q_{3month} *(in GJ)*	P *(in MWh.°C^{-1})*	T_0 *(in °C)*	Q_{2010} *(in GJ)*
Initial case (EC_{2010}=14,021,807.9)	4,285,202.0	444,3216.9 *(+3.62%)*	-2668.78	12.20	14,796,360.9 *(+5.37%)*
Compact scenario	4,977,520.7 (+14.94%)	5,162,179.4 *(+3.70%)*	-2922.6 (+9.07%)	12.26 (+0.40%)	16,325,437.6 (+9.82%)
Moderately compact scenario	5,424,813.1 (+23.47%)	5,627,278.5 *(+3.73%)*	-3179.2 (+17.45%)	12.30 (+0.81%)	17,847,143.5 (+18.69%)

Table 5.9: Building energy requirements and linear model parameters for each scenario. Relative differences between $Q_{3months}$ and $EC_{3months}$ are in *(italic)* and differences between the scenarios and the initial case in (regular).

Results displayed in table 5.9 show that the use of the linear model approximates well the space heating building energy loads. The errors in the building energy requirements estimations due to the use of the linear model are equal to about 3% with respect to the building energy requirements directly outputted from the WRF/ARW-BEP+BEM climate modeling system. Considering the whole year, the relative differences between the linear model estimations and the WRF/ARW climate modeling system outputs are equal to about 5%. Therefore the three months simulations are judged enough for computing the cold sensitivity and the base temperature of the study area and giving good estimations of the building energy load over the whole year.

When comparing the cold sensitivity and the base temperature for each scenario, it is observed that the cold sensitivity shows more significant differences between the development scenarios than the base temperature. The cold sensitivity and the building energy requirements are the highest in the moderately compact development scenario, the lowest in the initial case. The compact development scenario associated cold sensitivity and building energy requirements are higher than in the initial case, but lower than the moderately compact development scenario.

However the consideration of simple building energy requirements leads to miss-interpretations: the 2010-2030 urban development area provided by the SLEUTH* simulations is the highest in the moderately compact development scenario (1,864 ha) compared to the compact development scenario (1,185.24 ha). The 20% rules, which defines the amount of built-up areas that should be included in an atmospheric grid to consider it as an

urban grid, leads to neglect about 14% of the built-up area built by 2030 in the compact urban development scenario and about 13.6% of the built-up area built by 2030 in the moderately compact development scenario. Hence, it is more the SLEUTH* simulations that explain the differences in the building volume to be heated between the two scenarios. Because the difference in the volume of building to be heated prevents the comparison of the two scenarios, we consider the building energy requirements intensity that is the building energy requirement per floor square meter.

Table 5.10 gives the overall floor area for each scenario over the URSK domain. The highest floor area is observed in the moderately compact urban development and the lowest in the initial case. The floor area of the compact urban development scenario is higher than for the initial case, but lower than for the moderately compact development scenario.

Scenarios	*Floor areas*
Initial case	58,419,796 m^2
Compact	63,145,968 m^2
Moderately compact	68,172,584 m^2

Table 5.10: Simulated floor areas for each scenario.

Considering floor areas of table 5.10, a second linear model has been built by considering the heating energy intensity (figure 5.10). The cold sensitivity and the base temperature obtained through "the heating energy intensity-outdoor temperature" function are recalled P^* and T_0^* (table 5.11).

Scenarios	P^* *(in* $MWh.°C^{-1}.m^{-2}$*)*	T_0^* *(in* $°C$*)*
Initial Case	-4.57.10^{-5}	12.21
Compact scenario	-4.62.10^{-5} (+1.08%)	12.26 (+0.32%)
Moderately compact scenario	-4.66.10^{-5} (+1.95%)	12.30 (+0.40%)

Table 5.11: Cold sensitivities and base temperatures obtained by using heating energy intensity (in MWh.°C^{-1}.m^{-2}).

Table 5.11 evidences that the differences between the parameters of the linear fittings

are clearly lower.

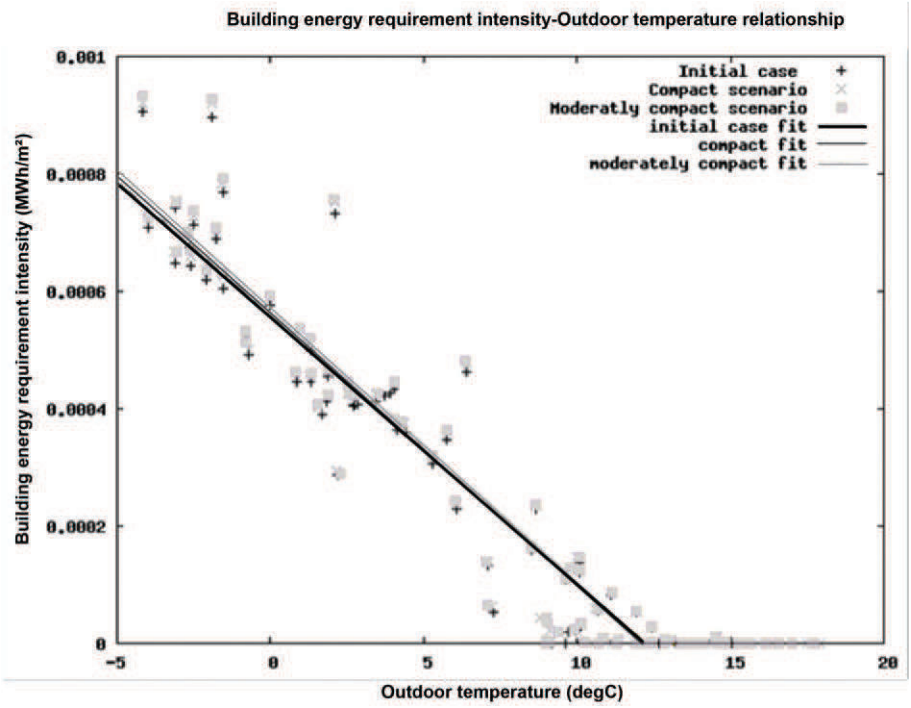

Figure 5.10: Building energy requirement intensity as a function of the daily outdoor temperature for each scenarios.

Thus the differences in the building energy requirements are mainly due to the differences in the building heated volume of each scenario. The locations of the new urban developments seem to have no influence on the building energy requirements.

For investigating the spatial pattern of the "building energy requirements-outdoor temperature" function, we computed for each urban grid the cold sensitivity P and base temperature T_0. The maps are presented in figures 5.11 and 5.12.

We observe in figures 5.11 and 5.12 that the cold sensitivity is higher in the center of the main agglomeration (that is also characterized by higher building density), and lower in its periphery (that is also characterized by lower building density) for the two scenarios. Those results are surprising. Yet many studies associate low density and sprawling patterns with increasing building energy requirements.
Few differences are observed in the base temperature (less than 1°C). The base temperature is in average equal to about 12°C but higher base temperatures that can reach 13°C are observed in few urban grids. This not surprising as the base temperature is often associated with the building energy performance and internal heat gains. The

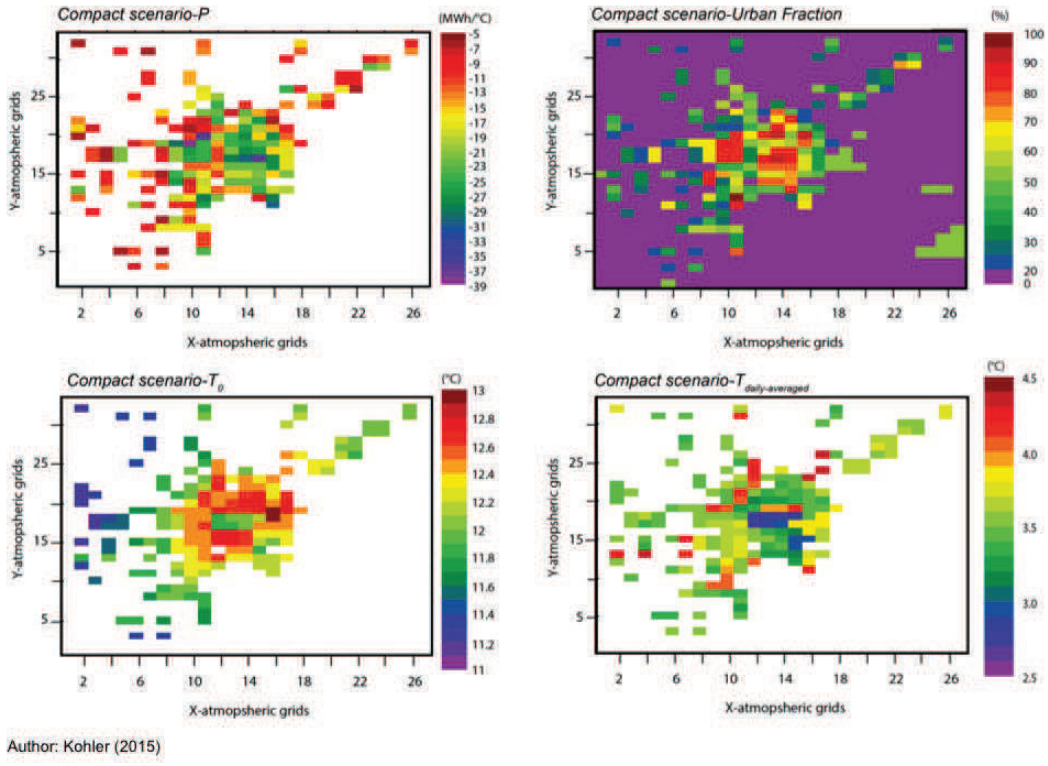

Figure 5.11: Compact development scenario: maps of the linear fitting parameters (cold sensitivity P and base temperature textitT_0), daily averaged urban temperature for the three selected months, and urban fractions

latter slightly vary over the URSK domain: we considered only three urban types in which the building characteristics for high and low intense residential are quite equal. At last, the daily average temperatures are the lowest in the dense urban core. This could be due to building shadowing effects that are enhanced in February and March. Then the daily average temperatures are the highest in the grids that are assigned to commercial and industrial types. In winter it is often showed that anthropogenic wasted heat contributes more than solar radiations to the warming of the air temperature [Sailor, 2011]. The wasted heat due to equipment in commercial and industrial grid is indeed the highest compared to the other urban types: the floor area of each building storey is 2100 m^2 for commercial and industrial buildings, 750 m^2 for high intense residential buildings, and 200 m^2 for low intense residential buildings.

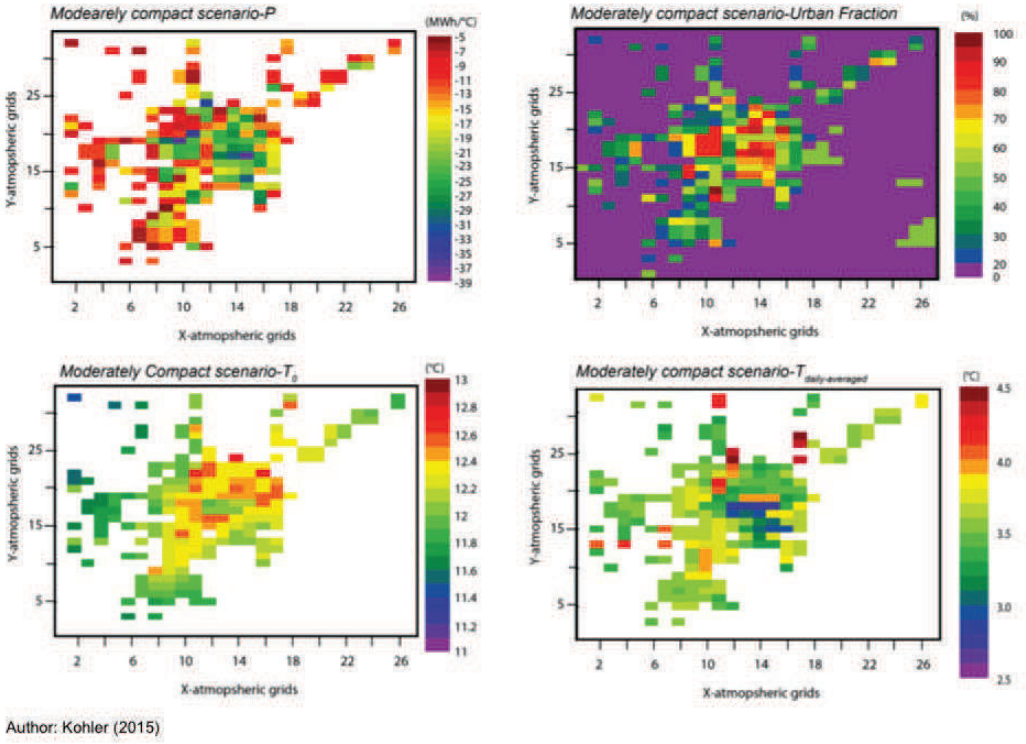

Figure 5.12: Moderately compact development scenario: maps of the linear fitting parameters (cold sensitivity P and base temperature T_0), daily averaged urban temperature for the three selected months, and urban fractions

When comparing the cold sensitivities and the urban fraction in the one hand, and the base temperature and the urban fraction in the other hand, it seems that the cold sensitivities are well correlated with the urban fraction neither do the base temperatures. The correlations between the urban fraction and the cold sensitivity are R=-0.90 for the two scenarios. The highest is the urban fraction the lowest is the cold sensitivity. The urban fraction is an estimate of the number of buildings included in each urban grid. The high correlations seem indicating building density effects on the space heating building energy requirements. When accounting for the vertical dimension of the buildings and considering the correlation between the total floor areas and the cold sensitivities, the correlations decrease (R=-0.76 and R=-0.77 for the compact and moderately compact scenarios, respectively). This decrease could be partly explained by changes in the ratio of the building envelop on the building volume (*i.e.* building surface on volume ratio). The building surface on volume ratio quantifies the amount of energy losses through the buildings facets on the energy required to heat the building volume. The floor area seems to increase the variability of the cold sensitivity compared to the number of buildings.

The correlations between the base temperature and the urban fraction are 0.42 and 0.32 for the compact and moderately compact urban development scenarios, respectively. The base temperature is not significantly correlated with the urban fraction. The number of buildings has few impacts on the building thermal equilibrium. In contrast, the correlations between the base temperature and the air temperature are equal to 0.79 and 0.71 for the compact and moderately compact development scenarios. Indeed the air temperatures influence the thermal equilibrium of the buildings, and especially the heat gains and losses through heat conduction in the building walls and natural ventilation.

Finally, we consider the building energy requirement intensity to make abstraction of the differences in the building volume to be heated between the scenarios. We computed the cold sensitivity P^* and base temperature T_0^* in each atmospheric grid. Figures 5.13 and 5.14 display the linear fitting parameters for each atmospheric grid.

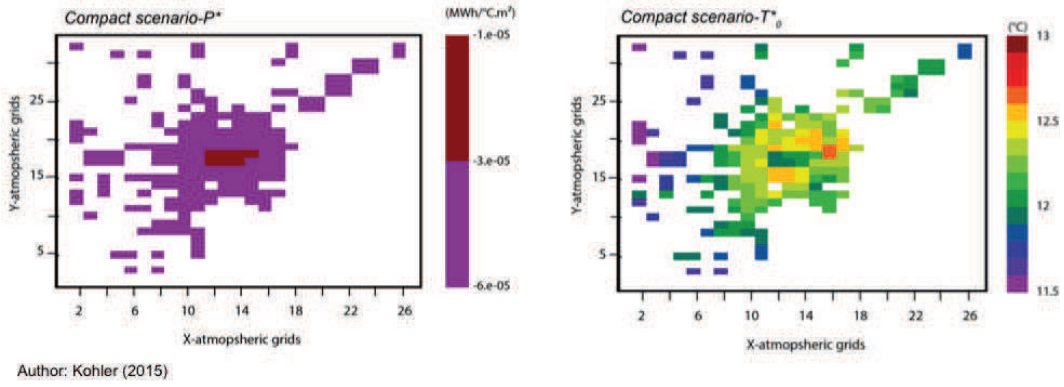

Figure 5.13: Linear fitting parameters considering the building energy requirements intensity for the compact development scenario. (Be careful the scale has been changed due to lower P^* compared to P)

Comparing figures 5.11 and 5.13 on the one hand, and figures 5.12 and 5.14 on the other hand, we observe that the cold sensitivities are mainly influenced by the building floor area unlike the base temperatures. A concentric gradient is observed in the cold sensitivity maps: the lowest cold sensitivities are found in the high dense urban core and the highest are observed in the periphery of the main urban agglomeration. This means that the buildings energy requirements in the dense urban core are less influenced by the cold temperatures compared to buildings that are located in its periphery. Figures 5.15 and 5.16 display in particular the building energy intensity requirements in function of the outdoor temperatures considering in the one hand the atmospheric

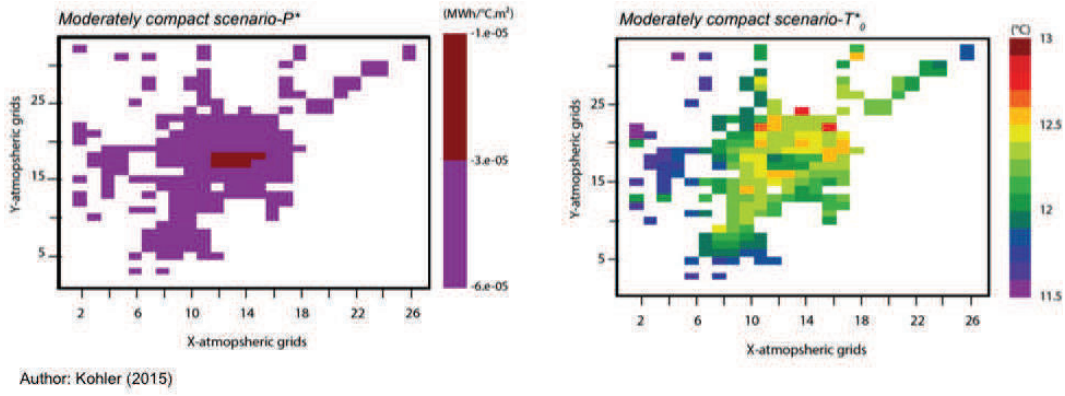

Figure 5.14: Linear fitting parameters considering the building energy requirements intensity for the moderately compact development scenario. (Be careful the scale has been changed due to lower $P*$ compared to P)

grids that are characterized by low cold sensitivities (class 1) and in the other hand the atmospheric grids that are characterized by high cold sensitivities (class 2) identified in figures 5.13 and 5.14. Clear differences in the building energy intensity requirements - outdoor temperatures functions, especially in the cold sensitivity are evidenced. Higher building density may reduce the losses of energy. The envelop on volume ratio is the highest for tall buildings reducing the energy exchanges of the buildings with their surrounds. In addition, the thermal radiations emitted by the surface are intercept and absorbed by adjacent building walls especially in narrow streets.

The base temperatures are the lowest in the dense urban core. They increase slightly by about 0.5 C in the vicinity of the urban core, and then decrease in the farthest periphery of the urban core. Nevertheless few differences are observed in the spatial pattern of the base temperatures when considering either the building energy requirement or the building energy intensity requirement.

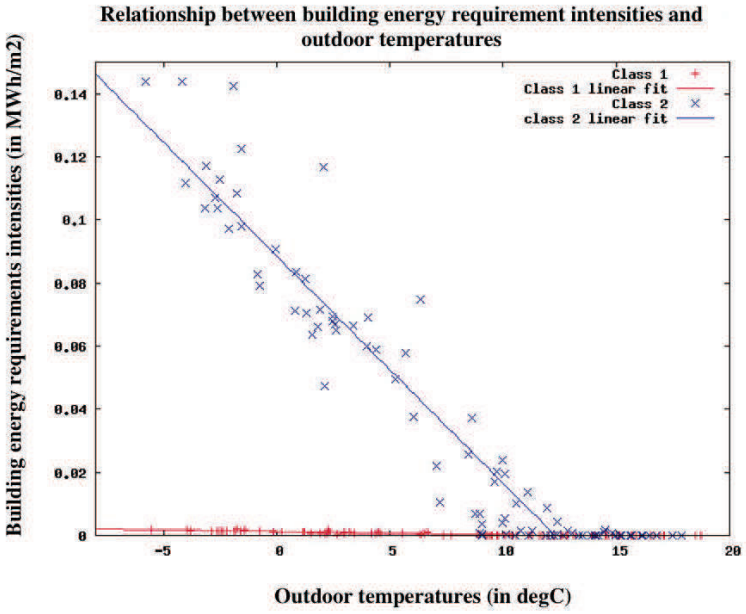

Figure 5.15: Relationship between the building energy requirement intensities and the outdoor temperatures for the two classes identified in figure 5.13 for the compact scenario. Class 1 (or 2) gathers the atmospheric grids that are characterized by low (or high) cold sensitivities.

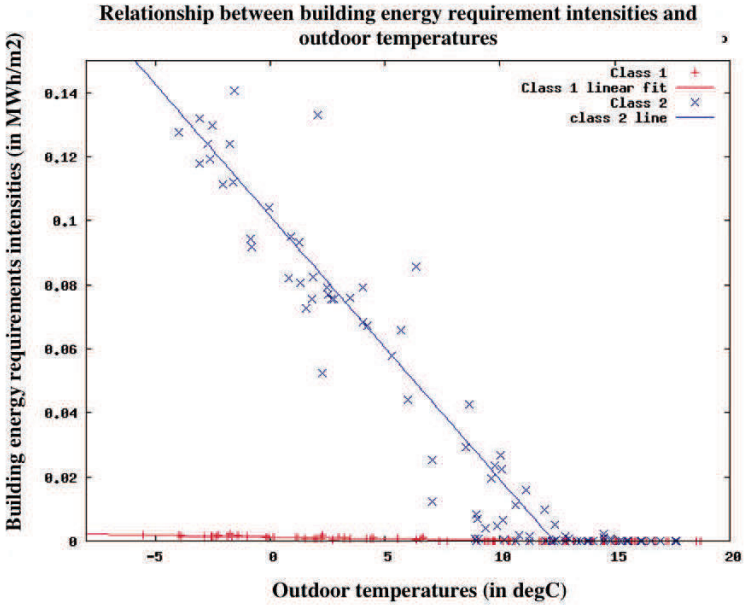

Figure 5.16: Relationship between the building energy requirement intensities and the outdoor temperatures for the two classes identified in figure 5.14 for the moderately compact scenario. Class 1 (or 2) gathers the atmospheric grids that are characterized by low (or high) cold sensitivities.

5.7 Conclusion

Like previous study we explored the effect of two planning rules (control of urban development and preservation of ecological habitat) on the urban climate (*e.g.* [Tokairin et al., 2010, Aguejdad et al., 2012, Masson et al., 2013, Stone and Rodgers, 2001, Stone et al., 2010, 2013] in association with the space heating building energy requirements. For this we use the WRF/ARW-BEP+BEM climate modeling system. The planning rules and mechanisms behind the urban development are explicitly taken into account through the design of non-developable land maps that are integrated in the SLEUTH* urban growth cellular automata. We investigate three contrasted and archetypal built-up types scenarios (the compact, moderately compact and spontaneous urban developments). Then the scenarios come in two versions in which the red squirrel forest habitat connectivity is preserved or not. Graphab [Foltête et al., 2012] is a landscape graph-based software that enables us to identify essential forest patches for ensuring the red squirrel ecological network connectivity while the MorphoLim [Tannier et al., 2011] computing program permits constraining the urban development either in the main built-up clusters or in their fringes. The resulting built up patterns appear to be not so different between scenarios that protect or not the red squirrel habitat. The scattered built-up patterns could not be evaluated by the climate modeling system: a grid is assigned to urban when more than 20% of its area is built-up. The built-up area is then under-estimated for scattered built-up patterns.
Therefore we only consider the compact and moderately compact built up patterns to assess the changes in the building energy requirements for heating and in the meteorological fields with the urban developments with the WRF/ARW-BEP+BEM climate modeling system. The built-up patterns serve to provide the $1km^2$ atmospheric grids land cover types and afferent physical static properties of the surfaces (*e.g.* roughness length, heat capacity, leaf area index, building heights, urban canyon dimensions and so on).

We firstly test the effect of the two urban development scenarios on the urban heat island intensity considering daily average, nocturnal and daytime urban and rural temperatures. Daytime temperature is taken as the average of the hourly temperatures included between 8 a.m. and 6 p.m. and conversely for the nocturnal temperature. The rural (or urban) conditions are taken as the average of all the non-urban (or urban) grids of the URSK domain. The urban heat island intensity appears to be weak. The averaging procedure is recognized to smooth the local differences in temperature, but

is more representative of the local climate. The UHI seasonal and daily patterns are well reproduced by the climate modeling system. The UHI intensity peaks in summer (September) and at night. The contrasts in temperature are indeed lower in wintertime when no evaporative cooling, shadowing effects and low solar radiation absorption are observed. Between the urban development scenarios slight differences are observed in the UHI intensity. Moreover the statistical distribution of the daily temperatures for the scenarios confirmed that the two scenarios have no effects on the urban temperatures. Significant warming locations are only observed in atmospheric grids for which the urban grid fraction has increased by more than 20% compared to the initial case. Besides this, the urban fraction is not significantly correlated with the average temperatures of the three months meaning that the temperature is more influenced by the synoptic conditions than by the shape of the built pattern.

Then we analyze the building energy requirements provided by the climate modeling system. Differences in the building energy requirement equal to +14% and +23% are reported for the compact and moderately compact development scenarios with respect to the initial case. The discrepancy in the building energy requirements estimates is less than 5% when considering the statistical model of the winter branch of the "Building energy requirement-daily outdoor temperature" relationship. The resulting cold sensitivities (the slope of the statistical model) quantify how much energy is required with temperature rise. They vary according to the scenarios. The base temperature is the temperature at which the building energy requirements. They are not sensitive to climate conditions (the interception of the statistical model with the temperature axis).
The moderately compact development scenario seems to have the highest building energy requirements and cold sensitivity. However the built patterns simulated by the SLEUTH* model are characterized by differences in the building volume to be heated. We therefore considered building energy requirement intensities. Then, the new cold sensitivities and base temperatures are quite similar between the two scenarios. Thus the changes in the building energy requirements between the scenarios come from the difference in the building volume to be heated. Two groups of urban grids emerge when mapping the new cold sensitivity. The first is characterized by relatively low cold sensitivity and are observed in the dense core of the main urban center. The second, located farthest from the dense urban core, is characterized by relatively high cold sensitivity. It corresponds to grids in which the building density is the lowest. The building density and building height may lower the cold sensitivity of the buildings. Physically the ratio of the building envelop on the building volume is higher in high

dense building area. Therefore the surface exchanges between the heated buildings and the colder outdoor are reduced. In addition the building density attenuates the surface longwave radiations losses towards the atmosphere meanwhile high building density favors the disconnection of the urban canopy flow with the above laying flow [Baik et al., 2003].
In opposite, no significant correlations are found between the base temperatures and the urban fraction. It seems that the base temperatures are more impacted by the building energy performance characteristics such as the performance of the insulation and internal heat gains. The base temperatures show lower values in the dense urban core, higher values in the first crown of the main agglomeration and finally decreasing values at the periphery of the main agglomeration. This pattern seems to be well correlated with the air temperature and internal heat gains through ventilation and conduction.

In conclusion, it seems that the urban climate modeling system is able to detect changes in the building energy requirements due to changes in the built-up area. It seems, however, unable to consider differences in the space heating requirements with respect to various built-up patterns. Two axes emerged from our study. The first plaids in favor reproducing more realistic building volume and details. This could be achieved by taking benefits of the highest resolution of the micro-scale and CFD models. The second scales back the role of the climate modeling system approach in assessing the building energy requirement. Indeed it appears that the sealing of the surface produces slight effects on the meteorological fields, in particular the temperature fields. Nevertheless, those results have to be confirmed by other study cases.
It is possible that the urbanization intensity in the URSK domain is too weak to impact the local climate. Other urban development simulations in fast developing countries and urban areas have to be performed and their incidence on the urban climate and energy requirement tested.
Second it seems that the chosen period of simulation is inadequate to observe local climate effects. The urban heat island intensity is indeed more intense at night, and in summer. The analyzes of the winter branch of the "energy-temperature" function and space heating energy, are realistic configurations for the study case, but is maybe not the best period to assess the ability of the climate modeling system to assess building energy requirements. It is possible that the climate modeling system approach is more adapted in summer and less in winter when the solar radiation forcings are weak and anticyclone conditions scarce. Again, further investigations are required.
Third, it is possible that the changes in the temperatures with respect to the scenario

are influenced by the atmospheric grid resolution. The 1 km grid resolution is indeed a compromise done between the computational time and the representation in details of the physical processes. Classical atmospheric grids range between 1 km and 5 km for considering anisotropic atmospheric grids and obstacle spatial average effects on the fluid flow. The grid resolution goes also hand in hand with the time steps used for simulating the various physical processes. A time scale characterizes each physical process. Small physical time scales require the use of small time steps. Hence for 1km atmospheric grids resolution, the usual time step adopted for solving the advection is about 100 second, for the acoustic waves 1 second and for the gravity wave 30 seconds. Hence the finest would be the atmospheric grid resolution the smallest should be the time step and the highest will be the computational time requirement.
To date, increasing the grid resolution raises, however, difficulties:

i) in representing the heterogeneity of the surface. Voogt and Oke [1998]reported that the urban surface anisotropy stays relatively constant as scales increase up to approximately 12 m up to 1000 m. Below this limit, the advection and fetch effects have to be considered. In this way, the tile approach that neglects the spatial topological information is no more adapted when using finer grids resolution. Advection and fetch effects have then to be considered.

ii) in representing more realistic urban components such as the trees and buildings. To date buildings are often viewed as uniform arrays of cubes leading to build idealized or correspondent building volume, but not real cities. In parallel the integration of the vegetation effects in the urban canopy models is at its beginning. Radiative, thermal, aerodynamic and humidity effects in such models are often taken into account for low vegetation while several studies pointed out the role of mature trees on building energy requirements according to the building exposition to solar radiations [Nowak, 2006].

Hence, the use of the climate modeling system to provide urban planning guidelines in the energy conservation outlook is not to date recommended. Careful attentions have to be paid on the interpretation of the results, and one should refrain, to date, from giving building energy performance policy advice to policy makers. Further researches on this field are required to adapt those climate modeling systems for operational urban planning and study the relationship between urban form, building energy and urban climate.

Chapter 6

Development of a 1D-canopy model under neutral atmospheric conditions

Abstract

The development of an interface canopy model (CIM) are presented in this chapter. This collaborative work carried in the EPAC team (LIVE, Strasbourg) were performed in the scope to more accurately reproduce the vertical structure of the meteorological quantities in the canopy layer, which profiles could be used as boundary conditions both in urban surface parameterizations immersed in atmospheric mesoscale models and in more resolved microscale meteorological models (domain of about 100 meters, horizontal grid size of 1-2m). The CIM canopy models relies on the previous work of Ikeda and Kusaka [2010] that stressed on the importance of multilayer canopy walls' thermal budgets resolutions and Müller [2007] that pointed out the sensitivity of the urban canopy parameterizations with the vertical resolution of the mesoscale atmospheric grids. In CIM canopy model, the 1-dimensional vertical transport equation for momentum is solved under neutral conditions using an adaptation of the parameterizations of the surface fluxes proposed by Martilli et al. [2002], a k-ε turbulence closure that uses an extension of the Santiago and Martilli [2010] mixing length formulation, and volume porosities like in Kondo et al. [2005] to account for the presence of buildings or other built elements in the largest canopy grids. In contrast to previous study, the obstacles have non-uniform x- and y- dimensions along with the z-dimension. Sensitive tests show that the CIM profiles show good agreements with the Monin-Obukhov theory for plane surface. More, the sensitive tests stress that the drag forces parameterizations and mixing length formulations are prevailing parameters that significantly influence the vertical wind speed profiles. The porosities in contrast show less influence on the vertical wind speed profiles when adopting uniform obstacles but considerably change the wind speed vertical profile when adopting non-uniform vertical volume porosities distributions, and produce considerable changes in the vertical turbulent kinetic energy profile. Nevertheless, those findings have to be confirmed by further experimentations, and the thermodynamics should be introduced in the transport equations to perform real atmospheric conditions studies. To such extent, Mauree [2014] in his PhD work already introduced the effect of the thermodynamic on the wind speed and turbulent kinetic energy vertical profiles. Those advance therefore permit research studies on the influence of the thermodynamics effects in the canopy layer as previous studies suggested major contributions of momentum drag forces compared to buoyancy forces in urban canopy layer allowing the simplification of the canopy layer models.

Keywords: *Atmospheric boundary layer Canopy model Surface-layer theory Turbulent kinetic energy Turbulence parametrization Urban meteorology Urban parametrization*

6.1 Introduction

Since the past decades, detailed urban canopy parameterizations (UCPs) that compute quasi-explicitly the three dimensional radiative and turbulent energy and momentum exchanges of the built elements of the urban canyon (*i.e.* walls, roofs and streets) with the atmosphere have been developed for mesoscale atmospheric modeling applications (see Chapter 2). The UCPs re-compute on their own urban canopy vertical grid the surface fluxes by introducing an extra-term in the Navier-Stokes conservative equations to accurately reproduce the vertical structure of the urban boundary layer. The structure of the urban boundary layer is particularly determinant in air quality and building energy issues, and a fortiori when the building energy use models are sensitive to the air ventilation and infiltration like in Bueno et al. [2011], and when building complex produces complex wind flows in the urban canopy layer. The obstacles indeed, modify the surface fluxes in the urban boundary layer and the urban canopy layer itself, but also influence the boundary layer above the urban canopy layer (the roughness sublayer) impacting weather mesoscale processes. The canopy meteorological quantities (*i.e.* canopy air temperature T_{can}, wind speed U_{can} and relative humidity q_{can}) that are used in the UCPs to re-compute the surface fluxes are either directly interpolated from the mesoscale vertical atmospheric grids at each calculation iteration [Martilli et al., 2002] or computed by using appropriate mean canopy meteorological quantities like in [Masson, 2000]. In the most sophisticated UCPs that reproduce the three dimensional effect of the obstacles on the energetics and dynamics of the airflow, one can referred to the single and multilayer urban canopy parameterizations depending whenever one or several levels describe the urban canopy layer. Both types of UCPs are acknowledged to show better accuracy with the observations compared to the classical roughness approach. Nevertheless, Ikeda and Kusaka [2010] by comparing the simulated aire temperatures provided by the single and multilayer urban effect parameterizations with observations recently demonstrated that the resolution of the wall heat budget for each level of a refined multilayer canopy grid produces better agreements with the 1-m temperature observations compared to the resolution of a single wall heat budget on a single canopy grid level. More, the quality of the simulations is showed to vary with the seasons (higher RMSE in winter) and the sky view factors (*i.e.* the hemispheric fraction of visible sky from ground) when using a single layer urban canopy parameterization.

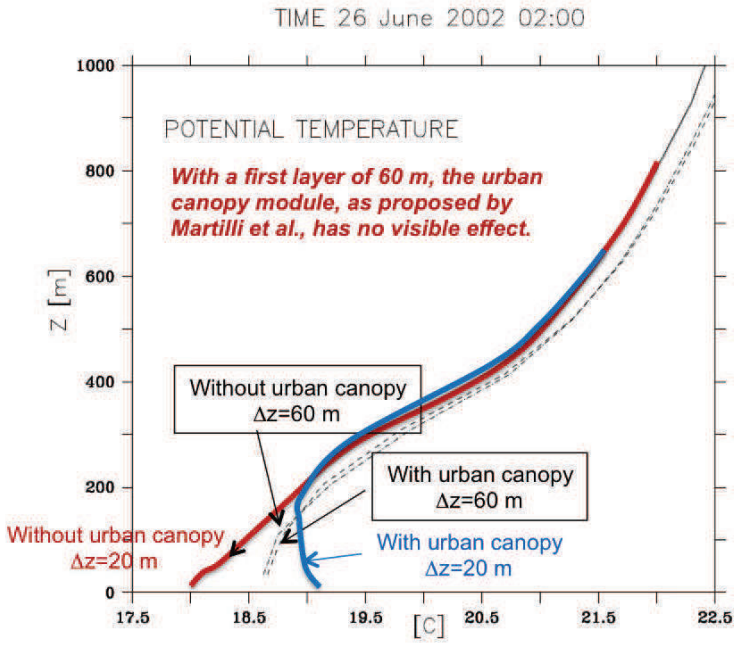

Figure 6.1: Simulated temperature (°C) showing the importance of the vertical resolution of the first mesoscale level and the improvement of the surface effect representations by using an urban canopy model (Adapted from Müller [2007]).

In parallel, Müller [2007] demonstrated that the multilayer UCPs are particular sensitive to the vertical resolution of the first level of the mesoscale atmospheric grid when testing the BEP urban canopy parameterization of Martilli et al. [2002] with decreasing resolution of the first vertical mescal atmospheric grid (taken respectively at 60 m and 20 m).

In particular, this study pointed out that the structure of the boundary layer varies with the vertical resolution of the mesoscale atmospheric grid (figure 6.1). The surface fluxes induced by the built-up surfaces are particularly underestimated when adopting a low vertical resolution (60 m) at the first level of the atmospheric grid. More, the nocturnal instable layer that is often found over the urban areas is not reproduced by the mesoscale atmospheric model. He then increased the vertical resolution of the first level of the mesoscale atmospheric grid (20 m). The nocturnal instable boundary layer and the surface fluxes are then fairly well reproduced. His results, therefore, plaid in favor of using more resolved mesoscale atmospheric grids at the vicinity of the surface to capture the specific energetics and dynamics of the urban boundary layer. Nevertheless, the use of refined vertical atmospheric grids resolution triggers increasing computational time demand. As a consequence, the same scholar proposed to implement a one-dimensional canopy model at the interface of the Swiss TVM mesoscale atmospheric model and the BEP urban canopy parameterization. The

mesoscale atmospheric model forces the top of the canopy grid at each iteration of the physical calculations. The canopy model computes the canopy wind, temperature and turbulent kinetic energy profiles using one-dimensional vertical transport equations. Those vertical profiles are then used in the BEP urban canopy parameterization to re-compute the surface fluxes that are transferred to the mesoscale atmospheric model. As presented in figure 6.1, the implementation of the canopy model allows a better representation of the surface effects even with low atmospheric grids vertical resolution.

6.2 Research objectives

Taken into account those advances, we propose to develop a canopy interface model (CIM). It is expected to: *i)* improve the representation of the boundary layer vertical structures in the mesoscale atmospheric models without increasing the computing demand; *ii)* improve the simulations of the microscale climate models like the building energy use models by considering the dynamic and energetic of the whole urban boundary layer, and more especially those of the urban canopy layer; *iii)* permits to interface any atmospheric mesoscale models and surface fluxes calculations to enlarge the number of available urban climate modeling systems that are designed for addressing urban environmental issues. The surface fluxes could issue from microscale models or any urban surface parameterizations that can include sophisticated building energy models or represent the microclimate induced by the presence of trees in the dense urban canopy such as their cooling effects.
We pay a particular attention to represent the aerodynamic effects of any elements of the urban canyon that can be a building or a tree. For this, we define at each level of the vertical canopy grid of the CIM canopy model dimensionless surface and volume porosities to describe the morphology of the obstacles immersed in the vertical canopy grid of the CIM canopy model. The developments of the CIM canopy model have been initiated in the FVM non-hydrostatic mesoscale atmospheric model of Clappier et al. [1996] and are presented in Kohler et al. [2012]. Latter, Mauree et al. [2014a] proposed further developments and validation against CFD modeling simulations. The CIM canopy model is now implemented in the well-known collaborative WRF-ARW mesoscale model of Skamarock et al. [2008] version 3.5. This chapter is dedicated to the presentation of the preliminary developments and the earliest results found in Kohler et al. [2012].

6.3 Description of the Canopy Interface model: CIM

6.3.1 Physical formulations

6.3.1.1 The vertical transport equation for momentum

At the scale of the street-canyons, the prevailing factors at the origin of the urban heat island phenomenon are the solar radiations and the prevailing winds [Bozonnet et al., 2007]. Therefore, the CIM canopy model is firstly developed to solve the 1D transport equation for momentum (ref. 6.1). In the canopy layer, the time variations of the wind speed (*term I* 6.1) are only due to changes in the surface forcings (*term III* in equation 6.1) and changes in the atmospheric turbulent fluxes (*term II* in equation 6.1 (see chapter 2). The surface forcings are induced by the surface roughness that originates pressure drag forces, and in turn losses of momentum at the fluid-surface interface. The atmospheric turbulent fluxes are induced by the exchanges of momentum between two flows with one flowing over each other at their interface, that are characterized by contrasted wind speeds.

$$\underbrace{\frac{\partial U_i}{\partial t}}_{\text{Term I}} = \underbrace{\frac{\partial}{\partial z}(\overline{u'w'})}_{\text{Term II}} + \underbrace{f_u^S}_{\text{Term III}} \tag{6.1}$$

6.3.1.2 The turbulent closure

We adopted the K-theory to model the atmospheric turbulent fluxes. The K-theory approximates the atmospheric turbulent fluxes by analogy with a molecular diffusion. The turbulent fluxes are then written according to a local wind speed gradient time an unknown coefficient of diffusion: the turbulent viscosity coefficient μ_t. Since the turbulent viscosity coefficient measures the ability of mixing of a flow, it is common to parameterize the turbulent viscosity coefficient like the product of a velocity $L.T^{-1}$ time a length L.
The velocity and the length are set in relation with the features of the turbulent flow.

The length is usually set equal to the size of the biggest eddy contained in the flow, while the velocity represents the local shear stress induced by the momentum exchanges between the two overlaying flows. Hence, according to the Prandtl parameterization the length L is the mixing length [Prandtl, 1925]. It defines by analogy to the mean free path ways of a molecule the distance that can cross an air parcel before be mixed with its surrounding. Over plane areas the mixing length is usually equal to the elevation $L = z$ or $L = kz$ with k the van kármán universal constant, assuming that the eddies increase linearly with the height.
In the presence of obstacles, the size of the eddies is, however, limited due to the flow obturations induced by the obstacles. To such extent, Santiago and Martilli [2010] demonstrated that the mixing length is close to a constant in the urban canopy layer, which mainly depends on the building density. Thus, we chose as a first approximation that L=W_x with W_x the street length in the x-direction in the urban canopy layer (for $z < H$).
In contrast to the Monin-Obukhov theory, the velocity that represent the friction velocity is parameterized by the local wind speed gradients. Thus, the turbulent viscosity coefficient is written according to the Prandtl theory like:

$$\mu_t = k^2 L^2 (\frac{\partial U}{\Delta z}) \tag{6.2}$$

The van kármán universal constant k is set equal to 0.41 according to Högström [1996], 0.35 according to Businger et al. [1971] or sometimes taken at 0.40 [Andreas et al., 2006]. Here we set k to be equal to 0.4 like in Martilli et al. [2002].

6.3.1.3 The resolved equation

Considering equation 2.16, the second term of equation 6.1 can be rewrite using the formulation of the K-theory. Thus, the vertical transport equation for momentum can be then written according to:

$$\underbrace{\frac{\partial U_i}{\partial t}}_{\text{Term I}} = \underbrace{\frac{\partial}{\partial z}(\mu_t \frac{\partial \overline{U_i}}{\partial z})}_{\text{Term II}} + \underbrace{f_u^S}_{\text{Term III}} \tag{6.3}$$

Term I represents the variation of the wind speed according to the time, *term II* rep-

resent the atmospheric turbulent fluxes. The atmospheric turbulent fluxes are set null at ground and are proportional to the turbulent viscosity coefficient μt described in the previous section. At last *term III* are the momentum losses induced by the presence of the ground, and the walls of the surface elements such as building or trees.

6.3.2 Grid and obstacle representations

The grid of the canopy model consists in a column composed by several vertical levels, which vertical resolution (Δz) and horizontal resolutions (Δx or Δy) are set constant throughout the z-direction. Each level of the column is described according to the center I of the grid volume and its faces (or interfaces) i. The obstacles that can be buildings or trees, are considered to be immersed in the column and occupy a fraction of the grid volume and facets at each level of the column. The obstacles are considered to be parallelograms that fill the entire vertical dimension of the canopy grid cell as showed in figure 6.2.

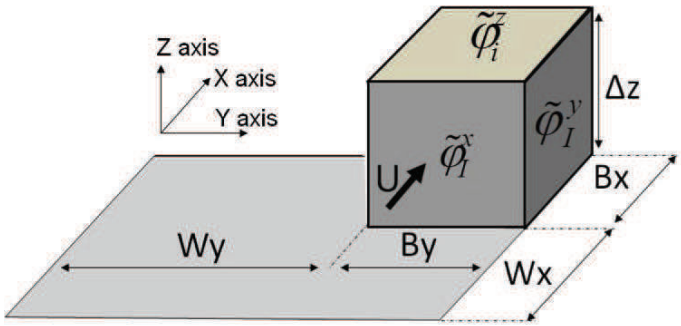

Figure 6.2: Representation of the obstacle's geometry. Bx and By are the obstacle's width while the street widths in x and y directions are respectively Wx and Wy. Δz is the vertical grid resolution.

Like Kondo et al. [2005], we consider the effect of the presence of buildings in larger volume of air through dimensionless porosities. They are used to attenuate the atmospheric exchanges in the urban canopy layer due to the presence of obstacles, and to weight as well the pressure drag forces acting on the facets of the obstacles. In this study, we consider tow kind of porosities: the volume and surface porosities. Each of them varies between 0 and 1. The volume porosity ϕ_I defines the fraction of air included in each canopy grid. The surface porosity ϕ_i represents the unoccupied fraction of the canopy girds faces .

Unlike Kondo et al. [2005], the volume and the surface porosities vary at each level of the vertical canopy grid considering that the size of the obstacles varies in height but also in width and length according to the height like in figure 6.3.

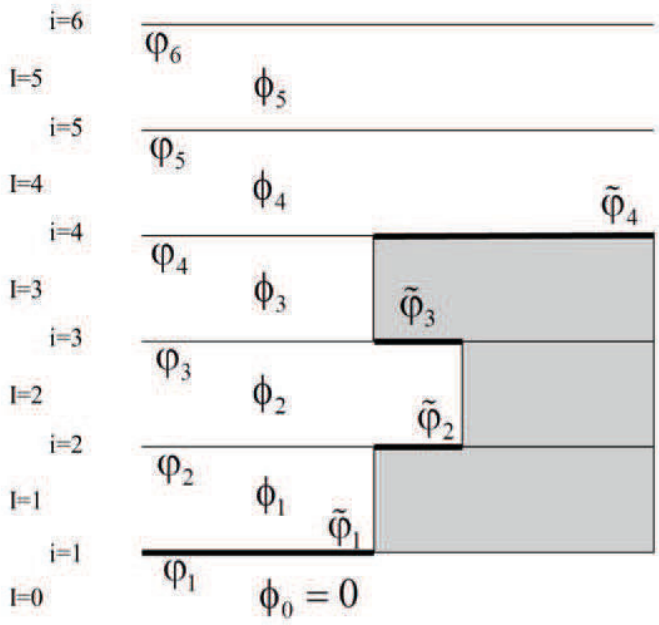

Figure 6.3: ϕ refers to the volume porosity. Small φ is for surface porosity (free surface) at interface i while the accent is for the obstacle z surfaces (**bold line**).

The volume porosity in the canopy gird cell I is:

$$\phi_I = 1 - \widetilde{\phi}_I \tag{6.4}$$

In which the occupied volume fraction of the canopy grid is defined by using the obstacle densities in x-direction and y-directions, like:

$$\widetilde{\phi}_I = \frac{B_{x,I} B_{y,I}}{(B_{x,I} + W_{x,I})(B_{y,I} + W_{y,I})} \tag{6.5}$$

This formulation enables us to consider the effect of various patterns of obstacle densities on the airflow. Indeed Baik and Kim [2003] found that the obstacle density triggers three types of flow regimes that are characterized by how much the turbulent eddies at the leeward side of the buildings interpenetrate the windward turbulent eddies of the next obstacle. Figure 6.4 depicts the three flow regimes. It is showed that the wake

zone (bounded by the dash line) of the buildings are disconnected in **(a)**, interpenetrate in **(b)** and quasi inexistent in **(c)**.

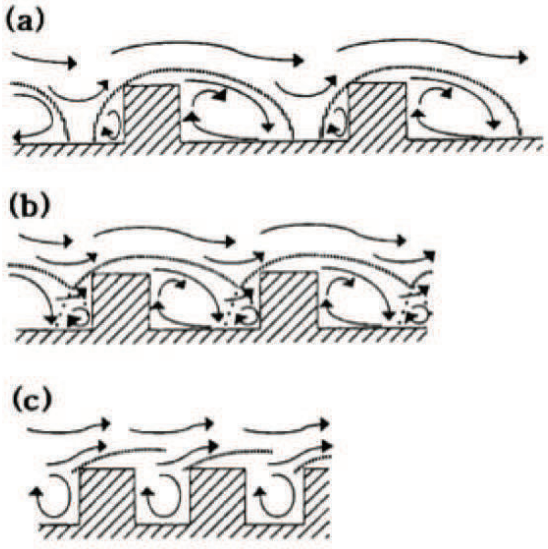

Figure 6.4: Sketch of the three flow regimes that can occur in the urban street canyons: (a) isolated roughness flow, (b) wake interference flow, and (c) skimming flow (from Oke 1988).

The isolated building flow regime is the regime in which the turbulent eddies are the less perturbed by the presence of other obstacles. The skimming flow is the flow regime in which the obstacle density is so much high that the airflow inside and outside the confined area of the street vary independently.

In our study, the obstacles density is defined by the number of obstacles n that are included in the canopy grid so that:

$$n = \frac{dx.dy}{(B_{x,I} + W_{x,I})(B_{y,I} + W_{y,I})} \tag{6.6}$$

Hence the highest is the obstacle density the least are the free volume in the canopy grid cell.
Finally, the surface porosities are the free fractions of any canopy grid interfaces i. The surface porosities are set equal to:

$$\varphi_i = min(\Phi_I - \Phi_{I-1}) \tag{6.7}$$

At the bottom of the canopy grid, a particular boundary condition is fixed:

$$\varphi_1 = 1 - \Phi_1 \tag{6.8}$$

6.3.3 Discretized equations

We use a finite volume method when discretizing the momentum transport equation so as to consider the presence of obstacles in larger air volume. The discretization of the transport equation for momentum gives for a any canopy grid I:

$$\frac{U_I^{t+1} - U_I^t}{\Delta t} = \frac{1}{\Phi_I V_I}(f_{i+1} - f_i) + \frac{1}{\Phi_I V_I} f_u^S \tag{6.9}$$

Where Δt is the time step, t the time of a simulation. The total volume of the canopy grid cell is V_I and the volume porosity is noted Φ_I. The source term is f_u^S and f_i is the atmospheric turbulent fluxes that exchange quantities at the canopy grid interfaces.

The atmospheric turbulent fluxes f_i are computed according to:

$$f_i = \varphi_i \mu_{t,i}(\frac{U_I - U_{I-1}}{\Delta z}) \tag{6.10}$$

With f_i is the atmopsheric turbulent fluxes at the interface i, φ_i the free horizontal surface of the interface i, $\mu_(t, i)$ the turbulent viscosity coefficient, and Δz the vertical resolution of the canopy grid.

6.3.4 Source terms

The source terms represents the momentum sinks induced by the resistance of the obstacles to the motion. We choose to distinguish the momentum sinks induced by

horizontal from the momentum sinks induced by the vertical building facets like in Martilli et al. [2002]. In the absence of alternative theory, the horizontal surface fluxes are computed according to the Monin Obukhov Similarity Theory given:

$$F_i^H = -\frac{|U_I^{hor}|k^2}{|ln(\frac{\Delta z/2}{z_0})^2|}U_I \tag{6.11}$$

Where $|U_I|$ is the norme of the horizontal wind speed and U_I is the U or V component of the wind speed. The roughness length is z_0 and k the Von Kármán constant (set equal to 0.41).

On the vertical obstacle walls, the drag forces are induced by the differential in the pressure distributions over the leeward and windward obstacle facets. Their are formulated by using the drag force approach proposed by Raupach [1992] and are distributed through along the obstacle height considering that the vertical facets at the leeward side of the obstacles are orthogonal to the fluid motion. It leads to:

$$F_{I,ort}^V = -Cd|U_I^{ort}|U_I \tag{6.12}$$

The drag coefficient Cd that assesses the resistance of an object immersed in a fluid environment is taken equal to 0.4 like in Martilli et al. [2002].

In addition, frictions forces that act on the obstacle walls placed parallel to the fluid flow are modeled by using the Monin-Obukhov Similarity Theory like in equation 6.11.

$$F_{I,hor}^S = \frac{1}{\Phi_I V_I}(\widetilde{\varphi_i^z}.F_i^H + \widetilde{\varphi_I^x}.F_{I,orth}^V + 2.\widetilde{\varphi_I^y}.F_{I,hor}^V \tag{6.13}$$

According to the tile approach, horizontal and vertical surface fluxes for momentum are averaged in the canopy grid cell according to their respective covering areas. The ratios of the obstacle surface on the air volume (refer figure 6.2) are called the specific

surface. They are described as follows for vertical surfaces perpendicular to the x- and y- axis (see):

$$\frac{\widetilde{\varphi_i^x}}{V_I} = \frac{B_{y,I}}{(B_{x,I} + W_{x,I})(B_{y,I} + W_{y,I})} \tag{6.14}$$

$$\frac{\widetilde{\varphi_i^y}}{V_I} = \frac{B_{x,I}}{(B_{x,I} + W_{x,I})(B_{y,I} + W_{y,I})} \tag{6.15}$$

And, for plane surfaces like the roofs or the streets:

$$\frac{\widetilde{\varphi_i^z}}{V_I} = \frac{\Phi_I - \Phi_{I-1}}{\Delta z} \tag{6.16}$$

6.4 Preliminary results and discussion

To understand the importance of each of the processes involved in the canopy wind profile, preliminary tests were conducted for a column height of 50 m and 5 m vertical canopy grid resolution. A building elevation of 25 m and a building and street widths of 10 m along the x and the y directions respectively, are assumed. A wind speed of 3 $m.s^{-1}$ is forced at the top of the column at each calculation iterations.

The simulation settings are:
Case 1. The mixing length is equal to the height (L=z) and frictions are only computed at ground.
Case 2. Same as case 1 but a volume and surface porosities are taken into account within the column.
Case 3. Same as case 2, but roof surfaces effects are added.
Case 4. Same as case 3 with additional drag forces due to walls.
Case 5. Same as previous case 4. Inside the canopy, the mixing length is limited by

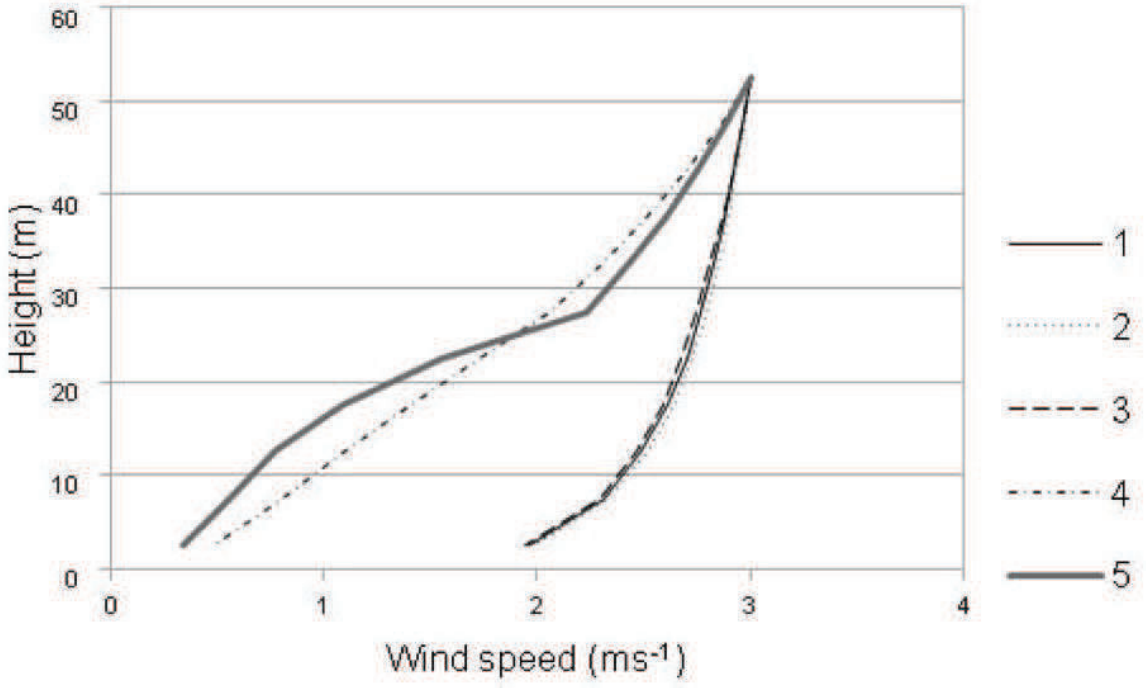

Figure 6.5: Vertical U wind profile for the cases 1 to 5 described below.

the street width.

With respect to the Prandtl theory, case 1 reproduces well the logarithmic profile found other flat surfaces. Starting from this base case, porosities are showed to produce slight effects on the vertical wind profile (case 2). This result can be partly explained by the non-consideration of the effects of the obstacle density in the mixing length formulation. More, the effects of the porosities have not been harshly tested by considering obstacle dimensions that do not vary with height. Further experimentations are then required to conclude on the effects of the porosities on the vertical wind profile.

In case 3, the momentum sinks induced by the roofs do not produce visible changes in the vertical wind profile. In contrast, the pressure forces acting on the building walls considerably reduce the wind speed in and out of the urban canopy layer (with elevation $z < 25$ m and elevation $z > 25$ m, respectively). The wind speed at the surface is reduced by about 1.5 $m.s^{-1}$, but remains unchanged at the top of the column due to the column forcings. In addition, the vertical wind profile is found to be no more logarithmic. The strength of the drag coefficient can explain the sensitivity of the vertical wind profile with the drag forces. The drag coefficient Cd is indeed 10 fold higher than the equivalent drag coefficient considered for horizontal surfaces when using the

Monin-Obukhov Similarity Theory.

Finally when limiting the mixing length according to the street width in the urban canopy layer significant modifications of the vertical wind profile are noticed. The logarithmic profile is displaced above the rooftop and the velocities are reduced below the building height. It depicts the well-known wind speed vertical profiles found by other studies and sketch in figure **??**. The mixing length is therefore a key point in the canopy wind profile modeling.

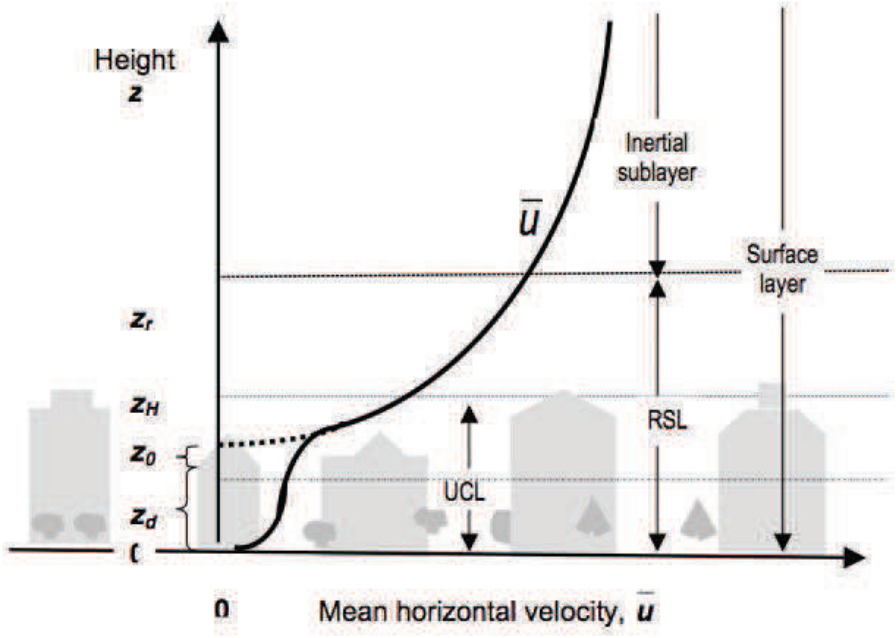

Figure 6.6: Generalized mean (spatial and temporal) wind velocity profile in a densely developed urban areas. The obstacle mean height is z_H, the roughness sublayer height is z_r, the roughness length is z_0 and the zero plane displacement length is z_d. The solid lines indicates the vertical mean wind profile while the dashed line indicates the extrapolated wind profil from the inertial sublayer. (from in World Metorological Organization [2006])

6.5 Conclusion

In this study, the early developments and results of the CIM canopy model have been presented. The developments of the CIM canopy model rely on two main objectives:

- the consideration of any obstacle perturbations on the airflow. The obstacles could be either trees or buildings;
- the interfacing of the CIM canopy model with any surface parameterizations.

The first objective is achieved by introducing surface and volume porosities in the transport equation for momentum in the terms that account for surface and atmospheric fluxes to consider the presence of obstacles in larger volume of air.
Up to now the surface and volume porosities are built by considering parallelograms, which lengths and widths can vary with height and various obstacle density distributions. The effects of the porosities on the vertical wind profile are slight, but *1)* more complex building form have to be tested before concluding, and *2)* case 5 suggests that the mixing length formulation is a prevailing factor in the vertical wind profile. By now the obstacle density is not taken into account in its formulation however Santiago and Martilli [2010] demonstrated that this parameters is crucial when modeling the air flow in the urban canopy layer.

The second objective is achieved by designing the frame of the CIM canopy model as flexible as possible to allow the consideration of any surface fluxes that are provided by other existant urban canopy parameterizations whatever their sophistications or philosophies. Hence, particular attentions have been paid in well separated the surface flux calculations that could come from any surface parameterizations from the diffusion and porosities calculations that are intrinsic to the CIM canopy model. More, the question of the parsimony of the inputed obstacle geometry datasets has been raised. The CIM canopy model is then able to compute the surface and volume porosities knowing two obstacle lengths and the obstacle height. This work was done by considering first the FVM non-hydrostatic mesoscale model of Clappier et al. [1996] that includes the BEP+BEM surface flux parameterizations of Martilli et al. [2002] and Krpo [2009] and neutral atmospheric conditions.

Taken into account those advances, Mauree et al. [2014a] developed the CIM canopy model for any atmospheric stability conditions and implemented some of the latter recommandations. Mauree et al. [2014a] (See in appendix of this chapter) adopted the formulation of Santiago and Martilli [2010] for the mixing length in which the effects of the building density on the mixing length is considered and developed the CIM canopy model so as to take into account non-uniform obstacle heights (through building height probability functions like in Martilli et al. [2002]).
First, a k-ϵ turbulence closure is adopted for parameterizing the turbulent viscosity coefficient. It accounts for the production of turbulence by shearing stress, but also by buoyancy forces. The k-ϵ turbulence closure has been first used under neutral conditions to test its ability to reproduce the vertical wind profile before being adapted to consider any atmospheric stability conditions. The k-ϵ turbulence closure is showed to accurately reproduce the shearing stress induced by the buildings, and in particular the momentum sink observed at the rooftop under neutral conditions. More, it is showed to be able to further consider any atmospheric stability conditions through the buoyant terms that are implemented in the turbulent kinetic energy transport equation.
Second, the mixing length is adapted from Santiago and Martilli [2010]. The volume porosities are introduced in the mixing length parameterization so as to take into account the modification of the eddy size with the building density.
Then, the wind and turbulent kinetic energy vertical profiles simulated by the CIM canopy model has been compared with the Santiago and Martilli [2010]'s CFD experimentations. The CIM canopy model is found to produce vertical wind and turbulent kinetic energy profiles that fit well with the CFD simulations.
In Mauree et al. [2014a], it is also showed that with uniform buildings size: *i)* the modified mixing length reduces the wind velocity but not as much as the vertical surface fluxes which effect is maximum at the top of the urban canopy; *ii)* the porosities have slight influence on the wind profile and turbulent kinetic energy.
With non-uniform building height, it is pointed out that adapted mixing length *i)* slightly modify the wind velocity profile; but *ii)* produce considerable effects on the turbulent kinetic energy profile. This latter finding has to be confirmed by further experimentations.

For building energy assessments' perspectives, the CIM canopy model has been implemented in the American WRF-ARW version 5.3.1 mesoscale atmospheric model of Skamarock et al. [2008] by Mauree et al. [2014b]. The CIM canopy model is directly coupled with the BEP parameterization of Martilli et al. [2002] for providing for each time step the canopy wind speed and temperature profiles to the BEP parameteriza-

tion.
The simulations performed by using a vertical resolution of 5 m in both the mesoscale atmospheric and CIM canopy models do not impact the temperature vertical profile, but however, triggers wind speed reductions in the canopy layer. To such extent, several studies pointed out the role of local wind on urban ventilation and local temperatures [Bozonnet et al., 2007, Kuttler et al., 1998a]. A reduction of the wind speed in the urban canopy layer may harsher the thermal comfort in summer increasing in turn the cooling energy loads in buildings. More, the reduction of the wind speed in the urban canopy may lower the air ventilation and infiltration: the building energy models such as Energy Plus are showed to be particularly sensitive to the air ventilation and infiltration as stressed by Bueno et al. [2011].
Hence the coupling of the CIM canopy model with any building energy models such as EnergyPlus may produce under-estimations of the building energy requirements in winter and over-estimations of the building energy requirements in summer.

The study of Yang et al. [2012] provide insight on the results that can provide the coupling of the CIM canopy model with the EnergyPlus and ENVI-met models. Those scholars coupled the ENVI-met micro-scale model of Bruse and Fleer [1998] that includes the microclimate effects of trees and detailed complex of buildings with the building energy EnergyPlus model. For this, they adapted in particular the walls convective heat transfer coefficients (CHTC) of the EnergyPlus model by calculating the CHTC as a linear function of the wind speed provided by the ENVI-met model. Their experimentations result in greater CHTCs, increasing heating loads by 1.8% in winter and decreasing cooling loads by 0.8% in summer. It is thus expected that the coupling of the CIM canopy model with the EnergyPlus model will reduce the wall CHTCs. It will in turn reduce the heating energy loads in winter and increase the cooling energy loads in summer. In such context, new developments and studies are welcome to confirm those hypothesis and improve further works.

At last, the coupling of the CIM canopy model with the WRF mesoscale atmospheric model was expected to save computational time. Like in Müller [2007] the coupling of the CIM canopy model with mesoscale atmospheric model is expected to produce fairly wind and temperature canopy profiles even with the use of coarse atmospheric grid resolutions. To test this assumptions, Mauree [2014] performed a study case in which the canopy grid resolution is taken at 5 m and the atmospheric grid resolution at 94 m. This scholar found a temperature under-estimations by up to 1°C compared to the case in which the atmospheric grid resolution is set equal to 5 m. Thus, another

expectation of the coupling of CIM with the WRF model is that the building energy requirements will be under (or over)-estimated in summer (or winter) even with the use of CIM canopy model when using coarse atmospheric grid resolutions. By now it seems that the use of the CIM canopy model in a climate modeling system cannot achieve saving computational time and if used with coarse atmospheric grids, the CIM canopy model is showed to produce high deviation of the vertical temperature profile.

As a conclusion, the CIM canopy model is by now developed. Nevertheless, further experimentations are required to test its reliability before permitting to give answers to building energy or air quality issues.

Appendices

Boundary Layer Meteorology manuscript No.
(will be inserted by the editor)

Development and validation of a new 1D Canopy Interface Model in a neutrally stratified atmosphere

Dasaraden Mauree · Manon Kohler · Nadège Blond · Alain Clappier

Abstract A new 1D canopy interface model (CIM) is developed to evaluate the influence of obstacles on the atmosphere in the boundary layer. The objective is to analyze the influence of urban parametrizations on spatially averaged variables (wind speed, turbulent kinetic energy, temperature and humidity) and to guarantee the coherence with past propositions. The development of the CIM is presented through the main governing equations and the modifications brought to these equations. Compared to previous studies, obstacle characteristics are computed using surface and volume porosities in each cell of the model domain. These porosities are used to weight several terms in the Navier-Stokes equations and have been introduced to prepare a coupling of the model with microscale model that could provide a better description of different kind of obstacles. A 1.5-order turbulence closure, using the turbulent kinetic energy, is used in the model. In order to ensure the coherence with Prandtl theory over plane surfaces, a modification of the usual constant values is proposed. In addition, the mixing length is modified to take into account the densityand height of obstacles in the canopy layer.

Results are compared with analytical solutions obtained in neutral atmospheric conditions over plane surfaces (no buildings), and also with data collected from a computational fluid dynamics (CFD) experiment with buildings. The comparison of results from the CIM with the analytical solutions, when no obstacles are present, establishes that the CIM is able to reproduce surface-layer processes. We demonstrate that over such a surface, a constant turbulent kinetic energy profile is obtained. The comparison of the CIM results with the CFD also show good agreements in the presence of obstacles. It is shown that the CIM is able to reproduce an inertial sub-layer as described by the Prandlt or constant-flux layer theory above a displacement height over a homogeneous canopy. Sensitivity analyses are performed in order to analyze the effect of obstacles on wind and turbulent kinetic energy profiles. The results indicate that fluxes from vertical surfaces and the mixing length have the most important effect.

D. Mauree · M. Kohler · N. Blond · A. Clappier
Université de Strasbourg, Laboratoire Image Ville Environnement, 3 rue de l'Argonne, 67000 Strasbourg, France

D. Mauree
Agence de l'Environnement et de la Maîtrise de l'Energie, 20 avenue du Grésillé, BP 90406, 49004 Angers CEDEX, France
Tel.: +33-3-68850971
E-mail: dasaraden.mauree@gmail.com

M. Kohler and N. Blond
CNRS, UMR 7362, Strasbourg, France

Keywords Atmospheric boundary layer · Canopy model · Surface-layer theory · Turbulent kinetic energy · Turbulence parametrization · Urban meteorology · Urban parametrization

1 Introduction

The study of the effects of urban areas on the boundary-layer structure and on wind fields were first motivated by the will to understand the dynamics of the planetary boundary layer with respect to pollutant dispersion (Delage and Taylor 1970; Bornstein 1975). The enhancement of computer performance in the last decades has also allowed more precise mesoscale models to be developed with several new propositions to parametrize surface fluxes and their diffusion (Masson 2000; Kusaka et al 2001; Martilli et al 2002). However in view of the current state of the art models and growth of computer performance, it is still not possible to use very high resolutions (e.g., 1 m) that would allow a better integration of obstacles (such as buildings or trees) in mesoscale models (Martilli 2007) while at the same time simulating large enough domains so as to capture large scale interactions.

Indeed the complexity and high heterogeneity of urban surfaces (buildings, roads, green spaces) make it very difficult to simulate the urban boundary layer. The surfaces and obstacles present in such areas modify the fluxes as well as the profiles of various meteorological variables inside the canopy itself (Oke 1987; Foken 2008). They also influence the boundary layer above the urban canopy impacting mesoscale weather processes (Craig Jr 2002). Since the turbulent fluxes of momentum, for example, is not constant with height anymore but instead decreases to zero up to the zero-displacement height, the use of traditional theories (such as the similarity theory), to simulate the boundary layer in an urban context, is not expected to work (Rotach 1993; Roth 2000).

Masson (2000) developed a single layer canopy model where an urban canopy parametrization is used to calculate the effects of urban areas on various meteorological variables. The first level of the meteorological model is displaced above the urban areas and a mean value of the variables in the canopy is used to calculate the source and sink terms due to urban areas. Martilli et al (2002) proposed another parametrization scheme in which they developed a multi-layer scheme that was fully integrated in a mesoscale model. Using the same methodology, Muller (2007) designed experiments to show that a canopy module can be used to enhance the computational time while decreasing the vertical resolution in the mesoscale model. Figure 1 shows that the use of a canopy module with a low resolution (60 m) in the mesoscale model, aLMo (Doms and Schättler 2002), gives the same trend as using a very high resolution (20 m) in this model (Muller 2007). The use of a canopy model is hence expected to reduce computational time while allowing at the same time a more precise integration of obstacles and calculation of the fluxes generated by the presence of these obstacles. However in this work, the canopy model developed by Muller (2007) was not totally independent of the mesoscale model and hence cannot be easily introduced into another model.

In order to overcome these shortcomings, a new canopy interface model (CIM) is designed and presented here. The objective is to develop a 1D model that could be used independently of a mesoscale model, by prescribing boundary conditions, but could also be coupled with a mesoscale model.

The multi-layer scheme developed by Martilli et al (2002), is modified to include a diffusion process based on a 1.5-order turbulence closure using the turbulent kinetic energy (e) in order to calculate a more precise vertical profile for the variables. A diagnostic mixing length is also used in the model based on the formulation proposed by Santiago and Martilli (2010). To be able to take into account any obstacle, an interface has been developed to represent the obstacle's effects in terms of porosities inside the Navier-Stokes equations. A coupling with a mesoscale model could be done to improve the urban boundary-layer description. It will also give the possibility to a user to couple a mesoscale model with a microscale model that could provide a more detailed representation

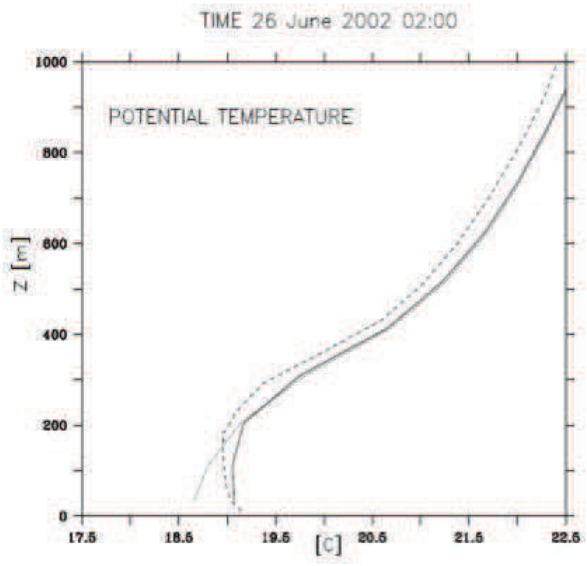

Fig. 1 Use of a canopy module allows low vertical resolution (results from Muller, C., 2007) Bold black line (**-**) high resolution (20 m) in mesoscale model; dotted line (- -) canopy model in mesoscale with low resolution (60 m); pale black line (-) mesoscale model with low resolution (60 m)

of the geometry of the surface obstacles (real building or urban vegetation shapes) or even compute surface fluxes.

When developing the model, various parametrizations schemes were tested in order to control their relative coherence. For that purpose, the model is first tested offline mode in neutral atmospheric conditions over a plane surface and results are compared to classical theories such as Prandtl surface-layer theory. Obstacles are then integrated in CIM and the results are compared with data issued from a computational fluid dynamics (CFD) experiment (Santiago et al 2007; Martilli and Santiago 2007).

In Section 2, the main assumptions and theories proposed to describe the surface layer are given. In Section 3, a complete description of the CIM and the set of equations on which the model is based are presented. Section 5 shows the comparison of the CIM, without obstacles and in neutral conditions, with an analytical solution obtained using Prandtl surface-layer theory. The profiles from the CIM, in the presence of obstacles, are then compared with results from a CFD experiment. A sensitivity analysis is also conducted to determine which terms have the most impact on the meteorological profiles. The results, their limits as well as the different perspectives for the CIM are finally discussed in Section 6.

2 The Surface Layer

A number of processes have been parametrized in the past to describe the flow in the surface layer. Important characteristics of the surface layer were first described by Prandtl (1925) and were afterwards recognized as the Prandtl or constant flux layer theories. Consequently, several studies were conducted to improve the mathematical representation of the different processes taking place in this surface layer and under different atmospheric stability conditions (Monin and Obukhov 1954; Foken 2006; Zilitinkevich and Esau 2007).

The surface-layer theory is commonly described using a series of theory and assumptions:

1. **Homogeneity assumption**
When considering large enough horizontal distances (i.e. large grid cell in the studied domain), it is assumed that the horizontal properties of a flow are homogeneous and hence that the vertical fluxes are relatively important compared to the horizontal fluxes.
Following this assumption, the averaged characteristics of the flow are considered to be a function of the z(vertical)-coordinate only.
2. **The K-Theory**
The vertical kinematic turbulent fluxes can then be approximated to:

$$\overline{u'w'} = -\mu_t \frac{\partial U}{\partial z} \tag{1}$$

where u' and w' are the fluctuations of the horizontal and vertical wind velocity components respectively, the over bar represents the ensemble average of these quantities, U is the horizontally averaged wind velocity (m s^{-1}) and μ_t is the eddy diffusion coefficient (m^2 s^{-1}).
3. **Boundary-layer theory**
The boundary-layer theory states that in the surface layer, above a plane surface, the vertical fluxes can be assumed constant (variation of less than 10% and while neglecting the effect of the Coriolis force). This surface layer is called the Prandtl or constant-flux layer. This gives rise to the boundary-layer assumption where

$$| \overline{u'w'} | = u_*^2 = constant \tag{2}$$

where u_* is the friction velocity.
4. **First-order turbulence closure in neutral conditions**
To compute the turbulent diffusion coefficient, an analogy with the molecular diffusion process is made. The diffusion coefficient can be described as the product of a velocity scale, V', times a length scale, l, similar to when describing the molecular diffusion and is given by Eq. 3:

$$\mu_t = V'l. \tag{3}$$

Over a plane surface, the length l is the mixing length. It is usually assumed to be equal to the height z or kz. This is the most common parametrization used in the mesoscale meteorological models. This parametrization was developed first by Prandtl (1925) and it has been the object of several studies (Therry and Lacarrère 1983; Watanabe and Kondo 1990; Coceal and Belcher 2004). k is the von Kármán constant, equal to 0.41 according to Högström (1996). Recent studies showed however that k is closer to 0.39 and suggest that this value can change with stability (Zhang et al 2008). If we follow the analogy with the molecular diffusion, we will consider that the mixing length is equal to z, as it could represent the maximum distance that an air parcel will travel before it touches the surface; it could also, in this way, represent the maximum size of the turbulent eddies. The velocity scale can be replaced by the friction velocity u_* and a constant k, yielding the following equation:

$$\mu_t = k u_* z. \tag{4}$$

These theories and assumptions all build together to produce the so-called **Prandtl surface-layer theory**. In these conditions, the wind profile can then be calculated using Eqs. 1, 2 and 4:

$$\frac{\partial U}{\partial z} = \frac{u_*}{kz}. \tag{5}$$

Integrating between z_0 (which is also commonly known as the roughness height and represents the height of obstacles that can be placed randomly on the ground and around which the mean

horizontal velocity is equal to zero) and a height, z, the following logarithmic profile is obtained:

$$U(z) = \frac{u_*}{k} \ln\left(\frac{z}{z_0}\right). \tag{6}$$

When the roughness elements are closely packed together, such as in a city or in a forest, the top of the elements act as a displaced surface (Stull 1988). The wind speed can then be assumed to be equal to zero at that displaced height. Equation 6 can be written as follows to take this into account:

$$U(z) = \frac{u_*}{k} \ln\left(\frac{z-d}{z_0}\right) \tag{7}$$

where d is the displacement height (m) and U is defined as being equal to zero when z is $d + z_0$.

3 Canopy Interface Model

The canopy interface model (CIM) is developed with the objective of testing the coherence between parametrizations proposed to represent the effects of built surfaces on the atmosphere, and to prepare a 1D-column model that could be used in an offline or online mode in a mesoscale model. One of the goals of CIM, is to prepare the coupling of meteorological mesoscale models with microscale models in such a way that the user of the microscale model may provide more accurate information concerning the geometry of the obstacle (such as volume or surface porosities) and if necessary also exchange surface fluxes. The coupling of the models is not presented here. The present article gives a description of the development of CIM and the methodology used to test the coherence with past propositions.

The CIM is first compared to Prandtl theory, which has been validated with measurements in numerous previous studies (Blackadar 1962; Foken 2006). It can be used to produce analytical solutions of the equations presented in Section 2 when no obstacles are present. To take into account complex surface areas, CIM was also developed following previous proposed urban parametrizations and studies. Indeed, the presence of urban surfaces inside the canopy has a significant influence on the air-flow due to:

1. Radiation trapping and heat conduction by building
2. Drag force induced by vertical and horizontal surfaces
3. New ways of transformation of mean kinetic energy into e.

Each of these effects are taken into account when applying CIM in real conditions and in a mesoscale meteorological model (Mauree 2014, chap. 5) as they impact the different meteorological variables (wind speed, e, temperature or humidity). However, in the present study, we will not describe the effect of buildings on the radiation and heat exchanges in order to focus the discussion on the analysis of mechanical effects only. For this purpose, we will only consider the atmosphere under neutral stability. Other developments and analyses in stratified conditions can be found in Mauree (2014, chap. 4).

3.1 Governing equation: momentum equation

The transport of a quantity can be written in a conservative form (Clappier et al 1996). The resulting equation calculates the mean momentum in the following way:

$$\frac{\partial U_i}{\partial t} + U_j \frac{\partial U_i}{\partial x_j} = -\delta_{i3} g + f_c \varepsilon_{ij3} U_j - \frac{1}{\overline{\rho}} \frac{\partial \overline{P}}{\partial x_i} + \nu \frac{\partial^2 U_i}{\partial x_j^2} - \frac{\partial (\overline{u_i' u_j'})}{\partial x_j} + f_u^s \tag{8}$$

where U_i or U_j are the time-averaged wind speed (m s^{-1}) with three components depending on i, j and k which are indices for each direction, x_i or x_j are the distance in each direction (m), t is the time (s), δ_{i3} is the Kronecker delta (a scalar quantity), g is the acceleration due to gravity(m s^{-2}), f_c is the Coriolis parameter (s^{-1}), ε_{ij3} is a unit tensor (also a scalar quantity), ρ is the density (kg m^{-3}), $\overline{P}$ is the time-averaged pressure component (kg m^{-1} s^{-2}), ν is the kinematic viscosity (m^2 s^{-1}) and $\overline{u_i' u_j'}$ are the ensemble average turbulent component of the wind (m s^{-1}).

The first term on the left hand side represents the time-evolution of the mean momentum. The second term corresponds to the advection of the mean momentum by the mean wind. The terms on the right hand side represents respectively the effect of gravity, the influence of the Earth's rotation (Coriolis force), the mean pressure-gradient forces, the influence of the viscous stress on mean motions, the influence of Reynolds stresses on the mean motions due to the air parcel's friction, and the specific sources of momentum f_u^s due to the friction of air with surfaces (bare soil, vegetation, buildings...). Additional information about these specific sources can be found in Martilli et al (2002) and Krpo (2009).

CIM is a 1D-column model. It was developed taking into account that:

1. when working at the neighborhood scale, it is possible to assume horizontal homogeneity, that is, it is assumed that the $\frac{\partial}{\partial x}$ and $\frac{\partial}{\partial y}$ terms are equal to zero
2. the subsidence can also be considered to be small (with the vertical wind component being of the order of mm s^{-1} as compared to the horizontal wind components which are of the order of m s^{-1}) (Stull 1988)
3. the Coriolis effect is negligible
4. viscous stress is very small as compared to the other terms in Eq. 8
5. the Reynolds stress can be approximated, under certain conditions, to a be proportional to the wind gradient (see Section 2)
6. advection processes as well as the mean pressure gradient are also neglected.

Using such approximations, Eq. 8 finally gives:

$$\frac{\partial U_i}{\partial t} = \frac{\partial}{\partial z}\left(\mu_t \frac{\partial U_i}{\partial z}\right) + f_u^s \tag{9}$$

where μ_t is the turbulent diffusion coefficient and U_i is the horizontal wind component in the $x-$ or $y-$directions. In CIM the turbulent diffusion coefficient is computed using a 1.5-order turbulence closure as described in Section 3.2.

3.2 1.5-order turbulence closure

When obstacles are present, it is no longer possible to make the same assumption on the mixing length which was made in the first-order turbulence closure (Coceal and Belcher 2004; Santiago and Martilli 2010). Furthermore u_* cannot be considered constant anymore in the presence of obstacles (Högström 1996; Roth 2000; Foken 2008). In such cases, Eq. 4 is thus not applicable and it was proposed to use a different calculation for the diffusion coefficient.

Besides the one derived from the K-Theory (Eq. 1), the turbulent diffusion coefficient can be computed using a 1.5-order turbulence closure using the e as given in the following equation:

$$\mu_t = C_k \sqrt{e} l \tag{10}$$

where l is the parametrized mixing length (as will be explained in Section 3.6.5). C_k is a constant with a value of 0.4 being used by different authors (Therry and Lacarrère 1983; Bougeault and Lacarrère 1989; Abart 1999). To further guarantee the coherence of the formulations that have been proposed, a different methodology to compute this value will be presented in Section 3.4 on the basis of statements discussed in Section 3.3.

3.3 Coherence between formulations of the turbulent diffusion coefficient

Equation 4 may be applied only over a plane surface in neutral conditions where no obstacles are present. However, Eq. 10 may be applied on any kind of surfaces and stability conditions. When developing the CIM, we made sure that these two formulations are coherent over plane surfaces and neutral conditions. In such cases, if the two different propositions for the turbulent coefficients are equal, then it can be shown that a constant turbulent kinetic energy profile will be obtained :

$$e = \left(\frac{ku_*}{C_k}\right)^2. \tag{11}$$

This coherence statement will be used to simplify the e governing equations which will be presented in Section 3.4.

3.4 Governing equation: turbulent kinetic energy equation

Assuming horizontal homogeneity, a prognostic equation, equivalent to the momentum, can be used to compute the e :

$$\frac{\partial e}{\partial t} = \frac{\partial}{\partial z}\left(\lambda_t \frac{\partial e}{\partial z}\right) + P - \varepsilon + f_e^s \tag{12}$$

where λ_t can be assumed to be equal to μ_t (Muller 2007).

Equation 12 gives the time-evolution of the e in neutral conditions and the buoyancy term is hence neglected here. The terms on right hand side represent respectively the diffusion term, the mechanical production term, the dissipation term and the fluxes due to the presence of obstacles.

The production term represents the wind shear caused by wind gradient and friction over surfaces and is given by the following equation:

$$P = -\overline{u'w'}\frac{\partial U}{\partial z} \tag{13}$$

where $\overline{u'w'}$ is the momentum flux. Note here that a negative sign is present so that the production term actually contributes positively to the generation of turbulence since $\overline{u'w'}$ is a negative term.

Based on the surface-layer theory, $\overline{u'w'}$ can be replaced using Eq. 1. This then yields a production term equal to:

$$P = \mu_t \left(\frac{\partial U}{\partial z}\right)^2. \tag{14}$$

The dissipation term represents the breaking down of the larger turbulent eddies into smaller ones and can be expressed as:

$$\varepsilon = C_\varepsilon^* \frac{e^{\frac{3}{2}}}{l} \tag{15}$$

where l is still the parametrized mixing length representing the maximum size of the turbulent eddies and C_ε^* a constant. One can note that the dissipation term is not written as usual: in other studies a specific dissipation length is defined (Chen and Kim 1987) with various formulations (Louis et al 1983; Delage 1974). This dissipation length is sometimes assumed to be different from the mixing length scales (Christen et al 2009; Santiago and Martilli 2010). It is argued in this article that the geometry of the canyon is the most important parameter and there should be no reason to use a different mixing length in the dissipation term. However, it is important to use a constant to scale the dissipation compared to the production. It should be recalled here that the mixing length is defined here as the maximum distance that could be reached by an air parcel (analogy with the molecular diffusion) and it hence is weighted in the dissipation term using only a constant. Thus the C_ε^* value is chosen to be different from the traditional C_ε.

Replacing Eqs. 14 and 15 in Eq. 12 yields:

$$\frac{\partial e}{\partial t} = \frac{\partial}{\partial z}\left(\mu_t \frac{\partial e}{\partial z}\right) + \mu_t \left(\frac{\partial U}{\partial z}\right)^2 - C_\varepsilon^* \frac{e^{\frac{3}{2}}}{l} + f_e^s. \tag{16}$$

Using Eq. 10 to replace the diffusion coefficient in Eq. 16, the following equation is obtained:

$$\frac{\partial e}{\partial t} = \frac{\partial}{\partial z}\left(\mu_t \frac{\partial e}{\partial z}\right) + C_k \sqrt{e} l \left(\frac{\partial U}{\partial z}\right)^2 - C_\varepsilon^* \frac{e^{\frac{3}{2}}}{l} + f_e^s. \tag{17}$$

Re-arranging Eq. 17:

$$\frac{\partial e}{\partial t} = \frac{\partial}{\partial z}\left(\mu_t \frac{\partial e}{\partial z}\right) + C_\varepsilon^* \frac{\sqrt{e}}{l}\left(e_{stat} - e\right) + f_e^s. \tag{18}$$

With this new formulation (Eq. 18) it is easier to compute the e by discretizing it with an implicit and explicit term (explanation on discretization with implicit and explicit schemes could be found in Ascher et al (1997)). e_{stat} represents the value of the e that is obtained over a plane surface under neutral and stationary conditions (i.e. when the local production of e is equal to the dissipation). It is written as follows:

$$e_{stat} = \frac{C_k}{C_\varepsilon^*} l^2 \left(\frac{\partial U}{\partial z}\right)^2. \tag{19}$$

From this, the value of C_k can be calculated. As mentioned in Section 3.3 both formulations of the turbulent diffusion coefficient (Eqs. 4 and 10) have to be equal. If it is assumed here again that the mixing length, l, is equal to the height and that the wind gradient is proportional to the friction velocity (as in Eq. 5), then it can be calculated that:

$$\frac{C_k^3}{C_\varepsilon^*} = k^4. \tag{20}$$

Thus, if we consider that the most important result is that the production term should be scaled compared to the dissipation term (or the countrary), it can be seen here that if a value of 1 is chosen for C_ε^*, C_k is equal to $k^{\frac{4}{3}}$ (0.30 as compared to a usual value of 0.4 as given by Bougeault and Lacarrère (1989) and Martilli et al (2002)).

If CIM is coupled with a mesoscale model, the top boundary conditions, for the different variables, are expected to come from the mesoscale model. In an offline mode, the values for the boundary conditions are prescribed and fixed. To sum up this section, it has been shown that CIM solves 1D transport equations. In order to bring coherence between past propositions, a new formulation for the computation of the e was derived.

3.5 Discretization

CIM uses a Finite Volume Method to find a solution, over a 1D-column, for the partial differential equation given in Eq. 21.

$$\frac{\partial U}{\partial t} = \frac{\partial}{\partial z}\left(\mu_t \frac{\partial U}{\partial z}\right) + f_u^s \tag{21}$$

where the term f_u^s is the source term representing the fluxes that will impact the flow. The discretization of the equations is only done here for the component of the momentum equation in the $x-$direction but the same methodology is applied for the component of the momentum in the $y-$direction as well as for the discretization of the e equation.

$$\int_{\delta V} \frac{\partial U}{\partial t} dV = \int_{\delta V} \frac{\partial}{\partial z} \left(\mu_t \frac{\partial U}{\partial z} \right) dV + F_u \tag{22}$$

where F_u is the integral over a volume of f_u^s (for additional information refer to (Martilli et al 2002)).

Using the Gauss-divergence theorem to change the volume integrals of the diffusion term into surface integrals:

$$\int_{\delta V} \frac{\partial U}{\partial t} dV = \int_{\delta S} \left(\mu_t \frac{\partial U}{\partial z} \right) dS + F_u. \tag{23}$$

Discretizing Eq. 23 to determine the solution:

$$U_I^{t+1} = U_I^t + \triangle t \frac{S_i}{V_I} \mu_{t_i} \frac{U_{I-1} - U_I}{\triangle z} + \triangle t \frac{S_{i+1}}{V_I} \mu_{t_{i+1}} \frac{U_I - U_{I+1}}{\triangle z} + \triangle t F_u \tag{24}$$

where S and V are the surface and volume characteristics of the grid cells respectively, $\triangle z$ is the vertical grid cell height and i and I are indices representing the cell face or centre respectively. These surfaces and volumes could be replaced by surface and volume porosities. These values can be obtained from a different model where the porosities are represented more precisely and would represent any obstacles (such as buildings or trees) present in the canopy.

3.6 Obstacle integration

CIM calculates the fluxes generated by horizontal and vertical surfaces, based on the formulation proposed by Martilli et al (2002) but reformulated here using porosities. The objective is to be able in the future to include any kind of obstacle present in the canopy.

3.6.1 Geometrical obstacles characteristics

Previous studies (Masson 2000; Martilli et al 2002) only described obstacles as an array of regular cubes. The novelty of our approach is that obstacles sizes are specified here *at each level* inside the urban canopy module for the x- and y-directions. Volume and surface porosities are computed from these dimensions and are then used in the calculation of the fluxes and the diffusion coefficient.

Obstacles 3D-geometry are described according to Krpo et al (2010); Kohler et al (2012) and are shown in Fig. 2. The obstacles (buildings and street canyons) are repeated to fill the space inside a grid cell. Surface and volume porosities are then defined as in Fig. 2 where I represents variables assigned to the cell centre and i to the cell face.

The geometrical characteristics of the obstacles are calculated as follows and their values vary from 0 to 1.

– The free volume porosity is given by:

$$\phi(I) = 1 - \hat{\phi}(I) \tag{25}$$

where the occupied volume $\hat{\phi}$ is given by:

$$\hat{\phi}(I) = \frac{B_x(I)}{(B_x(I) + W_x(I))} \frac{B_y(I)}{(B_y(I) + W_y(I))}. \tag{26}$$

– Based on volume porosity, the free surface porosity can be calculated as follows:

$$\varphi(i) = min(\phi(I), \phi(I-1)). \tag{27}$$

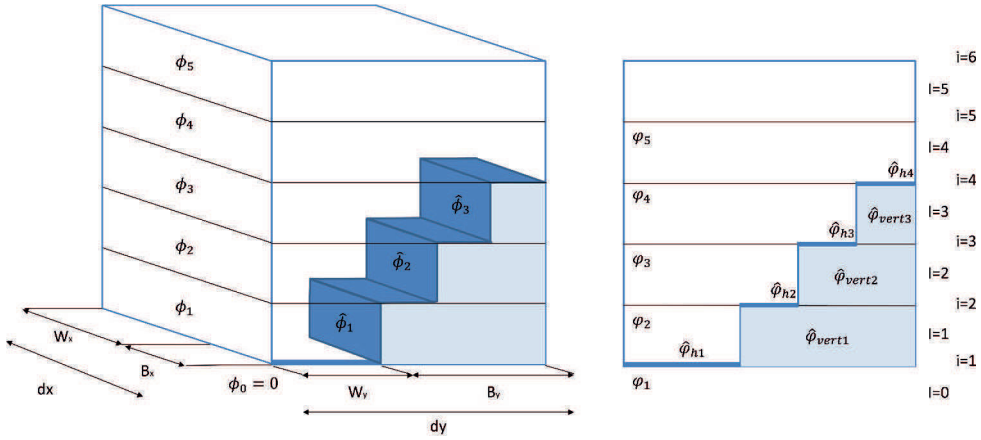

Fig. 2 On the left: 3D-view of obstacles with the occupied and free volume (B_x and B_y are the building length and W_x and W_y are the street width in the x- and y-directions respectively. dx and dy are the horizontal grid resolution while dz is the vertical resolution); on the right : side view of a section of the 1D-column showing the interpretation of the occupied surface and porosities in CIM

– The obstacles horizontal ($\hat{\varphi}_h$) and vertical ($\hat{\varphi}_{vert_x}$ and $\hat{\varphi}_{vert_y}$) surfaces (as shown on Fig. 2) are computed as follows:

$$\hat{\varphi}_h(i) = \phi(I) - \phi(I-1) \tag{28}$$

$$\hat{\varphi}_{vert_x}(I) = \frac{B_y(I)}{(B_y(I)+W_y(I))}\frac{B_x(I)}{(B_x(I)+W_x(I))}\frac{1}{(B_x(I))} \tag{29}$$

$$\hat{\varphi}_{vert_y}(I) = \frac{B_y(I)}{(B_y(I)+W_y(I))}\frac{B_x(I)}{(B_x(I)+W_x(I))}\frac{1}{(B_y(I))}. \tag{30}$$

3.6.2 Modification of the governing equations

The surface and volume porosities, as calculated with Eqs. 25 and 27 respectively, can be used to replace the S and V terms from Eq. 24.

$$U_I^{t+1} = U_I^t + \triangle t\frac{\varphi(i)}{\phi(I)\triangle z}\mu_{ti}\frac{U_{I-1}-U_I}{\triangle z} + \triangle t\frac{\varphi(i+1)}{\phi(I)\triangle z}\mu_{ti+1}\frac{U_I-U_{I+1}}{\triangle z} + \triangle t F_u \tag{31}$$

where F_u in Eq. 31 represents the additional forces that will impact the momentum.

As stated before, the presence of obstacles inside the canopy alters the flow pattern, the surface fluxes and the generation of turbulence. The influence of obstacles has been parametrized and used in previous models (Masson 2000; Martilli et al 2002). The parametrization of these fluxes is adapted from Martilli et al (2002). The geometrical variables given in Section 3.6.1 will influence the diffusion terms as shown in Eq. 31 and the calculations of the different term as shown in Sections 3.6.3 and 3.6.4.

3.6.3 Modification of the momentum flux terms

Horizontal surfaces in the canopy (roofs, streets...) induce a frictional force on the movement of air masses and lead to a loss of momentum. Above such surface, the surface-layer theory can be used to express the fluxes that are induced (Louis 1979; Martilli et al 2002). (Note that for simplicity,

we omit cell indices from the porosity and surface terms.)

$$\mathbf{F}u_I^H = -\rho \left[\frac{k}{\ln\left(\frac{\triangle z/2}{z_0}\right)} \right]^2 \mid U_I^{hor} \mid \mathbf{U_I} \frac{\hat{\varphi}_h}{\phi \triangle z} \tag{32}$$

where k is the von Kármán constant, z_0 is the roughness length (0.05 m), U_I^{hor} is the horizontal wind component at the I level, $\mathbf{U_I}$ is the wind component for both the $x-$ and $y-$directions at the I level and $\hat{\varphi}_h$ is the total horizontal surface of the obstacles at each level.

Vertical surfaces of the obstacles create a pressure gradient that is parametrized as a drag-force (Raupach 1992; Otte et al 2004; Martilli 2007; Hamdi and Masson 2008; Aumond et al 2013) in the momentum conservation equation. This drag-force can be calculated for both directions as follows:

$$\mathbf{F}u_I^{vert} = -\rho C_d \mid U_I^{ort} \mid \mathbf{U_I} \frac{\hat{\varphi}_{vert}}{\phi} \tag{33}$$

where C_d is the drag coefficient as parametrized by Santiago and Martilli (2010), $\hat{\varphi}_{vert}$ is the vertical surface of the obstacles in each direction at each level and U^{ort} is the wind speed orthogonal to the street direction and is calculated as:

$$U^{ort} = cos(drst) * U_x - sin(drst) * U_y \tag{34}$$

where $drst$ is the angle for the canyon direction and U_x and U_y are the wind speed in both directions.

3.6.4 Modification of the turbulent kinetic energy

Compared to previous formulations, in this paper it is proposed to weight the e production due to fluid-fluid interactions or air-surfaces frictions using respectively the surface porosities and the surface of each interfaces.

To calculate the production of e, due to the friction of the air on the horizontal surfaces of obstacles, it is possible to use the e_{stat} value given by Eq. 19 which has been obtained over a plane horizontal surface. Using Eq. 5 from the surface-layer theory, $\partial U/\partial z$ can be replaced to obtain the following equation:

$$e_{surf} = \frac{C_k}{C_\varepsilon^*} \left(\frac{u_*}{k}\right)^2. \tag{35}$$

It can clearly be seen, that when no obstacles are present and under stationary conditions, this value is constant with height as it is proportional to u_*^2.

To take into account these additional sources in the e equation in each grid cell, e_{surf}, is weighted by the obstacles horizontal surfaces, as this term is due to the production of e from the movement of fluids layers on horizontal surfaces, while e_{stat} is weighted by the 'free surface' porosity as this is due to fluid-fluid interactions.

$$e_{surf} = \frac{C_k}{C_\varepsilon^*} \left(\frac{u_*}{k}\right)^2 \frac{\hat{\varphi}_h}{\phi} \tag{36}$$

$$e_{stat} = \frac{C_k}{C_\varepsilon^*} l^2 \left(\frac{\partial U}{\partial z}\right)^2 \frac{\varphi}{\phi}. \tag{37}$$

Since both terms (from Eqs. 36 and 37) have been weighted proportional to the surface from which they have been generated they can simply be summed.

When vertical surfaces are present, there is additional transformation of Mean Kinetic Energy into e. The production of e by vertical surfaces is parametrized using Eq. 38:

$$Fe_I^{vert} = \rho C_d \mid U_I^{ort} \mid^3 \frac{\hat{\varphi}_{vert}}{\phi}. \tag{38}$$

3.6.5 Proposition to evaluate the mixing length in the presence of obstacles

Over a plane surface, the mixing length is usually evaluated using a linear function increasing with height. In the presence of obstacles this formulation is however not appropriat as the geometry of the obstacles will limit the maximum distance that an air parcel can travel.

A mixing length proposed by Santiago and Martilli (2010)
Santiago and Martilli (2010) proposed a new formulation that modifies the calculation of the mixing length taking into account the height of the building and the porosity. Inside the canopy, they argued that the mixing length is close to a constant which corresponds to results from Raupach et al (1996) but are however in contradiction with other results from Coceal and Belcher (2004). Santiago and Martilli (2010) proposed to calculate a displacement height (see Eq. 7) using the following equation:

$$d = h(1 - \phi)^{\alpha} \tag{39}$$

where h is the obstacle's height, ϕ is the volume porosity and α is a constant equal to 0.13.

The mixing length is then computed as follows:

$$l(i) = max(h - d, z(i) - d) \tag{40}$$

The mixing length is thus constrained inside the canopy by a constant value, while increasing linearly with height above the canopy.

Extension of the Santiago and Martilli (2010) mixing length taking into account the vertical distribution of porosity It is proposed in the present study to extend the proposition of Santiago and Martilli (2010) so as to account for a variation in the vertical distribution of porosity. The methodology is based on following steps:

1. the buildings are classified according to their height, i.e each class includes buildings with same height;
2. the ratio of each class in a grid cell is computed;
3. a mixing length for each building class is computed as if this one occupies the whole grid box, and
4. a mean mixing length is calculated based on the ratios of each building class in the grid box.

Figure 3 gives an example, where three classes of buildings are considered with seven buildings are present in the grid box.

Considering N classes of buildings with a height (denoted $H(n)$, $n = 1, N$) that follows the vertical grid (i.e. the top of each grid cell), the ratio of each class can be written using the occupied built volume in the grid as follows:

$$P(n) = \frac{1}{\hat{\phi}(1)} \sum_{I=1}^{N} \hat{\phi}(I) - \hat{\phi}(I+1)\delta_{In} \tag{41}$$

where δ_{In} is the Kronecker delta and is equal to 1 when I is equal to n. Note that here we assume that the first level is the most occupied level.

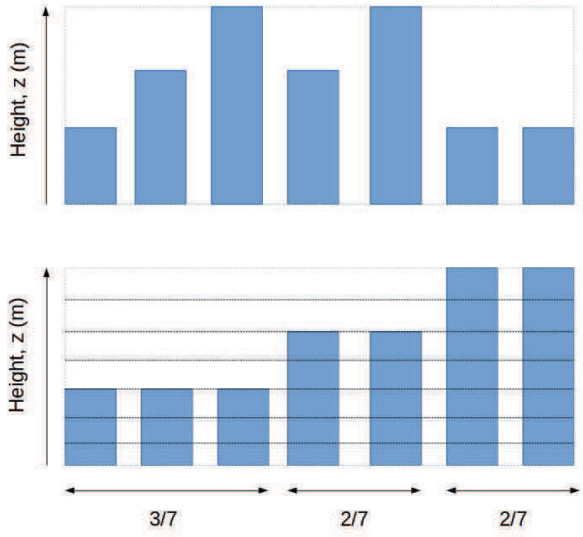

Fig. 3 Example of vertical distribution of buildings (top) and their classification in term of height (bottom). N=3 in this case.

A weighted mixing length can then be obtained with Equation 42:

$$l(i) = \sum_{n=1}^{N} P(n)L(i,n) \tag{42}$$

with:

$$L(i,n) = max(H(n) - D(n), z(i) - D(n)) \tag{43}$$

and where the displacement height for each building class is:

$$D(n) = H(n)(1 - \phi(n))^{\alpha} \tag{44}$$

with α still equal to 0.13 like in Santiago and Martilli (2010).

4 Experiments with CIM

In order to validate the assumptions made and strategies used to ensure the coherence with past propositions during the development of the CIM, the results are first compared to Prandtl theory over a plane surface and with a CFD simulation in presence of obstacles. Besides these tests, a sensitivity analysis using the separation methodology as proposed by Stein and Alpert (1993) is conducted.

Cubic obstacles of 25 m are integrated in CIM. Each of these simulations are performed in a unique 1D-column with a grid interval of 5 m and with a vertical height of 50 m that corresponds to twice the height of the obstacles that would be included in the domain. This is based on the fact

that the bottom of the inertial sub-layer can be considered to be twice that of the surface layer (Roth 2000).

When developing these tests, the meteorological boundary conditions for CIM are fixed at the top of the domain (50 m) with a wind speed of 9.68 m s^{-1} and a potential temperature of 293 K. The surface temperature inside the model is kept at 293 K such that a neutral atmospheric condition prevails. We do not fix any boundary condition for the e as CIM calculates the e on its own using the wind speed from the last grid cell.

4.1 Comparison of CIM with an analytical solution over a plane surface

CIM is first tested in the absence of obstacles under neutral conditions and its results are compared to the analytical solutions from Prandtl Theory. Using Eq. 6, a logarithmic profile of the horizontal wind can be computed and the same is expected from CIM. As for the e, from Eq. 11, a profile with a constant value should be obtained.

4.2 Comparison of CIM with a CFD model over an array of buildings

Known theories such as the surface-layer theory or the Monin-Obhukov Similarity Theory cannot be applied when there are obstacles (Högström 1996; Roth 2000), especially in urban areas. Even if there are a few experimental measurements in urban areas (Mestayer et al 2005; Rotach et al 2005; Lemonsu et al 2006; Christen et al 2009), it was difficult to use them to test CIM in neutral conditions and in a controlled environment.

In view of these constraints, it was chosen to compare results from CIM with a CFD experiment in the neutral case. The results used here to evaluate the capabilities of CIM, are from a CFD experiment performed by Santiago et al (2007); Martilli and Santiago (2007); Santiago and Martilli (2010).

Cubic obstacles with a height of 25 m are integrated in CIM. The width of the obstacles also correspond to the street (canyon) width such that the volume porosity, ϕ, is equal to 0.75, which is the value that was used in the CFD experiment from Santiago et al (2007); Martilli and Santiago (2007). As opposed to CIM, the CFD experiment used a higher (2.5) order turbulent closure to calculate the diffusion coefficient.

Boundary conditions for the wind speed and the temperature similar to before are also used here. A pressure gradient has been imposed in the CFD experiment to create an entrainment movement in the canopy, which is not present in CIM as we expect the fluxes coming from the surfaces to be sufficient to cause these movements. However, for comparison purposes with the CFD, a pressure gradient is added as an explicit term in the momentum equation.

In this configuration, the parametrization for the mixing length presented in Section 3.6.5 is used as it has been previously argued that this can have a major influence on the diffusion process (Coceal and Belcher 2004; Santiago and Martilli 2010).

4.3 Sensitivity tests to evaluate the impact of obstacles

The objective of this series of tests is to analyze how the presence of cubic obstacles inside the canopy model impacts the wind and e profiles. For that purpose, the factor seperation methodology as proposed by Stein and Alpert (1993) is used. Thus, the mechanical effect of the obstacles is studied as a function of several contributions:

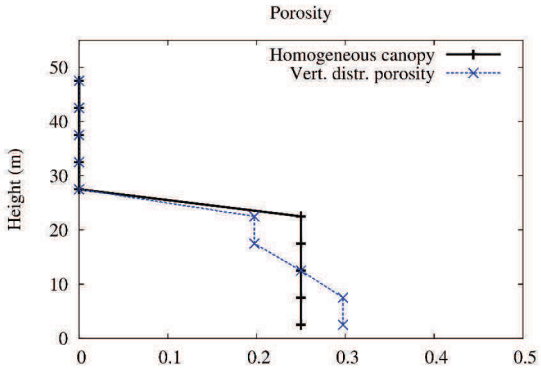

Fig. 4 Vertical distribution of occupied volume in the case of a homogeneous canopy and with a vertical distribution of the obstacles. Altitude is in metres.

- One simulation is done using a porosity terms in Eq. 31 equal to 1. The contribution of porosity terms is then calculated as the difference with the basecase and is noted $\hat{U}_{por}$.
- One simulation is done with removing the surface horizontal effects. The contribution of horizontal surfaces (denoted $\hat{U}_{FH}$) is the difference with the base case.
- A simulation is done with vertical fluxes equaled to zero. The contribution of the vertical flux from the vertical surfaces (denoted $\hat{U}_{FV}$) is calculated as the difference with the basecase.
- A simulation is done with a mixing length proportional to height. The difference with the base case is equal to the contribution the mixing length (denoted $\hat{U}_l$).
- The contribution of the interactions of each of these processes is noted $\hat{U}_{int}$.

A quantitative analysis of these effects can then be made using Eq. 45 (we take for example here the case of the wind speed):

$$U_{obs} = U_{noobs} + \hat{U}_{por} + \hat{U}_{FH} + \hat{U}_{FV} + \hat{U}_l + \hat{U}_{int} \tag{45}$$

where U_{obs} and U_{noobs} are the wind speed calculated in the presence of the obstacles and over a plane surface respectively. $\hat{U}_{int}$ can be computed as being the remaining contribution since all the other terms of the equation are known elements.

4.4 Vertical distribution of porosity

In order to analyze more in detail the effect of a vertical porosity (see Section 3.6.5), we compare simulations between two test cases: one with a regular array of cubes of 25 m high ($\phi = 0.75$) and the other one having a vertical distribution of obstacles as shown in Fig. 3 but with an average volume porosity over the whole column similar to that of the regular array (see Fig. 4). One can note however that the vertical forces are not conserved between the two tests. The difference between the two tests includes both a contribution of a change in the vertical mixing length and the vertical fluxes.

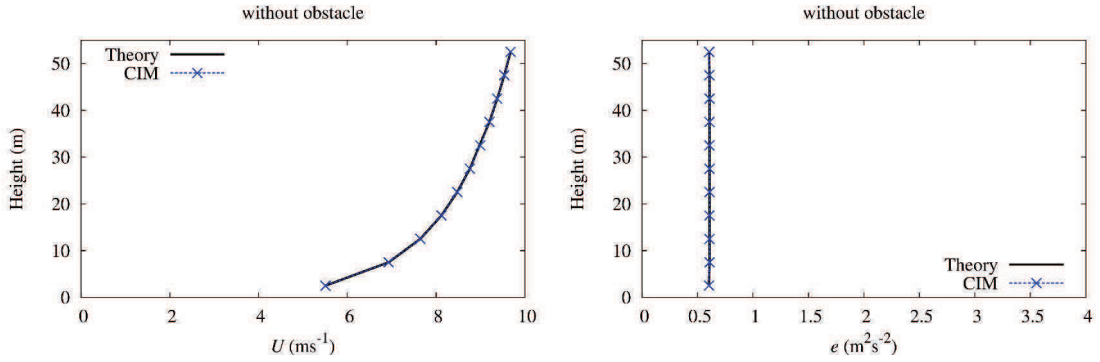

Fig. 5 Comparison of (a) the wind (in m s^{-1}) and (b) e (in m^2 s^{-2}) profiles computed using the analytical solution from the Prandtl surface-layer theory, CIM using formulation described in Section 3.4 and CIM using usual constants. Altitude is in metres.

5 Results in neutral atmospheric conditions

All following results were obtained in neutral atmospheric conditions. For this reason, it is chosen, in this particular context, not to show the potential temperature profiles (no interest in these conditions), but to present only the wind and e profiles.

5.1 Without obstacles

The first two set of calculations were performed considering a surface without any obstacles. Figure 5 shows the profiles obtained from these calculations: one set of profile is based on the Prandtl surface-layer theory, giving an analytical solution for the wind profile (Eq. 6) and a constant value for the e (Eq. 11); the other one is issued from a simulation with CIM.

A logarithmic wind profile and a constant e profile is obtained above the plane surface in both cases. It must be highlighted here that the wind and e profiles, that are obtained with the formulations we adopted in CIM, correspond exactly to what is expected from the theory.

5.2 With obstacles

In this section, CIM is compared with the results from a CFD experiment in presence of cubic obstacles (still in neutral conditions). CIM is then used to understand the impact of the porosity terms in the equations, the impact of the mechanical influence due the obstacles on the atmosphere through the friction of the air on horizontal (ground and building roofs) surfaces, the impact of the drag force due to the vertical surfaces and of the mixing length and the interactions of all processes using the separation methodology proposed by Stein and Alpert (1993).

5.2.1 Comparison with CFD: importance of a specific urban mixing length

Figure 6 shows the comparison between the CFD experiment (denoted "CFD") and CIM's simulation (denoted "CIM - modified l") for the wind and e profiles. Note that the CFD height was normalized and hence had to be multiplied by the height of our obstacles for a more appropriate comparison.

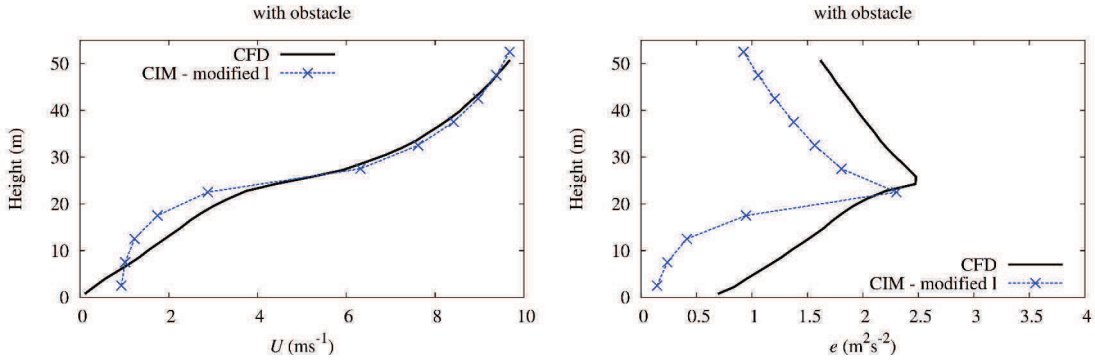

Fig. 6 Comparison of (a) the wind (in m s^{-1}) and (b) e (in m^2 s^{-2}) profiles obtained with obstacles from the CFD experiment and from CIM. Altitude is in metres.

It can be noted from Fig. 6 that the profiles calculated by CIM give a similar trends as compared to the profiles from the CFD. The differences in the wind profile between the CFD and CIM are less than 5%.

The decrease in e with altitude above the buildings top, that can be observed in both simulations, is due to the pressure gradient that was present in the CFD experiment. The presence of this pressure gradient hence modifies the expected constant e value which was expected above a plane surface or above the top of obstacles.

One can note however the differences in the e profile and more especially in the height at which the maximum e occurs. Santiago and Martilli (2010) also showed that they could not reproduce the height at which the maximum e occured. If the usual constants, as used by Santiago and Martilli (2010), were used in CIM to calculate the profiles (results not shown here), the differences between the CFD profiles and CIM profiles were more important. In order to explain and further understand these differences, a series of sensivity studies were developed (see Section 5.2.2).

5.2.2 Sensitivity tests to evaluate the impact of obstacles

Sensitivity tests are carried out to evaluate the contribution of several processes that determine the profile of the meteorological variables. Thus, four different scenarios were performed as explained in Section 4.3. The results are summarized in Figure 7.

Figure 7 shows that the vertical fluxes are the most important factors impacting the wind profile. They highly impact the wind speed and have a maximum effect at the top of the canopy. The new formulation of the mixing length also acts to reduce the wind speed but with less effects. Less influence is noted from porosity terms and even less from horizontal terms. When all these terms are considered together, these processes are mutually counterbalanced and hence reduce less wind speed than taken separately. One can note that the formulation of the mixing length in CIM tends to drastically reduce the e above the surface compared to the classical one based on a linear function of height but this effect is counterbalanced in the budgets since the mixing length is appearing in multiple equations (turbulent diffusion coefficients, dissipation and production of turbulent kinetic energy, etc). The differences observed when comparing the CIM with the CFD could also be due to porosity terms in the urban canopy and to mixing length formulation above (both of them having negative effects with could explain the CIM underestimating the e).

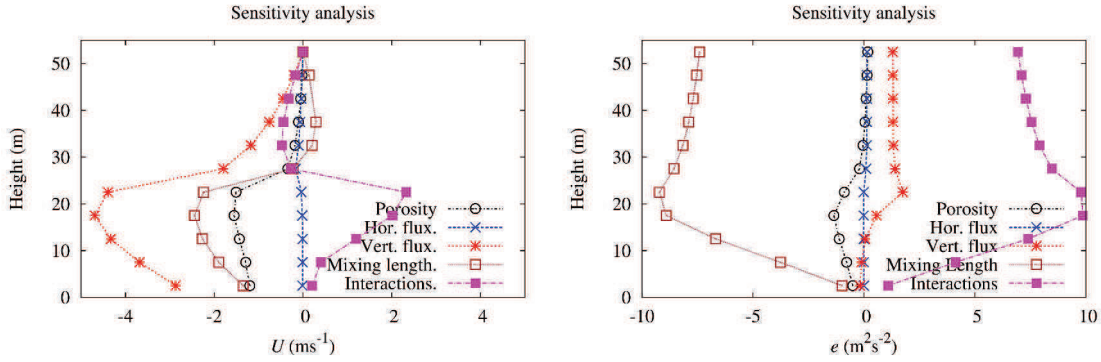

Fig. 7 Contributions of porosity terms (bullets), horizontal fluxes (crosses), vertical fluxes (stars), mixing length new formulation (empty squares) and their interactions (full squares) on wind (a) the wind (in m s^{-1}) and (b) e (in m^2 s^{-2}) profiles. Altitude is in metres.

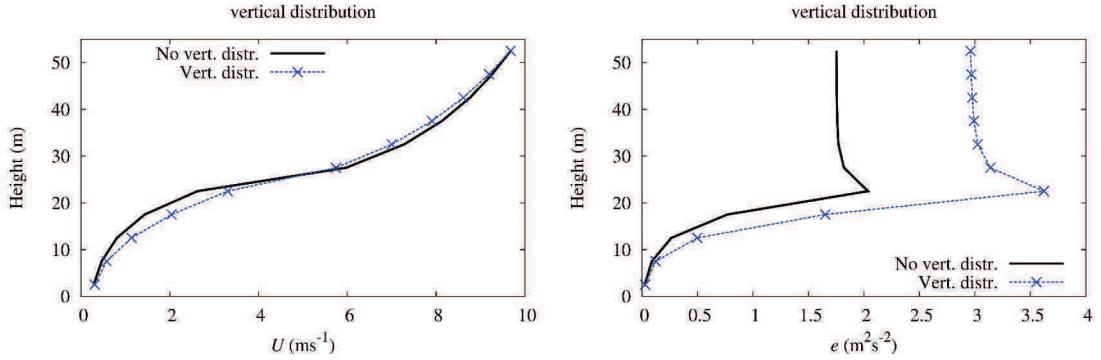

Fig. 8 Comparison of (a) the wind (in m s^{-1}) and (b) e (in m^2 s^{-2}) profiles computed with a vertical distribution of porosities (Vert. Distr) and with a regular array of cubes (No. vert. distr.). Altitude is in metres.

5.2.3 Extension of the mixing length to take into account the vertical distribution of porosity

This section is dedicated to analyse the effect of a non-homogenous vertical distribution of the porosity. Figure 8 shows the comparison between the wind and e vertical profiles obtained with a homogeneous and and a non-homogeneous vertical distribution of the porosity, keeping constant the average porosity for the whole column (see Figure 3). Note that the vertical fluxes are thus conserved in these two cases.

Figure 8 shows that the wind speed is slightly modified while e increases. It should be highlighted here that there is a strong increase in the e profile particularly near the top of the obstacles (40%).

6 Discussions and Conclusion

A canopy interface model was developed with a specific attention on the need to put previous theories in coherence and to prepare a 1D-column model that can be used as a coupling tool between mesoscale and microscale model. A new methodology was proposed for the calculation of the turbulent kinetic energy. It has been argued that in the canopy the most important parameter is the mixing length and that there is no need to use a different mixing length for the dissipation

term. It has been shown that there is a strong coherence between the formulation that has been adopted and what can be expected from the theory over a plane surface and in neutral conditions. Additionally, we proposed an original methodology for the numerical resolution of e in the CIM where a stationary value of e can be used to account for the presence of horizontal interfaces.

CIM was first run in neutral conditions over a plane surface and results were compared to the analytical solutions obtained using Prandtl surface-layer theory. The results were in very good agreement with what was expected. It was shown that over a plane surface a constant profile, corresponding to the stationary value of the e, is obtained. This shows that the mechanical production of turbulence and the diffusion processes are well represented in CIM. This also demonstrates that the hypothesis regarding the constants formulated in Section 3.4 are valid.

Results from CIM in a neutral case were then compared to results from a CFD experiment. The horizontal wind speed profile was in very good agreement with the experiment. Although the general trend for the turbulent kinetic energy corresponds to what is obtained from the CFD (increase in the canopy to a maximum at the top of the obstacle and a decreasing trend above), there are still discrepancies in the profile however. The e is under-estimated at the bottom of the domain (and more particularly near the ground) as well as above the obstacles. One of the reasons for this difference can also be due to wake production of e, for which no parametrization is included in CIM (Christen et al 2009). Further experiments are needed to understand the origin of these differences and how they can be addressed in models.

Sensitivity tests were built with CIM in order to analyze the effects of each of the factors influencing the meteorological variables on the wind and e profiles. It was seen that the mixing length as well as the various surface fluxes highly influence the determination of the wind and e profiles. More particularly, these separate tests have shown that the main momentum sinks inside the canyon are from the vertical surfaces. This can be explained from the formulation used to represent the horizontal and vertical forces respectively. This is in agreement with previous studies (Raupach 1992; Martilli et al 2002; Martilli and Santiago 2007; Hamdi and Masson 2008; Aumond et al 2013) stressing on the importance of the drag parametrization in urban canopy models but we presented here a quantitative evaluation of the impact of this drag force. This highlights the fact that future research need to concentrate on improving the parametrization of the impact of vertical surfaces.

Additionally, we also showed with these contributions, that the mixing length is also an important parameter. A new formulation for the mixing length was derived in order to account for the vertical distribution of obstacles. This new methodology was tested and the influence of this distributed mixing length was analysed on the calculation of the meteorological variables. Although we do not have any experimental measurement to confirm our findings, we showed that it was possible to extend the Santiago and Martilli (2010) mixing length to a more general formulation.

The use of CIM to calculate high-resolution profile inside a canopy, using mesoscale data as boundary condition, has been shown to be possible. This study was meant to demonstrate the capacity of CIM to compute and give appropriate result over a plane surface as well as when obstacles are present in neutral conditions. As Rotach (1995) stated, generally the roughness sub-layer is in near-neutral condition, we feel confident that CIM can be used very effectively to act as an interface between mesoscale and microscale model based on the results from this study. However, further improvements are needed to implement buoyancy effects in a modified version of CIM that would take into account different atmospheric stratification.

Acknowledgements The authors thanks ADEME, Region Alsace, REALISE, ZAEU for financial supports. This work was partially done in the framework of the ANR Trame Verte and the CCTV2 projects. We would like to thank José-Luis Santiago for providing the CFD data which was used in this paper and Alberto Martilli for the interesting discussions.

References

Abart B (1999) Modélisation de la turbulence en écoulement stratifiés pour la couche limite atmosphérique. PhD thesis. École Centrale de Nantes. 414 pp.

Ascher UM, Ruuth SJ, Spiteri RJ (1997) Implicit-explicit Runge-Kutta methods for time-dependent partial differential equations. Appl Numer Math 25:151-167. DOI http://dx.doi.org/10.1016/S0168-9274(97)00056-1, URL http://www.sciencedirect.com/science/article/pii/S0168927497000561, special Issue on Time Integration

Aumond P, Masson V, Lac C, et al (2013) Including the Drag Effects of Canopies: Real Case Large-Eddy Simulation Studies. Boundary-Layer Meteorol 146(1):65-80. DOI 10.1007/s10546-012-9758-x

Blackadar AK (1962) The vertical distribution of wind and turbulent exchange in a neutral atmosphere. J Geophys Res 67:3095-3102. DOI 10.1029/JZ067i008p03095, URL http://dx.doi.org/10.1029/JZ067i008p03095

Bornstein RD (1975) The two-dimensional URBMET urban boundary layer model. J Appl Meteorol 14:1459-1477.

Bougeault P, Lacarrère P (1989) Parameterization of Orography-Induced Turbulence in a Mesobeta-Scale Model. Mon Weather Rev 117:1872-1890.

Chen Y-S, Kim S-W (1987) Computation of turbulent flows using an extended k-epsilon turbulence closure model. NASA STIRecon Tech Rep N 88:11969.

Christen A, Rotach M, Vogt R (2009) The Budget of Turbulent Kinetic Energy in the Urban Roughness Sublayer. Boundary-Layer Meteorol 131:193-222. DOI 10.1007/s10546-009-9359-5

Clappier A, Perrochet P, Martilli A, et al (1996) A new non-hydrostatic mesoscale model using a CVFE (control volume finite element) Discretisation technique. Proc. EUROTRAC Symp. pp 527-531

Coceal O, Belcher SE (2004) A canopy model of mean winds through urban areas. Q J Roy Meteorol Soc 130:1349-1372. doi: 10.1256/qj.03.40 DOI 10.1256/qj.03.40

Craig Jr KJ (2002) MM5 Simulations of urban induced convective precipitation over Atlanta, GA. San Jose State University. 130 pp.

Delage Y (1974) A numerical study of the nocturnal atmospheric boundary layer. Q J Roy Meteorol Soc 100:351-364. DOI 10.1002/qj.49710042507

Delage Y, Taylor PA (1970) Numerical studies of heat island circulations. Boundary-Layer Meteorol 1:201-226. DOI 10.1007/BF00185740

Doms G, Schättler U (2002) A description of the nonhydrostatic regional model LM. Dtsch. Wetterd.

Foken T (2006) 50 Years of the Monin-Obukhov Similarity Theory. Boundary-Layer Meteorol 119:431-447. DOI 10.1007/s10546-006-9048-6

Foken T (2008) Micrometeorology. Springer. pp. 328

Hamdi R, Masson V (2008) Inclusion of a drag approach in the Town Energy Balance (TEB) scheme: Offline 1D evaluation in a street canyon. J Appl Meteorol Climatol 47:2627-2644.

Högström U (1996) Review of some basic characteristics of the atmospheric surface layer. Boundary-Layer Meteorol 78:215-246. DOI 10.1007/BF00120937

Kohler M, Mauree D, Blond N, Clappier A (2012) Development of a Canopy Model for a multiscale urban climate system. Proc. 8th Int. Conf. Urban Clim.

Krpo A (2009) Development and application of a numerical simulation system to evaluate the impact of anthropogenic heat fluxes on urban boundary layer climate. PhD thesis. École Polytechnique Fédérale de Lausanne, 233 pp.

Krpo A, Salamanca F, Martilli A, Clappier A (2010) On the Impact of Anthropogenic Heat Fluxes on the Urban Boundary Layer: A Two-Dimensional Numerical Study. Boundary-Layer Meteorol 136:105-127. DOI 10.1007/s10546-010-9491-2

Kusaka H, Kondo H, Kikegawa Y, Kimura F (2001) A Simple Single-Layer Urban Canopy Model For Atmospheric Models: Comparison With Multi-Layer And Slab Models. Boundary-Layer Meteorol 101:329-358. DOI 10.1023/A:1019207923078

Lemonsu A, Bastin S, Masson V, Drobinski P (2006) Vertical Structure of the Urban Boundary Layer over Marseille Under Sea-Breeze Conditions. Boundary-Layer Meteorol 118:477-501. DOI 10.1007/s10546-005-7772-y, URL http://dx.doi.org/10.1007/s10546-005-7772-y

Louis J-F (1979) A parametric model of vertical eddy fluxes in the atmosphere. Boundary-Layer Meteorol 17:187-202. DOI 10.1007/BF00119538

Louis J-F, Weill A, Vidal-Madjar D (1983) Dissipation length in stable layers. Boundary-Layer Meteorol 25:229-243 DOI 10.1007/BF00117978

Martilli A, Clappier A, Rotach MW (2002) An Urban Surface Exchange Parameterisation for Mesoscale Models. Boundary-Layer Meteorol 104:261-304. DOI 10.1023/A:1016099921195

Martilli A (2007) Current research and future challenges in urban mesoscale modelling. Int J Climatol 27:1909-1918. DOI 10.1002/joc.1620

Martilli A, Santiago J (2007) CFD simulation of airflow over a regular array of cubes. Part II: analysis of spatial average properties. Boundary-Layer Meteorol 122:635-654. DOI 10.1007/s10546-006-9124-y

Masson V (2000) A Physically-Based Scheme For The Urban Energy Budget In Atmospheric Models. Boundary-Layer Meteorol 94:357-397. DOI 10.1023/A:1002463829265

615 Mauree D (2014) Development of a multi-scale meteorological system to improve urban climate modeling. PhD
616 thesis. Université de Strasbourg, 184 pp.
617 Mestayer PG, Durand P, Augustin P, et al (2005) The urban boundary-layer field campaign in marseille (ubl/clu-
618 escompte): set-up and first results. Boundary-Layer Meteorol 114:315-365. DOI 10.1007/s10546-004-9241-4,
619 URL http://dx.doi.org/10.1007/s10546-004-9241-4
620 Monin AS, Obukhov AM (1954) Basic laws of turbulent mixing in the surface layer of the atmosphere. Contrib
621 Geophys Inst Acad Sci USSR 151:163-187.
622 Muller C (2007) Improvement of an urban turbulence parametrization for meteorological operational forecast and
623 air quality modeling. PhD thesis, École Polytechnique Fédérale de Lausanne, 208 pp.
624 Oke T (1987) Boundary layer Climates. Methuen and Co., Ltd., London. 435 pp.
625 Otte TL, Lacser A, Dupont S, Ching JK (2004) Implementation of an urban canopy parameterization in a
626 mesoscale meteorological model. J Appl Meteorol 43:1648-1665.
627 Prandtl L (1925) Report on investigation of developed turbulence. NACA Rep. TM-1231
628 Raupach MR (1992) Drag and drag partition on rough surfaces. Boundary-Layer Meteorol 60:375-395. DOI
629 10.1007/BF00155203
630 Raupach MR, Finnigan JJ, Brunei Y (1996) Coherent eddies and turbulence in vegetation canopies: The mixing-
631 layer analogy. Boundary-Layer Meteorol 78:351-382. DOI 10.1007/BF00120941
632 Rotach MW (1993) Turbulence close to a rough urban surface part I: Reynolds stress. Boundary-Layer Meteorol
633 65:1-28.DOI 10.1007/BF00708816
634 Rotach MW (1995) Profiles of turbulence statistics in and above an urban street canyon. Atmos Environ 29:1473
635 - 1486.
636 Rotach MW, Vogt R, Bernhofer C, et al (2005) BUBBLE - an Urban Boundary Layer Meteorology Project. Theor
637 Appl Climatol 81:231-261. DOI 10.1007/s00704-004-0117-9
638 Roth M (2000) Review of atmospheric turbulence over cities. Q J Roy Meteorol Soc 126:941-990. DOI 10.1002/
639 qj.49712656409
640 Santiago JL, Martilli A (2010) A Dynamic Urban Canopy Parameterization for Mesoscale Models Based on
641 Computational Fluid Dynamics Reynolds-Averaged Navier-Stokes Microscale Simulations. Boundary-Layer
642 Meteorol 137:417-439. DOI 10.1007/s10546-010-9538-4
643 Santiago J, Martilli A, Martín F (2007) CFD simulation of airflow over a regular array of cubes. Part I: Three-
644 dimensional simulation of the flow and validation with wind-tunnel measurements. Boundary-Layer Meteorol
645 122:609-634. DOI 10.1007/s10546-006-9123-z
646 Stein U, Alpert P (1993) Factor Separation in Numerical Simulations. J Atmospheric Sci 50:2107-2115. DOI
647 10.1175/1520-0469(1993)050⟨2107:FSINS⟩2.0.CO;2
648 Stull RB (1988) An Introduction to Boundary Layer Meteorology. Kuler Academic Publishers. 666 pp.
649 Therry G, Lacarrère P (1983) Improving the Eddy Kinetic Energy model for planetary boundary layer description.
650 Boundary-Layer Meteorol 25:63-88. DOI 10.1007/BF00122098
651 Watanabe T, Kondo J (1990) The influence of canopy structure and density upon the mixing length within and
652 above vegetation. J Meteorol Soc Jpn 68:227-235.
653 Zhang Y, Ma J, Cao Z (2008) The Von kármán constant retrieved from CASES-97 dataset using a variational
654 method. Atmos Chem Phys 8:7045-7053. DOI 10.5194/acp-8-7045-2008
655 Zilitinkevich S, Esau I (2007) Similarity theory and calculation of turbulent fluxes at the surface for
656 the stably stratified atmospheric boundary layer. Boundary-Layer Meteorol 125:193-205. DOI 10.1007/
657 s10546-007-9187-4

Chapter 7

Conclusion and perspectives

7.1 The background of the study

The climate change and the depletion of most of the affordable tanks of conventional fossil fuels in the next century challenge the contemporaneous societies in designing post-carbon society, and in achieving the energy transition towards low carbon energies. In France, buildings are a key point of the energy policies. They represent about 40% of the French final energy consumption in which residential buildings consume more than the two third (dedicated in particular for the space heating). In addition, buildings produce approximately 24% of the French greenhouse gases emissions.
In contrast, because the building design and defaults in the building construction can influence the building energy consumption for decades and since 56% of the French dwellings are built before 1975, the date of the adoption of the first thermal regulation, the buildings represent as well a high potential of energy savings and reductions of greenhouse gas emissions by improving solely the energy performance of the buildings. Since 2009 (law Grenelle 1) local authorities play a reinforced role in the energy policies designed to cope with the climate change impacts. For this, they require additional quantitative indices that could be integrated in most of the planning instruments, to assess the building energy performance, and assess the impacts of their planning and energy policies on the building energy patterns.

More, since the 1980's the rapid urbanization and the democratization of the automobile have trigger the spatial expansion of the urban areas out of their fringe in the farthest and farthest countryside. The sealing of vast arable lands, in particular for transportation infrastructures represents the equivalent of one district each 7 years and results in the fragmentation of the landscape, the alteration of the surface properties, and in turn the alteration of the local climate. The limitation of the residential urban development is by now managed by promoting urban densities, constructions in brownfields and hollow teeth, and urban greening policies that are also demonstrated to favor building energy savings for space heating by strengthening the urban heat island intensity [Owens, 1992]. The urban densities are also expected to lower the building energy use per capita and square meters by promoting multi-family housings. All those findings award an increasing role on local development policies in energy savings strategies. Nevertheless, in which extent the urban planning policies can influence the building energy requirements and the local climate? Which are the linkages between the urban form, the building energy requirement and the urban climate?

In the available methods that can be either surveys of the energy consumption of standard households, the analysis of the radiant energy emitted by the building envelops, or the analysis of the dwellings database, the dynamic of the meteorological conditions are often miss-evaluated. Those studies, indeed, consider standard climate to allow the comparison of the building energy demand patterns from one year to another, or use the unified degree-day method to characterize the thermal environment of the buildings. However, the air temperatures used to build the degree-days are often inherited from the fix meteorological observational network that monitor the synoptic weather conditions and circulations. Several studies, however, demonstrated that the negligence of the local warming or urban heat island, induced by the impervious built-up areas leads to over-estimate by up to +30% the building energy demand in urban areas. Indeed, the urban areas that experience slow nocturnal cooling rate can be warmer by up to +8°C compared to the moist surrounds at night under favorable conditions (*i.e.* anticyclone conditions, light wind).

In parallel and in the past decades, numerical mesoscale atmospheric models receive particular recognition in addressing urban environmental issues. The atmospheric mesoscale models that are initially used to provide throughout knowledge on the dynamic of the urban boundary layer, and the cross-scaled physical processes involved in the urban heat island effect, are since the 2000's enriched by sophisticated urban canopy parameterizations (UCPs) that model the 3-dimensional effects of simplified cubic building shape and uniform building complex on the energetic and dynamics of the airflow.
The UCPs reproduce the *i)* attenuation of the solar absorption in the urban canopy due to shading of the building facets; *ii)* the heat storage in the urban materials and their thermal inertia; *iii)* the multiple reflections of the longwave radiations emitted by the surfaces due to the presence of myriad of built-up facets in the urban canopy (*e.g.* street, walls, roofs); and at last *iv)* the alteration of the wind flow (*i.e.* wind speed reduction and turbulent exchanges) induced by the presence of obstacles. With increasing concerns on building energy issues, researchers developed in addition simplified building energy models that could be connected to the UCPs to assess the contribution of the anthropogenic heat emissions on the urban climate and the building energy requirements, considering in particular the effect of the urban heat island on the building energy requirements.
In particular, the building energy model computes the building skin temperatures and the indoor energy budget of a standard building that is represented like a box by accounting for *i)* the presence of windows; *ii)* the heat conduction through a layered wall

system; *iii)* the production of anthropogenic heat due to the use of the equipments and generated by human metabolism; *iv)* the unintentional natural ventilation; and *v)* the use of active air conditioning and heat pumps systems. The building energy models are then enabling to compute the building energy requirements for space heating or cooling for a determined thermal and humidity comfort range.
The all set of computing programs form as a whole, a climate modeling system that provide new opportunities to urban stakeholders to transfer the climate and energy knowledge in the urban planning and the energy policies at regional or local scale.

7.2 Objectives and adopted methodology

Taken in advantage those advances, this study questions the usefulness of such climate modeling system in helping urban planners to implement in the one hand energy saving strategies, and in the other hand, climate change mitigations and adaptation strategies (*e.g.* urban greenery, high-reflective surface, improvement of building energy performance through insulations, and so on). In particular, the capacities of such climate modeling systems to take into account the dynamic of the atmosphere, the urban heat island, and the dynamic of the urban development are addressed. The numerical approach is of particular interest since it permits to consider each of the physical processes involved in the urban climate separately. It also enables to consider all possible futures: urban development strategies, changes in the building stock properties.The second objective of this study is more thematic and questions the relationship that exist between the urban form, the building energy and the urban climate to stress on the importance of the urban planning in the building energy saving strategies.

To address those issues, we used in particular the proven American research WRF/ARW-BEP+BEM climate modeling system. The methodology consists in:

(1) Test the capacity of the climate modeling system to estimate the building energy requirements of a given area and period

We firstly carried out building energy and meteorological simulations across the Strasbourg-Kehl Urban Region (URSK), France and tested the sensitivity of the climate modeling system to the building parameters.The meteorological and the building energy simulations lasting from January 1^{st} 2010 up to the December 31^{st} 2010 (the reference

case). We designed four encapsulated domains centered on the Strasbourg agglomeration that are two-way nested to dynamically consider the influence of the urban areas on the atmosphere. The resolutions of the domains range from 45 km/ 9 km/ 3 km up to 1 km for the innermost domain (the URSK domain). We took advantage of the availability of the high-resolution regional land-use land-cover database provided by the regional cooperation CIGAL and the up-to-date building database provided by the INSEE institute. The latter covers the metropolitan area of Strasbourg. Both databases are used to accurately define the static physical conditions of the surface necessary to represent the various thermal environments across the URSK domains, and in particular the urban features.

(2) Test the capability of the WRF/ARW-BEP+BEM climate modeling system to account for the effect of realistic urban development strategies

We secondly explored the capability of the WRF/ARW-BEP+BEM climate modeling system to account for the effect of two realistic urban development strategies designed to cope with the negative impacts of the urban sprawl on the building energy requirements, and the urban climate. The urban development strategies consist in the conservation of the protected ecological habitats and the control of the urban development.
For this, we designed three contrasted urban development scenarios (*i.e.* spontaneous development, compact development and moderately compact development scenarios) that come into two scenario sub-sets that take into account or not the protection of the regional ecological network. We explicitly took into account the mechanisms behind the urban development by using the SLEUTH* cellular automata model of Doukari et al. [2013] for simulating the urban development at the time horizon of 2030. The urban planning policies are implemented in the SLEUTH* cellular automata model through developable land maps that constraint the urban development. The developable land maps of each scenario are built by using the Graphab and MorphoLim computing programs [Foltête et al., 2012, Tannier et al., 2011].
MorphoLim permits distinguishing the three contrasted urban types scenarios by delineating the built-up clusters across the urban region. The compact scenario corresponds to the densification of the existing built pattern in the core of the existing clusters. The moderately compact scenario corresponds to the reinforcement of the main urban centers by concentrating the development at their fringes. The spontaneous urban development scenario corresponds to the absence of control of the urban development except the one that is defined in the zoning of the local development plan.

The Graphab computing program is used to identify the ecological habitats that should be protected to ensure the ecological flow of a target species across the Strasbourg-Kehl urban region, here the red squirrel. We secondly used the simulated built-up maps of the scenarios for determining the static physical data of the WRF/ARW climate modeling system, and simulated the building energy requirements for each scenario.
At last the simulated built-up maps are used in the climate modeling system to provide the surface physical properties by 2030 of the new URSK domains and simulate the building energy requirements of each development scenarios.

(3) Develop a canopy interface model CIM to improve the representation of the surface in the climate modeling systems and account for the microclimate effects of the vegetation

One of the more important tasks of the land-use planning is to protect the natural resources. Since 2009 and the Grenelle 1 de l'environnement, the restoration and preservation of the green and blue ecological networks have been incorporated in the local development. They aim to facilitate the ecological flow across urbanized regions. In particular, trees (row of trees, urban forests) and green areas in general receive particular attention with the climate change and the harshening of the summer thermal conditions. In the ecological services provided by the vegetation, the provision of clean and fresh air (up to -2°C compared to the built-up surrounds) 100 m to 500m downwind to the green area is regularly mentioned to improve the urban environmental quality [Givoni, 1991, Nowak, 2006, Tyrväinen, 2001, Wilmers, 1991]. The cooling effects are mainly due to the evapotranspiration cooling and the reduction of the surface temperature of the sealed surfaces through the shade provided by the tree crown. Thus, the spatial topological information plays a key role in assessing the benefits of the trees on the building energy requirements. Several studies revealed that planting tree at the south and west sides of the buildings can save cooling energy (about 40%-30%) and heating energy (about 10%-20%) by providing shade for roofs and walls and by protecting, as well, the buildings from the prevailing wind [Heisler et al., 1986, Akbari and Taha, 1992, Simpson and McPherson, 1998, Sailor, 1998].
Nevertheless, in the urban canopy parameterizations, the vegetation present in an urban grid is often treated apart from the built-up areas through the tile approach. An urban grid is then composed by an urban and a non-urban fractions whatever the location of the two in the grid. The energy budget of each surfaces are computed separately assuming that the urban and non-urban surfaces do not interact before the first level of the atmospheric grid. There, the surface fluxes, the radiant energy, and the

skin temperatures of each surface are averaged with respect to their respective coverage in the mesoscale atmospheric grid. Although the tile approach is showed to yield reasonable results for the latent heat fluxes [Grimmond et al., 2011], the local wind shielding, shading and evapotranspiration cooling effects of the trees on the building thermal environment are miss-considered in mesoscale atmospheric models. This feature dramatically limits the usefulness of the climate modeling systems in assessing the ecological benefits of the vegetation in energy saving strategies.

To cope with this limits, we developed a canopy interface model (CIM) to improve the representation of the surface in the climate modeling systems by allowing the interfacing of the mesoscale atmospheric models with any existing sophisticated building energy model like EnergyPlus building of Birdsall et al. [1990] that considers the thermodynamic behavior of complex building geometries and wall systems through the use of Computer Assisted Designer interfaces that are often used by architects and engineers, or microclimate models that account for the spatial topology of the built-up elements and that explicitly consider the presence of tall vegetation in the urban fabrics like in the ENVI-met microscale model of Bruse and Fleer [1998].

The philosophy is that existing sophisticated microscale climate models that account for the thermodynamic effects of the vegetation and the topology of the various built and vegetation elements contained in the urban canopy layer, existing CFD models that resolve the whole scale of the turbulence spectrum contained in an airflow flowing across one or two complex building geometry, and existing sophisticated building energy models that account for the adaptive thermal comfort behavior of the building occupants and accurate indoor energy budget (urban dwellers in developed countries are showed to spend more than 70%-90% of their time indoors [Schweizer et al., 2007]) can better simulate the building energy requirements for space cooling and heating accounting than the usual urban canopy parameterizations.

The CIM canopy interface model resolves the vertical transport equation for momentum. It accounts for the airflow obstructions induced by complex obstacle morphology in larger atmospheric grids by considering surface and volume porosities.
Like in the urban canopy model of Kondo et al. [2005], the effect of the obstacles on the thermodynamic of the fluid are introduced in the transport equations trough the use of additional terms (*i.e.*the source terms). The surface and volume porosities are then introduced in the parameterization of the turbulent atmospheric fluxes and in the equations of the surface drag and friction forces.

By now, the CIM model considers parallelogram obstacles that can vary in size according to their width and length through along the obstacle height.
A sensitivity analysis, in which each terms of the vertical transportation equations for momentum are successively added, permited to highlight the contributions of each terms of the equation in the vertical wind speed profile.

7.3 The main results provided by this study

(1) Test the capacity of the climate modeling system to estimate the building energy requirements of a given area and period

We firstly highlighted that the WRF/ARW-BEP+BEM climate modeling system provides accurate meteorological conditions with regard to the 2 m near-surface temperatures and the 10 m wind fields recorded by the national meteorological institute Météo France at three meteorological stations included in the URSK domain. Nevertheless, the absence of a dense meteorological network in urban areas limits the significance of the validation of the simulated meteorological fields.

We secondly demonstrated that the WRF/ARW-BEP+BEM climate modeling system achieves to fairly estimate the building energy requirements over the study area. We focused on the building energy requirements for space heating of the administrative limit of the city council of Strasbourg (CUS) for which a previous analysis provided by the regional air quality association (ASPA) on the building energy consumption have been performed. The discrepancies between the annual estimations of the building energy consumptions provided by the regional air quality association (ASPA) and the WRF/ARW-BEP+BEM climate modeling system are equal to -23.55%. It sounds reasonable considering the approximations assumed by the climate modeling system and the large number of parameters and user inputs that have to be defined in the settings.

Thirdly, we showed that the climate modeling system is able to reproduce the non-linear building energy requirements-outdoor temperatures relationships observed and documented by Thom [1954], Valor et al. [2001] and Amato et al. [2005]. Those scholars, indeed, plotted the building energy consumptions provided by energy delivery census in function of the outdoor temperatures monitored at several meteorological

stations. They observed the non-linear building energy requirements-outdoor temperatures relationships and noticed that the relationship depict a winter branch and a summer branch linear trends. They, therefore, proposed to treat separately the winter branch and summer branch of the building energy requirements-outdoor temperatures relationships, and modeled the relationships by a statistical model consisting in the linearly fittings of the winter branch and summer branch separately. Doing so, they built a statistical model in which the slope of the linear fittings represents the sensitivity of the building energy requirements with the air temperatures, and in which the interception of the linear fittings with the air temperature axis provides the base temperatures, or the temperature at which the building energy requirements are no more climate sensitive.

Considering the simulations of the building energy requirements in the one hand and simulations of the outdoor air temperatures in the other hand provided by the climate modeling system, we also observed the non-linear building energy requirements-outdoor temperatures relationships and its linear decreasing trend with increasing simulated outdoor temperatures for wintertime. We therefore proposed to linearly fit the building energy requirements and outdoor temperature relationship to built the statistical model found by those previous studies, and quickly estimate for any periods the building energy requirements of a given area. Like in a degree day method, the simulated air temperatures and the base temperature of the statistical model can serve computing the degree-days of a given study area, meanwhile the sensitivity of the building energy requirements with the air temperature permits to find a correspondence between the degree-days and the building energy requirements for the space heating or cooling.
The discrepancies between the simulated and the estimated building energy requirements by using the WRF/ARW-BEP+BEM climate modeling system and the statistical model, respectively, are few (less than -5%).
More, the consideration of three appropriate months of the 2010 year (*i.e.*February, March and September) is demonstrated to be enough to estimate correctly the cold sensitivity and the base temperature found over the study area for the 2010 period, enabling to save computational time for the meteorological simulations.
Compared to the traditional degree-day method, the simulated statistical model enables to consider base temperatures and heating periods that are not defined a priori by convention but that are physically determined according to the building properties define in the user-settings and the meteorological conditions. More, it permits to consider the effect of the urban heat island on the building energy requirements.

At last, due to the physical significances of the base temperature and the sensitivity of the building energy requirements with the air temperature, those two statistical parameters can serve for defining new building energy performance indexes able to quickly assess energy saving strategies.
We tested their sensitivity by designing energy saving scenarios that consider successively *i)* the large adoption of reflective cool roofs; *ii)* the changes in the insulating properties; *iii)* the changes in the windows size, and *iv)* behavioral strategies that imply the management of the thermostat set point temperature. We intentionally neglected the urban greenery strategies. The local cooling effects induced by the trees due to shading, evaporation and transpiration are not yet accurately represented in the urban canopy parameterization implemented in the WRF/ARW-BEP+BEM climate modeling system. Doing this, we observed that the BEM model, included in the WRF/ARW-BEP+BEM climate modeling system is particularly sensitive to the building internal heat gains and thermal inertia. In particular, the changes in the insulation properties and the thermostat set point temperatures originate intense changes in both the simulated building energy requirements and base temperatures.
More, the sensitivity analysis of the building energy model with the settings parameters showed that the wasted heat generated by the equipments particularly modifies the building energy requirements. A fortiori the discrepancies of -23.55% in the estimations of the building energy requirements between this study and the ASPA study is revealed to be mainly due to differences in the base temperatures.

(2) Test the capability of the WRF/ARW-BEP+BEM climate modeling system to account for the effect of realistic urban development strategies

We observed that the simulations of the urban development result in three contrasted 2030 built-up patterns but that noticed that the ecological network policies have few impacts on the 2030 built-up patterns. This result is inherent to the study case, in which most of the ecological habitats identified by the Graphab computing programs are already in the protection zoning of the local development plan.
By performing a sensitive analysis of the land cover datasets with the dominant land cover approach adopted in the WRF/ARW-BEP+BEM climate modeling system. The dominant land cover approach consists in assigning an atmospheric grid to urban if the cumulative area of the built-up areas that are included in the atmospheric grid represents more than 20% of the atmospheric grid area. Doing so, we demonstrated that the use of the dominant land cover approach in the WRF/ARW-BEP+BEM climate modeling system fails to consider scattered built-up patterns when considering 1x1 km

mesoscale atmospheric grids.
We therefore simulated the effect of the compact and moderately compact built-up patterns on the urban climate and building energy requirements and compared the simulation outputs with the 2010 reference case.

We found that:

i) the simulated temperatures of the two scenarios are more sensitive to the large-scale weather system than the local climate and built-up fractions. Local warming of the air temperatures of about +0.7°C up to +1°C are only observed in atmospheric grids in which the land cover changes dramatically from natural to sealed surfaces. This result differs from the one of Lee et al. [2009], which reported significant increases in the air temperatures with increasing built-up fractions in particular for wintertime.

ii) the WRF/ARW-BEP+BEM climate modeling system is showed to fairly reproduce the seasonal and diurnal dynamic of the urban heat island revealing enhancing urban heat island in summer with increasing solar radiation forcings, and at night. Nevertheless, the average urban heat island intensities are weak (0.6°C in average). We considered the urban thermal conditions as the average temperature of all the urban grids and the rural thermal conditions as the average temperature of all the rural grids. Nevertheless, it seems that the urban heat island intensity suffers from a lack of standard. Oke [1987] and Stewart and Oke [2006] defined the urban heat island intensity as a temperature difference between the air within the urban canopy layer and the air in a rural reference area taken outside the urban settlement. Sailor [1998] defined the urban heat island intensity as the temperature difference between adjacent urban and rural regions. Cantat [2004] used a network of urban and rural meteorological stations that are considered to represent average urban and rural conditions respectively, to define the urban heat island intensity. Aguejdad et al. [2012] took the urban conditions as the horizontal temperature average of the atmospheric grids contained in a line of 5 km length centered at the city core and the rural conditions as the horizontal temperature average of the atmospheric grids contained in a line of 5 km width located 17 km upwind of the city center. By using the definition of Oke [1987] and considering the temperature of the atmospheric grid located at the Kléber square as the urban condition and the temperature of the atmospheric grid located at Entzheim airport as the rural conditions, we found an urban heat

island intensity of +1.97°C. It is therefore showed that the intensity of the urban heat island varies with respect to the definition of the urban and rural conditions: in the one hand the averaging procedure smooth the local variability of the urban heat island and in the other hand, the use of two single urban and rural stations questions the representativeness of the chosen stations in regard to the myriad of thermal environments present in the urban areas.

iii) no significant differences in the urban heat island intensity are showed between the scenarios. It seems that the urban development intensity and the location of the urban development have few impacts on the urban heat island intensities. This finding is confirmed by Atkinson [2003], which reported an increase in the temperature of solely +0.1°C when tripling the radius of the urban areas, Tokairin et al. [2010] that found a temperature increase of +0.6°C and +0.9°C in average when considering the extension of the Jakarta urban area between the 1970's and the 2000's. This result, are also in agreements with the finding of Sajjad [2013] that found an annual variation of the minimum and maximum urban temperatures with respect to increasing city radius scenario from 8 km, 12 km, 16 km and 20 km and in particular at night for a theoretical round city located at Faisalabad of 0.1314°C and 0.1090°C.
Like Hamdi and Schayes [2008] we concluded that the urban heat island intensity revealed small sensitivity to city size. Other urban parameters seem to be more significant in explaining the urban heat island intensity like the building density and design, or the anthropogenic heat produced by the human activities.

Finally, when exploring the building energy requirements of each built-up area development scenarios and built for each of them the statistical model, we found that at first glance the building energy requirements and the sensitivity of the buildings with the outdoor temperatures are the highest in the moderately compact scenarios and the lowest in the compact scenarios. Nevertheless, the compact and moderately compact simulated built-up patterns differ insofar as the compact urban development scenario is characterized by a smaller total built-up areas than the moderately compact scenario. By considering then, building energy intensities (*i.e.* the building energy requirement per floor area), we highlighted that the differences in the building energy requirements and the cold sensitivities between the development scenarios are mainly due to the differences in the building volume to be heated of each scenario. In the statistical parameters of the statistical model, the base temperature is showed to be less sensitive to the building volume. Spatially, the buildings are less sensitive to the cold temperatures

in the high dense urban core compared to the periphery of the main urban agglomeration in the compact and moderately compact scenarios demonstrating a dependence of the building thermal behavior of the envelop with the building design and density. The building design influence the amount of exposed facets of the building and the envelop on volume ratio. The building density influences the trapping of the thermal radiation in the street. Those findings have to be confirmed by other studies.

(3) Develop a canopy interface model CIM to improve the representation of the surface in the climate modeling systems and account for the microclimate effects of the vegetation

The preliminary results first indicate that the CIM model is able to reproduce the quasi-logarithmic vertical wind profile observed over plane areas. It is also able to reproduce the nearly logarithmic wind speed vertical profile found above the rooftop and the constant wind speed vertical profile observed in the urban canopy layer induced by the obstacle density. The sensitivity analysis, however, indicates that the wind speed vertical profile is not significantly impacted by the introduction of the surface and volume porosities in the atmospheric momentum turbulent fluxes. In contrast, the vertical wind speed profile is showed to be sensitive to the parameterization of the drag forces acting on the obstacle walls, and the parameterization of the mixing length parameterization included in the turbulent viscosity coefficient in the urban canopy layer.
Taken into consideration this advances, Mauree and Clappier [2014] continued to develop the CIM interface model for any atmospheric stability conditions. He implemented a k-ϵ turbulent closure to parameterize the turbulent surface fluxes, and therefore introduced a prognostic turbulent kinetic energy equation. He then found that the porosities have non-negligible effects on the vertical turbulent kinetic energy profile. In addition, he pointed out that the introduction of the porosities terms in the mixing length parameterization have significant incidence on the vertical wind profile of the urban canopy layer. This result is encouraging and further tests are then required to assess the effect of even more complex obstacle shape on the air thermodynamics.
At last, based on the work of Müller [2007] that found a sensitivity of the simulated vertical profile of the air temperature and wind speed with the vertical resolution of the vertical atmospheric grids, Mauree [2014] introduced the CIM interface model in the WRF/ARW-BEP+BEM climate modeling system. He showed that the coupling of the CIM interface model with the WRF/ARW-BEP+BEM climate modeling system slightly reduces the wind speeds in the canopy layer. It has, however, no incidence on

the vertical profile of the air temperatures.

7.4 Are the existing WRF/ARW climate modeling system suitable to provide urban planning guidelines?

The results of this study indicate that the climate-modeling systems like the WRF/ARW-BEP+BEM climate model system can achieve providing accurate estimates of the building energy requirements at macro-scale level and urban planning level (scale: 1:5,000 to 1:1,50 000) but not at the building lots or neighborhood. Their simulation outputs allow the construction of the well-documented building energy requirements-outdoor temperatures relationship that is suitable for a given area and that can serve for determining building energy performance indices. Despite this, some arguments limit their usefulness in urban climate operational studies.

First, the use of the climate modeling systems requires the basis knowledge in computing languages. It limits their direct applications by local practitioners that are regular costumer in GIS technics [Schwarz et al., 2012].

Second, few field campaigns in urban areas permit to validate the meteorological simulations provided by the climate modeling systems and improve their performance, in particular for wintertime. In Germany since the 1980's the penetration of the climate knowledge in the urban development strategies in regard to air quality and thermal comfort issues fosters the development of massive climate monitoring campaigns in most of the biggest and middle-sized urban areas of the country. Bochum, Essen, Stuttgart, Köln, and Muenchen are some of the study areas [Ren et al., 2011]. In the author knowledge, the meteorological field campaigns in urban areas are fewer in France and not as systematic. The energy and local climate preoccupations in France have recently penetrated the planning policies and instruments, and thus the permanent monitoring field campaign are scarce in urban areas. The fix meteorological network aims to measuring the synoptic circulation systems, and to such extent, the microclimates of the buildings and trees and the wasted heat due to human activities that are of interest in building energy or thermal comfort studies, are judged undesirables [**?**]. The inhomogeneity of the urban areas harsher the adoption of standard technic and increase the number of monitoring sites to depict the whole urban thermal environments of a given urban area. Nevertheless, several standardized methods have been developed

in the past to rationalize the number of stations and despite everything characterize the different thermal environments of the urban areas [Ellefsen, 1990/1, Stewart and Oke, 2006, Gill et al., 2008]. The standardization of the monitoring techniques seems promising in helping developing in the future vast urban meteorological network that can be used to validate the meteorological simulations provided by the atmospheric modeling systems.
Then, there is a clear trade-off between the level of information required in the climate modeling systems and the ease of use of the climate modeling systems. As climate modeling systems become more sophisticated, the amount of user inputs and the number of parameters that describe the average surface and building properties increase. Nevertheless, there are numerous sources of uncertainties in these parameters, and only few of them are revealed to be prevailing parameters in building energy simulations. In the parameters and user input, some can be directly obtained by treating aerial photography, airborne lidar or satellite images like the type of land cover, the height of the buildings, their orientations as well as the albedo of the urban materials. Others are more difficult to obtain and required time consuming treatments. For instance, the average building and street widths should be adapted to consider equivalent building walls surface and building volume that correspond to the complex building geometry. To such extent, Rasheed [2009] demonstrated that the form and length of the urban canyons have direct implications on the force drags acting on the urban canyon facets (*e.g.* street, wall and roof) and the distribution of the absorbed radiant energy. In this study, we also showed that the building envelop on volume can highly influence the building energy requirements and the thermodynamic behavior of the buildings with its surroundings. The peak heat emitted by the equipments that is defined for each urban type constitutes another user-input that contains numerous source of incertitude. It is, however, showed to be one of the prevailing parameters of the building energy model implemented in the WRF/ARW-BEP+BEM climate modeling system.

Other arguments are thematically relevant.
The horizontal resolution of the mesoscale atmospheric models used in climate modeling systems is taken large enough to consider isotropic surfaces and allow the simplification of the physical equations close to the surface. This implies the consideration of average physical properties, which significance can be questioned in regard to the transfer of climate knowledge in the urban planning. More, the planning strategies designed to cope with the rise of the local temperature (*e.g.* planting tree programs) and showed to reduce the building energy consumption are taken at the neighborhood and building lots level, for which the spatial topological informations and advection process are

crucial in determining the building surrounds and neighborhood climate conditions. At last, adaptation strategies are tied for existing situations [ONERC, 2003]. In the context of urban planning, one of the common postulates is that sprawled urban forms are the form the most land use consuming, the form the most energy use intensive mainly because sprawled built-up patterns are characterized by higher building energy use per capita compared to compact built-up patterns [Haines, 1986, Owens, 1992, Stone and Rodgers, 2001, INSEE, 2010], the form that enhance the most the greenhouse gases emissions due to the fossil fuel dependency of the journey-to-work car commuting, and the form of urban development that the most dramatically threaten the ecological diversity. It is, however and since the 1980's, the form of urban development that the urban stakeholders and local practitioners have to face every day. Nevertheless, in this study it has been showed that urban climate modeling systems like the WRF/ARW-BEP+BEM system cannot reproduce sprawled built-up patterns because the urban settlements are two small compared to the horizontal grid resolution of the mesoscale atmospheric model. So, how proposing high climatic future built-up patterns when local practitioners have not to date the capability to simulate appropriately the effect of the present sprawled built-up patterns on the urban climate and building energy requirements?

7.5 Which linkage between the urban form, the building energy requirements, and the urban climate?

The thematic objective of this study is the investigation of the interactions between urban form, urban climate, and energy taken under the focus of the building energy. Usually, the conceptual framework sketched in figure 7.1 is accepted.

The urban form is showed to influence the building energy consumption through three pathways.

1) The first pathway is inherent to the energy transmission and distribution losses. The repartitions of the population and the activities in the one hand and the localization of the energy production units in the other hand at national and regional levels influence the energy losses due to the transmission of the electricity from the source of

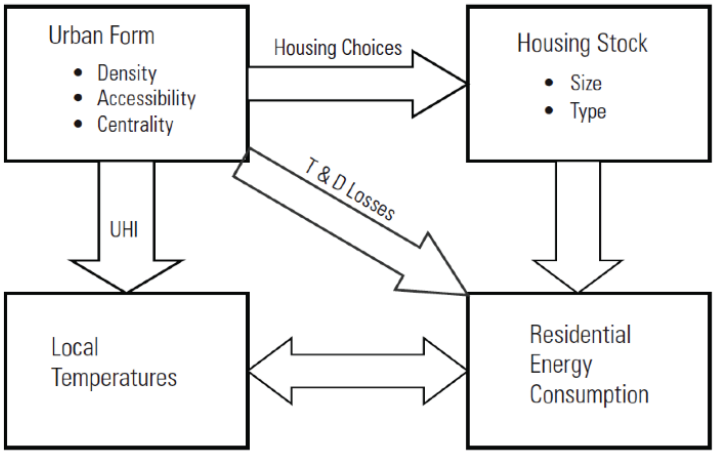

Figure 7.1: Casual paths often adopted between residential building energy consumption and urban form (From Ewing and Rong [2008])

the energy production to the source of energy consumption. The larger is the distance between these two sources, the more the amount of energy losses increases. More, the urban form is also expected to modify the type of fuel used in the cooling and heating systems. Compact urban forms are for instance expected to provide large opportunities to develop urban heating systems.

2) The second pathway is indirect and involves the housing stocks. Bigger houses require more energy than smaller houses because there are more surfaces to heat or cool than in smaller houses. Detached building houses require more energy since there is more exposed surface than in attached houses. The urban form influences the principle mode of transportation, employment and population distributions, but also the predominant housing structures. Haines [1986] associated the multinucleated built-up patterns with detached housings and multiple car ownerships. She associated the compact built-up patterns with multifamily housings and public services of transportations. Indeed the cost of the lands in high dense urban areas foresters the land developers to build compact form of buildings like multifamily and attached housings. Gusdorf et al. [2008] for instance used this postulate to constraint the urban development in the socio-economic urban expansion NEDUM model.

3) The third pathway, at last, is indirect and involves the urban climate and urban heat island effect. By changing the radiative, thermal and aerodynamic properties, sealed surfaces (*e.g.* pavements, parking lots, and buildings) contribute to warm the air up. Maximum differences between urban and rural temperatures are about 5-6°K to 6-8°K

in large cities on calm and clear night, and +1°C to +3°C at the annual scale according to Ketterer and Matzarakis [2014a]. In particular, Lee et al. [2009] highlighted that the warming of the air temperature is highly correlated to the fraction of built-up areas, and Ohashi et al. [2007] reported that the rise of +1°C of the daily maximum air temperature in Tokyo induces the rise of the electricity demand by +1.6 GW. Other studies of the late 1980's and 1990's pointed out that the building density promoted by the compact urban form can significantly reduce the energy consumption in winter by increasing the UHI intensity. Nevertheless, with the climate change most of the nowadays study investigate the effect of the UHI on the summer thermal comfort. To such extent, compact cities have been showed to accentuate the thermal discomfort in urban areas, especially in summer and at night by altering the capacity of rest of the urban dwellers [Matzarakis and Mayer, 1997]. This significant relationship between the urban air temperatures and the building energy requirements have put forward the urban planning in designing post carbon society and sustainable urban form.

In this study, the sealing of the surface originates few local warming in case of dramatically changes in the surface properties, but does not strengthen the urban heat island intensity whatever the considered built-up patterns. The changes in the building energy requirements between the simulated built-up patterns is showed to be only due to the amount of buildings and the volume of building to be heated. This result is surprising and limits the usefulness of climate modeling systems in such kind of experiences. Nevertheless, the horizontal resolution of the atmospheric grids can be too coarse compared to the changes in the land cover to "see" the climate feedback of the changes in the physical surface properties on the urban climate, and the air temperatures. This effect can also be due to the prevailing synoptic weather circulation in winter that can hide the local climate effects of the surface. More, the UHI intensity in winter is showed to be weak compared to summer as the solar radiations are low, the soil water capacity alters by the presence of solid precipitations, and the vegetation evapotranspiration function alter by the leaf-off period. Further experimentations have to be carried out to conclude on these points.

In this study, it is also showed that more than the urban form, the urban design and building form play prevailing roles in the building energy requirements. The building dynamical thermal behavior in case of cold temperatures is sensitive to the amount of exposed building facets to the airflow and building density. The basics geometry of the building and the building density then regulate the energy losses through the

building envelop and the multiple absorption of the thermal radiations emitted by the street-canyon surfaces at the building level. To such extent, the proportions of streets and the building heights that are controlled by the urban planning, influences the building density and its radiative effects [Strømann-Andersen and Sattrup, 2011]. It also influences the cold drainage in the core of the urban areas in case of flat terrain. In contrast, the architect and the developers are sought to regulate the building form, the thermal capacities of the building walls through the chosen materials and types of insulations, the amount of green area. Compared to urban planners, it seems that the land developers and the architects have direct and prevailing roles in the building energy requirements and that macroscale urban form have few impacts on the building energy requirements. Oke [1987], however, found a significant relationship between the populations considering as a proxy-index of the macroscale urban form with the intensity of the urban heat island. It can be here advocated that the population census can be more a proxy of the building density than a proxy of the size of the urban areas. We then recommend scaling down the scale of investigation at the neighborhood level by coupling mesoscale atmospheric models with resolved microscale climate models and building energy use models to analyze efficient building shapes and better represent the climate of the building neighborhood.

7.6 Perspectives

Simplifications of the climate modeling system have to be achieved for reducing the amount of parameters and user-inputs in the settings of the climate modeling systems, and permit the coupling of the mesoscale atmospheric model and CIM canopy interface model with any sophisticated building energy model, CFD models or microscale climate models. To such extent, further experimentations and sensitive analysis of the CIM interface model have to be performed before coupling it with microscale climate models to scale down the assessment of the building energy requirements at the building lots or neighborhood level.

Sensitivity and uncertainties analysis of the various parameters of the climate modeling system can help reducing the amount of user-setting parameters and save computing resource[Eisenhower et al., 2012].

Those efforts are of particular interest since most of the future investigations in applied urban climatology will belong to developing countries for which the geospatial surveys of the territories are recent [Matzarakis et al., 1998, Arnfield, 2003]. The parsimony of

the required informations in climate modeling systems becomes also even more crucial with the pursuit of the refinement of the grid cell resolutions in the recent applied urban climatology studies (*e.g.* 150 m, 250 m).
In the one hand, the smallest characteristic time scale of the panel of simulated physical processes governs the horizontal atmospheric grid resolution as well as the time steps adopted for the resolution of the physical processes. In the other hand, the anisotropy of the surface according to the chosen horizontal resolution influences the level of details of the surface that should be taken into account. The finest is the resolution, the more the surface are inhomogeneous, and the more the surface should be described in details. Describing the land cover by using the European Corine Land Cover for a resolution of 150 m is not the same as a resolution of 1 km. Thus, sensitivity analysis of the simulations provided by the climate modeling system with various horizontal atmospheric grid resolutions and surface static data when one is imposed fixed can help researchers to choose the optimal spatial resolutions.

In parallel, long-lasting field campaigns have to be encouraged in urban areas.In the field campaigns performed in France in the past decades, one inventories the ESCOMPTE field campaign in Marseille performed in summer 2001, the CAPITOUL field campaign in Toulouse that lasts one year between 2004 and 2005, and the RECLUS field campaign that hold in Strasbourg in summer 2002. As it can be showed the field campaigns last at best one year, but usually they focused on intensive summertime observational periods (IOP). The summer field campaigns permit to well appreciate the enhancing thermal stress induced by the urban heat island and the evaporative cooling induced by the trees and lawns. The urban heat island is indeed enhanced in summer with high solar forcings and enhanced evaporative cooling. Nevertheless, the absence of monitoring campaign in winter limits the investigation of the interactions between the urban climate and the building energy requirements in mid-latitude urban areas for which the space heating is the main end-uses in buildings. The validation of simulations provided by the climate modeling systems in winter season is particularly interesting as the hydrometeors (clouds and fogs) are particularly frequent at this period and because they are among the physical processes that are taken into account in the climate modeling systems maybe ones of the most challenging.

At last, the behavior of the urban dwellers has to be considered in the building energy study. Several building energy studies stressed the prevailing role of a-spatial variables

inherent to the lifestyle of the building occupants in the building energy requirements. Desjardin and Llorente [2009] for instance, stressed that the lifetime preferences can trigger differences in the energy consumption by factor 1-2 when analyzing the building energy consumption of two identical residential housings, which home equivalent socio-economic category of households. Other studies reported that the windows aperture can enlarged the thermal comfort sensation by +2°K to +4°K, depending whenever the arrival of fresh air is constant or temporary but frequent.
The rebound effect is a phenomenon of increasing building energy requirements with lower energy cost. This elasticity of the energy cost can be due to the improvement of the building thermal performance, the fluctuation of the cost of the fuel or to the changing in the household incomes. Whatever its cause, the elasticity of the energy consumption with respect to the cost of the energy provides much greater opportunities for households to tolerate lower temperature and making more effort to eliminate waste of energy [Owens, 1992, Crédoc, 2010].
To such extent, this study showed that the increase in the thermostat set point temperatures from 293°K to 294°K triggers changes in the building energy requirements equal to about +18%. More, Desjardin et al. [2011] carried out a sociological study on the energy behavior of interviewed French households. They noticed that the efforts to eliminate waste of energy are mainly done once, at the arrival of the households in their new houses, and rather implies the improvement of the energy efficiency of the wall insulations and windows systems. The household residential mobility that cause the urban areas to expand horizontally or vertically is then a key factor controlling the thermal efficiency of the buildings, and hence the building energy requirements.

At the scale of a day, the different thermal ambiance that have been crossed by the building occupants can play a significant role in the sensation of thermal comfort, and influence the thermostat set point temperatures. Studies like Ketterer and Matzarakis [2014b] focused on the characterization of the exposition of the human body to the thermal stress of various built-up thermal environments induced by the urban heat island intensity by using meteorological observations. Müller et al. [2014] investigated the changes in the PET indices considering the different land cover zones of Oberhausen, and changes in the vegetation type and covers using the ENVI-met microscale climate model. The postulate is that the sensation of comfort is mainly driven by the physiological regulation of the human body by thermo-regulatory mechanisms and circulation systems. As a consequence, this type of studies considers the energy budget of humans and its interactions with the surrounding thermal environments at a given time. Ketterer and Matzarakis [2014b] for instance used the Physiological Equiva-

lent Temperature (PET) of Höppe [1999]. It defines the equivalent air temperature at which, in standardized indoor settings (no winds, no solar radiations), and for a standardized person, the heat budget of the human body is balanced with the same core and skin temperatures as under the complex outdoor conditions to be assessed. It requires the definition of four environmental variables (*i.e.* the indoor temperature, the mean radiant temperature, the relative wind speed and the humidity) and two personal variables that are often difficult to obtain in practice: the activity level and the value of the clothing worn. Ranges of optimal thermal conditions are then defined to characterize the physiological stress on human being induced by the urban climate. Even more complex thermal comfort models like the one implemented in the building energy model EnergyPlus, account for the thermal history of the human beings through the use of a weighted air temperature that consists in the average of the air temperatures of the different thermal ambiances that have past cross by a group of individuals few hours before.

Because the location of the population and employments resources influences the daily commuting of the urban dwellers and the different thermal environments that are crossed in a day by individuals the transportation network and the net density (*i.e.* the density of the employments and population on a spatial unit) that are two discriminating factors of the urban form, play prevailing role in the thermal comfort of the urban dwellers. More the type of the building is showed to play a significant psychological influence on the thermal comfort of the urban dwellers. To such extent, Frontczak and Wargocki [2011] reported that people felt warmer at home and colder in their office, and that people in air-conditioned building are more sensitive to deviations in the thermal comfort. Thus, the consideration of sophisticated land use transport integrated (LUTI) models that simulate the residential and transport mobilities of the urban dwellers in the one hand, and the urban development in the other hand can help: *i*identifying the different thermal ambiances that are crossed by a group of individuals, *ii*help modeling the residential mobility and urban development. It therefore can provide the rate of renovation of the building insulations, the building properties and types, and give insight on the size of the newly constructed neighborhood's streets. The climate modeling systems can in parallel provide the different thermal ambiance that are cross by the individuals when coupling a mesoscale atmospheric model with the CIM canopy model, and a microscale climate model like EnviMet. From the system of urban climate models, it is then possible to calculate the PET indices of the different thermal ambiance crossed by the individuals or group of individuals. More, the climate modeling system can also provide the building energy requirements by coupling in addition to such climate modeling system, sophisticated building energy model like

EnergyPlus. Doing so, it seems therefore possible to investigate the link between the PET indices of a specific built-up areas characterized in terms of household category and building fabrics with the building energy demands.

In conclusion, the thermal comfort that is defined as the state of mind where a person expresses satisfaction with the thermal environment [ASHRAE, 2004] appears to be a central concept in the building energy studies. This concept directly links the lifestyle and activities of the individuals with their surrounding thermal environments and the heating or cooling building energy requirements. This concept also provides a new opportunities to study the interactions between the urban form, the building energy requirements and the urban climate: the various activities of the urban dwellers are mainly driven by spatial factors that influence the displacement of the urban dwellers like the distance of the home-to-work commuting, the mix of activities.

Bibliography

W. Abrahamse. A review of interventions studies aimed at household energy conservation. *Journal of environmental psychology*, 27:273–291, 2005. doi: 10.1016/j.jenvp.2005.08.002.

ADEME. Stratégie d?utilisation rationnelle de l'énergie : chapitre ii les bâtiments,. Technical report, 2005.

ADEME. Energie et climat - edition 2012. Technical report, 2012.

ADEUS. Les déplacements transfrontaliers des bas-rhinois. *Les notes de l'ADEUS*, Décembre 2011(60):4p, 2011.

ADEUS. Assurer une gestion économe de l'espace: Analyse des résultats de l'application du scoters. *The Journal of Bone & Joint Surgery*, (Mai 2012):44–53, 2012a.

ADEUS. Assurer une gestion économe de l'espace: Analyse des résultats de l'application du scoters. *Les notes de l'ADEUS*, Juin 2012(70):4p, 2012b.

ADEUS. La proximité, levier d'une organisation durable? *Les notes de l'ADEUS*, Juillet 2012(69):8p, 2012c.

ADEUS. Les évolutions récentes dans le bas rhin: des territoires plus spécialisés et plus interdépendants. *Les notes de l'ADEUS*, Décembre 2012(92):8p, 2012d.

ADEUS-AURM and DRE. Les déplacements transfrontaliers des bas-rhinois. page 82p, 2007.

Agreste. Les paysages agricoles dominent toujours le territoire français. *Agreste primeur*, Avril 2011(260):4p, 2011.

R. Aguejdad, J. Hidalgo, O. Doukari, V. Masson, T. Houet, and Météo-France CNRM. Assessing the influence of long-term urban growth scenarios on urban climate. *2012 International congress on environmental modeling and software managing ressources of a limited planet, proceedings*, 2012.

H. Akbari and H. Taha. The impact of trees and white surfaces on residential heating and cooling energy use in four canadian cities. *Energy*, 17:141–149, 1992.

H. Akbari, D. M. Kurn, S. E. Bretz, and J. W. Hanford. Peak power and cooling energy savings of shade trees. *Energy and buildings*, 25:139–148, 1997.

H. Akbari, S. Konopacki, and M. Pomerantz. Cooling energy savings potential of reflective roofs for residential and commercial buildings in the united states. *Energy*, 24(5):391–407, 1999.

H. Akbari, M. Pomerantz, and H. Taha. Cool surface and shade trees to reduce energy use and improve air quality in urban areas. *Solar energy*, 70:295–310, 2001.

E. Alexandri and P. Jones. Temperature decreases in an urban canyon due to green walls and green roofs in diverse climates. *Building and Environment*, 43(4):480–493, 2008.

L. Allen, F. Lindberg, and C.S.B. Grimmond. Global to city scale urban anthropogenic heat flux: Model and variability. *International Journal of Climatology*, 31(13):1990–2005, 2011.

A .D. Amato, M. Ruth, P. Kirshen, and J. Horwitz. Regional energy demand responses to climate change: Methodology and application to the commonwealth of massachusetts. *Climatic Change*, 71(1-2):175–201, 2005.

ANAH. Modélisation des performances énergétiques du parc de logements etat énergétique du parc en 2008. Technical report, 2008.

W. P. Anderson, P. S. Kanaroglou, and E.J. Miller. Urban form, energy and the environment: a review of issues, evidence and policy. *Urban studies*, 33(1):7 – 35, 1996. doi: 10.1080/00420989650012095.

E. L. Andreas, K. J. Claffey, R. E. Jordan, C. W. Fairall, P. S. Guest, P. Persson, and A. A. Grachev. Evaluations of the von kármán constant in the atmospheric surface layer. *Journal of Fluid Mechanics*, 559:117–149, 2006.

J.-P. Antoni and G. Vuidel. Mobisim: un modèle multi-agents et multi-scalaire pour simuler les mobilités urbaines. *Modéliser la ville. Forme urbaine et politiques de transport*, pages 50–77, 2010.

APUR. Analyse de la performance thermique des logements parisiens construits avant 1800. Technical report, 2011.

D. Arasteh, S. Selkowitz, J. Apte, and M. LaFrance. Zero energy windows. *Lawrence Berkeley National Laboratory*, 2006.

J. A. Arnfield. Two decades of urban climate research: a review of turbulence, exchanges of energy and water, and the urban heat island. *International Journal of Climatology*, 23(1):1–26, 2003. ISSN 1097-0088. doi: 10.1002/joc.859.

F. Asdrubali, C. Baldassarri, and V. Fthenakis. Life cycle analysis in the construction sector: Guiding the optimization of conventional italian buildings. *Energy and Buildings*, 64:73–89, 2013.

F. Asher. Metapolis ou l'avenir des villes. 1995.

ASHRAE Standard ASHRAE. Standard 90.1-2004, energy standard for buildings except low rise residential buildings. *American Society of Heating, Refrigerating and Air-Conditioning Engineers, Inc*, 2004.

"ASPA". Emissions de gaz à effet de serre et consommations d'énergie primaire sur les territoires de strasbourg et de la communauté urbaine de strasbourg. Technical report, 2006.

ASPA. Méthodologie de calcul des consommations d'énergie dans le secteur résidentiel-version v2012. Technical report, 2012.

N. Aste, A. Angelotti, and M. Buzzetti. The influence of the external walls thermal inertia on the energy performance of well insulated buildings. *Energy and Buildings*, 41(11):1181–1187, 2009.

B. W. Atkinson. Numerical modelling of urban heat-island intensity. *Boundary-Layer Meteorology*, 109(3):285–310, 2003.

J.-J. Baik and J.-J. Kim. A numerical study of flow and pollutant dispersion characteristics in urban street canyons. *Journal of Applied Meteorology*, 38:1576–1589, 2003.

J.-J. Baik, J.-J. Kim, and H. J.S. Fernando. A cfd model for simulating urban flow and dispersion. *Journal of Applied Meteorology*, 42(11):1636–1648, 2003.

A. Bailly and L. Bourdeau-Lepage. Concilier désir de nature et préservation de l'environnement: vers une urbanisation durable en france. *Géographie, économie, société*, 13(1):27–43, 2011.

A-B Barlag and W Kuttler. The significance of country breezes for urban planning. *Energy and Buildings*, 15(3):291–297, 1991.

M. Batty, Y. Xie, and Z. Sun. Modeling urban dynamics through gis-based cellular automata. *Computers, environment and urban systems*, 23(3):205–233, 1999.

W. Beckröge. Climate as a factor of a planning project?demonstrated by the example of dortmund bornstrasse. *Energy and Buildings*, 11(1):129–135, 1988.

P. Bergès, L.and Roche and C. Avon. Corridors écologiques et conservation de la biodiversité, intérêts et limites pour la mise en place de la trame verte et bleue. *Sciences Eaux & Territoires*, (3):34–39, 2010.

P. Bessy-Pietri. Les formes récentes de la croissance urbaine. *Économie et statistique*, 336(1):35–52, 2000.

M. J. Best. Representing urban areas within operational numerical weather prediction models. *Boundary-Layer Meteorology*, 114(1):91–109, 2005. ISSN 0006-8314. doi: 10.1007/s10546-004-4834-5.

M. J. Best, C. S. B. Grimmond, and M. G. Villani. Evaluation of the urban tile in moses using surface energy balance observations. *Boundary-Layer Meteorology*, 118 (3):503–525, 2006. ISSN 0006-8314. doi: 10.1007/s10546-005-9025-5.

B. Birdsall, W. F. Buhl, K.L. Ellington, A.E. Erdem, and F.C. Winkelmann. Overview of the doe-2 building energy analysis program, version 2. 1d. Technical report, Lawrence Berkeley Lab., CA (USA), 1990.

A. Bitan. The high climatic quality city of the future. *Atmospheric Environment. Part B. Urban Atmosphere*, 26(3):313 – 329, 1992. ISSN 0957-1272. doi: 10.1016/0957-1272(92)90007-F.

N. Blanc. *Vers une esthétique environnementale*. Editions Quae, 2008.

M. Bojic, F. Yik, and P. Sat. Influence of thermal insulation position in building envelope on the space cooling of high-rise residential buildings in hong kong. *Energy and Buildings*, 33(6):569–581, 2001.

M. Bonhomme. *Contribution á la géneralisation de bases de données multi-scalaires et évolutives pour une approche plurisdisciplinaire de l'énergie urbaine*. PhD thesis, Université de Toulouse, December 11st 2013.

M. Bonin. Les corridors, vecteurs d'aménagement durable de l'espace favorable à la protection des espèces. *Nature et sociétés*, 14(S67-S69):3p., 2006.

R. Bornstein and Q. Lin. Urban heat islands and summertime convective thunderstorms in atlanta: three case studies. *Atmospheric Environment*, 34(3):507–516, 2000.

R. D Bornstein. The two-dimensional urbmet urban boundary layer model. *Journal of Applied Meteorology*, 14(8):1459–1477, 1975.

P. Bougeault and P. Lacarrère. Parameterization of orography-induced turbulence in a mesobeta–scale model. *Monthly Weather Review*, 117(8):1872–1890, 1989.

J. Bouyer, C. Inard, and M. Musy. Microclimatic coupling as a solution to improve building energy simulation in an urban context. *Energy and Buildings*, 43(7):1549 – 1559, 2011. ISSN 0378-7788. doi: 10.1016/j.enbuild.2011.02.010.

E. Bozonnet, R. Belarbi, and F. Allard. Thermal behaviour of buildings: modelling the impact of urban heat island. *Journal of Harbin Institute of Technology*, 14(Sup.): 19–22, 2007.

R. Brännlund and T. J. Ghalwash. Increased energy efficiency and the rebound effect: effects on consumption and emissions. *Energy economicss*, 29:1–17, 2007.

R. E. Britter and S. R. Hanna. Flow and dispersion in urban areas. *Annual Review of Fluid Mechanics*, 35(1):469–496, 2003. doi: 10.1146/annurev.fluid.35.101101.161147.

M. Bruse and H. Fleer. Simulating surface-plant-air interactions inside urban environments with a three dimensional numerical model. *Environmental Modelling & Software*, 13(3-4):373 – 384, 1998. ISSN 1364-8152. doi: 10.1016/S1364-8152(98)00042-5.

M. M. Bryant. Urban landscape conservation and the role of ecological greenways at local and metropolitan scales. *Landscape and urban planning*, 76(1):23–44, 2006.

B. Bueno, G. Pigeon, L.K. Norford, and K. Zibouche. Development and evaluation of a building energy model integrated in the teb scheme. *Geoscientific Model Development Discussions*, 4(4):2973–3011, 2011. doi: 10.5194/gmdd-4-2973-2011.

A. J. Bunn, D. L. Urban, and T. H. Keitt. Landscape connectivity: a conservation application of graph theory. *Journal of Environmental management*, 59:265–278, 2000.

S. J. Burian et al. Urban morphological analysis for mesoscale meteorological and dispersion modeling applications: current issues. *5th AMS Urban Environment Conference, 23-26 August 2004, Vancouver BC*, 2004.

J. Businger, J. C. Wyngaard, Y. Izumi, and E.F. Bradley. Flux-profile relationships in the atmospheric surface layer. *Journal of the Atmospheric Sciences*, 28(2):181–189, 1971.

V. T. Ca, T. Asaeda, and Y. Ashie. Development of a numerical model for the evaluation of the urban thermal environment. *Journal of Wind Engineering and Industrial Aerodynamics*, 81(1/3):181 – 196, 1999. ISSN 0167-6105. doi: 10.1016/S0167-6105(99)00016-1.

O. Cantat. L'îlot de chaleur urbain parisien selon les types de temps. *Norois. Environnement, aménagement, société*, (191):75–102, 2004.

M. D. Cantwell and R.T.T. Forman. Landscape graphs: ecological modeling with graph theory to detect configurations common to diverse landscapes. *Landscape Ecology*, 8(4):239–255, 1993.

C. Cartalis, A. Synodinou, M. Proedrou, A. Tsangrassoulis, and M. Santamouris. Modifications in energy demand in urban areas as a result of climate changes: an assessment for the southeast mediterranean region. *Energy Conversion and Management*, 42(14):1647–1656, 2001.

B. Castéarn and L. Ricroch. Les logements en 2006 : le confort s'amliore, mais pas pour tous. *Cahier de l'INSEE-Juillet 2008*, (1202):4 p., 2008.

H .F. Castleton, V. Stovin, S. B. M. Beck, and J. B. Davison. Green roofs; building energy savings and the potential for retrofit. *Energy and Buildings*, 42(10):1582–1591, 2010.

CERTU. Protection des espèces et des habitats. *déecryptage Grenelle-Biodiversité*, (2):4 p., 2010.

CERTU/URB. Etude expérimentale : déetermination d'un mos et calcul d'une tache urbaine à partir de la bd topo de l'ign. *décryptage Grenelle-Biodiversité*, (dossier 33/06/34):70 p., 2008.

C. Chanard, M.-H. de Sède-Marceau, and M. Robert. Politique énergétique et facteur 4: instruments et outils de régulation à disposition des collectivités. *Développement durable et territoires. Économie, géographie, politique, droit, sociologie*, 2(1), 2011.

C.-R. Chang, M.-H. Li, and S.-D. Chang. A preliminary study on the local cool-island intensity of taipei city parks. *Landscape and Urban Planning*, 80(4):386–395, 2007.

E. Charmes, T. Souami, and Fondation Electricité de France. *Villes rêvées, villes durables?* Gallimard, 2009.

G. Chaudhuri and K. C. Clarke. The sleuth land use change model: A review. *International Journal of Environmental Resources Research*, 1(1):88–104, 2013.

F. Chen. The noah land surface model in wrf: a short tutorial. *LSM group meeting*, April 17, 2007.

F. Chen, H. Kusaka, R. Bornstein, J. Ching, C. S. B. Grimmond, S. Grossman-Clarke, T. Loridan, K. W. Manning, A. Martilli, S. Miao, D. Sailor, F. P. Salamanca, H. Taha, M. Tewari, X. Wang, A. A. Wyszogrodzki, and C. Zhang. The integrated wrf/urban modelling system: development, evaluation, and applications to urban environmental problems. *International Journal of Climatology*, 31(2):273–288, 2011. ISSN 1097-0088. doi: 10.1002/joc.2158.

J. Ching et al. National urban database and access portal tool, nudapt. *Bulletin of American meteorological society*, 90(7):1157–1168, 2011.

M. Christenson, H. Manz, and D. Gyalistras. Climate warming impact on degree-days and building energy demand in switzerland. *Energy Conversion and Management*, 47(6):671–686, 2006.

A. Clappier, P. Perrochet, A. Martilli, F. Muller, B. C. Krueger, et al. A new non-hydrostatic mesoscale model using a cvfe (control volume finite element) discretisation technique. In *Proceedings of EUROTRAC symposium*, volume 96, pages 527–531, 1996.

K. C. Clarke. A decade of cellular urban modeling with sleuth: Unresolved issues and problems. *Ch*, 3:47–60, 2008.

K. C. Clarke, G. Olsen, and J. A. Brass. Refining a cellular automaton model for wildfire propagation and extinction. *Proceedings of the Second International Conference on the Integration of geographic Information Systems and Environmental modeling, Breckenridge, CO.*, 1993.

C. G. Collier. The impact of urban areas on weather. *Quarterly journal of meteorological society*, 132, 2006a.

Commissariat général au développement durable. Etudes et documents: coûts et avantages des diffrentes formes urbaines : synthèse de la littérature économique. Technical Report 8, 2010.

C. Conner. The effect of exterior surface absorptivity and emissibity on energy use in residential buildings. *Unpublished report in Taha et. al 1988*, 1985.

D. B. Crawley, L. K. Lawrie, C. O. Pedersen, and F. C. Winkelmann. Energy plus: energy simulation program. *ASHRAE journal*, 42(4):49–56, 2000.

Crédoc. La température du logement ne dépend pas de la sensibilité écologique. Technical report, 2010.

CSTB. Méthode de calcul th-bce 2012. page 1377, 2012.

CUS. La cus en chiffre 2005: Strasbourg communauté urbaine en mouvement. Technical report, 2005.

CUS. Contribution à l'étude des performances énergétiques du parc de logements sur le territoire de la cus. Technical report, 2008.

CUS. Programme local de l'habitat: 4e plh de la cus: Potentiel de développement des communes. Technical report, 2009.

G. De Moor. Les théories de la turbulence dans la couche limite atmosphérique. *Direction de la météorologie*, 1983.

Delworth et al. Gfdl's cm2 global climate models. part i: formulation and simulation characteristics. *AMS Journal of climate-special section*, 19, 2003.

X. Desjardin and M. Llorente. Revue de la littérature scientifique sur le lien entre les formes d'organisation territoriale, les consommations énergétiques et les émissions de gaz à effet de serre. *Juin 2009 PUCA*, 2009.

X. Desjardin, L. Mettetal, L. Firdion, M. Peretti Ndiaye, R. Trehin Lalanne, and F. Beaucire. L'habiter périurbain face à l'enjeu énergétique. *Flux*, (89–90):46–57, 2011.

C. Dietzel and K. C. Clarke. Toward optimal calibration of the sleuth land use change model. *Transactions in GIS*, 11(1):29–45, 2007.

A. Dimoudi and M. Nikolopoulou. Vegetation in the urban environment: microclimatic analysis and benefits. *Energy and buildings*, 35(1):69–76, 2003.

O. Doukari, R. , and T. Houet. Sleuth*: a scenario-based version of sleuth for simulating breaking trends urban sprawl futures. *Comput. Environ. Urban Syst.(submitted)*, 2013.

DRE. Etude méthodologique: suivi de l'évolution des taches urbaines. *Réunion du groupe géomatique et connaissance des territoires*, 14 octobre 2008-CETE de l'Ouest, 2008.

J. Dudhia. Numerical study of convection observed during the winter monsoon experiment using a mesoscale two dimensional model. *Journal of Atmospheric science*, 46: 3077–3107, 1989.

S. Dujardin, A.-F. Marique, and J. Teller. Spatial planning as a driver of change in mobility and residential energy consumption. *Energy and Buildings*, 68:779–785, 2014.

S. Dupont, T. L Otte, and J. K. S. Ching. Simulation of meteorological fields within and above urban and rural canopies with a mesoscale model. *Boundary-Layer Meteorology*, 113(1):111–158, 2004.

B. Eisenhower, Z. O'Neill, V. A. Fonoberov, and I. Mezić. Uncertainty and sensitivity decomposition of building energy models. *Journal of Building Performance Simulation*, 5(3):171–184, 2012.

R Ellefsen. Mapping and measuring buildings in the urban canopy boundary layer in ten us cities. *Energy and Buildings*, 15-16:1025–1049, 1990/1.

Environmental Modelling Centre. The gfs atmospheric model, ncep office note 442, global climate and weather modelling branch. *Camp Springs, Maryland*, 2003.

EPA. http://energy.gov/energysaver/articles/cool-roofs. 2013.

R.L.H. Essery, Betts R.A. Best, M.J and, and P.M. Cox. Explicit representation of subgrid heterogeneity in gcm land surface scheme. *Journal of Hydrometeorology*, 4, 2003.

R. Ewing and F. Rong. The impact of urban form on u.s. residential energy use. *Housing Policy Debate*, 19(1):1–30, 2008. doi: 10.1080/10511482.2008.9521624.

L. Fischer. Etude de paramètres climatiques pertinents en vue de l'amélioration de la prébision des pointes de pollution par l'ozone dans l'agglomération de strasbourg. *Thèse de doctorat de l'Université Louis Paster*, 2001.

L. Fischer. Phénomènes radiatifs et îlot de chaleur urbain dans l'agglomération de strasbourg. *Revue Géographique de l'Est*, 45(2):99–112, 2005.

FLIR services. Guide de l'imagerie thermique pour les applications du bâtiment et des énergies renouvelables. page 68 p., 2011.

T. Foken. 50 years of the moninobukhov similarity theory. *Boundary-Layer Meteorology*, 119(3):431–447, 2006. ISSN 0006-8314. doi: 10.1007/s10546-006-9048-6.

J.-C. Foltête, C. Clauzel, and G. Vuidel. A software tool dedicated to the modelling of landscape networks. *Environmental Modelling & Software*, 38:316–327, 2012.

R. T. T. Forman. *Land mosaics: the ecology of landscapes and regions*. Cambridge University Press, 1995.

M. Franchomme, M. Bonnin, and C. Hinnewinkel. La biodiversité aménage-t-elle les territoires? vers une écologisation des territoires. *Déeveloppement durable et territoires. Économie, géographie, politique, droit, sociologie*, 4(1), 2013.

W. H. Frey and Z. Zimmer. Chapter: Defining the city. pages 14–25, 2001.

M. A. Friedl, D. K. McIver, J. C. F. Hodges, X. Y. Zhang, D. Muchoney, A. H. Strahler, C. E. Woodcock, S. Gopal, A. Schneider, A. Cooper, et al. Global land cover mapping from modis: algorithms and early results. *Remote Sensing of Environment*, 83(1): 287–302, 2002.

M. Frontczak and P. Wargocki. Literature survey on how different factors influence human comfort in indoor environments. *Building and Environment*, 46(4):922–937, 2011.

G. Galster, R. Hanson, M.R. Ratcliffe, H. Wolman, S. Coleman, and J. Freihage. Wrestling sprawl to the ground: defining and measuring an elusive concept. *House Policy Debate*, 12:12 p., 2001.

M. Garcia-Diez, J. Fernandez, L. Fita, and C. Yagüue. Seasonal dependence of wrf model biases and sensitivity to pbl schemes over europe. *Quarterly Journal of the Royal Meteorological Society*, 139:501–514, 2013.

K. J. Gaston and R. A. Fuller. The size of species? geographic ranges. *Journal of applied ecology*, 46:1–9, 2008.

N. Gazulis and K. C. Clarke. Exploring the dna of our regions : Classification of outputs from the sleuth model. *in EL Yacoubi, S., Chapard, B., and Bandini, S. (Eds.) Cellular automata, 7th International confrence on cellular automata for research and industry, ACRI 2006, Perpignan, France, September 2006. Proceedings. Lecture Notes in computer science*, 2006.

C. Giannakopoulos and B. E. Psiloglou. Trends in energy load demand for athens, greece: weather and non-weather related factors. *Climate research*, 31(1):97, 2006.

T. M. Giannaros, D. Melas, I. A. Daglis, I. Keramitsoglou, and K. Kourtidis. Numerical study of the urban heat island over athens (greece) with the {WRF} model. *Atmospheric Environment*, 73(0):103 – 111, 2013. ISSN 1352-2310. doi: 10.1016/j.atmosenv.2013.02.055.

S.E. Gill, J. F. Handley, A. R. Ennos, S. Pauleit, N. Theuray, and S. J Lindley. Characterising the urban environment of uk cities and towns: A template for landscape planning. *Landscape and Urban Planning*, 87(3):210–222, 2008.

L. Giovannini. *Urban scale phenomena and boundary layer processes in mountain valleys*. PhD thesis, University of Trento, 2012.

B. Givoni. Impact of planted areas on urban environmental quality: a review. *Atmospheric Environment. Part B. Urban Atmosphere*, 25(3):289–299, 1991.

Le Gleau, D. Pumain, T. Saint-Julien, et al. Villes d'europe: à chaque pays sa définition. *Economie et statistique*, 294(1):9–23, 1996.

Global-Chance. Les secteurs résidentiel et tertiaire. Technical Report Janvier 2010, 2010.

L. Godet. La "nature ordinaire" dans le monde occidental. *l'Espace Géographique*, 4: 295–308, 2010.

S. Godinot. Les plans climat énergie territoriaux: voies d'appropriation du facteur 4 par les collectivités et les acteurs locaux? *Développement durable et territoires. Économie, géographie, politique, droit, sociologie*, 2(1), 2011.

C. Gordon, C. Cooper, C. A. Senior, H. Banks, J. M. Gregory, T. C. Johns, J. F. B. Mitchell, and R. A. Wood. The simulation of sst, sea ice extents and ocean heat transports in a version of the hadley centre coupled model without flux adjustments. *Climate Dynamics*, 16:147–168, 2000.

L. A. Greening, D. L. Greene, and C. Difiglio. Energy efficiency and consumption- the rebound effect-a survey. *Energy policy*, 28:389–401, 2000.

G. A. Grell, J. Dudhia, D. R. Stauffer, et al. A description of the fifth-generation penn state/ncar mesoscale model (mm5). 1994.

C. S. B. Grimmond. Aerodynamic roughness of urban areas derived from wind observations. *Boundary-Layer Meteorology*, 89(1):1–24, 1998.

C. S. B. Grimmond and T. R. Oke. Aerodynamic properties of urban areas derived from analysis of surface form. *Journal of applied meteorology*, 38(9):1262–1292, 1999a.

C. S. B. Grimmond and T.R. Oke. Evaporation rates in urban areas, impacts of urban growth on surface water and groundwater quality. volume 259, pages 235–243, 1999b.

C. S. B. Grimmond, M. Blackett, M. J. Best, J. Barlow, J. J. Baik, S. E. Belcher, S. I. Bohnenstengel, I. Calmet, F. Chen, A. Dandou, et al. The international urban energy balance models comparison project: first results from phase 1. *Journal of Applied Meteorology and Climatology*, 49(6):1268–1292, 2010.

C.S.B. Grimmond, M. Blackett, M. J. Best, J.-J. Baik, S. E. Belcher, J. Beringer, S. I. Bohnenstengel, I. Calmet, F. Chen, A. Coutts, A. Dandou, K. Fortuniak, M. L. Gouvea, R. Hamdi, M. Hendry, M. Kanda, T. Kawai, Y. Kawamoto, H. Kondo, E. S. Krayenhoff, S.-H. Lee, T. Loridan, A. Martilli, V. Masson, S. Miao, K. Oleson, R. Ooka, G. Pigeon, A. Porson, Y.-H. Ryu, F. Salamanca, G.J. Steeneveld, M. Tombrou, J. A. Voogt, D. T. Young, and N. Zhang. Initial results from phase 2 of the international urban energy balance model comparison. *International Journal of Climatology*, 31(2):244–272, 2011. ISSN 1097-0088. doi: 10.1002/joc.2227.

S. Grossiord. Modélisation de l?impact des bâtiments sur le climat urbain. *Stage de master professionnel 1 en Ingnierie Environnementale*, Master Gosciences, Environnement et Risques , Universit de Strasbourg, 2009.

F. Gusdorf, S. Hallegatte, and A. Lahellec. Time and space matter: how urban transitions create inequality. *Global Environmental Change*, 18(4):708–719, 2008.

S. Guy. Consumption, energy and environment. *Encyclopedia of energy*, 1:687–695, 2004.

V. A. Haines. Energy and urban form: A human ecological critique. *Urban Affairs Review*, 21:337–353, 1986. doi: 10.1177/004208168602100304.

M. L. Hall, P. W. W. Lurz, M. D. F. Shirley, S. Rushton, R .M. Fuller, and K. Wolff. Impact of landscape management on the genetic structure of red squirrel populations. *Science*, 293/5538:2246–2248, 2001.

R Hamdi and V. Masson. Inclusion of a drag approach in the town energy balance (teb) scheme: Offline 1d evaluation in a street canyon. *Journal of Applied Meteorology and Climatology*, 47(10):2627–2644, 2008.

R. Hamdi and G. Schayes. Sensitivity study of the urban heat island intensity to urban characteristics. *International Journal of Climatology*, 28(7):973–982, 2008. ISSN 1097-0088. doi: 10.1002/joc.1598.

G. M. Heisler et al. Energy savings with trees. *Journal of arboriculture*, 12(5):113–125, 1986.

H. Herring and R. Roy. Technological innovation, energy efficient design and the rebound effect. *Technovation*, 27(4):194–203, 2007.

K. M. Hinkel, F. E. Nelson, A. Klene, and J. H. Bell. The urban heat island in winter at barrow (canada). *Journal of arboriculture*, 23:1889–1905, 2003.

K. M. Hinkel, F.E. Nelson, A. Klene, and J.H. Bell. Tevaluation of the impact of the urba heat island on residential and commercial energy consumption in tokyo. *Energy*, 37:371–383, 2012.

M. Hoel and S. Kverndokk. Depletion of fossil fuels and the impacts of global warming. *Resource and energy economics*, 18(2):115–136, 1996.

U. Högström. Analysis of turbulence structure in the surface layer with a modified similarity formulation for near neutral conditions. *Journal of the atmospheric sciences*, 47(16):1949–1972, 1990.

U. Högström. Review of some basic characteristics of the atmospheric surface layer. *Boundary-Layer Meteorology*, 78(3-4):215–246, 1996. ISSN 0006-8314. doi: 10.1007/BF00120937.

U. Högström, H. Bergström, and H. Alexandersson. Turbulence characteristics in a near neutrally stratified urban atmosphere. *Boundary-Layer Meteorology*, 23(4):449–472, 1982. ISSN 0006-8314. doi: 10.1007/BF00116272.

E. Holden and I.T. Norland. Three challenges for the compact city as a sustainable urban form: household consumption of energy and transport in eight residential areas in the greater oslo region. *Urban studies*, 42(12):2145–2166, 2005.

P. Höppe. The physiological equivalent temperature–a universal index for the biometeorological assessment of the thermal environment. *International Journal of Biometeorology*, 43(2):71–75, 1999.

Houdin et al. The lmdz4 general circulation model: climate performance and sensitivity to parametrized physics with emphasis on tropical convection. *Climate dynamic*, 27: 787–813, 2006.

Y. J. Huang, H. Akbari, H. Taha, and A. H. Rosenfeld. The potential of vegetation in reducing summer cooling loads in residential buildings. *American meteorological society*, pages 1103–1116, 1987.

A. Hunt and P. Watkiss. Climate change impacts and adaptation in cities: a review of the literature. *Climatic Change*, 104(1):13–49, 2011.

IAU. Les îlots de chaleur urbains: l?adaptation de la ville aux chaleurs urbaines. Technical report, 2010.

IAURIF. Contraintes énergétiques et mutations urbaines. Technical report, 2008.

T. Ichinose, K. Shimodozono, and K. Hanaki. Impact of anthropogenic heat on urban climate in tokyo. *Atmospheric Environment*, 33(24):3897–3909, 1999.

IEA. World energy outlook. Technical report, 2008.

IEA. World energy outlook: Executive summary. Technical report, 2012.

IEA. Key world energy statistics. Technical report, 2013.

R. Ikeda and H. Kusaka. Proposing the simplification of the multilayer urban canopy model: Intercomparison study of four models. *Journal of Applied Meteorology and Climatology*, 49(5):902–919, 2010.

T.R. Oke in World Metorological Organization. Initial guidance to obtain representative meteorlogical observations at urban sites. Technical Report WMO/TD-No. 1250, 2006.

INSEE. Aire urbaine de strasbourg : une population qui augmente. Technical Report 42, 2007.

INSEE. La facture énergétique des ménages serait 10% plus faible sans l'étalement urbain des 20 dernières années. Technical report, 2010.

INSEE. Le découpage en unités urbaines de 2010: l'espace urbain augmente de 19% en une décennie. Technical Report 1364, 2011.

INSEE. Logement : la construction moins dynamique que prévu. Technical Report 20, 2013.

INSEE and ADEUS. La cus dans la dynamique des migrations résidentielles. Technical Report 29, 2012.

IPCC. *Fourth Assessment Report: Climate Change 2007: The Physical Science Basis. Contribution of Working Group I to the Fourth Assessment Report of the Intergovernmental Panel on Climate Change*. Geneva: Intergovernmental Panel on Climate Change, 2007.

M. Z. Jacobson. *Fundamentals of atmospheric modeling*. Cambridge University Press, 1999.

C.A. Jantz, S.J. Goetz, and M.K. Shelley. Using the sleuth urban growth model to simulate the impacts of future policy scenarios on urban land use in the baltimore-washington metropolitan area. *Environmental planning B: Planning and Design 2003*, 30:251–271, 2004.

P. Jones, J. Patterson, and S. Lannon. Modelling the built environment at an urban scale?energy and health impacts in relation to housing. *Landscape and Urban Planning*, 83(1):39–49, 2007.

P. Kastendeuch, P. Lacarrere, G. Najjar, J. Noilhan, F. Gassmann, and P. Paul. Mesoscale simulations of thermodynamic fluxes over complex terrain. *International journal of climatology*, 20(10):1249–1264, 2000.

C. Ketterer and A. Matzarakis. Comparison of different methods for the assessment of the urban heat island in stuttgart, germany. *International journal of biometeorology*, pages 1–11, 2014a.

C. Ketterer and A. Matzarakis. Human-biometeorological assessment of the urban heat island in a city with complex topography–the case of stuttgart, germany. *Urban Climate*, 10:573–584, 2014b.

Y. Kikegawa, Y. Genchi, H. Yoshikado, and H. Kondo. Development of a numerical simulation system toward comprehensive assessments of urban warming countermeasures including their impacts upon the urban buildings' energy-demands. *Applied Energy*, 76(4):449 – 466, 2003. ISSN 0306-2619. doi: 10.1016/S0306-2619(03)00009-6.

P. Kindelmann et al. When is landscape matrix important for determining animal fluxes between resource patches? *Ecological complexity*, 2:150–158, 2005.

M. Kohler, D. Mauree, N. Blond, and A. Clappier. Development of a canopy model for a multiscale urban climate system. In *Proceedings of the 8th International Conference on Urban Climate*, 2012.

H. Kondo, Y. Genchi, Y. Kikegawa, Y. Ohashi, H. Yoshikado, and H. Komiyama. Development of a multi-layer urban canopy model for the analysis of energy consumption in a big city: Structure of the urban canopy model and its basic performance. *Boundary-Layer Meteorology*, 116(3):395–421, 2005. ISSN 0006-8314. doi: 10.1007/s10546-005-0905-5.

E. Kossecka and J. Kosny. Influence of insulation configuration on heating and cooling loads in a continuously used building. *Energy and Buildings*, 34(4):321–331, 2002.

A. Krpo. *Development and application of a numerical simulation system to evaluate the impact of anthropogenic heat fluxes on urban boundary layer climate*. PhD thesis, École Polytechnique Fédérale de Lausanne, 233 pages, 2009.

H. Kusaka and F. Kimura. Thermal effects of urban canyon structure on the nocturnal heat island: Numerical experiment using a mesoscale model coupled with an urban canopy model. *Journal of applied meteorology*, 43(12):1899–1910, 2004.

H. Kusaka, H. Kondo, Y. Kikegawa, and F. Kimura. A simple single-layer urban canopy model for atmospheric models: Comparison with multi-layer and slab models. *Boundary-Layer Meteorology*, 101(3):329–358, 2001. ISSN 0006-8314. doi: 10.1023/A:1019207923078.

W. Kuttler, D. Dutemeyer, and A. B. Barlag. Influence of regional and local winds on urban ventilation in cologne, germany. *Meteorologische Zeitschrift*, 7(2):77–87, 1998a.

W Kuttler, D Dutemeyer, and AB Barlag. Influence of regional and local winds on urban ventilation in cologne, germany. *Meteorologische Zeitschrift*, 7(2):77–87, 1998b.

Wilhelm Kuttler. *Climate Change on the Urban Scale-Effects and Counter-Measures in Central Europe*. INTECH Open Access Publisher, 2012.

K. Kylski. Spatial and seasonal distribution of anthropogenic heat emissions in lodz, poland. *Atmospheric Environment*, 30:3397–3404, 1996.

H. Laborit. *L'homme et la ville*. Champs Flammarion, 1971.

H. Landsberg. The meteorologically utopian city. *Bulletin of the American Meteorological Society*, 54(2):86–89, 1973.

J. H. Lee, M. Shahgedanova, and K. White. The role of urban parameters in the development of urban heat island: analysis and statistical modelling. page 4 p., 2009.

A. Lemonsu, A. Leroux, S. Belair, S. Trudel, and J. Mailhot. A general methodology of urban land cover type classification for atmospheric modeling. *CRTI scientific report*, pages 1–45, 2008.

A. Lemonsu, V. Masson, L. Shashua-Bar, E. Erell, and D. Pearlmutter. Inclusion of vegetation in the town energy balance model for modelling urban green areas. *Geoscientific Model Development*, 5(6):1377–1393, 2012. doi: 10.5194/gmd-5-1377-2012. URL http://www.geosci-model-dev.net/5/1377/2012/.

J. Lepart and P. Marty. Des réserves de nature aux territoires de la biodiversité. *Annales de géographie*, 115(651):485–507, 2006.

K. Liu and J. Minor. Performance evaluation of an extensive green roof. *Presentation at Green Rooftops for Sustainable Communities, Washington DC*, pages 1–11, 2005.

N. Long. Analyses morphologiques et aérodynamiques du tissu urbain : application à la micro-climatologie de marseille pendant la campagne escompte. *PhD report-Universit Lille1 - Sciences et Technologies*, 2003.

Loriot. Tache urbaine. *Présentation : Atelier gomatique, CETE-SO du 26/09/07*, 2007.

J.E. Loverland and G.Z. Brown. Impacts of climate change on the energy performance of buildings in the united states. *technical report*, 1989.

R. Mahmood, R. A. Pielke, K. G. Hubbard, D. Niyogi, P. A. Dirmeyer, C. McAlpine, A. M. Carleton, R. Hale, S. Gameda, A. Beltrán-Przekurat, B. Baker, R. McNider, D. R. Legates, M. Shepherd, J. Du, P. D. Blanken, O. W. Frauenfeld, U.S. Nair, and S. Fall. Land cover changes and their biogeophysical effects on climate. *International Journal of Climatology*, pages n/a–n/a, 2013. ISSN 1097-0088. doi: 10.1002/joc.3736.

A. Martilli. Numerical study of urban impact on boundary layer structure: Sensitivity to wind speed, urban morphology, and rural soil moisture. *Journal of Applied Meteorology*, 41(12):1247–1266, 2010.

A. Martilli. An idealized study of city structure, urban climate, energy consumption, and air quality. *ICUC8: The 8th International Conference on Urban Climate and the 10th Symposium on the Urban Environment*, 10(Part 2):430–446, 2012. doi: 10.1016/j.uclim.2014.03.003.

A. Martilli. An idealized study of city structure, urban climate, energy consumption, and air quality. *Urban Climate*, 10:430–446, 2014.

A. Martilli, A. Clappier, and M. W. Rotach. An urban surface exchange parameterisation for mesoscale models. *Boundary-Layer Meteorology*, 104(2):261–304, 2002. ISSN 0006-8314. doi: 10.1023/A:1016099921195.

T. Maruyama. Surface and inlet boundary conditions for the simulation of turbulent boundary layer over complex rough surfaces. *Journal of wind engineering and industrial aerodynamics*, 81(1):311–322, 1999.

V. Masson. A physically-based scheme for the urban energy budget in atmospheric models. *Boundary-Layer Meteorology*, 94(3):357–397, 2000. ISSN 0006-8314. doi: 10.1023/A:1002463829265.

V. Masson, C. Marchadier, G. Bretagne, M.-P. Moine, T. Houet, and M. Bonhomme. Projet acclimat : adaptation aux changements climatiques de lagglomération toulousaine. *Theoretical and Applied Climatology*, page 60p., 2013.

A. Matzarakis and H. Mayer. Heat stress in greece. *International Journal of Biometeorology*, 41(1):34–39, 1997.

A. Matzarakis and H. Mayer. Learning from the past: Urban climate studies in munich. In *5th Japanese–German Meeting on Urban Climatology*, pages 271–276, 2008.

A. Matzarakis, W. Beckröge, and H. Mayer. Future perspectives in applied urban climatology. In *Proc Second Japanese-German meeting, Report of Research Center for Urban Safety and Security, Kobe University, Special Report*, volume 1, pages 109–122, 1998.

D. Mauree. *Development of a multi-scale meteorological system to improve urban climate modeling*. PhD thesis, Université de Strasbourg, 184 pp., 2014.

D. Mauree, M. Kohler, N. Blond, and A. Clappier. Development of a 1D Canopy Interface Model. Part I: Neutral case and comparison with a C.F.D. *In preparation*, Chapter 3, 2014a.

D. Mauree, M. Kohler, N. Blond, and A. Clappier. Multi-scale modeling of the urban meteorology: integration of a new canopy model in WRF model. *In preparation*, Chapter 5, 2014b.

N. Mauree, D.and Blond and A. Clappier. Development of a 1D Canopy Interface Model. Part II: Stable and Unstable case - modification brought to the T.K.E equation. *In preparation*, Chapter 4, 2014.

L. Mehdi, C. Weber, F. Di Pietro, and W. Selmi. Evolution de la place du végétal dans la ville, de l'espace vert à la trame verte. *VertigO,-la revue électronique en science de l"environnement [en ligne]*, 12(2), 2012. doi: 10.4000/vertigo.12670.

Y. Miao, B. Liu, S.and Chen, B. Zhang, S. Wang, and S. Li. Simulating urban flow and dispersion in beijing by coupling a cfd model with the wrf model. *Advances in Atmospheric Sciences*, 30:1663–1678, 2013.

N. L. Miller, K. Hayhoe, J. Jin, and M. Auffhammer. Climate, extreme heat, and electricity demand in california. *Journal of Applied Meteorology and Climatology*, 47 (6):1834–1844, 2008.

E. S. Minor and D. L. Urban. Graph theory as a proxy for spatially explicit population models in conservation planning. *Ecological applications*, 17/6, 2007.

A. S. Monin and A. M. Obukhov. Basic laws of turbulent mixing in the surface layer of the atmosphere. *Contrib. Geophys. Inst. Acad. Sci. USSR*, 151:163–187, 1954.

C. Müller. *Improvement of an urban turbulence parametrization for meteorological operational forecast and air quality modeling*. PhD thesis, École Polytechnique Fédérale de Lausanne, 208 pp., 2007.

Nicole Müller, Wilhelm Kuttler, and Andreas-Bent Barlag. Counteracting urban climate change: adaptation measures and their effect on thermal comfort. *Theoretical and applied climatology*, 115(1-2):243–257, 2014.

G. Najjar, P. Kastendeuch, P. Stoll, J. R. Colin, F. Nerry, N. Ringenbach, J. Bernard, A. De hatten, R. Luhahe, and D. Viville. Le projet reclus, télédétection, rayonnement et bilan d'énergie en climatologie urbaine à strasbourg. *La Météorologie.*, 46, 2004.

National academy of technology of France. Prospective sur l'énergie au xxie siècle, synthse de la commission energie et environnement. Technical report, 2004.

D. J. Nowak. Assessing environmental functions and values of veteran trees. Nicoleeti G. and P. Gonthier (eds), 2004.

D. J. Nowak. Institutionalizing urban forestry as a "biotechnology" to improve environmental quality. *Urban Forestry and Urban Greening*, 5, 2006.

OECD and IEA. Energy efficiency requirements in building codes, energy efficiency policies for new buildings. Technical report, 2008.

Y. Ohashi, Y. Genchi, H. Kondo, Y. Kikegawa, H. Yoshikado, and Y. Hirano. Influence of air-conditioning waste heat on air temperature in tokyo during summer: numerical experiments using an urban canopy model coupled with a building energy model. *Journal of Applied Meteorology and climatology*, 46(1):66–81, 2007.

T. R. Oke. Towards a prescription for the greater use of climatic principles in settlement planning. *Energy and Buildings*, 7:1–10, 1984.

T. R. Oke. *Boundary layer Climates*. Methuen and Co., Ltd., London, 435 pp., 1987.

T. R. Oke. The urban energy balance. *Progress in Physical Geography*, 12(4):471–508, 1988. doi: 10.1177/030913338801200401.

G. B. Oleson, K. W .and Bonan, J. Feddema, M. Vertenstein, and C.S.B. Grimmond. An urban parameterization for a global climate model. part i: Formulation and evaluation for two cities. *Journal of Applied Meteorology and Climatology*, 47(4): 1038–1060, 2008a.

K. W. Oleson, G. B. Bonan, J. Feddema, and M. Vertenstein. An urban parameterization for a global climate model. part ii: Sensitivity to input parameters and the simulated urban heat island in offline simulations. *Journal of Applied Meteorology and Climatology*, 47(4):1061–1076, 2008b.

ONERC. Villes et adaptation au changement climatique. Technical report, 2003.

T. L. Otte, A. Lacser, S. Dupont, and J. K. S. Ching. Implementation of an urban canopy parameterization in a mesoscale meteorological model. *Journal of Applied Meteorology*, 43(11):1648–1665, 2004.

S. Owens. Energy, environmental sustainability and land use planning. *In M.Bregeny (ed) Sustainable Development and Urban form, London: Pion*, 1992.

D. E. Parker. A demonstration that large-scale warming is not urban. *Journal of Climate*, 19(12):2882–2895, 2006.

L. Pascual-Hortal and S. Saura. Impact of spatial scale on the identification of critical habitat patches for the maintenance of landscape connectivity. *Landscape and Urban Planning*, 83(2):176–186, 2007.

L. Peeters, R. de Dear, J. Hensen, and W. D'haeseleer. Thermal comfort in residential buildings: comfort values and scales for building energy simulation. *Applied Energy*, 86(5):772–780, 2009.

M. Pehnt. Dynamic life cycle assessment (lca) of renewable energy technologies. *Renewable energy*, 31(1):55–71, 2006.

L. Pérez-Lombard, J. Ortiz, and C. Pout. A review on buildings energy consumption information. *Energy and Buildings*, 40(3):394 – 398, 2008. ISSN 0378-7788. doi: 10.1016/j.enbuild.2007.03.007.

R. A. Pielke and D. Niyogi. *The role of landscape processes within the climate system, In Landform - Structure, Evolution, Process Contro*, volume 115. NY: Springer, 2011.

G. Pigeon, K. Zibouche, B. Bueno, J. Le Bras, and V. Masson. Improving the capabilities of the town energy balance model with up-to-date building energy simulation algorithms: an application to a set of representative buildings in paris. *Energy and Buildings*, 76:1–14, 2014.

L. Prandtl. Report on investigation of developed turbulence. *NACA Report TM-1231*, 1925.

R. G. Quayle and H. F. Diaz. Heating degree day data applied to residential heating energy consumption. *Journal of Applied Meteorology*, 19(3):241–246, 1980.

A. Rasheed. *Multiscale modelling of urban climate*. PhD thesis, ÉCOLE POLYTECHNIQUE FÉDÉRALE DE LAUSANNE, 2009.

M.R. Raupach. Drag and drag partition on rough surfaces. *Boundary-Layer Meteorology*, 60(4):375–395, 1992. ISSN 0006-8314. doi: 10.1007/BF00155203.

C. Ren, E. Y.-Y. Ng, and L. Katzschner. Urban climatic map studies: a review. *International Journal of Climatology*, 31(15):2213–2233, 2011.

H. Richardson, S. Basu, and A. A. M. Holtslag. Improving stable boundary-layer height estimation using a stability-dependent critical bulk richardson number. *Boundary-Layer Meteorology*, 148(1):93–109, 2013. ISSN 0006-8314. doi: 10.1007/s10546-013-9812-3.

N. Ringenbach. *Bilan radiatif et flux de chaleur en climatologie urbaine: mesures, modélisation et validation sur Strasbourg*. PhD thesis, Ecole Nationale Supérieure de Physique de Strasbourg, 2009.

A. H. Rosenfeld, H. Akbari, S. Bretz, B. L Fishman, D. M. Kurn, D. Sailor, and H. Taha. Mitigation of urban heat islands: materials, utility programs, updates. *Energy and buildings*, 22(3):255–265, 1995.

A. H. Rosenfeld, H. Akbari, J. J Romm, and M. Pomerantz. Cool communities: strategies for heat island mitigation and smog reduction. *Energy and Buildings*, 28(1): 51–62, 1998.

M. W. Rotach. Turbulence close to a rough urban surface part i: Reynolds stress. *Boundary-Layer Meteorology*, 65(1-2):1–28, 1993. ISSN 0006-8314. doi: 10.1007/BF00708816.

M. Roth. Review of atmospheric turbulence over cities. *Quarterly Journal of the Royal Meteorological Society*, 126(564):941–990, 2000. ISSN 1477-870X. doi: 10.1002/qj.49712656409.

M. W. Rothach. On the influence of the urban roughness sublayer on turbulence and dispersion. *Atmospheric Environment*, 33:4001–4008, 1999.

RTE. Bilan électrique 2012. Technical report, 2012.

D. J. Sailor. Simulations of annual degree day impacts of urban vegetative augmentation. *Atmospheric Environment*, 32(1):43–52, 1998.

D. J. Sailor. A review of methods for estimating anthropogenic heat and moisture emissions in the urban environment. *International Journal of Climatology*, 31(2): 189–199, 2011. ISSN 1097-0088. doi: 10.1002/joc.2106.

H. S. Sajjad. Observational and modelling approaches to study urban climate: application on pakistan. *Thèse de l'université de Strasbourg*, page 175, 2013.

F. Salamanca, A. Krpo, A. Martilli, and A. Clappier. A new building energy model coupled with an urban canopy parameterization for urban climate simulations:part I. formulation, verification, and sensitivity analysis of the model. *Theoretical and Applied Climatology*, 99(3-4):331–344, 2010. ISSN 0177-798X. doi: 10.1007/s00704-009-0142-9.

F. Salamanca, A. Martilli, M. Tewari, and F. Chen. A study of the urban boundary layer using different urban parameterizations and high-resolution urban canopy parameters with wrf. *Journal of Applied Meteorology and Climatology*, 50(5):1107–1128, 2011.

F. Salamanca, A. Martilli, and C. Yagüe. A numerical study of the urban heat island over madrid during the desirex (2008) campaign with wrf and an evaluation of simple mitigation strategies. *International Journal of Climatology*, 32(15):2372–2386, 2012.

M. Santamouris. Energy and climate in the built environment. *Solar Energy*, 1:402 p., 2001. Earthscan (ed.).

M. Santamouris, N. Papanikolaou, I. Livada, I. Koronakis, C. Georgakis, A. Argiriou, and D. N. Assimakopoulos. On the impact of urban climate on the energy consumption of buildings. *Solar Energy*, 70(3):201 – 216, 2001. ISSN 0038-092X. doi: http://dx.doi.org/10.1016/S0038-092X(00)00095-5. ¡ce:title¿Urban Environment¡/ce:title¿.

J. L. Santiago and A. Martilli. A dynamic urban canopy parameterization for mesoscale models based on computational fluid dynamics reynolds-averaged navier-stokes microscale simulations. *Boundary-Layer Meteorology*, 137(3):417–439, 2010. ISSN 0006-8314. doi: 10.1007/s10546-010-9538-4.

S. Saura and L. Rubio. A common currency for the different ways in which patches and links can contribute to habitat availability and connectivity in the landscape. *Ecography*, 33(3):523–537, 2010.

J. Schatz and C. J. Kucharik. Seasonality of the urban heat island effect in madison, wisconsin. *Journal of Applied Meteorology and Climatology*, 53(10):2371–2386, 2014.

B Schmitt, F Goffette-Nagot, et al. Defining rural areas? from a difficult conceptual definition to a necessary statistical delineation. *Économie Rurale*, (257):42–55, 2000.

N. Schwarz, U. Schlink, U. Franck, and K. Großmann. Relationship of land surface and air temperatures and its implications for quantifying urban heat island indicator:an application for the city of leipzig (germany). *Ecological Indicators*, 18:693–704, 2012.

C. Schweizer, R. D. Edwards, L. Bayer-Oglesby, W. J. Gauderman, V. Ilacqua, M. J. Jantunen, H. K. Lai, M. Nieuwenhuijsen, and N. Künzli. Indoor time–microenvironment–activity patterns in seven regions of europe. *Journal of Exposure Science and Environmental Epidemiology*, 17(2):170–181, 2007.

N. L. Seaman, F. L. Ludwig, E. G. Donall, T. Warner, and C. M. Bhumralkar. Numerical studies of urban planetary boundary-layer structure under realistic synoptic conditions. *Journal of Applied Meteorology*, 28(8):760–781, 1989.

J. H Seinfeld and S. N Pandis. *Atmospheric chemistry and physics: from air pollution to climate change*. John Wiley & Sons, 2012.

P. Seljom, E. Rosenberg, A. Fidje, J. E. Haugen, Meir, M., J. Rekstad, and T. Jarlset. Modelling the effects of climate change on the energy system-a case study of norway. *Energy policy*, 39:7310–7321, 2011.

A. Sellé. Bibliothèque des matériaux de construction 2010, avril 2011. URL http://www.maison.com/architecture/maison-basse-consommation/bibliotheque-materiaux-construction-4818/.

W. Selmi, C. Weber, and L. Mehdi. Multifonctionnalité des espaces végétalisés urbains. *VertigO-la revue électronique en sciences de l'environnement*, 13(2), 2013.

S. Shafiee and E. Topal. When will fossil fuel reserves be diminished? *Energy policy*, 37(1):181–189, 2009.

L. Shashua-Bar, D. Pearlmutter, and E. Erell. The cooling efficiency of urban landscape strategies in a hot dry climate. *Landscape and Urban Planning*, 92(3):179–186, 2009.

J. R. Simpson and E. G. McPherson. Simulation of tree shade impacts on residential energy use for space conditioning in sacramento. *Atmospheric Environment*, 32(1): 69–74, 1998.

A. L. Sizling, E. Sizlingová, D. Storch, J. Reif, and K. Gaston. Rarity, commonness, and the contribution of individual species to species richness patterns. *The American naturalist*, 174(1):82–93, 2009.

W. C. Skamarock, J. B. Klemp, J. Dudhia, D. O. Gill, D. M. Barker, W. Wang, and J. G. Powers. A description of the advanced research wrf version 2. Technical report, DTIC Document, 2005.

W. C. Skamarock, J. B. Klemp, J. Dudhia, D. O. Gill, D. M. Barker, M. Duda, X.Y. Huang, W. Wang, and J. G. Powders. A description of the advanced research wrf version 3. Technical report, NCAR Technical Note, NCAR/TN-475+STR, 2008.

B. Smit and J. Wandel. Adaptation, adaptive capacity and vulnerability. *Global environmental change*, 16(3):282–292, 2006.

C. Smith and G. Levermore. Designing urban spaces and buildings to improve sustainability and quality of life in a warmer world. *Energy policy*, 36(12):4558–4562, 2008.

C. Spitz. *Analyse de la fiabilité des outils de simulation et des incertitudes de métrologie appliquée à l'efficacité énergétique des bâtiments*. PhD thesis, Grenoble, 2012.

I. D. Stewart and T. R. Oke. Methodological concerns surrounding the classification of urban and rural climate stations to define urban heat island magnitude. *preprints of ICUC6 Göteborg*, 431, 2006.

B. Stone, J.J. Hess, and H. Frumkin. Urban form and extreme heat events: are sprawling cities more vulnerable to climate change than compact cities. *Environmental health perspectives*, 118(10):1425–1428, 2010.

Jr. Stone, J. Vargo, P. Liu, Y. Hu, and A. Russell. Climate change adaptation through urban heat management in atlanta, georgia. *Environmental science & technology*, 47 (14):7780–7786, 2013.

Jr. B. Stone and M. O. Rodgers. Urban form and thermal efficiency: how the design of cities influences the urban heat island effect. *Journal of the American Planning Association*, 67(2):186–198, 2001.

Jakob Strømann-Andersen and Peter Andreas Sattrup. The urban canyon and building energy use: Urban density versus daylight and passive solar gains. *Energy and Buildings*, 43(8), 2011.

R. B. Stull. *An Introduction to Boundary Layer Meteorology*. Kuler Academic Publishers, 666 pp., 1988.

M. Szymanowski and M. Kryza. Local regression models for spatial interpolation of urban heat island?an example from wrocław, sw poland. *Theoretical and Applied Climatology*, 108(1-2):53–71, 2012.

H. Taha. Urban climates and heat islands: albedo, evapotranspiration, and anthropogenic heat. *Energy and Buildings*, 25(2):99 – 103, 1997. ISSN 0378-7788. doi: 10.1016/S0378-7788(96)00999-1.

H. Taha, H. Akbari, A Rosenfeld, and J. Huang. Residential cooling loads and the urban heat island-the effects of albedo. *Building and environment*, 23(4):271 – 288, 1988.

C. Tannier. Formes de villes optimales, formes de villes durables : Réflexion partir de l'étude de la ville fractale. *Espaces et sociétés*, 138(3):153–171, 2009.

C. Tannier and I. Thomas. Defining and characterizing urban boundaries: A fractal analysis of theoretical cities and belgian cities. *Computers, Environment and Urban Systems*, 41:234–248, 2013.

C. Tannier, I. Thomas, G. Vuidel, and P. Frankhauser. A fractal approach to identifying urban boundaries. *Geographical Analysis*, 43:211–227, 2011.

C. Tannier, J.-C. Foltète, and X. Girardet. Assessing the capacity of different urban forms to preserve the connectivity of ecological habitats. *Landscape and Urban Planning*, 105:128–139, 2012.

P. D. Taylor, L. Fahring, K. Henein, and G. Merriam. Connectivity is a vital element of landscape structure. *Oikos*, pages 43–48, 1993.

H. Tennekes and J. L. Lumley. *A first course in turbulence*. MIT press, 1972.

M. Tewari, H. Kusaka, F. Chen, W. J. Coirier, S. Kim, and T.T. Wyszogrodzki, A.A.and Warner. Impact of coupling a microscale computational fluid dynamics model with a mesoscale model on urban scale contaminant transport and dispersion. *Atmospheric Research*, 96(4):656 – 664, 2010. ISSN 0169-8095. doi: http://dx.doi.org/10.1016/j.atmosres.2010.01.006.

H. C. S. Thom. The rational relationship between heating degree days and temperature 1. *Monthly Weather Review*, 82(1):1–6, 1954.

G. Thompson, R. M. Rasmussen, and K. Manning. Explicit forecasts of winter precipitation using an improved bulk microphysics scheme. part i: Description and sensitivity analysis. *Monthly Weather Review*, 132(2):519–542, 2004.

T. Tokairin, A. Sofyan, and T. Kitada. Effect of land use changes on local meteorological conditions in jakarta, indonesia: toward the evaluation of the thermal environment of megacities in asia. *International journal of climatology*, 30(13):1931–1941, 2010.

L. Tyrväinen. Economic valuation of urban forest benefits in finland. *Journal of environmental management*, 62(1):75–92, 2001.

UN. World Urbanization Prospects: The 2011 Revision, CD-ROM Edition. Technical report, Department of Economic and Social Affairs, Population Division, 2012.

J. Unger. Urban–rural air humidity differences in szeged, hungary. *International Journal of Climatology*, 19(13):1509–1515, 1999.

I. Uno, H. Ueda, and S. Wakamatsu. Numerical modeling of the nocturnal urban boundary layer. *Boundary-Layer Meteorology*, 49(1-2):77–98, 1989.

D. L. Urban and T. Keitt. Landscape connectivity: a graph-theoretic perspective. *Ecology*, 82(5):1205–1218, 2001.

D. L. Urban, E. S. Minor, E. A. Treml, and R. S. Schick. Graph models of habitat mosaics. *Ecology letters*, 12(3):260–273, 2009a.

D.L. Urban, E. S. Minor, E.A. Treml, and R. S. Schick. Graph models of habitat mosaics. *Ecology letters*, 12(3), 2009b.

US Climate change science program. Effects of climate change on energy production and use in the united states. Technical report, 2008.

E. Valor, V. Meneu, and V. Caselles. Daily air temperature and electricity load in spain. *Journal of applied Meteorology*, 40(8):1413–1421, 2001.

L. B. Verboom and R. Van Apeldoorn. Effects of habitat fragmentation on the red squirrel, sciurus vulgaris. *Landscape Ecology*, 4(2/3):171–176, 1990.

J. Viard. *La société d'archipel ou les territoires du village global*. ed. de l'Aube, 1974.

P. Viejo-Garcia and C. Keim. Simulation model of heat and power demand in a german region until 2030: Stuttgart metropolitan region as case study. *Architecture and Urban Planning (DDSS 2008). University of Technology Eindhoven, HJP Timmermans, B. de Vries (eds.)*, page 14, 2008.

V. Viguié and S. Hallegatte. The impact of a carbon tax on paris metropolitan area and its population. *2011, soumis à Environmental and Ressource Economics*, 2011.

J.A. Voogt and T.R. Oke. Effects of urban surface geometry on remotely-sensed surface temperature. *International Journal of Remote Sensing*, 19(5):895–920, 1998.

L. Wallace. Errors in estimating temperatures using the average of tmax and tmin-analysis of the uscrn temperature stations. 2012. URL http://wattsupwiththat.com/2012/08/30/errors-in-estimating-temperatures-using-the-average-of-tmax-and-tmin-analysis-of

S. Wang, C. Yan, and F. Xiao. Quantitative energy performance assessment methods for existing buildings. *Energy and Buildings*, 55:873–888, 2012.

weather.msfc.nasa.gov. URL http://www.weather.msfc.nasa.gov/.

R. L. Willby, M. L. Wigley, D. Conway, P. D. Jones, B. C. Hewitson, J. Main, and D. S. Wilks. Statistical downscaling of general circulation model output: a comparison of methods. *Water resources research*, 34:2995–3008, 1998.

F. Wilmers. Effects of vegetation on urban climate and buildings. *Energy and Buildings*, 15(3):507–514, 1991.

A. Xiu and J. E. Pleim. Development of a land surface model. part i: Application in a mesoscale meteorological model. *Journal of Applied Meteorology*, 40(2):192–209, 2001.

P. Xu, Y. J. Huang, N. Miller, and N. Schlegel. Effects of global climate changes on building energy consumption and its implications on building energy codes and policy in california. *peer final project report, September 2009, CEC-500-2009-006*, page 118 p., 2009.

L. Yang, H. Yan, and J. C. Lam. Thermal comfort and building energy consumption implications–a review. *Applied Energy*, 115:164–173, 2014.

X. Yang, L. Zhao, M. Bruse, and Q. Meng. An integrated simulation method for building energy performance assessment in urban environments. *Energy and Buildings*, 54(0):243 – 251, 2012. ISSN 0378-7788. doi: 10.1016/j.enbuild.2012.07.042.

G. J. Zhang, M. Cai, and A. Hu. Energy consumption and the unexplained winter warming over northern asia and north america. *Nature Climate Change*, 2013.

Chapter 8

Résumé (version française)

Résumé

A l'heure actuelle, la lutte contre le changement climatique et ses impacts se décline au niveau local. Depuis 2009, les plans climat énergie territoriaux sont obligatoires pour les agglomérations de plus de 50,000 habitants. Ils engagent les collectivités territoriales à quantifier les émissions de gaz à effet de serre et les dépenses énergétiques des principaux secteurs économiques hébergés sur leur territoire. Parmi ces secteurs, le bâtiment et notamment les bâtiments résidentiels, représentent plus de 40% des dépenses énergétiques françaises et constituent du fait de leur durée de vie et de l'ancienneté du parc immobilier français un fort potentiel de réduction des dépenses énergétiques.
En parallèle, depuis une dizaine d'année maintenant, la communauté des climatologues urbains développe des systèmes de modèles climatiques capables de simuler en moyenne l'effet des bâtiments sur la thermodynamique de l'atmosphère et les dépenses énergétiques des bâtiments.

Cette présente étude vise à évaluer les potentiels d'application à l'échelle d'un territoire de ces systèmes de modèles climatiques dans l'élaboration des inventaires énergétiques et dans le transfert des connaissances climatiques et énergétiques dans les principaux documents d'urbanisme. En outre, cette étude questionne le lien entre la forme urbaine, les dépenses énergétiques et le climat urbain.

Dans cette étude, nous avons successivement appliqué le système de modèles climatiques WRF/ARW-BEP+BEM de Skamarock et al. [2008] au territoire de la communauté urbaine de Strasbourg (France) en 2010 et à la région urbaine de Strasbourg-Kehl en 2030 en considérrant alors, des scénrios de développement résidentiel archétypaux. Ce faisant nous avons évalué la capacité des systèmes de modèles climatiques à estimer les dépenses énergétiques d'un territoire sur une période donnée et à prendre en compte la dynamique du dévelopment urbain. Enfin, afin d'améliorer la représentation de la surface, et notamment de la végétation, dans les systèmes de modèles climatiques nous avons développé un modèle de canopée urbaine, CIM, résolvant les profils verticaux de vents, de température et d'humidité et pouvant être couplé avec n'importe quels modèles de surface (paramétrisation urbaine, modèles climatiques microéchelles plus résolus).

Mot-clés: *paramétrisation urbaine-modèle atmosphérique mésoéchelle- performance énergétique des bâtiments -aire urbaine*

8.2 Introduction

Actuellement, le Groupement Intergouvernemental des Experts sur le Climat (GIEC) estime que la consommation croissante des hydrocarbures fossiles contribuerait à augmenter les températures de surface de +2°C à +6°C d'ici la fin de ce siècle. Les impacts de tels réchauffements seront tout particulièrement sensibles en milieu urbain qui concentre la population et où, à cette chaleur additionnelle, s'ajoute un effet de réchauffement de l'air local appelé îlot de chaleur urbain. Ce dernier est principalement imputable à l'imperméabilisation des sols et à la présence d'obstacles tels que les bâtiments qui modifient les échanges dynamiques et énergétiques entre la surface et l'atmosphère. Aussi, on estime que le réchauffement climatique influencera les dépenses énergétiques dans les bâtiments en réduisant notamment les besoins en chauffage mais concourra à l'utilisation croissante d'électricité en été dans les systèmes d'air conditionné.

Afin de lutter contre les impacts du changement climatiques, les Etats et plus particulièrement l'Union Européenne se sont dotés d'objectifs en matière de réduction de Gaz à effet de serre (GES). Au niveau national, il s'agit de réduire par 4 les émissions de GES en référence aux émissions 1990 d'ici 2050 (loi POPE de 2005). Le secteur du bâtiment est l'une des principales cibles des stratégies d'atténuation et d'adaptation au changement climatique. Il représente 43% (24% des émissions de GES) des dépenses énergétiques finales, principalement à des fins de confort thermique.
Par ailleurs, il incombe aux collectivités territoriales aux travers des Plans Climat Energie Territorial (Grenelle 1 et 2 de l'environnement) de constituer des inventaires chiffrés de leurs dépenses énergétiques et émissions de GES. Ces inventaires doivent renforcer la connaissance des collectivités locales sur leurs dépenses énergétiques à l'échelle de leur territoire et constituer un point d'appui à l'élaboration de stratégies locales luttant contre les effets du changement climatique.

Les inventaires de dépenses énergétiques des bâtiments à l'échelle de la ville sont souvent construits à partir de campagnes thermographiques aériennes des toitures [APUR, 2011] ou d'analyses statistiques multi-variées. Ces dernières s'appuient sur la connaissance de la consommation énergétique de bâtiments prototypes et des caractéristiques du parc immobilier d'un territoire. Peu de méthodes utilisées pour réaliser de tels inven-

taires considèrent l'influence du climat local sur les dépenses/demandes énergétiques des bâtiments. Parmi les outils numériques, qui permettent de tester a priori différents scénarios d'atténuation et d'adaptation (albédo, ombrage) au réchauffement climatique et qui considèrent l'influence du climat, figurent les modèles physiques micro-échelles (résolution du mètre) d'énergie du bâtiment. Ils calculent les demandes énergétiques d'un bâtiment prototype dont la géométrie et les propriétés radiatives et thermiques sont très proches de la réalité. Ils considèrent les échanges thermiques et dynamiques à l'intérieur d'un bâtiment soumis à des variations météorologiques et à l'influence de son environnement proche (*ex.* effet ombrage) ainsi que la dynamique d'activation des systèmes climatisés tels que les systèmes d'air conditionné ou les pompes à chaleur. Toutefois, les conditions météorologiques en entrée de ces modèles sont des données climatiques standards établies à l'aide de moyennes statistiques (30 ans) effectuées sur des observations météorologiques mesurées bien souvent à l'extérieur de l'aire urbaine. De ce fait, l'influence du climat sur les demandes énergétiques est surévaluée.

Dès lors, il apparait que les outils actuels dont disposent les collectivités territoriales en matière d'évaluation des dépenses énergétiques des bâtiments sur leur territoire ne sont pas optimisés à une vision prospective des différents effets des stratégies territoriales mises en place pour lutter contre les impacts du changement climatique.

Par ailleurs, la dynamique du développement résidentiel est souvent peu prise en compte dans les études d'inventaires. Or de précédentes études ont mis en avant le rôle croissant des choix de formes urbaines dans la construction de villes post-carbones et durables. Les formes compactes qui sont notamment mises en avant par les études d'énergétique du transport, induisent des densités urbaines en termes de bâtiments et de population plus fortes que les formes induites par l'étalement urbain. L'intensité des dépenses énergétiques par personne ou par mètre carré bâti est ainsi réduite en comparaison de celle observée dans les formes étalées des périphéries des villes. De surcroît, les fortes densités urbaines de par la prépondérance des surfaces imperméables artificielles et de la concentration des émissions de chaleur anthropiques concourreraient à intensifier les effets locaux d'îlot de chaleur, réduisant de ce fait les dépenses énergétique en chauffage. Néanmoins, ces formes compactes sont aussi réputées pour accroître à un seuil donné les effets de congestion du trafic routier, la pollution atmosphérique et les effets de dilatation des espaces de vie de la population urbaine vers les espaces verts des périphéries de ces mêmes villes. L'engouement pour les espaces verts et la maison

individuelle familiale des citadins tend en effet à s'accroître avec l'augmentation de la densité du bâti, contribuant à renforcer l'étalement urbain.
Des politiques de limitations de l'étalement urbain et des trajets automobiles fortement dépendant des ressources d'hydrocarbures fossiles sont ainsi mises en oeuvre pour contrecarrer les effets négatifs de l'étalement urbain (augmentation des consommations et de l'intensité énergétiques dans le transport et les bâtiments respectivement, fragmentation du paysage et mise en péril de la diversité écologique). Toutefois, peu d'études d'impact de ces stratégies d'aménagement sur le climat urbain et les dépenses énergétiques sont réellement menées : la question de la densité urbaine en termes de bénéfices énergétiques dans les bâtiments et écologiques reste posée.

8.3 Objectif

L'objectif de cette étude est de proposer une nouvelle méthodologie d'évaluation des dépenses/demandes énergétiques des bâtiments à l'échelle d'une aire urbaine et de tester différentes stratégies d'atténuation et d'adaptation au changement climatique. Cette méthodologie devra prendre en compte la complexité d'échelle du climat urbain notamment de l'îlot de chaleur urbain, ainsi que la dynamique de croissance des aires urbaines qui, en modifiant les propriétés de surfaces, altèrent également les conditions météorologiques locales. Ce faisant, l'interaction entre la forme urbaine, les dépenses énergétiques des bâtiments et le climat urbain sera questionnée.

8.4 La méthodologie

Depuis quelques décennies, les modèles régionaux du climat qui calculent l'évolution des conditions météorologiques moyennes sur des volumes élémentaires d'air de l'ordre du 1 km^3, ont connu des améliorations considérables en matière de représentations des surfaces urbaines (paramétrisation urbaine). Ces paramétrisations reproduisent en moyenne l'effet de plusieurs obstacles sur l'écoulement du vent, les échanges énergétiques et radiatifs. Les paramétrisations urbaines les plus accomplies considèrent les effets tridimensionnels des obstacles dans la canopée urbaine, couche d'air incluse dans la rue,

à l'instar du modèle TEB de Masson [2000] et BEP de Martilli et al. [2002]. Les obstacles d'un tissu urbain donné y sont traditionnellement modélisés comme une succession uniforme de cubes séparés par des rues (les canyon-rues) pour lesquels des flux de surfaces de mouvement, d'énergie, et d'humidité distinctifs sont calculés pour chacune des surface du canyon-rue (*ex.* rue, toit, mur). Ces flux de surface sont ensuite moyennés en fonction de leur surface dans la maille et de la représentativité du tissu urbain et des types de surface dans cette maille. Les flux de surfaces sont alors introduits dans le modèle atmosphérique comme un terme additionnel des équations atmosphérique de conservation de Navier-Stokes. Par ailleurs, et cela depuis les années 2000, de nombreux modèles énergétiques de bâtiments ont été implémentés dans les paramétrisations de canopée urbaine tel que le modèle BEM [Salamanca et al., 2010] qui a été couplé à la paramétrisation de canopée urbaine BEP et intégré dans le modèle méso-échelle non-hydrostatique WRF (Weather Research Forecasting model). Le modèle BEM calcule en particulier un bilan énergétique à l'intérieur du bâtiment en considérant les apports de chaleur passifs (solaires, anthropiques) et un modèle de pompe à chaleur qui estime la demande énergétique de chauffage/climatisation par rapport à un seuil fixé de confort en température et en humidité . Le tout forme alors un système de modèles météorologiques capable de prendre en considérations les interactions entre le climat urbain et les dépenses énergétiques dans les bâtiments ainsi que la complexité d'échelle inhérente au climat urbain.

Mon travail a consisté en plusieurs étapes :

(1) Tester la capacité d'un système de modèles météorologiques à construire un cadastre des demandes énergétiques sur un territoire donné .

Dans un premier temps, la capacité du système de modèles météorologiques WRF/ARW-BEP+BEM à fournir un cadastre des demandes énergétiques sur un territoire donné a été testée. WRF a ainsi été appliqué sur le territoire de la Communauté Urbaine de Strasbourg (CUS) pour l'année 2010. Quatre domaines emboités ont été construits. Le plus résolu se focalise sur la région urbaine de Strasbourg-Kehl. Ils se caractérise par une résolution horizontale de 1 km. Les conditions météorologiques de ce dernier domaine sont héritées (forçage climatique) des domaines-parents, moins résolus (45 km, 9 km, 3 km respectivement) tandis que le forçage météorologique du premier domaine s'appuie sur les ré analyses météorologiques des sorties du modèle climatique global AVN. Les données de surface et notamment la description de l'occupation du sol, la morphologie et l'orientation des canyons-rues sont issues de traitements géo-spatial de

bases de données locales fournies à hautes résolutions (BDOcs_2008 de la coopération CIGAL, BDtopo® de l'IGN). Les résultats de cette simulation permettent d'obtenir un cas de référence qui a été confronté aux observations météorologiques et énergétiques fournies par Météo France et l'Association pour la surveillance et l'étude de la pollution atmosphérique en Alsace (ASPA), respectivement, à des fins de validation et comparaison.

(2) Proposer une méthode rapide de calcul des demandes énergétiques prenant en compte la complexité du climat urbain.

S'appuyant sur la relation significative observée entre les températures de l'air et les dépenses énergétiques lors de précédentes études et sa simplification selon un modèle linéaire statistique [Thom, 1954, Amato et al., 2005], une nouvelle méthode d'estimation des demandes énergétique dans le bâtiment a été développée. Elle s'appuie sur l'utilisation des températures de l'air et des demandes énergétiques simulées par le système de modèles météorologiques WRF/ARW-BEP+BEM et la traditionnelle méthode des dégré-jours. Cette dernière repose sur la correspondance entre les besoin énergétiques des bâtiments pour le chauffage ou la climatisation et la distribution des gradients de températures dans un laps de temps donné entre la température de l'air extérieur et une température de référence, la température de base (T_0) qui caractérise quant à elle, l'équilibre thermique du bâtiment avec son environnement. La relation entre la température et les besoins énergétiques s'appuie sur la définition de la sensibilité climatique des bâtiments (P) qui mesure la propension des bâtiments à demander de l'énergie pour chaque degré Celsius supplémentaire. La méthode numérique comparativement à la méthode traditionnelle qui repose sur des observations de la température de l'air et des dépenses énergétiques présente l'avantage :
i) de considérer la complexité du climat urbain, *ii)* de pouvoir être établie relativement rapidement sur n'importe quel territoire et laps de temps, et *iii)* de ne pas définir à priori les paramètres du modèle linéaire statistique comme la température de base ou la sensibilité climatique des bâtiments.
Cette méthode a été développée sur le territoire administratif de la communauté urbaine de Strasbourg (CUS) à partir des résultats de l'étape (1). Elle a ensuite été optimisée à l'aide de test de sensibilité afin de réduire la durée des simulations et les besoins en ressources numériques. Enfin la relation linéaire statistique a permis de tester différentes stratégies de réduction des besoins énergétiques souvent mises en exergue dans la littérature tels que l'augmentation de la réflectivité des toits ou l'abaissement

de la température de confort dans les bâtiments.

(3) Tester l'influence de politiques de développement urbain durable sur les demandes énergétiques.

Dans un second temps, la capacité du système de modèles météorologiques WRF/ARW-BEP+BEM à prendre en compte les changements d'occupation du sol qui résultent des politiques de lutte contre l'étalement urbain a été éprouvée (*ex.* conservation de la trame verte, promotion de la densité urbaine et du renouvellement urbain). Une version modifiée du modèle américain d'automate cellulaire SLEUTH* de Doukari et al. [2013], a été utilisé à cette fin. Elle a permis de simuler le dénveloppement résentiel de scénrios de dénveloppements urbains archétypaux. Comme tout modèle d'automate cellulaire, les changements d'occupation du sol d'une cellule interviennent à partir de la connaissance de l'environnement voisin de la cellule. Un algorithme de Monte Carlo et trois règles simples (développement concentrique (edge growth), linéaire (road influenced growth) et spontané (spontaneous growth) permettent de contraindre le développement urbain. Afin d'imposer des contraintes plus réaliste au modèle, le PLU de la communauté urbaine de Strasbourg ainsi que les modèles MorphoLim et Graphab ont été utilisés [Tannier et al., 2011, Foltête et al., 2012]. À l'aide de la théorie des fractales, MorphoLim délimite des agrégats bâtis cohérents tandis que le second identifie les habitats à protéger impérativement pour le maintien de la connectivité écologique du paysage. Pour l'heure, Graphab a la capacité de considérer une seule espèce-cible. L'écureuil roux, espèce commune des aires boisées a été choisie. Sa forte répartition sur le territoire et sa faible distance de dispersion en font une espèce particulièrement sensible à la fragmentation du paysage écologique. L'ensemble de cette chaîne de modèles a ainsi été appliqué à la partie française de l'aire urbaine de Strasbourg-Kehl en considérant une résolution de la cellule de 20 m et une échelle temporelle de 20 ans correspondant à l'horizon temporelle des principales décisions territoriales. Les changements d'occupation du sol ont ensuite été agrégés à la résolution du modèle météorologique (1 km) afin d'y renseigner les propriétés physiques (*ex.*radiatives, aérodynamiques, thermiques, etc.) des nouvelles cartes d'occupation du sol.

(4) Proposer une amélioration de la représentation des obstacles urbains dans les paramétrisations urbaines et notamment de la végétation.

Afin de mieux représenter l'influence de la surface dans les modèles climatiques régionaux, le développement d'un modèle colonne de canopée urbaine (Canopy Interface Model ou CIM) a été initié. Il a pour objectif d'améliorer le calcul des flux de surface dans les modèles météorologiques méso-échelles. Son développement s'appuie sur les travaux de Müller [2007] qui a constaté la sensibilité du modèle de surface BEP à la résolution verticale des modèles climatiques régionaux. En effet la résolution verticale d'un modèle méso-échelle ne peut guère descendre au niveau du mètre (limite numérique et physique) tandis que la diminution de la résolution du modèle BEP fait perdre tout intérêt à l'utilisation de la paramétrisation dans les modèles climatiques régionaux. L'idée est alors d'effectuer un calcul plus résolu du profil de vitesse de vent, de température et d'humidité sur une grille verticale immergée dans la couche atmosphérique de canopée urbaine par un modèle de canopée urbaine à proprement dit, placé à l'interface du modèle de surface et du modèle météorologique mésoéchelle. Les profils simulés à l'aide du modèle CIM sont alors fournis en entrée des modèles de surface BEP+BEM ou de tous autres modèles micro-échelles plus résolus calculant les flux de surface et prenant en compte la topologie des éléments urbains à l'échelle du quartier. Les flux de surface sont ensuite directement interpolés sur la grille méso-échelle comme précédemment.

Le modèle de canopée résout pour l'heure l'équation de transport vertical de quantité de mouvement en présence d'obstacles et en conditions atmosphériques neutres. Les effets induits par la thermique sur l'écoulement du vent ne sont ainsi pas pris en compte dans un premier temps. L'équation de transport vertical de la quantité de mouvement est discrétisée à l'aide de la méthode des volumes finis afin de bien considérer l'effet de la présence d'une série d'obstacles dans une maille plus large. Des porosités de volume et de surface (*i.e.* volumes et surfaces libres des mailles) ont été introduites dans l'équation de transport dans le terme représentant les forces de trainées et de frictions, induites par la résistance des obstacles à l'écoulement de l'air, et dans les termes représentant la diffusion turbulente. Ces porosités dépendent de la densité des obstacles dans la maille et sont pour l'heure calculées en considérant des parallélépipèdes de longueur et largeur uniformes dans une maille mais pouvant varier d'une maille à l'autre sur toute la hauteur des obstacles.

Les flux turbulents entre les couches d'air sont paramétrés en analogie à la diffusion moléculaire à l'aide de la K-théorie où ils sont fonction d'un coefficient d'échanges turbulents (coefficient de viscosité turbulente). Ce dernier a la dimension du produit d'une vitesse par une longueur. La vitesse est généralement associée au cisaillement de deux

couches d'air s'écoulant à des vitesses différentes et considérée comme étant la vitesse de friction u_*. La longueur est prise en fonction de la taille maximale des tourbillons présente dans l'écoulement turbulent. Plusieurs paramétrisations de ce coefficient ont été testées au cours de cette étude.

8.5 Les résultats

Dans un premier temps, les comparaisons des simulations fournies par le système de modèles climatiques WRF/ARW-BEP+BEM avec les données d'observation de surface issues de 3 stations météorologiques (les seules disponibles) exploitées par Météo France montrent des biais de températures moyennes de l'ordre de +1°C à +2°C avec la station dite "urbaine". Cette station est toutefois localisée dans le jardin botanique. Aussi sa représentativité est mise en doute. La station représentative de la circulation atmosphérique synoptique localisée à l'aéroport d'Entzheim (Sud-Ouest de l'agglomération de Strasbourg) présente une sous-estimation des températures de l'ordre de -1°C qui tend à diminuer en période hivernale. La station "non-urbaine" de La Wantzenau (au Nord Est de l'agglomération de Strasbourg) en revanche montre des écarts de températures plus faibles et variables tout au long de l'année pouvant être positifs ou négatifs. Toutefois, le système de modèles climatiques WRF/ARW-BEP+BEM simule correctement les températures de l'air puisque le coefficient de corrélation entre les températures simulées et observées est de 0,90.
Pour le vent, le système de modèles climatiques WRF/ARW-BEP+BEM semble peiner à reproduire les vents forts ($> 2.5 m.s^{-1}$) qui sont pourtant fréquents sur la zone d'étude, et qui apparaissent notamment dans les directions principales des vents (Nord/Nord Est et Sud/Sud Ouest). Toutefois le coefficient de corrélation entre les vitesses de vent simulées et observées est relativement significatif (R=0.60) et permet de conclure que les champs de vent sont globalement bien pris en compte par le système de modèles climatiques WRF/ARW-BEP+BEM. A fortiori, les directions sont globalement bien reproduites.
Enfin, les comparaisons des demandes énergétiques simulées par le modèle sur le territoire de la communauté urbaine de Strasbourg avec les estimations de consommations d'énergie fournies par l'ASPA pour ce même territoire montrent une différence relative de -23,55%. Au vu du nombre de paramètres d'entrée et des approximations réalisées dans le système de modèles climatiques, cette différence est jugée acceptable. Plusieurs facteurs peuvent expliquer cette différence (*ex.* considération du climat local dans la

présente méthode, estimation des consommations et non des demandes énergétiques dans la méthode de l'ASPA, caractéristiques des bâtiments) mais il semblerait que la principale source des différences observées entre les deux études, proviennent des caractéristiques des bâtiments et notamment de la prise en compte des apports de chaleur interne dans les bâtiments tels que la chaleur dégagée par l'utilisation des équipements électriques. En effet une étude de sensibilité a montré que ce paramètre influence fortement les estimations des besoins énergétiques : la prise en compte de la chaleur dégagée par les équipements électriques permet de réduire les demandes énergétiques d'un facteur 1,85. Toutefois très peu de données sont disponibles sur l'incertitude d'un tel paramètre. Ces résultats encourageants demandent cependant une validation supplémentaire de la méthodologie sur d'autres agglomérations et encouragent également des travaux d'amélioration de la prise en compte des comportements énergétiques des ménages présents dans les bâtiments.

Le modèle linéaire statistique a ensuite été établi sur le territoire de la CUS en considérant les températures de l'air et les besoins en chauffage simulés par le système de modèles climatiques WRF/ARW-BEP+BEM. Il a permis de déterminer la température de base T_0 et la sensibilité climatiques P représentatives du parc immobilier de la CUS. Cette relation linéaire statistique permet de connaître à partir de la distribution des températures de l'air d'une période donnée et des deux paramètres P et T_0, les besoins en chauffage en commentant des erreurs d'estimations de l'ordre de -5%. Afin de gagner du temps de calcul, cette relation linéaire statistique a ensuite été optimisée. Il apparait que 3 mois suffisent pour déterminer les paramètres du modèle linéaire statistique. En utilisant ces nouveaux paramètres et la distribution des températures annuelles, les estimations de la consommation énergétiques sont entachées d'une erreur d'environ 2% comparé au cas de référence. Enfin, à partir de cette dernière relation linéaire, plusieurs stratégies de réduction des besoins énergétiques dans le bâtiment ont été testées (*ex.* isolation des bâtiments, utilisation de matériaux réfléchissant sur les toits, augmentation de la température de confort, de la fraction de fenêtre sur les murs). Il apparait que le système de modèles météorologiques est plus sensible aux variations des paramètres internes des bâtiments (température de confort, isolation) qu'aux changements intervenant sur l'environnement immédiat du bâtiment (albédo).

Dans un second temps, les travaux menés sur les scénarios d'aménagement urbain à l'aide du modèle SLEUTH* ont questionné la capacité des modèles météorologiques

à constituer des outils d'aide à la décision à l'échelle des aménageurs. Le système de modèle météorologique montre en effet peu de sensibilité aux changements d'occupation du sol et, notamment, n'arrive pas à reproduire les occupations du sol résultant de l'étalement urbain. Plusieurs explications peuvent être avancées :

- La faible extension spatiale de l'agglomération : entre 2000 et 2008 un taux d'artificialisation de 93,22 ha/an a été calculé à partir de l'étude diachronique de la base de données d'occupation du sol CIGAL.
- L'inadéquation de la résolution du modèle météorologique (1 km) comparée aux changements d'occupation du sol (20 m). Cette hypothèse conduit à modifier le système de modèles météorologiques afin que celui-ci puisse être utilisé à de plus grandes résolutions spatiales.

Enfin, les simulations météorologiques et énergétiques des différentes occupations du sol montrent peu de différence entre les différentes formes urbaines. Il apparait que le volume de chauffe et le rapport enveloppe sur volume des bâtiments aient des rôles prépondérants dans le calcul de la sensibilité au froid des bâtiments sur l'aire d'étude. Les bâtiments situés au centre-ville dense sont ainsi moins sensibles aux variations climatiques que les bâtiments situés en périphérie. Il semblerait de ce fait que la densité du bâti et la forme des bâtiments soient des critères prépondérants expliquant les besoins énergétiques dans notre cas d'étude. S'il est vrai qu'une forme urbaine compacte peut induire des formes de bâtiments plus compactes, il apparait que les différentes stratégies d'aménagement du territoire contribuant à ces formes urbaines aient moins de poids que les actions menées à l'échelle du quartier par les développeurs ou les architectes.

Les travaux précédents ayant démontré la nécessité d'adopter une résolution spatiale plus fine, un nouveau modèle de canopée (CIM) a été développé dans le but de permettre un calcul plus résolu des flux de surface pris en compte dans les modèles régionaux climatiques. Il doit permettre l'interfaçage de modèles méso-échelles avec des modèles climatiques micro-échelles (échelle du quartier) qui représentent de manière plus précise la surface, notamment les bâtiments et la végétation, et qui considèrent les effets de topologie des divers éléments urbains sur le microclimat. Certains d'entre-eux, à l'instar d'EnviMet [Bruse and Fleer, 1998] inclus notamment la végétation arborée dans la maille urbaine sous la forme d'un modèle colonne.
Mon travail a consisté à mettre en place ce nouveau modèle de canopée (CIM) et en

particulier d'y décrire les obstacles (bâtiment ou végétation) en termes de porosités. Des tests de sensibilité montrent que l'influence de la porosité sur les profils verticaux de vent est moindre comparé aux effets des forces de traînées opposées à l'écoulement du vent par les parois verticales des bâtiments. Toutefois, la réduction de la taille des tourbillons dans la canopée urbaine modifie considérablement le profil de vitesse et des travaux futurs devront intégrer les porosités de surface et de volume dans sa paramétrisation. Ce travail a été repris par Mauree [2014]. Il a continué le développement des paramétrisations turbulentes, a validé le modèle CIM en utilisant les sorties de simulations de l'écoulement de l'air de modèle plus résolus, tel que les CFD et a introduit CIM dans le système de modèles climatiques WRF/ARW-BEP+BEM [Mauree and Clappier, 2014, Mauree et al., 2014b]. Ce faisant, il a démontré que le profil vertical d'énergie cinétique turbulente est significativement influencé par la présence des porosités tout comme le profil de vent dès lors que les termes de porosités sont intégrés dans la paramétrisation de la taille des tourbillons dans la canopée urbaine. Il a également démontré que l'introduction du modèle CIM dans le système de modèles climatiques WRF/ARW-BEP+BEM concourrait à réduire la vitesse du vent dans la canopée urbaine.

8.6 Conclusion

L'étude présente a permis de mettre en place un système de modèles climatiques sur le territoire de la communauté urbaine de Strasbourg afin d'évaluer ses besoins énergétiques en chauffage. Si la méthodologie adoptée parait encourageante lorsque l'on compare les demandes énergétiques avec les estimations de consommations énergétiques issues d'autres méthodes de type inventaire, elle a permis de questionner son efficience dans un contexte de développement urbain modéré et hétérogène. En effet, l'hétérogénéité de la surface urbaine y est encore reproduite de manière trop simplifiée : les différentes occupations du sol sont traitées par des modèles de surface distinctifs qui ne communiquent pas tandis que la faible résolution du modèle. De ce fait, la méthode ne permet pas encore de répondre aux questionnements que se posent les collectivités territoriales : quelle est l'influence d'un point d'eau/végétation d'une superficie de quelques mètres carrés sur le confort thermique des piétons ? Quelles en sont la/les configurations optimales dans une perspective de conservation de l'énergie ? Si le modèle de canopée CIM répond pour partie aux enjeux d'échelles, son utilisation idéale avec d'autres modèles de surface plus résolus demande encore des simplifications

de la physique reproduite dans les systèmes de modèles climatiques afin de pallier la contrainte numérique du temps de calcul et les incertitudes liées à certains paramètres. En effet, le simplification géométriques des obstacles sous forme de cubes induit des approximations des surfaces des enveloppes des bâtiments et du volume de chauffe qui sont pourtant déterminants dans l'estimation des besoins énergétiques. Par ailleurs, cette simplification comme l'a démontré Rasheed [2009] influence également l'intensité des forces de traînées agissant sur les parois des obstacles et de l'absorption des rayonnements solaires et thermiques.

D'un point de vue thématique, la forme urbaine semble dans le cas d'étude présent avoir peu d'impact sur la relation existant entre les températures de l'air et les besoins en chauffage. Ce résultat devra être confirmé sur d'autres cas d'études. Enfin, de nombreuses études tendent à mettre en avant le rôle prépondérant des styles de vie des occupants des bâtiments dans les besoins énergétiques. Les besoins en énergie semblent très liés à l'élasticité des prix, aux performances énergétiques des bâtiments (isolation) et au contrôle actif de la température de consigne des thermostats des appareils de chauffage et moyens de ventilations (fenêtre). Une hausse des prix entraine bien souvent une baisse de la température de consigne des thermostats des appareils de chauffage. Par ailleurs des enquêtes sociologiques ont également démontrées que les rénovations thermiques de l'enveloppe du bâtiment sont souvent corrélées à la phase d'installation des ménages dans un nouveau logement. Aussi, il semblerait que la mobilité résidentielle joue un rôle non négligeable dans les besoins énergétiques des bâtiments. Cette mobilité est contrôlée pour partie par les politiques d'aménagements du territoire (loi de l'offre et de la demande). Enfin, il apparaît que le contrôle de la température de consigne des thermostats des appareils de chauffage est inhérent à la sensation de confort thermique des habitants. Cette sensation de confort thermique est physiologique, psychologique, et dépend aussi des différentes ambiances thermiques traversées par les individus au cours d'une journée. Aussi, il est possible autour de la notion centrale de confort thermique d'investiguer sous un nouvel aspect les interactions existantes entre la forme urbaine, les dépenses énergétiques dans les bâtiments et le climat urbain.

Manon KOHLER

Apport de la modélisation météorologique à l'évaluation des besoins énergétiques des bâtiments

Résumé

Les bâtiments représentent 40 pourcents de la consommation finale d'énergie. Ils sont ainsi le fer de lance des politiques de réduction des dépenses énergétiques. Récemment, des systèmes de modèles climatiques qui incluent un modèle atmosphérique régional et des paramétrisations urbaines sophistiquées ont été développés. Ils considèrent la complexité de l'îlot de chaleur urbain et ses interactions avec les besoins énergétiques des bâtiments. Dans quelle mesure ces systèmes constituent-ils des outils d'aide à la décision pour les autorités locales ? Cette étude menée sur le territoire de l'Eurodistrict (Strasbourg-Kehl) en 2010, puis en 2030, à l'aide du système de modèles de climat WRF/ARW-BEP+BEM a démontré que si le système de modèles estimait de manière fiable les besoins en chauffage des bâtiments, ces derniers étaient davantage sensibles aux caractéristiques intrinsèques des bâtiments qu'aux formes urbaines et à l'îlot de chaleur urbain induit par ces formes.

Energie des bâtiments - Climat urbain - Ilot de chaleur urbain - Modèle atmosphérique meso-échelle - Paramétrisation urbaine – Aménagement du territoire

Résumé en anglais

Buildings represent 40 percent of the end-use energy. Thus, they constitute a key point of the energy saving policies. Recently, climate modeling systems that include a mesoscale atmospheric model and sophisticated urban parameterizations have been developed to account for the complexity of the urban heat island and its interactions with the building energy loads. This study aims to assess the capability of such climate modeling systems to provide climate and energy guidelines to urban planners.

For this, we used the research WRF/ARW-BEP+BEM climate modeling system and performed sensitivity tests considering the territory of the Eurodistrict (Strasbourg-Kehl) in 2010, and then in 2030. The results reveal that the climate modeling system achieves estimating the building energy needs over the study area, but also indicate that the building energy needs are more sensitive to the building intrinsic properties and occupant behavior than to the urban forms and their induced urban heat island.

Building energy – Urban climate – Urban heat island - Mesoscale atmospheric model – Urban parameterization – Urban planning